Poznan University of Technology
Faculty of Civil and Transport Engineering

Doctoral Dissertation

Evaluation of selected properties of welded joints in PVC profiles for civil engineering applications

Marek Kozielczyk

Supervisor:
dr hab. inż. Marta Paczkowska, prof. PP

Auxiliary Supervisor:
dr hab. inż. Jakub Kowalczyk

Poznań 2026

Scientia vincere tenebras

— Université libre de Bruxelles

Abstract

This thesis examines how welding conditions influence the weld structure formed in hybrid unplasticized poly(vinyl chloride) (PVC-U) window profiles reinforced with a glass-fibre composite insert. Such hybrid profiles are of growing interest in civil engineering, where structural reliability and long-term durability are essential performance requirements. In this configuration, the weld zone becomes an interaction region between constituents with markedly dissimilar thermomechanical responses, so the process settings govern not only joint load-bearing capacity but also the propensity for irreversible changes within the weld material and the heat-affected zone. The central objective was therefore to determine how processing conditions influence the resulting weld-zone structure and to delineate a stable processing window that delivers repeatable joint quality without indications of material degradation.

The work comprises a theoretical section that primarily systematises the relevant material and technological constraints, followed by an experimental programme structured into three complementary stages. The first stage focused on the constituent materials of the profile and provided the baseline required to interpret phenomena within the weld. The second stage consisted of pilot trials aimed at selecting welding parameters and identifying the boundaries of process stability. The third, principal stage delivered a multi-method verification of weld-zone changes using hardness testing, microscopy, DSC, and FTIR-ATR.

The preliminary investigations demonstrated a pronounced asymmetry in the thermomechanical behaviour of PVC-U and the composite insert during welding, since PVC-U underwent plasticisation while the glass-fibre composite remained essentially dimensionally stable due to its substantially higher effective melting or softening threshold. The composite contained approximately 52% glass fibre by mass and, relative to PVC-U, exhibited markedly higher stiffness and strength alongside an extremely limited strain capacity. Thermal testing corroborated this mismatch in the welding context, because the heat deflection temperature of PVC-U was several times lower than that of the composite despite similar Vicat softening temperatures. During plasticisation and bead formation, these disparities between those materials promote non-uniform compliance and local stress concentration at the joint, which necessitates operating within a tightly controlled parameter window.

During the pilot stage, joint quality was assessed concurrently in mechanical terms through failure load, in geometric terms through symmetry and dimensional deviation, and in qualitative terms through bead continuity, weld bead colour, and overload events. The results showed that welding-head kinematics act as the governing control variable. Within the investigated range, a head feed rate of 0.25 mm/s provided the most favourable compromise between load-bearing performance and process stability when compared with 0.19 mm/s and 0.31 mm/s. In parallel, machining of the composite by milling proved to be a boundary condition for quality. Milling depths above 1.0 mm produced bead discontinuities and disqualified the welds despite locally high failure loads, whereas a depth of 1.0 mm delivered the best repeatability while preserving joint integrity. The analysis of temperature and plasticisation time further indicated that reducing temperature, down to 247 °C with a melting time of 30 s, progressively narrowed the stability margin until geometric nonconformities and machine overload errors emerged. By contrast, shortening the melting time to 22 s at 264 °C remained feasible without loss of quality, whereas further reduction to 21 s, compensated by increasing temperature into the 270–280 °C range, led to bead discoloration and symptoms of

thermal overloading, indicating a technologically unacceptable intensification pathway. On this basis, a processing window was established comprising welding at 264 °C with a melting time of 22 s, a head feed rate of 0.25 mm/s, and milling of the composite insert to a depth of 1.0 mm.

In the principal stage, the combined evidence from hardness testing, microscopy, DSC, and FTIR-ATR demonstrated that reducing the melting time from 30 s to 22 s at 264 °C preserved the material integrity of the weld zone relative to the reference condition. For welds produced between 256 °C and 264 °C, hardness remained at approximately 65–75 N/mm², and no statistically meaningful difference was detected between the welds produced at 264 °C with a melting time of 22 s and those produced at 264 °C with a melting time of 30 s, although weld hardness was lower than that of the parent PVC. Microscopy confirmed the absence of degradation features in welds produced between 256 °C and 264 °C, whereas the boundary condition of 270 °C with a melting time of 21 s produced discoloration penetrating into the weld bead, interpreted as evidence of PVC degradation. DSC provided no basis to conclude that welding at 264 °C with a melting time of 22 s induced any distinct structural change from the reference condition at 264 °C with a melting time of 30 s, as the observed differences were subtle and local. The decisive confirmation of chemical stability within the weld zone was delivered by FTIR-ATR spectra. Comparing welds produced at 264 °C with melting times of 22 s and 30 s revealed neither the emergence of new bands nor the disappearance of diagnostic bands, supporting the conclusion that the chemical type of the weld material remains unchanged within the recommended processing window.

The principal scientific contribution of the dissertation is the establishment of a quantitatively substantiated relationship between welding-process variables and the mechanical response of welded corners in PVC-U profiles reinforced with glass-fibre composite inserts, while demonstrating that this response cannot, by itself, define process acceptability. The regression-based part of the study showed that failure load varies systematically with welding temperature and melting time within the investigated process domain, thereby providing a basis for model-supported interpretation of the strength response. Its significance lies not in replacing technological qualification, but in demonstrating that strength prediction must be integrated with dimensional stability, weld morphology, and verification of the material state within the weld zone. The convergence of failure-load results, microscopic observations, DSC response, and FTIR-ATR spectra demonstrated that reducing the melting time from 30 s to 22 s at 264 °C does not induce detectable adverse material or microstructural changes in the weld zone relative to the reference condition produced at the same welding temperature. Overall, the dissertation provides implementable recommendations for the design and control of welded corner joints in civil-engineering applications, delineates a technological window for hybrid PVC-U/composite profile systems, and demonstrates that parameter selection must integrate strength-based criteria with material-state indicators of safety. Conditions that appear acceptable when evaluated solely by failure load may nevertheless initiate degradation processes that remain beyond the resolution of the failure-load metric alone.

Streszczenie

Niniejsza rozprawa dotyczy wpływu warunków zgrzewania na strukturę zgrzeiny powstającej w hybrydowych profilach okiennych z nieplastyfikowanego poli(chlorku winylu) (PVC-U), wzmacnianych wkładką kompozytową z włóknem szklanym. Tego rodzaju profile hybrydowe zyskują coraz większe znaczenie w budownictwie, gdzie niezawodność konstrukcyjna i trwałość długoterminowa stanowią zasadnicze wymagania użytkowe. W analizowanej konfiguracji, strefa zgrzeiny staje się obszarem oddziaływania składników o wyraźnie odmiennych odpowiedziach termomechanicznych. Parametry procesu determinują zatem nie tylko nośność połączenia, lecz także podatność materiału zgrzeiny i strefy wpływu ciepła na występowanie zmian nieodwracalnych. Głównym celem pracy było w związku z tym określenie, w jaki sposób warunki technologiczne wpływają na strukturę strefy zgrzeiny, oraz wyznaczenie stabilnego okna procesowego zapewniającego powtarzalną jakość połączenia bez oznak degradacji materiału.

Praca obejmuje część teoretyczną, ukierunkowaną przede wszystkim na usystematyzowanie istotnych uwarunkowań materiałowych i technologicznych, oraz program badań eksperymentalnych podzielony na trzy komplementarne etapy. Pierwszy etap dotyczył materiałów składowych profilu i pozwolił określić stan odniesienia niezbędny do interpretacji zjawisk zachodzących w zgrzeinie. Drugi etap obejmował badania pilotażowe służące doborowi parametrów zgrzewania i identyfikacji granic stabilności procesu. Trzeci, zasadniczy etap badań, umożliwił wielometodową weryfikację zmian w strefie zgrzeiny z wykorzystaniem pomiarów twardości, mikroskopii, DSC oraz FTIR-ATR.

Badania wstępne wykazały wyraźną asymetrię zachowania termomechanicznego PVC-U i wkładki kompozytowej podczas zgrzewania. PVC-U ulegał uplastycznieniu, natomiast kompozyt z włóknem szklanym pozostawał zasadniczo stabilny wymiarowo ze względu na znacznie wyższy efektywny próg topnienia lub mięknienia. Kompozyt zawierał około 52% włókna szklanego w ujęciu masowym i w porównaniu z PVC-U, charakteryzował się wyraźnie większą sztywnością oraz wytrzymałością, przy jednocześnie bardzo ograniczonej zdolności do odkształcenia. Badania cieplne potwierdziły tę niezgodność w kontekście procesu zgrzewania, ponieważ temperatura ugięcia pod obciążeniem dla PVC-U była kilkukrotnie niższa niż dla kompozytu, mimo zbliżonych temperatur mięknienia Vicata. Podczas uplastyczniania i formowania wypływki zgrzeiny różnice między tymi materiałami sprzyjają nierównomiernej podatności oraz lokalnej koncentracji naprężeń w obszarze połączenia. Wymusza to prowadzenie procesu w ściśle kontrolowanym zakresie parametrów.

Na etapie badań pilotażowych jakość połączenia oceniano równocześnie w ujęciu mechanicznym, geometrycznym i jakościowym. Kryterium mechaniczne stanowiło obciążenie niszczące. Kryteria geometryczne obejmowały symetrię oraz odchyłki wymiarowe, natomiast ocena jakościowa dotyczyła ciągłości wypływki, barwy wypływki zgrzeiny, oraz występowania przeciążeń maszyny. Wyniki wykazały, że kinematyka głowic zgrzewających stanowi kluczową zmienną sterującą procesem. W badanym zakresie prędkość posuwu głowicy wynosząca 0.25 mm/s zapewniała najkorzystniejszy kompromis między nośnością połączenia a stabilnością procesu, w porównaniu z wartościami 0.19 mm/s oraz 0.31 mm/s. Równolegle wykazano, że obróbka kompozytu przez frezowanie stanowi warunek brzegowy uzyskania wymaganej jakości. Głębokości frezowania większe niż 1.0 mm prowadziły do nieciągłości wypływki i dyskwalifikowały zgrzeiny, mimo lokalnie wysokich wartości obciążenia niszczącego. Głębokość 1.0 mm zapewniała natomiast najlepszą powtarzalność przy zachowaniu integralności połączenia. Analiza temperatury i czasu

uplastyczniania wykazała ponadto, że obniżanie temperatury do 247 °C przy czasie topienia 30 s stopniowo zawężało margines stabilności procesu, aż do wystąpienia niezgodności geometrycznych i błędów przeciążenia maszyny. Z kolei skrócenie czasu topienia do 22 s przy temperaturze 264 °C pozostawało możliwe bez utraty jakości. Dalsze skrócenie czasu do 21 s, kompensowane podwyższeniem temperatury do zakresu od 270 do 280 °C, prowadziło jednak do przebarwienia wypływki oraz objawów przeciążenia cieplnego, wskazując na technologicznie niedopuszczalną ścieżkę intensyfikacji procesu. Na tej podstawie wyznaczono okno procesowe obejmujące zgrzewanie w temperaturze 264 °C przy czasie topienia 22 s, prędkości posuwu głowicy 0.25 mm/s oraz frezowaniu wkładki kompozytowej do głębokości 1.0 mm.

W etapie zasadniczym zbieżne wyniki pomiarów twardości, obserwacji mikroskopowych, DSC oraz FTIR-ATR wykazały, że skrócenie czasu topienia z 30 s do 22 s przy temperaturze 264 °C pozwala zachować integralność materiałową strefy zgrzeiny względem warunku referencyjnego. Dla zgrzein wykonanych w zakresie od 256 °C do 264 °C twardość pozostawała w przybliżeniu na poziomie 65–75 N/mm². Nie stwierdzono statystycznie istotnej różnicy między zgrzeinami wykonanymi w temperaturze 264 °C przy czasie topienia 22 s a zgrzeinami wykonanymi w tej samej temperaturze przy czasie topienia 30 s, mimo że twardość zgrzeiny była niższa niż twardość materiału rodzimego PVC. Obserwacje mikroskopowe potwierdziły brak cech degradacji w zgrzeinach wykonanych w zakresie od 256 °C do 264 °C. Warunek graniczny odpowiadający temperaturze 270 °C i czasowi topienia 21 s powodował natomiast przebarwienie wnikające w wypływkę zgrzeiny, interpretowane jako przejaw degradacji PVC. Analiza DSC nie dostarczyła podstaw do stwierdzenia, że zgrzewanie w temperaturze 264 °C przy czasie topienia 22 s wywołuje odrębną zmianę strukturalną względem warunku referencyjnego, odpowiadającego temperaturze 264 °C i czasowi topienia 30 s, ponieważ zaobserwowane różnice były subtelne oraz lokalne. Rozstrzygające potwierdzenie stabilności chemicznej w strefie zgrzeiny uzyskano na podstawie widm FTIR-ATR. Porównanie zgrzein wykonanych w temperaturze 264 °C przy czasach topienia 22 s oraz 30 s nie wykazało ani pojawienia się nowych pasm, ani zaniku pasm diagnostycznych, co wspiera wniosek, że charakter chemiczny materiału zgrzeiny pozostaje niezmieniony w zalecanym oknie procesowym.

Główny wkład naukowy rozprawy polega na ustaleniu ilościowo uzasadnionej zależności między zmiennymi procesu zgrzewania a odpowiedzią mechaniczną zgrzewanych narożyprofili PVC-U wzmacnianych wkładkami kompozytowymi z włóknem szklanym, przy jednoczesnym wykazaniu, że sama odpowiedź mechaniczna nie może definiować akceptowalności procesu. Część badań oparta na analizie regresyjnej wykazała, że obciążenie niszczące zmienia się systematycznie wraz z temperaturą zgrzewania i czasem topienia w badanym obszarze procesu, dostarczając podstaw do interpretacji odpowiedzi wytrzymałościowej wspieranej modelem. Znaczenie tej analizy nie polega na zastąpieniu kwalifikacji technologicznej, lecz na wykazaniu, że predykcja wytrzymałości musi być zintegrowana ze stabilnością wymiarową, morfologią zgrzeiny oraz weryfikacją stanu materiału w strefie zgrzeiny. Zbieżność wyników obciążenia niszczącego, obserwacji mikroskopowych, odpowiedzi DSC oraz widm FTIR-ATR wykazała, że skrócenie czasu topienia z 30 s do 22 s przy temperaturze 264 °C nie powoduje wykrywalnych niekorzystnych zmian materiałowych ani mikrostrukturalnych w strefie zgrzeiny względem warunku referencyjnego uzyskanego przy tej samej temperaturze zgrzewania. Całościowo rozprawa dostarcza możliwych do wdrożenia zaleceń dotyczących projektowania i kontroli zgrzewanych połączeń narożnych w zastosowaniach budowlanych, wyznacza okno technologiczne dla hybrydowych systemów profili PVC-U/kompozyt oraz wykazuje, że

dobór parametrów musi integrować kryteria wytrzymałościowe ze wskaźnikami bezpieczeństwa odnoszącymi się do stanu materiału. Warunki, które mogą wydawać się akceptowalne przy ocenie prowadzonej wyłącznie na podstawie obciążenia niszczącego, mogą mimo to inicjować procesy degradacyjne pozostające poza rozdzielczością tej pojedynczej miary.

Résumé

La présente thèse examine l'influence des conditions de soudage sur la morphologie du joint formé au sein de profilés de fenêtres hybrides en polychlorure de vinyle non plastifié (PVC-U), renforcés par un insert composite à fibres de verre. Ces profilés suscitent un intérêt croissant en génie civil, un secteur où la fiabilité structurelle et la durabilité à long terme constituent des exigences de performance absolues. Dans une telle configuration, la zone de soudure devient une interface d'interaction entre des constituants aux réponses thermomécaniques très contrastées. Par conséquent, les paramètres du procédé ne régissent pas seulement la capacité portante de l'assemblage, mais également le risque d'altérations irréversibles au cœur du matériau soudé et dans la zone affectée thermiquement (ZAT). L'objectif central de ces travaux consistait donc à déterminer l'impact des conditions de mise en œuvre sur la structure finale de la soudure, et à définir une fenêtre d'opérabilité stable, garantissant une qualité d'assemblage hautement répétable et exempte de toute dégradation du matériau.

Le manuscrit s'articule autour d'un volet théorique, principalement dédié à la systématisation des contraintes matérielles et technologiques inhérentes, suivi d'un programme expérimental structuré en trois phases complémentaires. La première phase s'est concentrée sur les matériaux constitutifs du profilé, permettant d'établir l'état de référence indispensable à l'appréhension des phénomènes se manifestant au sein de la soudure. La deuxième phase, sous forme d'essais pilotes, a visé à sélectionner les paramètres optimaux et à cerner les limites de stabilité du procédé. La troisième phase, cœur de l'étude, a reposé sur une caractérisation multimodale des altérations de la zone soudée via des essais de dureté, des analyses microscopiques, la calorimétrie différentielle à balayage (DSC) et la spectroscopie infrarouge à transformée de Fourier en réflexion totale atténuée (FTIR-ATR).

Les investigations préliminaires ont révélé une asymétrie marquée dans le comportement thermomécanique du PVC-U et de l'insert composite lors du soudage. Le PVC-U entrait en phase de plastification, tandis que le composite à fibres de verre conservait une intégrité dimensionnelle quasi totale en raison d'un seuil effectif de fusion (ou de ramollissement) considérablement plus élevé. Ce composite, chargé à hauteur d'environ 52 % en masse de fibres de verre, affichait une rigidité et une résistance nettement supérieures à celles du PVC-U, combinées à une capacité de déformation extrêmement restreinte. Les essais thermiques ont confirmé cette inadéquation : la température de fléchissement sous charge (HDT) du PVC-U s'est avérée plusieurs fois inférieure à celle du composite, en dépit de températures de ramollissement Vicat comparables. Durant la plastification et la formation du cordon de soudure, ces dissimilitudes exacerbent l'hétérogénéité de la déformation et génèrent des concentrations de contraintes localisées au droit du joint. Cette dynamique impose de fait la restriction du procédé à une fenêtre paramétrique rigoureusement contrôlée.

Lors de la phase pilote, la qualité de l'assemblage a été évaluée simultanément sous des prismes mécanique (charge de rupture), géométrique (symétrie et déviations dimensionnelles) et qualitatif (continuité et coloration du cordon, détection de surcharges). Les résultats ont démontré que la cinématique de la tête de soudage constitue le paramètre de contrôle prépondérant. Sur la plage étudiée, une vitesse d'avance de 0,25 mm/s a offert le meilleur compromis entre les performances mécaniques et la stabilité du procédé, surpassant les vitesses de 0,19 mm/s et 0,31 mm/s. En parallèle, la préparation du composite par fraisage s'est imposée comme un facteur critique. Des profondeurs de fraisage excédant 1,0 mm ont induit des discontinuités dans le cordon, entraînant le rejet systématique des soudures malgré

des charges de rupture localement élevées. À l'inverse, un usinage de 1,0 mm a garanti la meilleure répétabilité tout en préservant l'intégrité structurelle de l'assemblage. Par ailleurs, l'analyse des couples température/temps de plastification a souligné qu'un abaissement de la température à 247 °C (pour un temps de fusion de 30 s) réduisait progressivement la marge de stabilité, jusqu'à l'émergence de non-conformités géométriques et de mises en sécurité de l'équipement par surcharge mécanique. Au contraire, une réduction du temps de fusion à 22 s sous 264 °C s'est avérée viable, sans aucune perte de qualité. Une réduction plus drastique à 21 s, bien que compensée par une élévation de la température (270–280 °C), s'est traduite par une décoloration du cordon et des stigmates de surcharge thermique, illustrant une voie d'intensification technologiquement inacceptable. Fort de ces constats, une fenêtre opératoire optimale a été arrêtée : un soudage à 264 °C avec un temps de fusion de 22 s, une avance de tête de 0,25 mm/s, et un fraisage de l'insert composite à une profondeur de 1,0 mm.

Dans la phase principale, le croisement des données issues de la dureté, de la microscopie, de la DSC et de la FTIR-ATR a prouvé que l'optimisation du temps de fusion (de 30 s à 22 s à 264 °C) préservait l'intégrité physico-chimique de la zone de soudure par rapport aux conditions de référence. Pour les soudures opérées entre 256 °C et 264 °C, la dureté s'est stabilisée autour de 65–75 N/mm². Aucune variation statistiquement significative n'a été relevée entre les assemblages réalisés à 264 °C (qu'ils soient à 22 s ou 30 s), bien que la dureté globale de la soudure reste en deçà de celle du PVC de base. L'analyse microscopique a corroboré l'absence de tout faciès de dégradation pour les échantillons soudés entre 256 °C et 264 °C. En revanche, le régime limite (270 °C pour 21 s) a provoqué une décoloration se propageant au cœur du cordon, témoignant sans équivoque d'une dégradation thermique du polymère. L'analyse DSC n'a mis en exergue aucune modification structurale probante entre le régime à 22 s et celui de référence à 30 s, les rares écarts observés demeurant infimes et ultra-localisés. La validation définitive de la stabilité chimique a été actée par la spectroscopie FTIR-ATR. La comparaison des spectres n'a révélé ni l'apparition de nouvelles bandes d'absorption, ni la disparition des bandes caractéristiques, attestant de la totale conservation de la signature chimique du matériau au sein de la fenêtre préconisée.

La contribution scientifique majeure de cette thèse réside dans l'établissement d'une corrélation quantitative robuste entre les variables du procédé de soudage et le comportement mécanique des assemblages d'angle pour ces profilés hybrides. Surtout, elle démontre que la réponse mécanique seule ne saurait dicter la validité du procédé. Le volet fondé sur la régression a mis en lumière une variation systématique de la charge de rupture en fonction de la température et du temps de fusion, posant ainsi les jalons d'une interprétation de la résistance étayée par la modélisation. La portée de ce travail ne vise pas à supplanter les qualifications technologiques d'usage, mais à prouver que l'anticipation de la résistance mécanique doit impérativement s'articuler avec la stabilité dimensionnelle, la morphologie du cordon et la vérification de l'état microstructural dans la ZAT. La convergence de l'ensemble des résultats atteste que l'optimisation du temps de fusion n'induit aucune altération matérielle ou microstructurale délétère. En définitive, cette thèse délivre des préconisations concrètes pour la conception et la maîtrise des assemblages d'angle soudés en génie civil. Elle délimite une fenêtre technologique stricte pour les systèmes PVC-U/composite, et souligne que la sélection des paramètres doit indissociablement lier les critères de résistance aux indicateurs de sécurité physico-chimiques. Une configuration de soudage d'apparence optimale, si elle n'est jugée qu'à l'aune de sa charge de rupture, peut en réalité dissimuler l'amorçage de processus de dégradation invisibles aux yeux de cette seule métrique.

Table of Contents

List of abbreviations

Notation	Meaning
A	Geometrical parameter in the corner failure-load test
ATR	Attenuated total reflection
C=O	Carbonyl group
CNC	Computer numerical control
CO	Carbon monoxide
CO_2	Carbon dioxide
C–Cl	Carbon–chlorine bond
C–H	Carbon–hydrogen bond
C–O	Carbon–oxygen bond
C–O–C	Skeletal vibration associated with ether or ester groups
D	Composite-insert milling depth
DMA	Dynamic mechanical analysis
DP	Degree of polymerisation
DSC	Differential scanning calorimetry
E	Young's modulus
e	Eccentricity parameter in the corner failure-load test
EPDM	Ethylene propylene diene monomer rubber
FTIR-ATR	Fourier-transform infrared spectroscopy with attenuated total reflection
GFRP	Glass-fibre-reinforced polymer
H1	Welding head 1
H2	Welding head 2
H3	Welding head 3
H4	Welding head 4
HCl	Hydrogen chloride
HDT	Heat deflection temperature
HRC	Rockwell hardness, C scale
IGU	Insulating glass unit
ISO	International Organization for Standardization
K value	Fikentscher constant
L	Mean failure load of welded joints
Li	Geometrical parameter in the corner failure-load test
Ln	Geometrical parameter in the corner failure-load test
LOI	Limiting oxygen index
low-E	Low-emissivity coating
Lz	Geometrical parameter in the corner failure-load test
Mn	Number-average molar mass
Mv	Viscosity-average molar mass
Mw	Weight-average molar mass
O–H	Hydroxyl group
P	Welding-head feed rate
P1	Commanded physical welding-head feed rate

P2	Effective feed rate at the 45° faying surface
PE	Polyethylene
PN-EN	Polish implementation of a European standard
PTFE	Polytetrafluoroethylene
PUR	Polyurethane
PV	Photovoltaic
PVC	Poly(vinyl chloride)
PVC-P	Plasticised poly(vinyl chloride)
PVC-U	Unplasticised poly(vinyl chloride)
R	Correlation coefficient
Rm	Tensile strength / maximum stress before fracture
Ru	Ultimate stress at complete failure
T	Welding temperature
t	Melting time
Tg	Glass transition temperature
TPE	Thermoplastic elastomer
UV	Ultraviolet radiation
VC	Vinyl chloride monomer
ΔCp	Change in heat capacity at the glass transition

1. Introduction

The rapid development of contemporary construction, coupled with rising expectations for occupant comfort and energy efficiency, means that window joinery is no longer viewed solely as a means of daylighting and ventilation. Instead, it has become a critical component of the external envelope with quantifiable in-service performance and growing relevance in civil engineering. A window, understood as a construction product closing an opening in the building enclosure, comprises the frame, sash, infill, most commonly glazing, seals, hardware, and installation details, which collectively govern thermal and acoustic insulation, air and water tightness, resistance to wind loading, durability, and safety [1–2]. From a civil engineering perspective, it is important that the evolution of window solutions has been driven not only by materials advances and the industrialisation of manufacture, but also by urbanisation and the progressive tightening of expectations regarding building energy performance [3–5]. In practical terms, this shifts emphasis from the product to the installed system. Final in-service quality depends not only on the intrinsic performance of the window, but also on its interaction with the wall and on the installation approach, which can introduce material thermal bridges and reduce surface temperatures in the reveal zone [5–6].

A further, closely related background factor is the parallel development of glazing technology. The widespread adoption of insulating glazing units and the refinement of the edge zone, including spacers and seal systems, have led to the window being treated as a coupled glass–cavity–edge assembly, in which durability and energy performance increasingly depend on the quality of detail design and execution [4], [7]. The continued tightening of thermal requirements has been reinforced by the dissemination of low-emissivity coatings, whose market diffusion has been correlated with energy crises and with increasingly stringent requirements on building energy use [5]. Consequently, contemporary window solutions are designed as part of the building’s energy strategy rather than merely as an architectural component.

Against this backdrop, multi-chamber frame systems have gained particular relevance, including solutions based on unplasticised PVC (PVC-U), which combine relatively low thermal conductivity with the ability to industrially form complex cross-sections and to produce repeatable corner joints by welding [8]. At the same time, window design remains a compromise between thermal insulation, stiffness, durability, and the manufacturing constraints associated with profiles and joints [9]. Improving frame insulation often necessitates materials with lower conductivity, which typically exhibit reduced stiffness and therefore require reinforcement [9–10]. In PVC-U profiles, this role has traditionally been fulfilled by steel sections, which increase load-bearing capacity but also introduce thermal bridges and create a thermally and mechanically heterogeneous system [10]. The drive to minimise the thermal penalty associated with metal and to reduce structural mass is therefore a direct motivation for the development of composite reinforcements and for the search for solutions that preserve the required quality of corner joints.

The literature identifies several complementary research directions that underscore the currency of this problem. First, state-of-the-art reviews of spacers and sealants in insulating glazing units emphasise the importance of limiting linear thermal bridges in the edge zone and highlight the role of warm-edge solutions in reducing condensation risk and improving the thermal balance [7]. Second, building-physics studies show that, even when the product itself performs well, significant losses and local temperature reductions may be generated by installation thermal bridges, which depend on window position within the insulation layer and

on the reveal detail [5–6]. Third, thermoplastic composite reinforcements manufactured by continuous methods, such as pultrusion, have been proposed as a means of improving the thermal performance of sashes and frames relative to steel-based variants, provided that joining technology in the multi-material system is adequately developed [11]. Fourth, strictly technological studies indicate that welding parameters and the preparation of profile ends, including machining of composite reinforcement in the corner region, directly determine the load-bearing capacity and repeatability of welded joints in composite-reinforced profiles [12], [13], [14].

Despite intensive research into window systems, including analyses of the quality and strength of welded PVC-U profile corners, a gap remains in coherently linking welding parameters to the material response in a profile–glass-fibre-reinforced composite system, evaluated directly within the weld zone. Although multiple joining methods exist, hot-plate butt welding remains the dominant industrial solution because it provides through-thickness joint continuity, corner tightness, and high repeatability in high-volume manufacture [15], [16]. The literature also highlights the sensitivity of weld quality even to small parameter deviations, which can reduce load-bearing capacity or tightness. This justifies the use of standardised assessment criteria, including corner failure load testing [16–18]. With composite reinforcement, the technological challenge becomes more complex. Achieving sufficient plasticisation of the region that encompasses both PVC and the reinforcing material may require greater thermal input, which in turn increases the risk of PVC degradation within the weld zone. This necessitates concurrent balancing of reinforcement geometry in the corner, end-preparation strategy, and welding-cycle parameters, including times and head feed kinematics, to preserve PVC-U quality and to limit defects at the PVC–composite interface [12–13].

In response to this research need, the present work focuses on the material properties of PVC-U and a glass-fibre-reinforced composite, and then analyses their interaction within a welded profile corner in the context of parameter selection, rationalisation, and the resulting weld-zone response. On the one hand, the study anchors the joint strength requirements in empirically determined material behaviour and in process parameters selected and optimised through experiments using robust weld-quality criteria. On the other hand, it verifies whether the process conditions induce undesirable material changes within the weld zone. In consequence, the work emphasises the critical role of joining technology and weld integrity in civil engineering as determinants of durability, safety, and the energy performance of built assets.

2. Description of the State of the Art

2.1. Window Systems Used in Civil Engineering

2.1.1. Historical Development of Window Systems

From a terminological standpoint, a window is a construction product intended, inter alia, to close an opening in the building envelope, such as an external wall or a pitched roof. The relevant standard also addresses daylight provision and the facilitation of ventilation. Within this scope, the term encompasses the frame and one or more sashes with an infill, most commonly glazing [1]. In practice, the history of window systems is the history of progressively tightening the envelope opening and formalising its performance. The window has evolved from a simple means of admitting daylight and enabling airing to a highly integrated product [2–3]. In such assemblies, components including the frame, sash, glazing, seals, hardware, and installation details jointly determine quantifiable properties, such as thermal and acoustic insulation, air and water tightness, resistance to wind loading, durability, and safety. From a civil engineering perspective, it is essential that this development has not been linear. Instead, it has been shaped by external drivers, including shifts in material technologies (glass, timber, metals, polymers), the industrialisation of manufacture, urbanisation, and increasingly stringent expectations of comfort and building energy efficiency.

In the earliest arrangements, the window effectively functioned as an opening in masonry, provisionally protected from precipitation and wind. Over time, solid closures emerged, for example timber shutters, which improved security and reduced infiltration, albeit at the expense of daylight admission. The maturation of timber joinery as a craft drove two material developments. First, it enabled improved dimensional stability of elements such as frames, sashes, and glazing bars. Second, it promoted the refinement of rebates and grooves, which acted as the earliest form of sealing against wind-driven rain [3]. In this period, in-service performance depended predominantly on workmanship, joint fit, and the practitioner’s experience, rather than on calculation or formal standardisation.

In parallel with the evolution of frames, glass advanced as a construction material. In the early stages it was scarce, and manufacturing methods did not allow large, flat panes with consistently high optical clarity [3], [19]. Glazing therefore tended to be small-format, while larger window areas were achieved by subdividing the opening into smaller fields using glazing bars or dense frame divisions. Technically, this is significant because the window was already more than a frame with inserted glass. It was an assembly in which glass had to interact mechanically with timber or metal elements. Glass and the frame respond differently to temperature variations. The frame may deform and transmit vibrations, whereas glass is brittle and has limited tolerance to localised stresses. In addition, windows were exposed to dynamic actions, including wind-induced vibration and incidental impacts during use, which demanded stable seating of the pane. As a result, constructional solutions began to crystallise that remain recognisable today in adapted form: the glazing rebate as the interface for supporting the glass edge within the frame, the glazing bead as the clamping and retaining element, and support blocks that carry the self-weight of the glass while limiting in-frame movement.

The nineteenth-century expansion of the construction industry accelerated the dissemination of tools and techniques that enabled repeatable manufacture [3]. The window

consequently ceased to be an exclusively bespoke product. Standardised configurations emerged, including box windows and double-sash arrangements, which in practice improved insulation by introducing an additional air layer and reducing the direct action of wind on the inner sash. During the twentieth century, hygienic and usability requirements gained prominence, including daylight provision, ventilation, ease of operation, and safety. This, in turn, drove the diversification of opening typologies, such as casement, tilt, pivot, and sliding systems, and increased the role of hardware as a system component governing both ergonomics and tightness.

Vertically sliding windows became particularly widespread in response to the need for controllable ventilation and spatial constraints. Casement windows remained common, while tilt-and-turn systems gained traction because they combine safe airing with the option of fully opening the sash. Sliding solutions increased in relevance alongside the proliferation of large glazed areas and the modernisation of dwelling layouts and service buildings [3]. As urbanisation progressed and traffic-related noise intensified, acoustic insulation became a material design criterion. This indirectly reinforced the demand for improved sealing and multi-layer glazing concepts [4]. Concurrently, closing hardware and locking mechanisms evolved to enable tighter engagement between the sash and the frame. With improved manufacturing accuracy, this progressively reduced infiltration and enhanced comfort.

The transition from basic hinge-and-latch arrangements to perimeter hardware with adjustable keeps supported a gradual, operational tightening of the window. Compression adjustment mechanisms, including eccentric compression rollers, together with multi-point locking, enabled a more uniform distribution of contact pressures on seals around the sash perimeter. This translated into more stable air and water tightness under service loads and in the presence of material ageing [20]. As system solutions matured, the standardisation of functional requirements and test methods also advanced, improving product comparability and structuring the market. Contemporary window assessment relies on harmonised classes of, among others, air permeability, watertightness, and resistance to wind loading, supported by unified testing and calculation procedures. This enables constructional solutions to be directly related to in-service and energy-relevant performance parameters [2].

A pivotal technological breakthrough was the industrial production of high-quality flat glass in large formats. In practice, a key milestone was the float process, developed in the 1950s, with the concept formulated in 1952, a pilot line commissioned in 1954, and commercial implementation achieved in 1959. This route delivered high flatness and sheet uniformity at substantial throughput, thereby reducing the cost of window glass within the post-war industrialisation of construction [19], [21]. It enabled larger glazed areas, supported the emergence of modernist architecture, and subsequently facilitated mullion-and-transom and modular façade systems.

At the same time, awareness of heat losses through transparent envelope elements increased. The corresponding response was the development of insulated glazing, in which two, and later three, panes are separated by a cavity filled with air or a gas with more favourable thermal properties (Fig. 2.1). Although concepts of insulated glazing appeared already in the nineteenth century, industrial uptake accelerated in the twentieth century, particularly in the interwar and post-war periods, when advances in edge-sealing technologies and quality control made stable production of insulated glazing units (IGUs) feasible for a rapidly expanding construction market [4], [7]. In system terms, this marked a shift whereby

the thermal performance of a window was no longer a property of the frame alone. It became a result of the coupled interaction between the glass, the cavity, and the edge zone.

With the proliferation of IGUs, the perimeter region, including spacer bars and sealants, assumed critical importance because it governs the durability of the cavity, gas retention, and resistance to moisture ingress. In parallel, the issue of thermal bridging at the glass perimeter became more prominent, driven by spacer conductivity and the geometry of glass-to-frame contact. These constraints stimulated the development of warm-edge spacer bars and the refinement of sealing systems. This can be interpreted as a maturation of the window concept towards a product in which durability and performance depend on detail quality as much as on material selection. A particularly consequential step occurred towards the end of the twentieth century, when aluminium spacers began to be replaced by lower-conductivity alternatives, including stainless steel, polymers, and composite materials, in order to reduce the linear thermal bridge and limit condensation risk in the IGU edge zone [7].

Fig. 2.1. Representative construction of an insulating glass unit (IGU). Source: Author's own work

A subsequent phase of development involved functional coatings applied to glass, most notably low-emissivity (low-E) coatings. These reduce heat losses associated with radiative exchange while maintaining high visible light transmittance. In chronological terms, the origins of low-E technology can be traced to the 1960s. Its industrial deployment and rapid market diffusion occurred primarily in the 1970s and 1980s, closely linked to the energy crises and the tightening of requirements for building energy use [5]. In practice, low-E coatings enable substantially lower glazing thermal transmittance without an excessive increase in the number of panes. In parallel, selective coatings and solutions aimed at controlling solar gains advanced, reflecting the need for thermal comfort and the growing role of air conditioning in office buildings.

As energy requirements in construction became more stringent, the emphasis shifted from the window as a product to the entire window junction. This was the stage at which the window became an element of the building's energy strategy. Selection criteria extended beyond aesthetics and durability to include the balance between heat losses and gains. In this framing, the final in-service quality of a window depends not only on product parameters, but also on its interaction with the wall and the method of installation. Research in building physics indicates that the window's position relative to the insulation layer and the detailing

of the reveal materially affect linear thermal transmittance and local surface temperature reductions, thereby influencing comfort and long-term robustness [5–6]. Layered installation systems also became more widespread, in which airtightness is shaped by a set of layers with distinct functions. Consequently, the outcome becomes particularly sensitive to workmanship quality [22].

The history of window frames is essentially a history of compromise between load-bearing capacity, dimensional stability, durability, and insulation performance. For centuries, timber was the dominant material, offering favourable thermal conductivity and ease of machining, while requiring protection against moisture and UV exposure. With the development of steel and aluminium, slender, high-capacity constructions became feasible, enabling large glazed areas [23–24]. At the same time, the high thermal conductivity of metals exposed energetic limitations, which drove the adoption of thermal breaks and the development of multi-chamber and hybrid profiles.

The widespread adoption of unplasticised PVC in the second half of the twentieth century created a new class of systems based on extruded multi-chamber profiles, joined at corners by welding [3], [25]. Historically, this transition is significant because it shifted the basis of window quality from craftsmanship to a controlled industrial process. Profile design, material consistency, weld repeatability, and compatibility with hardware and seals became central determinants of performance. In subsequent decades, steel reinforcements were developed and have more recently been supplemented by composite solutions, alongside multi-seal configurations, in response to tightening requirements for airtightness and insulation. Timber–aluminium and PVC–aluminium systems can be interpreted as a further stage in this evolution. They sought to combine the thermal benefits of timber or PVC with improved exterior aesthetics and weathering resistance provided by aluminium cladding profiles [24]. These solutions illustrate a broader contemporary trend in which a single material is increasingly not selected in isolation. Instead, layered assemblies and joints are designed to allocate specific functions, such as load-bearing, insulation, and protection. A similar logic applies to façade systems, where the frame forms part of the envelope structure, and the sealing and water-drainage concept is critical for reliability [20].

The most recent history of window systems is closely associated with low-energy buildings and the ambition to further reduce window thermal transmittance while retaining core functional requirements. Two parallel trajectories are evident. The first concerns the refinement of established solutions, including improved spacer bars, more stable sealing systems, optimisation of profile geometry, and the reduction of linear thermal bridges [7]. The second trajectory develops high-performance technologies, such as vacuum glazing, ultra-low-conductivity fills, and multi-layer systems in which the transparent element comprises several interacting layers and combines thermal insulation with solar-gain control [26].

The concept of an active or adaptive window is also advancing, in which solar energy transmittance and light transmission are modulated over time. This includes both passive approaches, such as thermochromic materials, and active solutions, such as electrochromic systems, integrated with building automation [26]. In historical terms, this represents a substantive shift because the window is no longer treated as an element with fixed properties. Instead, it is increasingly regarded as a device with a controllable performance profile. In design practice, this necessitates revised approaches to reliability, maintenance, and the assessment of effectiveness.

Table 1 provides a concise overview of the evolution of window systems.

Table 1. Development of window systems [3–5], [7], [19], [23–28]

Historical period	Dominant solutions	Key driver of development	Implications of implementation
Up to the 18th century	Timber joinery, small glazed panes with muntins	Need for daylight and ventilation indoors; development of craftsmanship	Limited airtightness; high variability in quality
19th century	Box windows; gradual refinement of closing hardware	Industrialisation; urbanisation	Improved control of infiltration; greater repeatability
1st half of the 20th century	Larger glazed areas; steel and aluminium in architecture	Modernism	Greater diversity of sash functions and window configurations with increasing glazing share; increasing heat losses
2nd half of the 20th century	Widespread adoption of insulating glass units (IGUs) and solutions improving joint airtightness; PVC-U in architecture	Need for comfort; mass production	Parameterisation of airtightness; development of system junction details
21st century	Solutions reducing losses at the glass–frame interface and at the glazing-edge region: triple glazing, warm edge, smart windows	Energy requirements and comfort	Reduction of thermal bridges; integration with building automation

2.1.2. Overview of Window Systems

In civil engineering practice, a window system denotes not merely a product understood as a frame–sash–glazing set, but a family of structural and material solutions that enables the design of windows with defined thermal, acoustic, mechanical, and in-service performance across a wide spectrum of opening typologies, load cases, and environmental conditions. Contemporary reviews of window systems are typically organised by the dominant frame material, namely PVC-U, aluminium, timber, steel, façade systems, and hybrid configurations, because the frame material governs the prevailing load-transfer mechanisms, the nature of thermal bridging, the scope for sectional geometry, and the dominant durability-related risks. The literature emphasises that the ultimate energy and functional performance of a window arises from a coupled interplay between material properties, section geometry, joint quality, glazing selection, and the alignment of installation solutions with building-physics principles [8], [29–30].

PVC-U systems constitute one of the key families of window solutions in residential and public buildings, because they combine the manufacturability of the production route, notably the extrusion of profiles with complex geometry, with the relatively favourable thermal insulation of the base material. From a system perspective, a PVC-U profile should not be treated as a standalone component. It forms part of an assembly comprising the frame and

sash geometry, the glazing unit, seals, and the approach adopted for reinforcement and for fixing hardware. This component architecture simultaneously governs thermal performance, stiffness, in-service durability, and manufacturing repeatability, which is consistently emphasised in review studies on window design optimisation [8], [29].

At the core of the system is the multi-chamber profile, in which air cavities provide insulation and create functional zones, including rebates, seal grooves, and chambers for reinforcements and hardware. A decisive design aspect is the mechanism by which stiffness and load-bearing capacity are ensured. Traditionally, this has relied on steel reinforcements, although composite inserts are increasingly being adopted to reduce the proportion of steel within the profile cross-section [8], [29]. PVC-U profile solutions are developed as variants with rebate sealing (AD) and with a central gasket (MD), across different installation depths and glazing capacities. System-level analyses therefore specify reference conditions for thermal declarations, including calculation and test methods, because the outcome depends on the combined configuration of frame, glazing, and spacers [30]. In practice, comparability of PVC-U solutions requires clarification as to whether declared values relate to the profile, the complete window, or a defined configuration, for example a specific frame width, spacer type, and glazing unit. Reviews of methods for assessing the thermal transmittance of PVC windows underline that, even for the same profile family, calculated or measured results may vary materially with geometric details and methodological assumptions. Accordingly, comparisons require explicit and consistent reporting of the adopted premises [30].

From a quality perspective, the surface ageing of PVC profiles under UV exposure is relevant, particularly for dark colours, alongside the quality control of raw materials and protective layers. Studies on the chalking of PVC profiles indicate a pronounced influence of formulation choices, including surface-layer design and stabiliser packages [31]. In parallel, profile recycling strategies are being developed. Investigations of the mechanical properties of recycled material show that parameter stability requires stringent process control, and that property scatter may be material from the standpoint of system reliability [32]. From a manufacturing viewpoint, PVC profiles are characterised by corner welding and the consequent need to control joint quality, including material distribution within the core, residual stresses, and sensitivity to process parameters. Analyses of the load-bearing capacity of PVC profile corners indicate that the welding regime is critical for repeatability and reliability, particularly under variable production conditions [17].

System variants with reduced steel content, such as glass-fibre-reinforced composite inserts, are being advanced in response to energy-driven pressures and the trend towards larger glazed areas. Research on solutions that simultaneously improve thermal and mechanical performance suggests that achieving a stable outcome requires an integrated approach, encompassing material selection, geometry, joint reinforcement, and glazing configuration, together with verification under the reference conditions prescribed by the assessment methodology [11], [30]. The market development of PVC-U systems is typically pursued through system-supplier product platforms, within which thermal and mechanical performance is scaled through parameters including installation depth, sealing concept, permissible glazing thickness, and reinforcement type. For example, systems such as IDEAL 7000 [33], SOFTLINE 82 MD [34], and solutions incorporating composite reinforcements, such as ThermoFibra [35] and ARTEVO [36], are presented as responses to energy requirements and the trend towards larger glazed areas. Interpretation of declared values should, in each case, take account of the window configuration and the applied assessment methodology [30], [33–37].

Aluminium systems are particularly advantageous where high stiffness, slender sightlines, and compatibility with large glazed areas are prioritised. Unlike PVC-U or timber, aluminium enables very high load-bearing capacity with comparatively small cross-sections, which is especially relevant for large-format systems and for architectural requirements that impose minimal visible frame widths. At the same time, aluminium's high thermal conductivity makes the thermal break a constitutive feature of contemporary solutions. The literature highlights the critical role of thermal-break geometry and the separation strategy between the internal and external parts of the section in limiting the thermal bridge while retaining mechanical stability, which places thermal-break design at the interface of thermal and structural requirements [29], [38].

From an energy-assessment perspective, it is essential to model heat transfer through thermally broken sections with appropriate fidelity. Studies on the estimation of thermal transmittance for aluminium frames indicate that reliability depends on the consistent application of standardised methods and the accurate representation of the section geometry [38]. For comparative evaluations, it is important to distinguish between the quality of geometric representation and heterogeneous zones, methodological assumptions in the calculations, and the influence of glazing-seat and sealing details that can alter the effective heat-transfer path through the frame [38]. From a mechanical standpoint, the effect of the thermal break on sectional stiffness is also material. Experimental investigations of profiles with thermal breaks point to the need for cautious interpretation of data and targeted verification for large sashes [39]. In this sense, the thermal break is not solely a thermal feature, but a component that may modify the effective section properties, particularly under service and wind loading [39]. Recent work on thermally broken window configurations further indicates that improving thermal performance requires concurrent optimisation of both the frame and the glazing, and that the outcome reflects the overall configuration rather than any single element in isolation [40].

Timber systems are based on solid-wood or laminated timber sections, where raw-material selection and grain orientation materially influence dimensional stability and susceptibility to deformation under coupled moisture and temperature cycling. Compared with metallic systems, timber offers more favourable insulation performance, which supports the reduction of thermal bridging within the frame. However, material hygroscopicity means that durability and in-service parameters are strongly contingent on surface protection and on constructional details that limit wetting. Reviews addressing ageing resistance emphasise that durability is governed in particular by effective water shedding, the continuity and substrate compatibility of coating systems, and resistance to UV exposure and weathering actions [41].

In operational terms, timber systems should therefore be assessed not only through thermal metrics, but also through maintenance requirements, including inspections, coating refurbishment, and monitoring of joints and seals, because degradation of the protective layer can trigger accelerated ageing and geometric changes in the elements [41]. Accordingly, comparisons between timber systems and alternatives such as PVC-U and aluminium should explicitly differentiate assessment criteria, including insulation performance, durability and maintenance cycle, UV and water resistance, and long-term dimensional stability, because material trade-offs are effectively unavoidable in practice [8], [41]. A further variant comprises timber–aluminium systems, which transfer a substantial share of weather-resistance demands to an external aluminium cladding while retaining a timber core on the interior side. This hybrid architecture reduces the exposure of timber to atmospheric actions, while also

implying that in-service behaviour results from both material compromise and the quality of joint and sealing details. Consequently, system-level analyses should compare such solutions under consistent reference conditions and clearly specified configurations, analogously to the assessment of other frame systems [8].

Steel systems in façade engineering remain relevant where very slender, stiff profiles with high load-bearing capacity are required, particularly in refurbishment projects, buildings with elevated security demands, special-purpose solutions that require geometric stability and resistance to deformation, and architectural or artistic constructions (Fig. 2.2). At the same time, owing to the high thermal conductivity of steel, such profiles require the mitigation of thermal bridging through thermal breaks and insulating inserts. Analyses of metal-frame solutions indicate that improved thermal performance depends on both the separation strategy and the optimisation of the interface zones with the glazing unit and sealing system, because these regions concentrate heat losses and leakage risks [42]. In design practice, it is crucial to distinguish material-level assessment, where the benefits are high capacity and slenderness, from envelope-level assessment, where the governing factors are thermal balance and airtightness. In narrow sections, a substantial share of losses may be driven by linear thermal-bridge effects in the vicinity of the glass interface, spacer, and seals. Accordingly, the energy performance of steel profiles requires careful verification under the relevant assessment methodology and within a consistent whole-window configuration, rather than on the basis of the profile alone [8], [42].

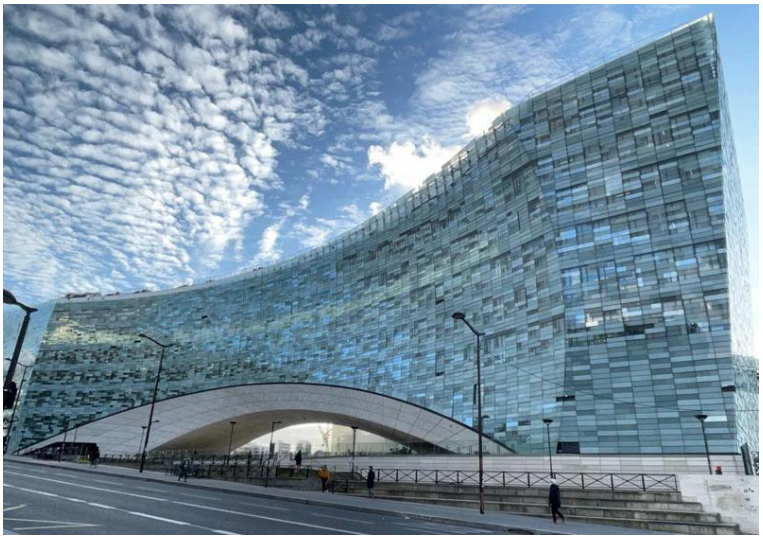

Fig. 2.2. Steel primary load-bearing structure (Paris, 13th arrondissement, France) [43]

Façade systems, including mullion-and-transom, unitised, and structural glazing solutions, integrate the transparent envelope into a larger load-bearing arrangement. They transfer wind actions and glass self-weight to the building structure (Fig. 2.3(a) and (b)). Unlike conventional façade windows, performance is governed by repeatable junctions and by the continuity of details at interfaces, including mullion–transom connections, anchorage zones, and glazing perimeters. This increases the relevance of linear thermal bridges within connection regions. The available literature indicates that a robust thermal assessment of curtain-wall façades requires a consistent computational approach aligned with the methodology prescribed for such envelopes, including ISO 12631, together with the analysis of characteristic details, because junctions and connections materially shape the thermal balance [44]. High-performance solutions increasingly adopt multi-layer arrangements in which the envelope combines insulation and solar-control functions. In these configurations,

the outcome is sensitive to workmanship quality and to the long-term retention of sealing performance [44]. In parallel, within the domain of intelligent window and façade solutions, the literature reports growing emphasis on active and energy-related functions, including the integration of energy-generating concepts and advanced optical functionalities. This extends assessment criteria beyond thermal transmittance alone and shifts the analysis towards the trade-off between thermal, optical, and functional performance [45].

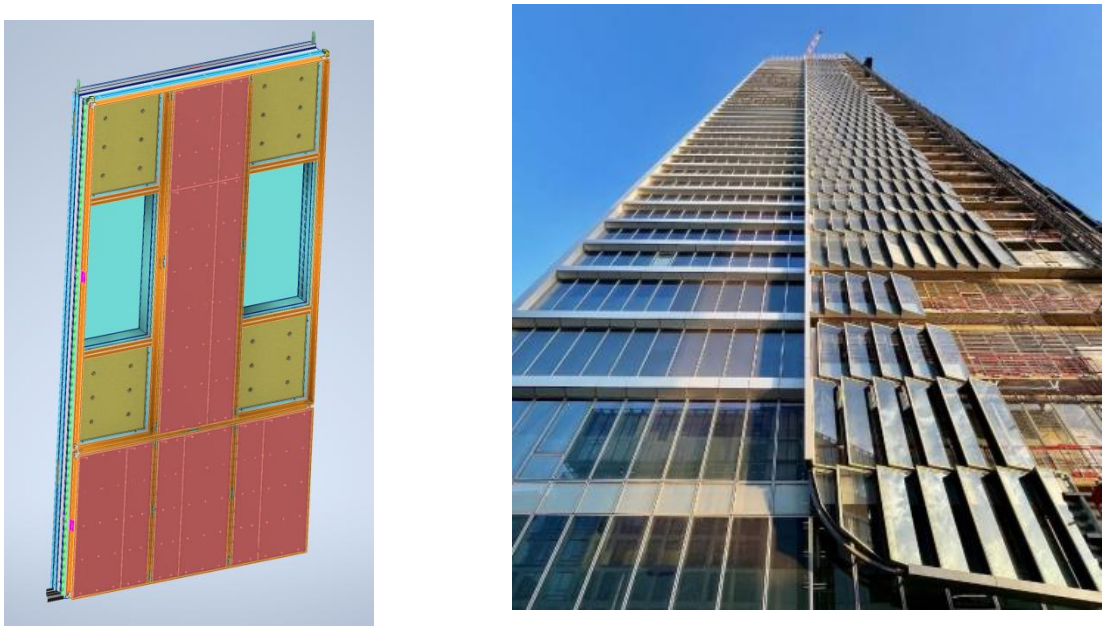

(a) (b)

Fig. 2.3. Segmented aluminium unitized façade system: (a) virtual model, (b) photovoltaic (PV)-integrated double-skin façade (Puteaux, Île-de-France, France). Source: Author's own work

Table 2 synthesises the advantages and limitations of five families of window systems from a qualitative perspective, highlighting two principal domains. The first is the thermal balance, which is governed by material conductivity, section geometry, and the design of thermal breaks and reinforcements. The second is reliability and durability, which depend on joints, sealing systems, and surface resistance. In line with experimental findings and conclusions from the reviewed literature, system comparisons should be anchored in a defined configuration and a clearly stated assessment methodology, because outcomes depend on the combined frame–sash–glazing arrangement and on sectional detailing [8], [29–30]. For PVC-U, insulation performance is supported by multi-chamber geometry, whereas durability and in-service quality depend, inter alia, on UV resistance and the repeatability of corner welding. Where recyclate is used, process control becomes an additional determinant [17], [31–32]. Metal systems compensate for unfavourable thermal conductivity through thermal breaks and insulating inserts. The credibility of thermal assessment is particularly sensitive to faithful representation of sections and junctions [38–39], [42], [44]. Timber systems, in turn, offer a favourable thermal balance, yet their durability is strongly contingent on coating systems and on water-shedding detailing [41].

Table 2. Comparison of selected building envelope system families [8], [17], [29], [31–32], [38–42], [44]

System family	Benefits	Limitations and risks	Applications
PVC-U systems	Good insulation due to multi-chamber profile geometry; flexible cross-section design; possibility of using recycled feedstock under controlled quality	Surface ageing and UV-induced chalking (especially in dark colours); corner quality and load capacity depend on welding parameters; when recyclate is used, strict control of the process and properties is required	Residential and public buildings; energy retrofits
Aluminium alloys systems	High stiffness and slenderness; favourable for large glazed areas; broad scope for designing profiles with thermal breaks	Aluminium's high thermal conductivity necessitates thermal breaks; thermal performance assessment is sensitive to cross-section geometry and detailing; the spacer may affect the effective stiffness of the cross-section	High-glazing buildings; commercial buildings; sliding systems
Timber systems	Favourable thermal performance compared with metals; architectural value; renewability through refurbishment of protective coatings	Hygroscopicity; durability depends on the coating system and water-drainage detailing; maintenance requirements	Buildings with elevated architectural requirements; premium buildings
Steel systems	High load capacity and stiffness; possibility of slender frames in curtain wall systems; evolving strategies to improve the thermal performance of steel profiles	Thermal bridges in metal sections; need for thermal breaks and insulating inserts, as well as refined glazing and sealing detailing	Renovations; special-purpose buildings; façade elements and curtain walls
Façade systems	Integration of the transparent enclosure with the load-bearing system; mullion-and-transom and unitised solutions; ability to design details at façade	Linear thermal bridges at junctions and connections, high sensitivity to workmanship quality and airtightness; thermal assessment requires a consistent methodology and	Mullion-and-transom, unitised and structural façades; commercial buildings

scale	analysis of characteristic details

PVC-U solutions with composite reinforcement warrant particular attention. In comparative studies, a PVC-U system with composite reinforcement was reported to exhibit improved thermal performance relative to a steel-reinforced variant. The sash thermal transmittance was lower by 12%, and the frame by 13% [11]. In the same tests, the load-bearing capacity of corner joints for the composite variant, welded integrally with the profile, was approximately twice that of the steel-reinforced solution [11]. These findings support development pathways that reduce steel content and thermal bridging while preserving the required structural stability. This direction is also reflected in system solutions described by manufacturers, for example glass-fibre technologies positioned as substitutes for conventional reinforcement strategies [35].

2.1.3. General Characteristics of System Families

A window is a multi-component construction product in which structural, hygrothermal, acoustic, safety, and operational functions are delivered by a set of mutually coupled components. Regardless of the system family, including polymer-based, timber, aluminium alloys, steel, or façade configurations, a recurring division can be identified between the load-bearing element, such as a frame and sash or mullions and transoms, the transparent infill, namely monolithic glass or an insulated glazing unit, and the functional connection layer comprising seals, connectors, and fittings (Fig. 2.4). This configuration determines an extensive bill of materials, while individual elements operate under distinct service conditions. Some components transfer loads and stabilise geometry, others mitigate heat losses, and others must maintain airtightness despite ageing, ultraviolet exposure, and cyclic wetting. Consequently, material design for window systems is, in practice, the management of trade-offs between insulation performance, load-bearing capacity, durability, and the feasibility of industrial manufacture for both profiles and joints [9].

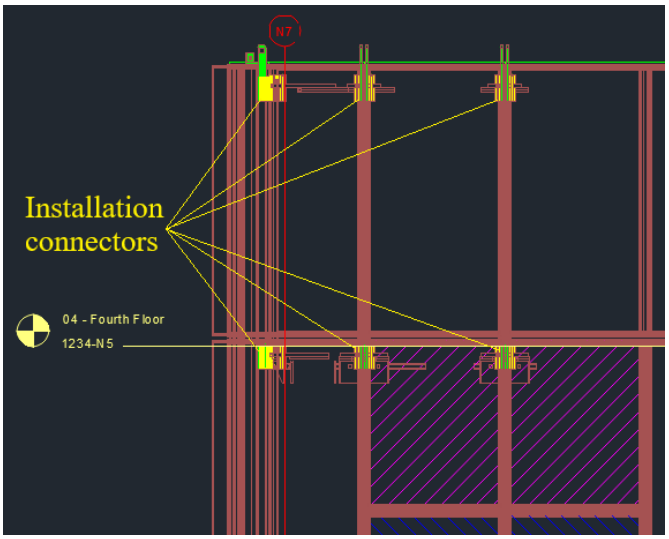

Fig. 2.4. Representative schematic of connectors installation for a modular block assembly. Source: Author's own work

A typical window incorporates, inter alia:

- frame and sash profiles, or façade profiles, often incorporating thermal breaks and reinforcements,

- glazing and the edge-seal concept of the insulated glazing unit, including the spacer bar, sealing system, and cavity gas (Fig. 2.5),
- gaskets and compression elements that govern airtightness and watertightness,
- hardware, connectors, installation components, and ancillary materials, such as adhesives, sealants, setting blocks, and protective coatings.

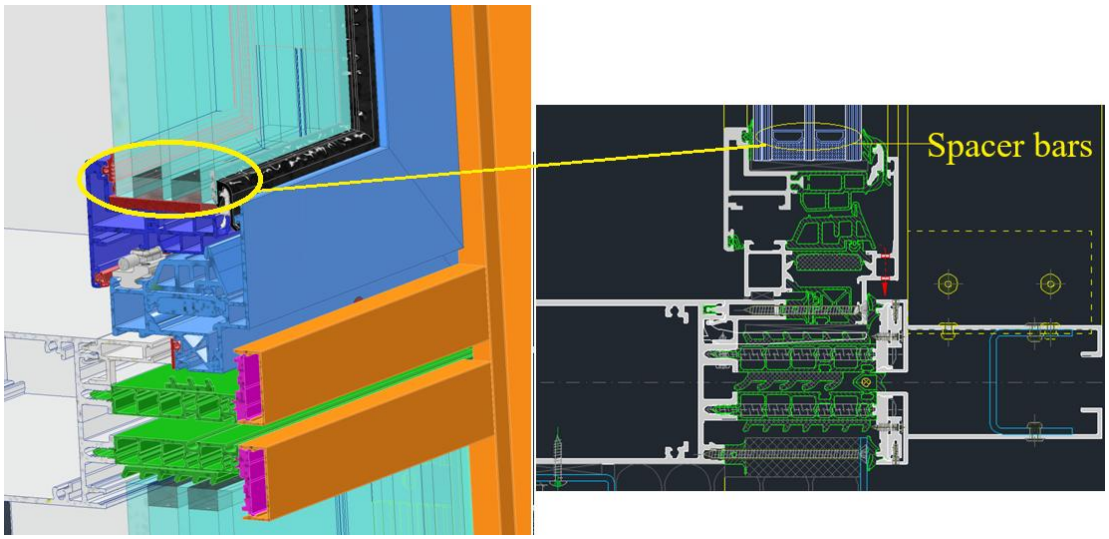

Fig. 2.5. Virtual model of spacer-bar positioning in the insulating glass unit. Source: Author's own work

For material analysis, it is often more informative to group materials by their function within the window than by system family. From a chronological perspective, structural profile materials should be considered first, followed by materials that limit heat conduction and provide tightness, and finally by auxiliary materials that enhance durability and aesthetics. This logic clarifies why windows with enhanced insulation performance are increasingly hybrid in character. They combine several materials to satisfy thermal and mechanical requirements simultaneously [9].

In practice, the following set of material groups predominates:

- profile materials: PVC-U, aluminium, timber, including laminated timber, and steel;
- thermal-break and insert materials used to mitigate thermal bridging: glass-fibre-reinforced polyamides, foams, and insulating inserts;
- sealing materials: elastomers, including ethylene propylene diene monomer (EPDM) rubber, thermoplastic elastomers, and sealants;
- specialised materials: glass-fibre-reinforced polymer composites, used as profiles or reinforcements in energy-efficient windows.

A primary criterion for selecting profile materials is the relationship between thermal conductivity and stiffness. High-conductivity materials, such as metals, enable slender sections and high load-bearing capacity, yet increase the risk of thermal bridging. Lower-conductivity materials, such as PVC-U, timber, and composites, support insulation performance, but often require reinforcement or larger sections to limit deflections. Consequently, improved thermal performance is achieved principally either by separating temperature zones using a thermal break, or by adopting low-conductivity materials while maintaining the required stiffness through reinforcement or composite architectures [9].

In PVC-U profiles, multi-chamber geometry combined with the polymer's low conductivity limits heat flow, although the elastic modulus of PVC-U is relatively low. Therefore, particularly for larger sashes and long spans, steel reinforcements are used to stabilise geometry under mechanical loading and thermal actions. Analyses of deformation in PVC profiles with a steel core indicate that such reinforcement materially alters structural response under temperature differentials and solar radiation, while also revealing the thermal and mechanical heterogeneity of the PVC–steel system [10]. This heterogeneity, in turn, motivates the adoption of reinforcements with lower conductivity, including composite reinforcements, in energy-efficient windows.

Aluminium profiles provide high strength and dimensional stability, which facilitates the design of slender sections, large sashes, and façade systems. However, aluminium's high conductivity means that, without additional measures, the profile would act as a dominant thermal bridge. The established solution is the use of thermal breaks that separate the exterior and interior parts of the profile. In practice, glass-fibre-reinforced polyamide sections are employed, enabling load transfer across the joint while substantially reducing thermal conductivity within the bridge region [46]. Environmental performance is increasingly reported through Environmental Product Declarations, which are used in life-cycle assessment studies [47].

For timber systems, material selection is largely determined by a favourable stiffness-to-weight ratio and low thermal conductivity, which supports meeting energy requirements without extensive thermal-break complexity. Timber is, however, hygroscopic. Accordingly, frame performance depends strongly on dimensional stability under variable moisture conditions and on the quality of surface protection that limits degradation under UV exposure and rainwater [47].

Alongside established materials, new hybrid solutions are gaining prominence, in which components with markedly different properties are combined within a single profile geometry. This is particularly relevant for energy-efficient windows, where reducing thermal bridging must be achieved without sacrificing load-bearing capacity and dimensional stability. For this reason, glass-fibre-reinforced polymer (GFRP) composites are increasingly introduced in framed and mullion-and-transom constructions, where they are viewed as enabling reduced heat conduction through the frame section while retaining the required stiffness [9]. In multi-material solutions, adhesion, chemical compatibility, and mismatches in thermal expansion at material interfaces become critical, because they directly govern the durability of connecting junctions and the stability of in-service performance [48].

Window performance is also strongly influenced by glazing and glass products. The baseline is float glass, whereas applications requiring safety and enhanced mechanical resistance commonly employ tempered and laminated glass. The glass type is selected in accordance with the anticipated action scenarios and relevant standard requirements [49–50]. In insulated glazing units, the edge seal is decisive, comprising the spacer system and the sealing arrangement. The quality of these elements determines the retention of airtightness and the long-term stability of thermal performance during service [48].

Perimeter sealing is provided primarily by elastomeric gaskets, whose function is to accommodate installation tolerances and service-induced deformations while maintaining the required air and water tightness. In practice, EPDM is frequently selected as the base material because of its resistance to ageing and weathering, as well as the stability of its properties over the typical operating temperature range of windows [48], [51]. Alternatives include TPEs

and silicone elastomers, which can simplify processing and integration with the profile, but require careful selection with respect to compressive creep under sustained sealing pressure.

High-insulation solutions also employ very low-thermal-conductivity materials in zones that, in conventional profiles, act as pathways for intense heat flow. This concerns, inter alia, thermal breaks and insulating infills, such as PUR elements placed within profile chambers, to reduce frame thermal transmittance and to limit linear losses in the region where the frame meets the insulated glazing unit [48]. Such measures are particularly relevant for windows with a high frame-to-area ratio, where section-level improvements translate directly into the thermal transmittance of the whole window.

Material selection in window systems is therefore not a single-point decision. It reflects the need to balance thermal, mechanical, durability-related, manufacturing, and environmental requirements. As expectations for energy efficiency increase, the role of multi-material solutions and insulating materials within the frame section grows, alongside the deliberate selection of joints and sealing strategies that govern the stability of performance across the product life cycle [9], [48].

2.2. Poly(vinyl chloride) as a Structural Material

2.2.1. General Remarks on Poly(vinyl chloride)

The term polimer entered scientific usage around 1832, when Jöns Jacob Berzelius classified polymers among compounds of higher molar mass. A further milestone followed in 1839 with the first isolation of styrene. In 1868, Alfred Nobel synthesised nitrocellulose [52–54]. The industrial-scale development of polymeric materials began to accelerate around 1909, when Leo Hendrik Baekeland obtained phenol–formaldehyde resins. Subsequent research enabled the creation and implementation of new polymer families that were adopted widely. In the 1920s and 1930s, the German chemist Hermann Staudinger refined the polymer concept by framing polymers as large macromolecules. During this period, in 1933, Imperial Chemical Industries pioneered industrial polyethylene production using a high-pressure route [55–58]. Another landmark was the synthesis of nylon by the American chemist Wallace Hume Carothers, who also introduced terminology associated with condensation reactions. The Second World War period was marked by intensified research activity and rapid technological progress. In the 1950s, mass production of expanded polystyrene was initiated, among others, by Badische Anilin- & Soda-Fabrik (BASF) [59–62]. From the 1970s onwards, research expanded at a particularly fast pace, encompassing new polymer classes, including semiconducting polymers, nanostructured polymers, and self-healing polymer systems.

A polymer is a macromolecular compound. It is formed by organic, and in some cases inorganic, macromolecules and can be represented as a chain of repeating structural units. These basic units are termed mers, and their number typically ranges from 10,000 to 1,000,000 or more [63]. Macromolecules are associated through bonding interactions mainly covalent and Van der Waals [64]. Polymer properties depend, inter alia, on the nature of these interactions and include physicochemical, mechanical, processing, and in-service characteristics.

The degree of polymerisation, also denoted DP (Degree of Polymerisation), indicates how many mers constitute a macromolecule. This descriptor is important because polymers typically comprise macromolecules with a non-uniform degree of polymerisation. Moreover,

the chain ends differ structurally from the repeat units in the interior of the chain [65]. Macromolecular mass can be expressed either as atomic mass, commonly reported in atomic mass units (u), or as molar mass, expressed in g/mol. Owing to molar-mass non-uniformity, macromolecules are described using average molar masses. These may be characterised using number-based and mass-based contributions of macromolecules, while the breadth of the molar-mass distribution is captured by the degree of polydispersity.

Polymers may occur as synthetic polymers, biopolymers, or modified variants [66–68]. An additional important class comprises copolymers, understood as a set of macromolecules formed from two or more different mer types. During polymerisation, the sequence of mers may adopt distinct arrangements, which leads to differences in the configurational organisation of macromolecules. Three basic sequence orderings can be distinguished: head-to-tail, head-to-head, and tail-to-tail [69–73].

To classify polymers, three primary criteria are commonly distinguished, namely chemical structure, physical structure, and rheological behaviour [65], [75]. The first criterion, chemical structure, may be discussed in terms of the main chain and the side groups. With respect to the main chain, polymers are often described as having either homogeneous or heterogeneous chains. With respect to side groups, a distinction is made between polymers whose repeat units comprise only carbon atoms and polymers incorporating heteroatoms, such as PVC. The second criterion, physical structure, differentiates thermoplastic, thermosetting, and chemically cured polymers. Thermoplastics share characteristic features, including linear or branched structure that may form amorphous or crystalline arrangements. They soften and flow upon heating and are readily processable. When subjected to repeated heating and cooling below the degradation threshold, they do not undergo degradation. By contrast, thermosetting and chemically cured polymers share a high degree of crosslinking. They neither melt nor flow, are not readily processable, and, when heated beyond the curing regime, they tend to degrade. The third criterion, rheological behaviour, divides polymers into elastomers and plastomers, with plastomers further subdivided into thermoplastics and duroplastics. Elastomers exhibit high deformability, with rubber representing a typical example. By contrast, plastomers show comparatively low deformability [65], [75]. The classification of selected polymers according to rheological behaviour is presented in Table 3.

Table 3. Classification of selected polymers by rheological behaviour [65], [75]

Thermoplastics		Thermosets	
Amorphous	Crystalline	Chemically curing	Thermally curing
Poly(vinyl chloride)	Polyethylene	Epoxy resins	Phenol-formaldehyde resins
Polystyrene	Poly(tetrafluoro-ethylene)	Unsaturated polyesters	Urea resins
Poly(methyl methacrylate)	Polypropylene	Silicones	
Polycarbonates	Poly(methylene oxide)	Polyurethanes	
Polysulfones	Poly(ethylene oxide)		
Poly(phenylene oxide)	Polyamides		
	Poly(ethylene terephthalate)		
	Poly(butylene terephthalate)		

Polyoxymethylene
Polyetherketones

Monosubstituted polyolefins and vinyl polymers can form three configurational arrangements, namely atactic, isotactic, and syndiotactic. Considering physical structure and its relationship to properties, polymers can be divided into three categories [65–68], [75]. The first is the amorphous, or non-crystalline, structure, characterised by the lack of long-range ordering in macromolecular arrangement. The second is the crystalline structure, in which ordering is present to a greater or lesser extent. The third is the semicrystalline structure, which represents an intermediate case in which macromolecules are partly arranged as in an amorphous phase and partly as in a crystalline phase [77–78].

It should be noted that amorphous polymers may occur in several physical states, including glassy, elastic, and plastic states. Figure 2.6 illustrates the evolution of physical states during polymer heating. Crystalline polymers, in turn, are typically considered to exist in two physical states, namely crystalline and liquid. Thermosetting and chemically cured polymers are associated with a single physical state, the glassy state. Crosslinked elastomers exhibit a slightly broader range, commonly described as glassy or elastic. Polymer transitions are governed by specific characteristic temperatures. The brittleness temperature denotes the onset of brittle behaviour and the transition towards a state of forced elasticity within the glassy regime. The flow temperature denotes the transition between the elastic and plastic states, depending on the heating or cooling path. The glass transition temperature denotes the transition between the glassy and elastic states, again depending on the thermal path. The melting temperature denotes the transition to the molten state in crystalline or semicrystalline systems [65–68], [76].

Polymeric materials, also referred to as plastics, comprise a broad category because, in addition to the base polymer component that forms the core, they contain numerous auxiliary constituents. These include fillers, carriers, and stabilisers, as well as softeners, namely plasticisers. Additional additives may include curing agents, foaming agents, dyes and pigments, antistatic agents, flame retardants, and many others. Current global production of polymers and polymeric materials exceeds 360 million tonnes per year, while the production of coatings and adhesives is approximately 50 million tonnes per year [65–68], [76]. Among the several thousand grades available, vinyl polymers, including poly(vinyl chloride) and polystyrene, account for a dominant share, estimated at around 70–80%.

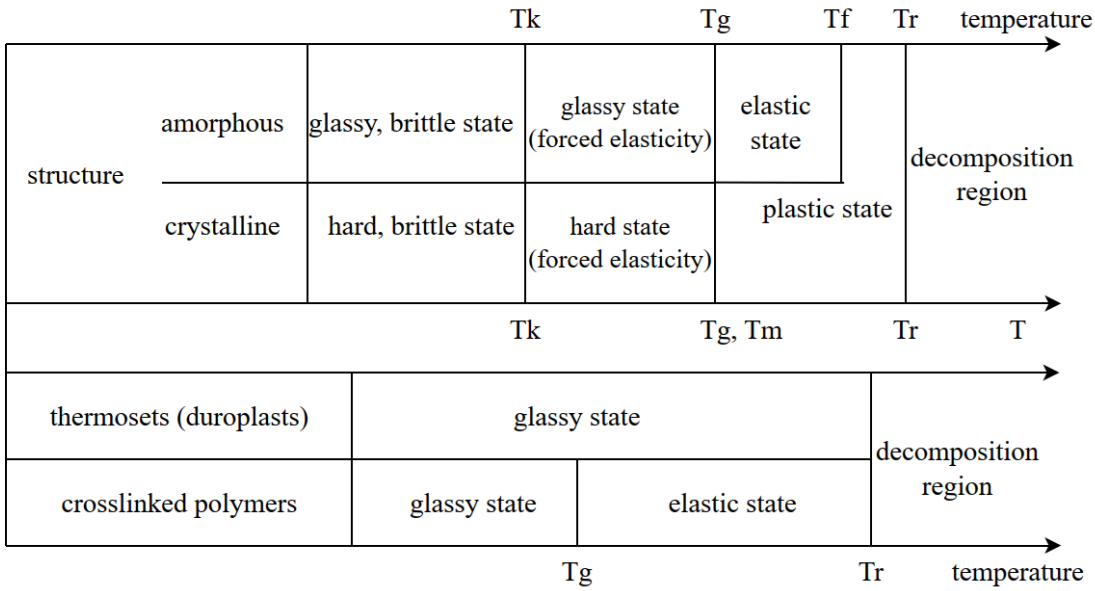

Fig. 2.6. Changes in physical states during polymer heating [65]

One of the earliest synthetically produced polymers manufactured on a broader industrial scale was poly(vinyl chloride) [52], [54], [79]. It is a thermoplastic material that occurs in both pigmented and unpigmented forms. It is also non-flammable and resistant to inorganic chemicals. It is used across many areas of everyday and industrial practice, including structural applications, household goods, and flooring products [80]. In Polish usage, the abbreviation PCW is also used in place of the full name poli(chlorek winylu). This abbreviation is employed in the context of vinyl chloride polymerisation products obtained in emulsion, suspension, bulk, or solution routes, using peroxides, azo compounds, or redox systems as initiators [81–82]. In most international contexts, however, the acronym PVC, derived from “poly(vinyl chloride)”, is used more frequently [82–83].

The first recorded discovery of the vinyl chloride monomer, VC (vinyl chloride), dates to the nineteenth century, when Henri Victor Regnault reported it in 1835 in France. A subsequent milestone was the polymerisation of vinyl chloride by the German chemist Eugen Baumann in 1872, achieved by exposing tubes containing vinyl chloride to sunlight. The first documented routes for producing poly(vinyl chloride) are reflected in patents filed in the United States in the early twentieth century. The development of core apparatus and pilot installations for PVC manufacture is commonly associated with the 1930s [52], [54–55], [57], [59-62], [79]. PVC production expanded markedly during the Second World War period. Since then, PVC has remained among the most widely used synthetic materials across multiple industrial sectors.

Industrial polymers are produced predominantly via radical, ionic, coordination, or addition polymerisation routes [84], [75]. The homopolymer of poly(vinyl chloride), defined as a chain comprising only one mer type, contains 56.7% chlorine [79]. This high chlorine content is directly associated with the comparatively low cost of this thermoplastic. In practice, poly(vinyl chloride) is most often compounded with additives, including stabilisers, plasticisers, fillers, and other modifiers [81]. Only after compounding does PVC attain its full in-service property profile.

On the basis of formulation and resulting behaviour, two principal variants of poly(vinyl chloride) are distinguished. The first is rigid PVC, also referred to as PVC-U (unplasticised

PVC) [85]. The second is flexible PVC, also referred to as PVC-P (plasticised PVC) [86]. Rigid products contain only small amounts of plasticiser and are characterised by resistance to corrosion, oils, chemicals, and weathering. They are readily processed, joined, coloured, and printed. Products made of PVC are also relatively light, the density of PVC is approximately 20% of iron and 10% of lead by mass [79]. Additional features include flame resistance and self-extinguishing behaviour, alongside insulating properties [87–90]. PVC-U products can be manufactured in transparent, semi-transparent, and opaque variants. Representative applications include cold-water piping, window profiles, containers, sheets, and bottles. Flexible products, by contrast, are characterised by good transparency, flexibility, and tear resistance [91–93]. PVC-P is also pliable and weather-resistant. It further exhibits low permeability to oxygen and odours. Typical applications include cable insulation, footwear soles, floor coverings, and horticultural films [79], [81], [94]. PVC-based windows, doors, and flooring are now widely embedded in the built environment, as are pipelines and electrical cabling. Taken together, these applications indicate that PVC remains a structurally important material in everyday use.

The technological processing of polymers is governed by multiple factors, including monomer type and composition, step-growth or chain-growth polymerisation, the polymerisation environment, initiator type, the monomer phase state during polymer formation, and core process parameters. Additional determinants include the reaction medium, coagulation or precipitation method, and the type of apparatus and equipment employed [95–99]. In contrast to many other thermoplastics, poly(vinyl chloride) is processed not only as a powder obtained directly from polymerisation. Instead, it is commonly converted into compounds and granulates through the incorporation of stabilisers, plasticisers, lubricants, and other auxiliaries [79], [81]. The purpose of these additives is to produce a formulation suitable for processing by, inter alia, improving flow behaviour, providing protection against thermal decomposition under processing conditions, and tailoring the properties of the final product.

Vinyl chloride (1-chloroethylene), with the molecular formula CH_2=CHCl, exhibits the properties summarised in Table 4.

Table 4. Properties of vinyl chloride [79], [81], [100]

Property	Value and unit
Colour	Colourless
Odour	Pleasant, sweetish
Molecular weight	62.50
Physical state (at 20.0 °C)	Gas
Gas density (-13.9 °C, 1013 hPa)	3.01 g/dm^3
Liquid density (-20.0 °C)	0.9834 g/cm^3
Relative gas density to air (15.0 °C, 1013 hPa)	2.15
Melting point (1013 hPa)	113.45K (-159.70 °C)
Boiling point (1013 hPa)	259.25K (-13.90 °C)
Flash point	Not applicable
Autoignition temperature	472.0 °C
Lower explosion limit (mixture with air)	3.60% vol.
Upper explosion limit (mixture with air)	33.00% vol.
Lower explosion limit (mixture with oxygen)	4.00% vol.
Upper explosion limit (mixture with oxygen)	70.00% vol.

Stoichiometric concentration	7.75% vol.
Vapour pressure (at a temperature of 20.0 °C)	0.34 MPa
Vapour pressure (at a temperature of 30.0 °C)	0.46 MPa
Saturated vapour concentration	Not applicable
Solubility in water (20.0 °C, 1013 hPa)	0.10% wt.
Solubility in other solvents	Soluble in most organic solvents
Critical temperature	156.5 °C
Critical pressure	5.59 MPa
Viscosity (15.0 °C, 1013 hPa)	0.0105 mPa·s
Specific heat capacity (25.0 °C, 1013 hPa)	0.858 J/(g·K)
Heat of vaporisation at the boiling point	334.3 J/g
Heat of polymerisation	1138.8 J/g

Poly(vinyl chloride) depending on the polymerisation method and catalyst type, may adopt stereoregular forms, commonly described as syndiotactic, which are associated with head-to-tail sequencing. It may also occur in non-stereoregular, atactic forms, which are associated with head-to-head or tail-to-tail sequencing [74].

Poly(vinyl chloride) is obtained via free-radical polymerisation of vinyl chloride, initiated by peroxides, using bulk, solution, or emulsion processes. The characteristics of poly(vinyl chloride), including its molar mass, are governed by the initiator type, the selected route, and the polymerisation temperature. PVC is a thermoplastic polymer typically produced as a white powder. A characteristic feature is its low crystallinity, of the order of 10%. Its glass transition temperature is close to 80 °C, while the softening temperature is commonly reported in the range 145–170 °C. Exposure to temperatures above 130 °C entails a risk of thermal decomposition accompanied by HCl evolution and progressive discoloration from pale yellow through red and brown to black [94], [101]. This behaviour is associated with the formation of conjugated unsaturated sequences.

PVC is most readily dissolved in cyclohexane, whereas esters, ketones, and chlorinated solvents are less favourable media. It is also resistant to water, acids, and alkalis, both dilute and concentrated. Resistance extends to ozone and oxygen, as well as to petrol, mineral oils, and crude oil derivatives. At room temperature, PVC is relatively stiff, while at low temperatures it becomes brittle. This is commonly attributed to the presence of polar C–Cl bonds and restricted macromolecular mobility.

To attain practical property profiles, PVC is modified either through external plasticisation, achieved physically by incorporating softeners and blending with other polymers, such as impact modifiers, or by chemical modification, including copolymerisation with comonomers such as olefins or vinyl acetate. Hot compounding is typically conducted in two configurations. The first yields rigid PVC by mixing with stabilisers, pigments, and fillers. The second yields flexible PVC by incorporating plasticisers. Under suitable processing and conditioning, the content of residual volatile species can be reduced markedly, with reported levels below 1 ppm [91–92]. Removal of residual vinyl chloride monomer is generally more effective from powdered PVC, which has a high specific surface area, and from plasticised formulations than from certain discrete compositions.

Chemical modification of poly(vinyl chloride) can, in principle, increase formulation homogeneity, improve compatibility with auxiliary agents, reduce the glass transition

temperature, enhance low-temperature impact performance, and alter the kinetics of energy absorption. Poly(vinyl chloride) is processed in two principal forms. The first is rigid PVC, colloquially referred to as “winidur”, commonly manufactured by extrusion, injection moulding, or sintering. The second is the softened, plasticised form, colloquially termed “winiplast”, processed by calendering, extrusion blow moulding, casting or dipping, and gelation in moulds. To mitigate thermal degradation during processing, thermal stabilisers are incorporated, including organotin compounds, esters of dicarboxylic and sulphur-containing acids, and barium, calcium, or zinc stearates [93], [102].

Chlorinated poly(vinyl chloride), with a chlorine content in the range 60–68%, is produced by chlorinating PVC at 80–120 °C in solvents such as dichloroethane, chlorobenzene, or tetrachloroethane, typically in the presence of free-radical initiators [94], [101]. Chlorinated PVC also has a broad application base, including use in the production of varnishes, coatings, fabrics, and electrical insulation materials.

Plasticisers, also referred to as softeners, are organic liquids with relatively high boiling points. They may also comprise organic compounds with low melting temperatures. A key distinction between such liquids and other low-molecular species in polymer matrices concerns volatility, often discussed in terms of vapour pressure. Liquid plasticisers incorporated into a polymer matrix form plastisols, also described as organosols and organogels [91], [93].

2.2.2. Processing Methods

One of the oldest approaches to vinyl chloride polymerisation is emulsion polymerisation. This route can be operated either continuously or in batch mode, including configurations employing a seed latex. The continuous variant is typically implemented in vertical reactors with volumes of 12–20 m^3. The batch variant is used in larger vessels, commonly 60–200 m^3. In practice, however, many installations favour a greater number of smaller reactors, with capacities of 6–12 m^3, and medium-size units in the range 16–40 m^3 [108]. The described emulsion polymerisation is carried out using water-soluble initiators, typically inorganic peroxides, at levels of 0.02–0.2 wt% relative to VC. Emulsifiers are essential and are most often anionic. Latex properties depend strongly on emulsifier selection, including particle size, particle-size distribution, and mechanical stability.

Process control requires avoiding extremes. Insufficient emulsifier may lead to latex coagulation, whereas an excessive emulsifier dose can impair latex characteristics. This may cause technical difficulties during drying and transport of PVC due to powder caking and agglomeration. Latex formation is governed by key emulsifier attributes, including the critical micelle concentration and the aggregation number. In continuous emulsion polymerisation, the monomer, an aqueous emulsifier solution, initiators, and pH buffers are introduced at the top of the vessel, while latex is withdrawn from the bottom. A recognised drawback of continuous operation is reactor fouling by polymer deposition, which, inter alia, degrades heat transfer. In batch emulsion polymerisation, the polymerisation mixture is charged into the reactor before the reaction is initiated. A critical objective is to obtain PVC latex with suitable paste-forming properties, which is achieved by adding a seed latex. At the end of polymerisation, the latex is transferred to an equalisation tank, and latex isolation proceeds analogously to the continuous route [109].

A second polymerisation route for vinyl chloride is suspension polymerisation. Unlike emulsion polymerisation, it is operated in batch mode only. It is carried out in vertical reactors with capacities of 10–200 m^3. A further distinction is that suspension polymerisation uses initiators soluble in the monomer phase, whereas emulsion polymerisation employs initiators soluble in water. Suspension polymerisation is typically conducted at 40–70 °C in the presence of protective colloids, also termed suspension stabilisers. Emulsifiers are used only very rarely and may be applied to increase plasticiser uptake by PVC. Free-radical initiators used in suspension polymerisation include dialkyl and diacyl peroxides, ketone peroxides, and related species. The polymerisation temperature is a key parameter because it is linked to PVC molecular weight. As the temperature increases, the molecular weight of the polymer decreases.

Other polymer properties depend primarily on interfacial tension at the water–monomer interface. This is influenced by reactor hydrodynamics, the aqueous-to-organic phase ratio, and the suspension stabilisers. The polymerisation sequence begins with charging the aqueous phase, comprising demineralised water, solutions of suspension stabilisers, and other water-soluble additives. The reactor is then evacuated, purged with nitrogen, and evacuated again under vacuum to remove oxygen. This is essential because oxygen inhibits vinyl chloride polymerisation. An unfavourable feature from the standpoint of process integrity is HCl evolution, which can promote equipment corrosion and the formation of PVC chains containing labile groups that are more susceptible to degradation. Both effects are associated with the decomposition of vinyl chloride polyperoxides formed in the presence of oxygen, which break down under polymerisation conditions and release these species. The prepared reactor is subsequently charged with VC and heated, via the jacket, using water or steam to the set polymerisation temperature. Once the setpoint is reached, initiators are added and the pressure drop is monitored as an indicator of achieving the desired monomer conversion. Reaching the target pressure drop marks the transition to degassing of unreacted monomer, which is transferred to rectification equipment. After cooling, the suspension is routed to filtration and product-drying units. The final stage comprises cleaning the reactor with high-pressure water and treating the vessel walls and agitator to mitigate polymer build-up [79].

A further route for vinyl chloride polymerisation is bulk polymerisation. Unlike suspension and emulsion polymerisation, it contains neither an aqueous phase nor emulsifiers or suspension stabilisers. Consequently, it should yield polymer grains with the highest attainable purity. Early bulk polymerisation was performed in vertical reactors. However, these did not deliver polymer quality at the required level. This motivated the introduction of a two-stage cycle, which was subsequently refined repeatedly.

In the first stage, vinyl chloride is polymerised in a vertical vessel, also referred to as a prepolymeriser. The polymerisation mixture is then transferred gravitationally to a horizontally arranged polymeriser, where conversion is increased. A further step in improving bulk polymerisation involved a return to vertical vessels. This became feasible through progressive redesign of the mixing concept until the desired outcomes were achieved. The initiators used in bulk polymerisation are analogous to those employed in suspension polymerisation, which is advantageous because they are soluble in the monomer phase. Grain size and grain morphology depend on mixing conditions in the prepolymeriser. Heat exchange occurs through monomer evaporation and subsequent condensation on the reactor walls and in the reflux condenser. Effective removal of the reaction heat is therefore critical. Favourable conditions include a sufficiently large cooling surface to condense the evaporated monomer and an adequate monomer inventory to dissipate excess heat via evaporation [79].

Processing, also referred to as polymer conversion, denotes the set of operations by which polymers are transformed into final products with precisely defined geometry and mechanical performance. It is an advanced process in which the material undergoes diverse physicochemical phenomena alongside substantial geometric reshaping. These effects arise from the combined input of thermal and mechanical energy, the action of forces and stresses, and the occurrence of thermally driven reactions, including polymerisation, crosslinking, oxidation, and degradation, also described as depolymerisation. Additional contributions stem from interfacial and contact phenomena, including adsorption, adhesion, and tribomechanical friction [110–113]. The principal routes of polymer processing are illustrated in Fig. 2.7.

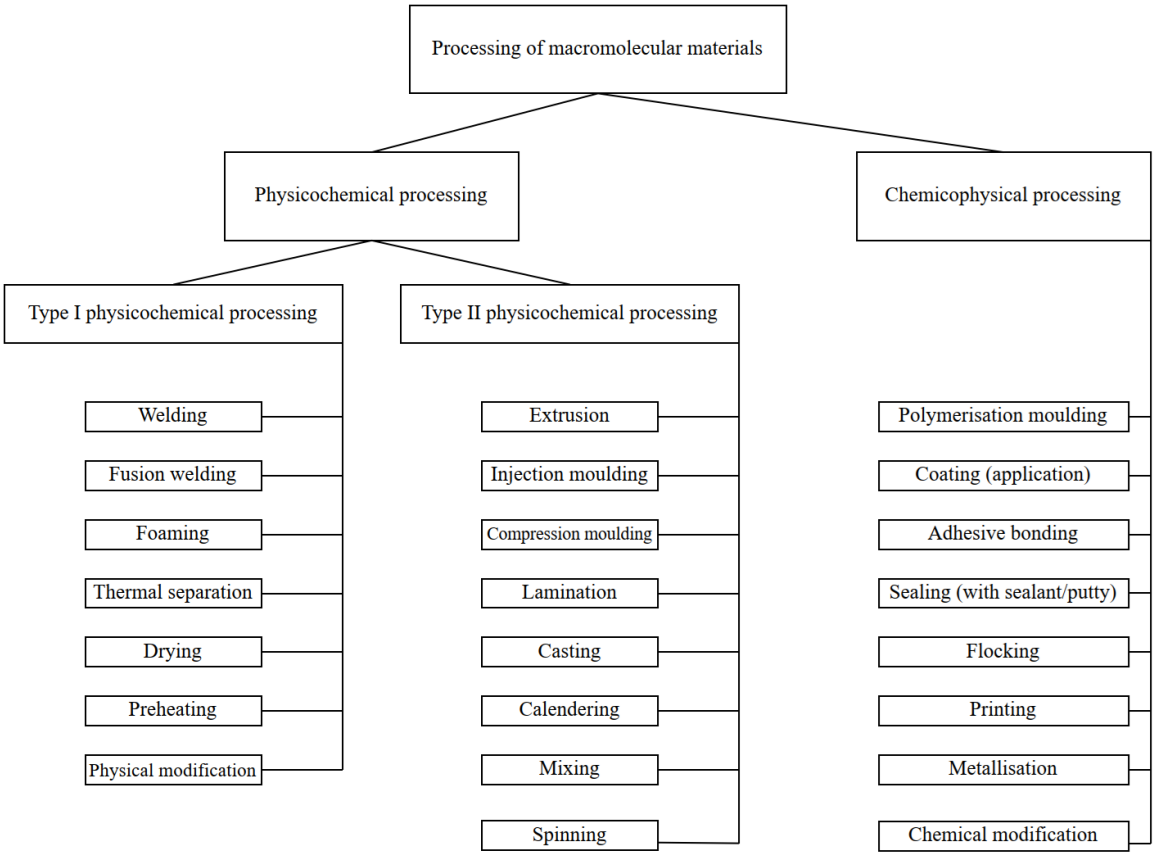

Fig. 2.7. Types of polymer processing methods [74]

A primary preparatory step in processing is the mixing of the polymer with additives, often termed auxiliaries, which facilitate processing and improve in-service performance. Such agents include pigments and dyes, thermal stabilisers, fillers, and softeners, namely plasticisers. They also include antioxidants, photostabilisers, and flame-retardant additives. The incorporation of auxiliaries aims to obtain an intermediate form suitable for subsequent conversion, such as granulate, a pre-impregnated feedstock, or a moulding compound [110–113]. The actual conversion stage then comprises shaping operations, including injection moulding, extrusion, and forming.

The processing industry for poly(vinyl chloride) can, in broad terms, be divided into two principal technological routes, namely those associated with forming rigid products (Fig. 2.8) and those associated with plasticised, flexible products (Fig. 2.9).

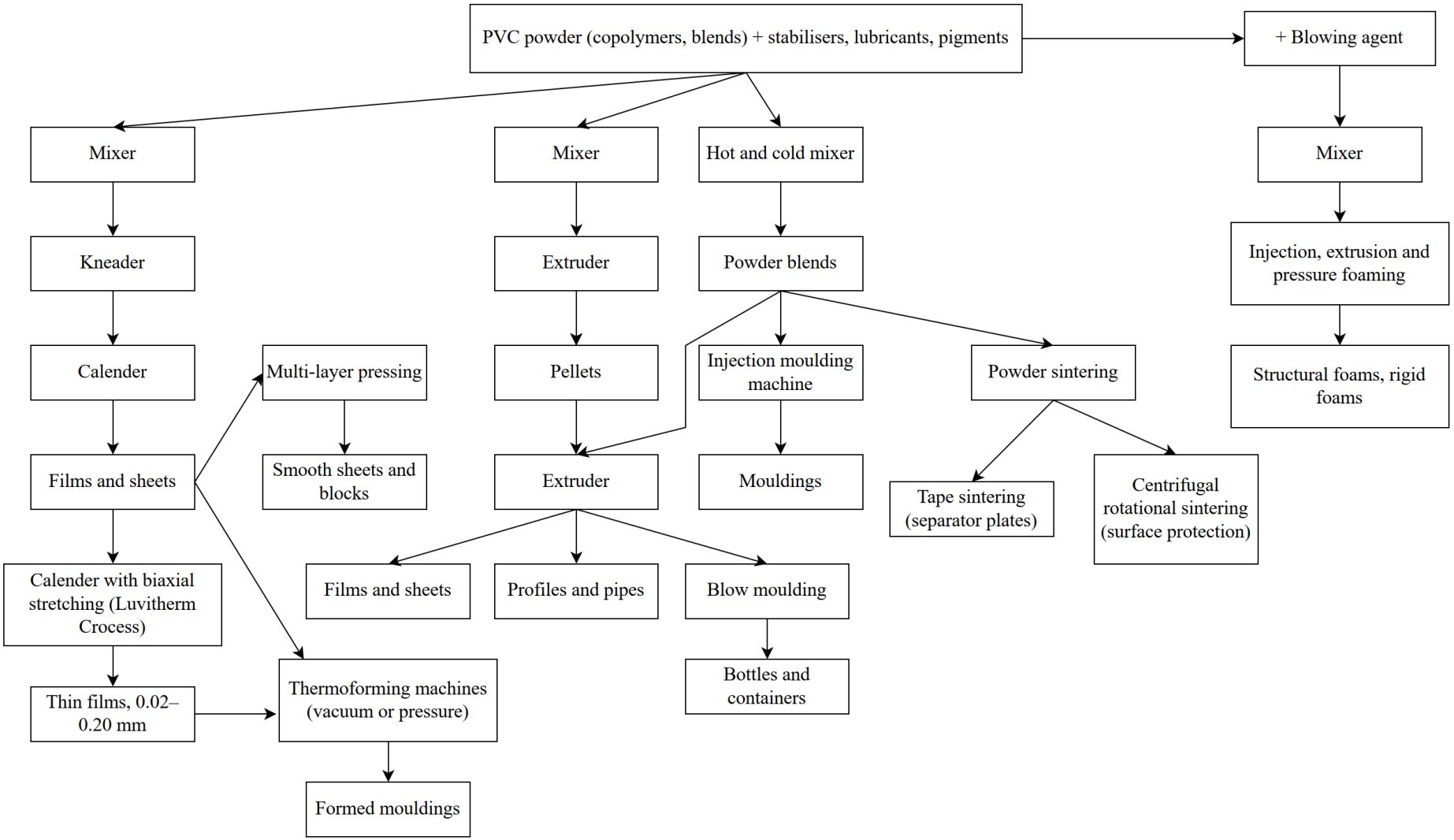

Fig. 2.8. Processing industry for poly(vinyl chloride) intended for rigid products [114]

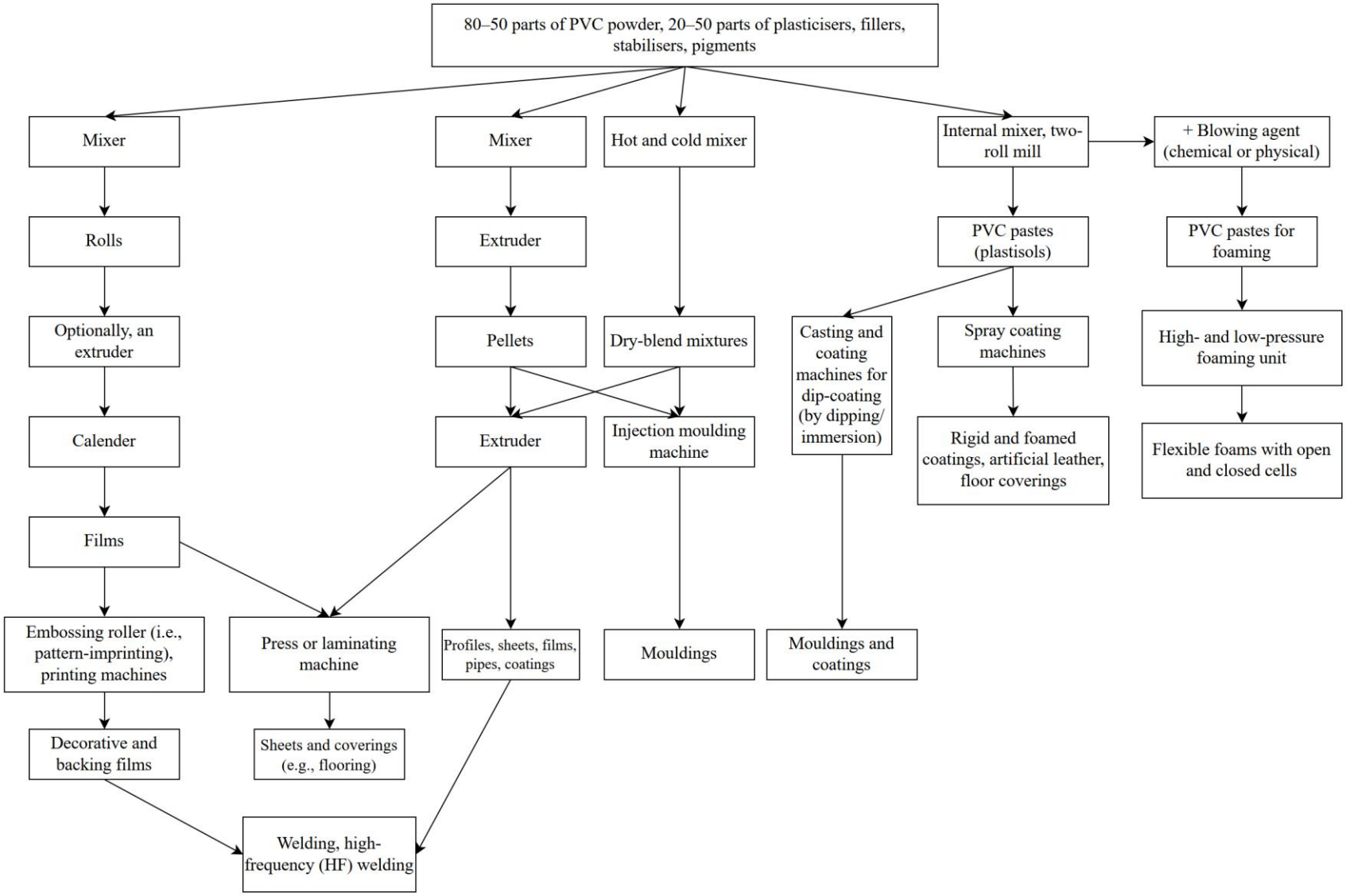

Fig. 2.9. Processing industry for poly(vinyl chloride) intended for plasticised products [114]

2.2.3. Properties of Poly(vinyl chloride)

By its nature, the vinyl chloride molecule is asymmetric. The polymer chain structure, however, may adopt two principal sequencing motifs, namely head-to-tail and head-to-head. The preferred arrangement is head-to-tail, which is associated with higher thermal stability. Nevertheless, the formation of some head-to-head segments cannot be eliminated completely. Additional chain defects may also occur, including impurities, branching, residual initiator fragments, and related irregularities. Collectively, these features adversely affect the properties of the polymerisation product.

Head-to-tail sequencing favours a higher degree of chain ordering and promotes syndiotacticity, which is linked to the formation of a crystalline phase. For poly(vinyl chloride), this is associated with a syndiotactic diad content exceeding 54.5% [115]. Above this threshold, which reflects the level of structural ordering, polymers exhibit notably high thermal stability. This behaviour is plausibly related to the presence of a certain fraction of crystalline material. The crystallites can act as physical crosslink points, thereby stabilising the structure under processing conditions.

The suitability of poly(vinyl chloride) grains for specific processing techniques is governed by grain morphology. The relationship between polymerisation conditions and grain morphology is therefore critical. Understanding this relationship enables polymerisation to be planned so as to obtain the targeted morphology. PVC grains formed during polymerisation can be classified, and specific grain types can be associated with particular methods and polymerisation conditions. Five grain types are commonly distinguished, including three single-cell types and two multi-cell types [116–117]. Single-cell grains may be partially porous with closed pores, porous with open pores, or non-porous, described as glassy. Multi-cell grains may be macrocellular, containing a small number of larger cells, or microcellular, containing a larger number of smaller cells.

High homogeneity is typically achieved in the presence of single-cell grains. Agglomerated grains statistically contain each of the aforementioned single-cell types. A further observation is that grains at a given conversion level tend to exhibit markedly higher porosity. This is associated not only with pores within cells, but also with porous intercellular spaces. Open-pore single-cell grains are produced by bulk polymerisation. Notably, they are not surrounded by a suspension-stabiliser film, unlike suspension polymers. Consequently, their porosity is substantially higher than that of suspension-derived PVC. Another characteristic of grains obtained by bulk polymerisation is a relatively narrow grain-size distribution. Multi-cell grains produced by suspension polymerisation are surrounded by a suspension-stabiliser film. They comprise a mixture of single-cell grains exhibiting differing porosity levels.

Bulk polymerisation offers the potential to establish broadly uniform conditions for all cells. This is because, in bulk polymerisation, the reaction is not compartmentalised into isolated droplets, and the forming grains are therefore exposed to broadly similar polymerisation conditions. By contrast, suspension polymerisation proceeds within isolated monomer droplets. These droplets do not experience identical polymerisation conditions because of non-uniform mixing across the reactor volume, heterogeneity in droplet characteristics, including different initiator concentrations, and differences in local heat transfer. Deformation of the droplet boundary film is also relevant and may arise from earlier droplet collisions. As a consequence of these factors, suspension polymerisation yields a more

diverse grain population. This diversity is, however, accompanied by heterogeneity in porosity, which may introduce production-related difficulties [105].

Considering the structured course of polymerisation, it can be stated that grain character is already discernible at approximately 10% monomer conversion. Grain nuclei form in the monomer droplet at conversions below 1% and typically measure 0.1–0.2 μm. As conversion increases towards 5%, the nuclei grow to about 0.6–0.8 μm. A subsequent stage is grain agglomeration, which occurs at conversions of 3–10%. Agglomeration entails the formation of clusters whose sizes range from 1–3 μm up to approximately 10 μm. The next stage of polymerisation is the development of the final grain, with a particle size of 50–250 μm, at which point conversion reaches 80–90% [79].

Within PVC morphology, no distinction is typically emphasised between domains of approximately 200 nm and microdomains of approximately 20 nm. This is because, at higher conversion levels in the polymerisation product, no discernible remnants of these features remain. Notably, domains can be identified at conversions below 2%, whereas microdomains, which represent the smallest identifiable poly(vinyl chloride) entities, comprise aggregates on the scale of fewer than 50 polymer chains [105].

The majority of commercial poly(vinyl chloride) grades exhibit molecular weights in the range 50,000–200,000, depending on the averaging definition applied (Mn, Mw, or Mv) and the measurement method. Differentiation of PVC grades with dissimilar molecular weights can be supported by the Fikentscher constant, also referred to as the K value, which is linked to the viscosity of polymer solutions [79].

Poly(vinyl chloride) differs from polyolefins, namely polyethylene and polypropylene, and from polystyrene primarily because chlorine atoms presence. This increases polarity and interchain interactions, which translates into higher stiffness at room temperature. It also results in a higher material density relative to hydrocarbon polymers. In practical terms, PVC is therefore more often selected where dimensional stability and resistance to ignition are important, and less often where minimising component mass is the overriding priority [122].

These differences are evident when basic physical and mechanical properties are compared. For typical unplasticised materials, poly(vinyl chloride) has a density of approximately 1.35–1.45 g/cm³, which is clearly higher than polyethylene and polypropylene at about 0.90–0.93 g/cm³, and higher than polystyrene at about 1.05 g/cm³. At the same time, the Young's modulus of PVC typically falls within 1.3–3.3 GPa, which is comparable to polypropylene and higher than for most polyethylene grades, although often lower than for polystyrene at 2.4–4.1 GPa. A key distinction concerns ductility. Typical elongation at break for PVC, reported as 10–150%, is materially lower than for polyethylene at 100–1000% and polypropylene at 50–550%, which indicates a lower tolerance to local stress concentrations. Polystyrene combines high stiffness with very low elongation at break of about 1–2.5%, and is therefore often even more brittle in practical service [123].

From a fire-safety standpoint, a major advantage of PVC over hydrocarbon polymers is its limited flammability. The limiting oxygen index (LOI) for rigid PVC is reported at approximately 44–49% oxygen by volume, which implies a limited ability to sustain flaming under an atmosphere close to air composition [122]. By contrast, LOI values for polypropylene, polyethylene, and polystyrene are close to 17–19%, reflecting a substantially greater propensity for sustained combustion in these materials [124]. This difference has direct implications for flame-retardancy strategies. Polyolefinic materials more often require

intensive additive systems or broader modification, whereas PVC can achieve high resistance to ignition with less demanding formulation requirements [125].

At the same time, PVC exhibits constraints that arise not from mechanics, but from thermal sensitivity. Thermal studies on composite profiles with a PVC matrix indicate a relatively high glass transition temperature of about 78–80 °C, while the softening temperature measured by the Vicat method is approximately 75–77 °C [126]. This profile supports stiffness retention under ambient conditions, yet approaching the range 70–80 °C leads to a pronounced reduction in modulus and dimensional stability. The literature further suggests that typical service temperatures for PVC lie broadly between about -10 °C and 60 °C, and that exceeding this range accelerates unfavourable property changes [122].

A critical mechanism limiting both the processing window and elevated-temperature durability is the thermal degradation of poly(vinyl chloride). It initiates with hydrogen chloride elimination, namely dehydrochlorination, and progresses towards the formation of conjugated double-bond sequences, commonly described as polyenes. The process is accompanied by autocatalysis. The released hydrogen chloride can accelerate further degradation in the solid phase, as demonstrated in kinetic studies [127]. As a result, beyond reductions in molar mass and deterioration of mechanical performance, discoloration is observed, including yellowing and browning, alongside increased brittleness and the emission of acidic products. These effects are particularly relevant in corrosion-sensitive assemblies or in applications that require a high-purity service environment [128]. In practice, this necessitates the use of thermal stabilisers and strict control of the thermal regime during processing and service. Thermogravimetric data indicate that major decomposition stages may manifest above 200 °C, for example at 211–217 °C as reported for the investigated profiles. Nonetheless, the initiation of unfavourable changes may begin substantially earlier, already within temperature ranges characteristic of processing [122], [126].

Against the broader spectrum of polymers, it is also important to note that most plastics, irrespective of type, are poor thermal conductors. Consequently, where an application requires effective heat dissipation, the standard strategy is to introduce fillers and engineer conductive pathways within the composite, rather than relying on the conductivity of the polymer itself [129]. For PVC, this means that its benefits in terms of stiffness and resistance-related performance do not automatically resolve thermal challenges in components operating near heat sources. In such cases, material selection is often governed not only by degradation, but also by composite-layer design and the architecture of the filler system. Selected properties of PVC in comparison with other polymers are summarised in Table 5.

Table 5. Summary of selected properties of PVC and other polymers [122–124], [126], [130–132]

Property	Unit	PVC	Polypropylene	Polyethylene	Polystyrene
Density (specific gravity)	g/cm³	1.35–1.45	0.90	0.93	1.05
Young's modulus	GPa	1.3–3.3	1.3–1.8	0.6–1.4	2.4–4.1
Tensile strength	MPa	41–52	27–41	14–55	42–69
Strain at break	%	10–150	50–550	100–1000	1–2,5
Limiting oxygen index (LOI)	% O_2 (vol.)	44–49	17.6	18.4	18.2
Glass transition temperature (Tg)	°C	78–80	−10	−123	100

Vicat softening temperature	°C	75–77	150.6	126.4	97.7

2.2.4. Effect of Temperature on the Properties of Poly(vinyl chloride)

Poly(vinyl chloride) exhibits a relatively high glass transition temperature, which directly governs its behaviour under typical service conditions. For many formulations, including semi-rigid grades and building profiles based on PVC, Tg determined by DSC or DMA typically lies at approximately 76–80 °C. This implies that, at room temperature, PVC remains in a glassy state characterised by high stiffness and limited segmental mobility of the chain [122], [126]. For a representative PVC formulation, a tensile strength of about 49 MPa and a Young's modulus of approximately 2390 MPa have been reported, which is consistent with rigid PVC materials containing low plasticiser contents [122]. This already indicates that the temperature response of PVC cannot be reduced to a single parameter. It encompasses both purely mechanical phenomena, such as viscoelasticity, and chemical processes, including ageing and degradation.

From the standpoint of temperature effects, the transition through Tg is critical because the viscoelastic response changes rapidly in the vicinity of Tg. Below Tg, elastic deformation dominates and creep is comparatively limited. As temperature increases towards Tg, the contribution of segmental relaxation grows, which reduces the modulus and increases the propensity for permanent deformation. DMA results are illustrative. For the same PVC formulation, the storage modulus G′ at 30 °C was reported as 899 MPa, whereas at 90 °C, that is, close to and above Tg, it decreased to only a few MPa [122]. This change does not imply material failure. It reflects a shift in the dominant deformation mechanism. In practice, this translates into a higher sensitivity of PVC components to sustained loading at elevated temperatures. Under the same force, deformation may accumulate more rapidly. After unloading, a larger permanent strain component may remain.

Assessment of PVC performance therefore requires separating immediate effects, which are associated with viscoelasticity, from time-dependent effects, which arise from ageing and degradation. A review addressing PVC in the environment reported that neat PVC is typically used in a range of approximately -10 °C to 60 °C, whereas at higher temperatures the risk of accelerated property change increases. The same source indicated that visible signs of decomposition may appear from about 135 °C [133]. In practical terms, even if a component is not exposed to temperatures approaching processing conditions, long-term operation above the typical service range may accelerate processes that lead to colour change, embrittlement, or reduced dimensional stability. The time–temperature relationship is central. Temperature alone is not the only variable because many processes, including creep and chemical ageing, are cumulative in nature.

In structural applications, in addition to Tg, parameters describing softening under combined thermal and mechanical loading are important, including softening temperature, for example in Vicat-type testing. For composite profiles with a PVC matrix intended for façade applications, a softening temperature of 75 °C and Tg of approximately 78–80 °C were reported [126]. In terms of temperature effects, it is material that the vicinity of 70–80 °C constitutes a regime in which selected properties, including stiffness and creep resistance, may change substantially even without chemical degradation. Accordingly, these temperatures are critical in the design of components operating under solar exposure, elevated ambient temperatures, or near heat sources. If a sustained load is also present, for example

deflection, compression, or installation pressure, the relevance of stress relaxation and creep increases, and so does the risk of losing geometric tolerances or joint tightness.

In [134] it was observed that at moderately elevated temperatures, on the order of 60–80 °C, chemical ageing processes may occur before a pronounced decline in mechanical performance becomes apparent. In a study on the combined influence of heat and humidity on unplasticised PVC (PVC-U), accelerated conditions at 60 °C and 80 °C produced spectral changes indicative of the formation of conjugated double bonds, namely polyenes, which correlated with sample yellowing. The authors emphasised that concurrent interpretation of mechanical and chemical results is necessary because a material may appear to retain load-bearing capacity while entering a stage of slow structural transformations that subsequently facilitate further degradation. For PVC, this means that increasing temperature can initiate a chemical change pathway even when a clear reduction in strength is not yet observed in standard short-term tests.

Beyond a certain temperature, chemical instability becomes the dominant factor for PVC. Unlike many hydrocarbon polymers, the principal degradation route for PVC is not depolymerisation to monomer. It is hydrogen chloride elimination, namely dehydrochlorination, which leads to the formation of polyene sequences and initiates a cascade of secondary reactions, including cyclisation, crosslinking, and aromatisation [128]. This mechanism is initiated by structural defects in the chain, including allylic and tertiary chlorides. The generated HCl can act catalytically, accelerating further HCl elimination within the material, which is an autocatalytic effect [127]. In terms of temperature influence, this implies that above a threshold one observes not only “softening” and viscoelastic changes, but a genuine change in chemical composition and macromolecular structure. As a result, colour stability declines, brittleness increases, micro-defects and changes in surface properties may develop, and mechanical properties may ultimately deteriorate.

The relationship between temperature and visible degradation effects is well illustrated by the role of polyenes. In an analysis of PVC degradation, it was reported that HCl elimination produces conjugated double-bond sequences, and that when at least about seven conjugated double bonds occur within a chain, discoloration becomes visible within the visible-light range [135]. In practice, yellowing, browning, or blackening of PVC constitutes a macroscopic manifestation of processes occurring at the level of polymer-chain structure. Importantly, such changes may develop locally, for example in zones with poorer heat dissipation or in regions of stress concentration. Temperature therefore affects a component not only globally, but also locally through temperature gradients and transient overheating.

The temperature sensitivity of PVC is the direct reason for using thermal stabilisers during processing, including extrusion, injection moulding, and calendering. Stabilisers reduce the dehydrochlorination rate, inter alia by binding HCl and deactivating labile sites in the polymer chain, thereby increasing stability within the processing window. In a study addressing the influence of an organic stabiliser on PVC pipes, improved thermal-stability parameters were reported following modification of the stabilising system [136]. From a service perspective, comparisons of PVC temperature resistance must take formulation into account, since otherwise they do not provide a reliable basis for material assessment. Two PVC-based materials may exhibit similar Tg values, yet differ markedly in resistance to thermal degradation, yellowing rate, or the quantity of emitted degradation products.

Temperature also affects the emission of degradation products, which is relevant in both environmental and materials terms, including corrosion of the surrounding environment and interactions with adjacent materials. In a study on the emission of acidic products from PVC, the release of HCl was shown to be potentially two-stage. In addition to HCl, other organic acids, such as formic and acetic acid, may be formed and emitted [137]. Consequently, with increasing temperature, not only does the rate of internal changes rise, but so does the potential for PVC to affect its surroundings through volatile products. In practical service, elevated temperature may therefore increase the risk of accelerated ageing of neighbouring elements, for example metallic components, or contribute to odour and hygiene issues in enclosed spaces.

It can therefore be concluded that temperature affects PVC through two complementary pathways. The first is the change in viscoelastic response in the vicinity of Tg. The second is the initiation and acceleration of chemical degradation at higher temperatures. In practice, the safe selection of PVC for elevated-temperature service requires the simultaneous consideration of multiple factors, including temperature and load duration, which governs creep, environmental conditions, such as moisture and oxygen availability, and formulation, including stabiliser and additive systems. Only such an integrated approach enables a reliable judgement as to whether an observed deterioration is driven mainly by passage through Tg or by progressive dehydrochlorination and the emission of decomposition products [127–128], [137].

2.2.5. Toxicology and Recycling of Poly(vinyl chloride)

Monomers and polymers, as well as polymer-based materials more broadly, can exert effects on the human body. Upon contact with the organism, they may induce local tissue responses, including burns, irritation, or allergy. They may also elicit systemic toxic side effects and teratogenic outcomes, manifested as foetal defects [138–142]. Particular attention should also be paid to additives, including fillers. One example is asbestos, whose dust can be carcinogenic. Its crystallites are very small and exhibit sharp edges, which promotes their penetration into cellular structures. Particles with sizes up to about 10 μm are also highly hazardous to human health and life. These are fragments derived from polymeric materials and plastics that, once ingested, may translocate through the intestinal wall into the bloodstream, potentially triggering multiple pathological responses [138–141]. In developing the concept of the amount of a toxic substance that causes death in a test animal, the notion of acute oral lethal toxicity was established [143].

Given the chemical reactivity of monomers, most can be classified as more or less toxic [142]. Vinyl chloride may cause skin and respiratory irritation. It is hazardous to the eyes and can damage the liver. Vinyl chloride also exhibits confirmed carcinogenic effects, including an association with tumours of the lungs, brain, and liver. Its adverse role has additionally been documented for neoplasms of the circulatory and lymphatic systems [144–148]. Toxic and other adverse effects on the human body have also been confirmed for other monomers. Ethylene and propylene may contribute to asphyxia. Tetrafluoroethylene, ethylene oxide, and styrene may be responsible for irritation of the skin and respiratory tract, with tetrafluoroethylene additionally implicated in renal degeneration. Exposure to acrylonitrile may cause nausea as well as abdominal and headache symptoms. Formaldehyde, phenol, and bisphenol A may induce skin and respiratory irritation. Phenol may be associated with coma and convulsions, whereas bisphenol A may be linked to arrhythmias and spasms. Threshold concentrations for individual monomers used in production technologies are defined as

workplace-assigned maximum concentrations, technical guidance values, and exposure equivalents for carcinogenic substances [144–148].

Polymers, unlike monomers, are in most cases relatively inert with respect to the human body. They are not subject to mandatory registration and assessment [149]. They do not typically contain sensitising reagents nor do they constitute agents of acute toxic poisoning. Adverse effects associated with their presence or contact are generally attributed to residual unreacted monomer or polymerisation catalysts. Despite their low intrinsic toxicity, polymers may still affect the human body to some degree. Poly(vinyl chloride) used as part of polymeric products, such as floor coverings or wallpapers, may contain up to 50 wt% plasticiser, for example di(2-ethylhexyl) phthalate. This compound readily migrates into water or food. It can enter via the respiratory route and, after gastrointestinal uptake into the blood, may cross the placental barrier. This underpins the view that PVC floor coverings should not be used for excessive periods, given intensive abrasion and the aggregation of dust particles. Because of their adverse implications for human health, frequent ventilation and airing of indoor spaces is recommended [150–151]. Adverse effects have also been reported for other polymers, including polyethylene, polypropylene, and polystyrene, which may be associated with the formation of local tumours. Polytetrafluoroethylene may be linked to neoplasms, including sarcoma. Silicones have been associated with autoimmune-related conditions and lymph-node enlargement. Natural latex that has not been adequately purified from proteins, and is used, inter alia, in glove production, may cause severe allergic reactions, asthma, or anaphylactic shock [150–151].

It is well established that polymeric materials, in addition to their principal constituent, namely the polymer itself, contain a wide range of additives, including plasticisers, colourants, thermal stabilisers, flame-retardant additives, and many others. These are used to manufacture products such as packaging, kitchenware, and toys. Accordingly, when considering the effects of monomers and polymers on the human body, the impact of additives must also be taken into account. To ensure safety, additives must not contain toxic or health-damaging substances [152–155]. In this context, flame-retardant additives warrant attention. They are intended to delay burning, yet they may be associated with serious neurological outcomes, including disruption of foetal thyroid-hormone function. This may entail changes in brain anatomy, including effects on cognitive development, attention-related disorders, or spatial-orientation difficulties. In view of these risks, certain substances of this class have been prohibited or restricted in the United States and in many EU countries. The European Commission has published a materials list for the manufacture of polymers and plastic articles intended for food contact. Continuous updating of the list of monomers and other raw materials is intended to provide ongoing control in this area. For polymeric materials, an overall migration limit of 60 $mg \cdot kg^{-1}$ applies, and the corresponding limit expressed per surface area is 10 $mg \cdot dm^{-2}$ [152–155].

Toxic substances that are harmful to human health and life may also be released during fires. Building services systems and buildings contain polymeric materials as load-bearing and structural elements. They also appear as equipment, accessories, and decorative components. Of particular concern is the formation of smoke during a fire. Ignition may occur via a candle flame, a spark, a cigarette butt, or a range of other factors. Such triggers ignite the polymer locally, causing progressive heating and ultimately flaming. Heat release increases, accompanied by fire growth and smoke generation. Subsequently, the products of thermal breakdown, namely degradation and depolymerisation of the polymer, may ignite. Flame spread then creates new fire seats [156–158]. Fire is inherently rapid. Within a few minutes,

substantial quantities of heat, smoke, and gases are generated. This is a physicochemical process governed by multiple factors, including the chemical composition of the burning materials, their volume, density, and shape, the ignition mechanism, such as explosion, friction, or flame, as well as heat-transfer dynamics and the presence of flame-retardant agents.

Polymer combustion is typically multi-stage and occurs predominantly at the surface. Heat drives polymer degradation, producing large quantities of volatile combustible products. Pyrolysis then proceeds, effectively gasifying the polymer and generating smoke. This is followed by conversion of chemical energy into thermal energy and the luminous emission of the flame. Once the environment and combustion mode stabilise, and the associated parameters, such as temperature, oxygen concentration, thermal uniformity of the polymer, specimen geometry, and flame characteristics, become established, the flame may remain localised or expand across the specimen, creating new ignition sites. One commonly used measure of polymer flammability is the oxygen index. It is defined as the lowest oxygen concentration in an oxygen–nitrogen mixture required to sustain combustion of a polymer specimen with dimensions 150 × 13 × 13 mm [156–158]. Oxygen-index values for individual polymers are listed in Table 6.

Table 6. Limiting oxygen index of selected polymers [159]

No.	Polymer	Limiting oxygen index
1	Poly(ethylene oxide)	0.150
2	Polyformaldehyde	0.151
3	Poly(methyl methacrylate)	0.175
4	Polypropylene	0.180
5	Polyethylene	0.180
6	Polyacrylonitrile	0.180
7	Polystyrene	0.181
8	Polybutadiene	0.185
9	Cellulose	0.190
10	Poly(ethylene terephthalate)	0.210
11	Poly(vinyl alcohol)	0.220
12	Polyamide 66	0.250
13	Polycarbonate	0.270
14	Aromatic polyamide (Kevlar)	0.290
15	Phenol-formaldehyde resin	0.350
16	Polybenzimidazole	0.415
17	Poly(vinyl chloride)	0.450
18	Poly(vinylidene chloride)	0.600
19	Carbon fibre	0.600
20	Poly(tetrafluoroethylene)	0.950

Based on Table 6, poly(vinyl chloride) ranks 17th among the 20 examples presented. It therefore belongs to the group of polymers that require a relatively high index, and thus a relatively high oxygen concentration, to sustain combustion. This is favourable in practical terms because, given the range of PVC applications, reduced flammability constitutes a useful performance attribute.

Smoke is an integral component of a fire. The amount of smoke generated during polymer combustion is as important as the rate of CO and CO_2 formation. This reflects the fact that fatalities due to smoke inhalation exceed those caused by direct flame exposure [156–158]. Smoke-emission characteristics during the burning of selected polymers are presented in Table 7.

Table 7. Smoke-emission characteristics during the burning of selected polymers relative to poly(acrylonitrile-co-butadiene-co-styrene) [159]

No.	Polymer	Maximum smoke density factor
1	Poly(acrylonitrile-co-butadiene-co-styrene)	1.00
2	Poly(vinyl chloride)	0.65
3	Polystyrene	0.59
4	Polisulfon	0.29
5	Polycarbonates	0.27
6	Polyamidoimides	0.21
7	Polyacrylates	0.14
8	Polytetrafluoroethylene	0.12
9	Phenolic resins	0.09
10	Polyethersulfones	0.06

Beyond fire performance, the widespread use of PVC also necessitates consideration of its environmental footprint, particularly in relation to large-scale production, waste accumulation, and end-of-life management. It is estimated that during the period of intensified, large-scale global production of polymeric materials and polymers, namely from the 1950s to 2018, total output reached approximately 9 billion tonnes [160–167]. Commodity plastics, including poly(vinyl chloride), polyethylene, polypropylene, polystyrene, and poly(ethylene terephthalate), account for 78% of global production, which is reported at around 360 million tonnes. Only about 8% has been recycled, 12% incinerated, whereas the largest share, approximately 80%, has accumulated in landfills, thereby generating an environmental burden and persistent disorder in the natural environment. When the statistics are restricted to Europe, approximately 30% of polymeric materials are recycled, up to 40% are incinerated, and around 30% are landfilled [160–167]. These waste streams mainly comprise packaging products for food and industry, natural and synthetic carpets, materials used in personal and mass transport, and diverse materials employed across multiple sectors, including construction, the chemical industry, and electrical engineering. A critical point is that the primary challenge in eliminating such waste is not its mass, but rather its long degradation time and substantial volume [160–167]. Nevertheless, waste can be processed and redirected to secondary use. For example, it may serve as production scrap suitable for direct re-use, as a feedstock for recovering monomers, or as a source of energy via incineration.

Recycling, also referred to as recovery or waste treatment, denotes processing operations applied to polymeric waste. Its principal objectives include reducing pollution and supporting environmental restoration, as well as recovering end products in the form of monomers, intermediate products in the form of degradation compounds, and, where feasible, polymeric materials suitable for re-use [168–172]. Current recovery pathways include mechanical recycling aimed at producing a regranulate that substitutes virgin material, feedstock recycling aimed at recovering monomers, thermal recovery aimed at generating additional energy, bio-organic routes aimed at producing biofuels and compost, and physicochemical

approaches. The products obtained via these routes are commonly referred to as recyclates. A practical and important premise is that a recyclate should ideally be derived from a single polymer type. This is, however, difficult to achieve because waste streams typically contain mixtures of different polymers [168–172].

Recycling of poly(vinyl chloride) is strongly conditioned by product type and intended application. Accordingly, effective PVC recycling requires classification by end-of-life assortment. The recycling structure for PVC waste is illustrated in Fig. 2.10. Waste generated during production and processing is typically consolidated and returned directly to manufacturing, because it may function as a fully valuable feedstock [173–175].

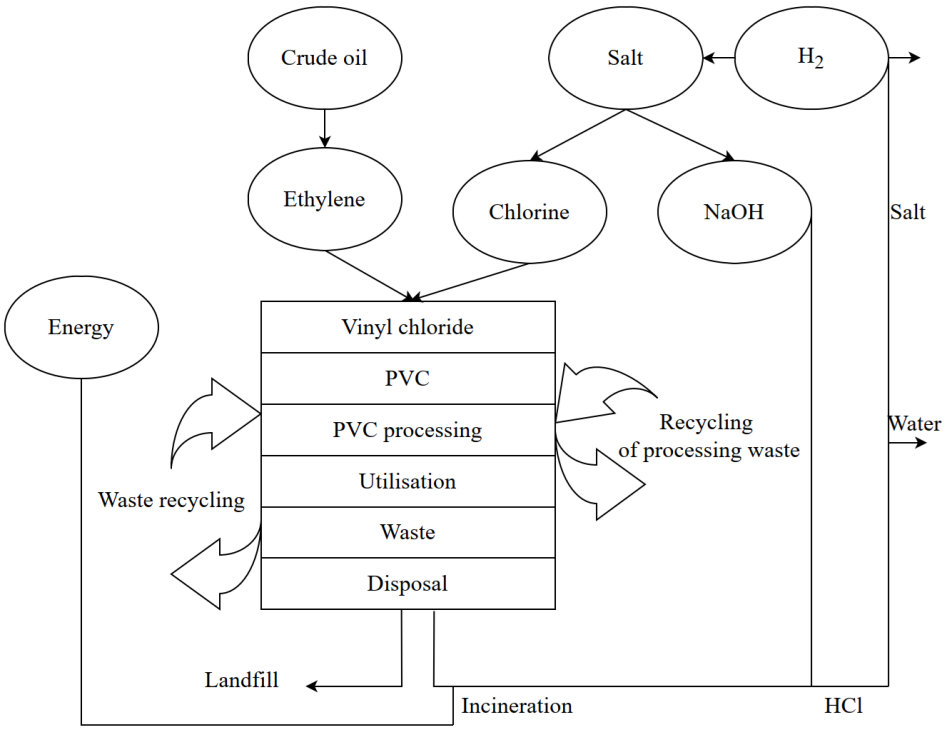

Fig. 2.10. Recycling framework for PVC waste [159], [172–175]

In most cases, mechanical recycling of PVC comprises the following stages. The first is segregation and comminution of PVC from other constituents, including glass, metallic components, rubbers, and adhesives. The second stage is washing. This is followed by grinding PVC into a regranulate. The final stage is reprocessing into target products using available methods, such as injection moulding for items including bottles, or extrusion for profiles and films [169–170], [176]. Not all waste streams are suitable for such re-use. Packaging that enters mixed municipal waste is typically directed to incineration. In that case, the sole benefit is the recovery of thermal energy. It should be noted that incineration of PVC is technically demanding because of its thermal degradation behaviour. The main combustion products are CO_2 and H_2O, yet HCl is also an integral component of the process due to the presence of chlorine in the material. Moreover, the process may promote the formation of polycyclic compounds, including benzo[a]pyrenes, and chloroaromatic species, with the potential formation of highly toxic dioxins. Harmful substances in flue gases are treated via wet or dry cleaning. This is commonly performed using CaO, $Ca(OH)_2$, or $CaCO_3$, as indicated in the cited sources [169–170], [176]. Aqueous suspensions of calcium compounds, dispersed via a hot air stream to fragment larger particles, neutralise acidic gases. Water subsequently evaporates, and dry calcium salts of mineral acids are formed.

PVC products that cannot be recycled are either landfilled or incinerated. The presence of stored PVC waste in landfills is often regarded as not inherently hazardous to the environment, because poly(vinyl chloride) is not biodegradable. However, PVC contains multiple additives, including plasticisers, stabilisers, and pigments. These constituents may pose environmental risks through leaching into landfill filtrate, thereby loading soil and groundwater with hazardous substances, including heavy metals. This concern primarily applies to plasticised, so-called soft PVC. For rigid PVC, the risk is considered lower because such components are not readily released. During the incineration of poly(vinyl chloride), catalysed by KCl and $CuCl_2$ at 300–400 °C, organic compounds known as dioxins may be released [177]. These highly harmful, toxic, and carcinogenic species can enter soil and water. They may also enter the human body, particularly through dairy products and fats. Large-scale transmission is further amplified by transport via chimney gases [177].

Some products can be manufactured from poly(vinyl chloride) and fibre-reinforced composites. These are typically reinforced with glass, natural, or carbon fibres [178–180]. Carbon fibres are predominantly allocated to commercial aviation and wind-power installations. Their recycling relies on multiple methods, with key determining factors including fibre type, component size, and mechanical performance. Such classification enables more effective recycling routes. A further reinforcement used in PVC, including in window-profile manufacture, is glass fibre. Small glass-fibre composites may be directed to incineration. Larger parts are cut and stored. Composites with natural-fibre or carbon-fibre reinforcements are mechanically comminuted to a granular form and may subsequently serve as fillers for new products [178–180].

2.2.6. Applications

Poly(vinyl chloride) produced by emulsion polymerisation is used primarily for paste formulations. Their share of emulsion PVC production is estimated at approximately 90% [79]. These pastes enable the manufacture of coated products, including artificial leather, floor coverings, and various coatings produced by casting and dipping methods. Pastes are also manufactured from microsuspension PVC, as well as from special PVC grades obtained by bulk polymerisation and from copolymers of vinyl chloride with vinyl acetate. Other applications of emulsion PVC include the manufacture of battery separator plates using powder sintering technology [93–94].

Poly(vinyl chloride) produced by suspension polymerisation and bulk polymerisation is suitable for manufacturing both rigid and plasticised products. A substantial share, exceeding 55%, is used in the construction sector for long-life goods, including window profiles, pipes, and technical compounds [79], [88–89]. More than 10% of applications relate to electrical engineering, including cable insulation and fittings. Further applications include soft and rigid films, which encompass packaging, as well as medical products, such as blood bags and drainage tubing.

When applications are expressed as percentage shares, approximately 60% of PVC production is dedicated to rigid products. This primarily relates to the construction sector, including window profiles, shutters, pipes, doors, roof gutters, and packaging [87–90]. It also includes the automotive and electrical industries [91–94], [181–182]. Within this group, approximately 31% of production is allocated to pipes and a further 8% to tiles. Another 8%

comprises extruded window profiles. Flat and corrugated sheets account for 6%. Injection-moulded products represent the smallest share, at around 2%.

The remaining share of PVC applications is allocated to plasticised products. These include, inter alia, floor coverings, cable insulation, and garden hoses [91–94]. In quantitative terms, plasticised products also include 16% for films and sheets, 10% for cables, 7% for extruded profiles, 6% for artificial leather, and a further 6% for floor and textile coverings [183]. Poly(vinyl chloride) products also have medical applications, including tubing for infusion fluids, catheters, blood containers, and disposable gloves. Products made from chlorinated poly(vinyl chloride), with a chlorine content of 60–68%, are used in the manufacture of varnishes and enamels, various coatings, including anticorrosive and water- and oil-resistant systems, fabrics, including flame-retardant fabrics intended for anti-rheumatic underwear, and packaging films [91–94]. More than 64% of poly(vinyl chloride) products are long-life goods, with durability reported to reach up to 100 years. A smaller share, 24%, comprises products with a service life of approximately 15 years. Only 12% falls within the least durable group, with a life expectancy of around 2 years [183].

Applications of different PVC types, together with the corresponding Fikentscher K-value, are presented in Table 8.

Table 8. Applications of different PVC types, including the Fikentscher constant range. Notes: I – range 50–55, II – range 56–60, III – range 61–65, IV – range 66–70, V – range 71–75, VI – range 76–80 [79], [88–94], [183]

PVC type	Rigid PVC			Plasticised PVC		
	Emulsion	Suspension	Bulk	Emulsion	Suspension	Bulk
Processing route	Fikentscher number					
Calendering	II, III	II, III	II, III	IV, V, VI	III, IV	IV
Films	V, VI					
Floor coverings				III, IV, V, VI	III, IV	
Extrusion of rigid PVC						
Pressure pipes		V	IV, V			
Window profiles	III, IV	III, IV	II, III, IV			
Sheets and flat films	II, III	II	II			
Blown films	II	II	II			
Extrusion of flexible PVC						
General				III, IV	III, IV	III, IV
Cable insulation					III, IV, V, VI	III, IV
Particularly favourable					IV	IV
Blow moulding		I, II	I, II		III, IV, V, VI	II, III
Injection moulding		I, II	I, II		III, IV, V, VI	I, II
Paste technologies				IV, V, VI	IV, V, VI	

2.3. Challenges in Joining PVC Window Profiles Emphasising Welding

Welding is one of the principal methods for producing permanent joints in thermoplastic components. In process terms, it involves bringing the contacting surfaces into a plasticised state through partial melting at the interface, followed by consolidation under controlled conditions. After cooling, the joint forms a weld of adequate load-bearing capacity and tightness. Joint formation is governed by diffusion and interpenetration of polymer chains within the plasticised layer, coupled with microstructural reconstruction during cooling. Welding is selected when high durability, repeatability, and sealing performance are required, and where mechanical fastening or adhesive bonding would be less efficient or more difficult to control in serial production [184–185].

For joinery produced from unplasticised poly(vinyl chloride) (PVC-U), welding is critical because the quality of corner welds directly determines the load-bearing capacity, tightness, and long-term durability of window frames and sashes. In industrial practice, the dominant solutions are those that enable rapid and repeatable joining while allowing control of key process variables, including temperature, time, and consolidation force [15–16].

The plastics industry employs a range of welding methods that differ in how thermal energy is delivered to the joint, in joint geometry, and in typical application domains. Methods most frequently discussed in the literature include hot-tool or hot-plate welding, friction welding, including vibration welding, ultrasonic welding, hot-gas welding, and specialist techniques, such as electromagnetic-field or laser welding [184–185]. Method selection depends on polymer type, component thickness and geometry, required throughput, dimensional tolerances, and the quality requirements imposed on the weld.

For PVC-U window profiles, two constraints are decisive. The first is the complex, multi-chamber cross-section combined with a 90° corner joint. The second is the requirement for high repeatability under mass-production conditions. Consequently, some methods, such as ultrasonic welding or vibration friction welding, are restricted in practice due to tooling and geometric challenges. Manual methods, including hot-gas welding, do not meet the throughput and repeatability expected in window manufacture [184–185]. For these reasons, butt welding using heated plates is widely regarded as the standard approach in PVC joinery production [15–16].

In the context of joining PVC-U window profiles, three solution families are used in practice: welding as the primary method for serial production, mechanical joints for specialist or service applications, and adhesive bonding, usually as an auxiliary measure, for example for applied cover elements. Hot-plate welding is preferred because it can produce a continuous weld across the joint cross-section and deliver high corner tightness. The process is readily automated, although it requires ongoing process control [15–16].

Methods widely described in the literature for other thermoplastic products have limited utility for PVC-U window profiles. Ultrasonic welding is highly effective for small parts with well-defined joint geometry. For large, multi-chamber profiles it would require complex sonotrodes and uniform energy delivery across the entire joint interface, which is difficult to achieve in industrial practice. Vibration friction welding offers high productivity, yet it is typically applied to simpler joint geometries. For window-profile corners, repeatable motion guidance and control of expelled material in visible surface regions become limiting factors [184–185].

In practice, the following can be identified for PVC-U window profiles [15–16], [184–185]:

- the primary method is hot-plate butt welding (serial production),
- auxiliary methods include mechanical joining and adhesive bonding (special and service applications),
- ultrasonic and vibration friction methods are rarely used and are economically unattractive for mass production due to geometric and tooling constraints.

Hot-plate welding is widely regarded as the reference method in PVC joinery manufacture because it enables rapid, repeatable corner welding while maintaining the required tightness and load-bearing performance. The process comprises, in essence, a heating stage, in which the profile end faces are plasticised through contact with the heated plate, a transition stage, in which the plate is withdrawn and the parts are aligned, and a consolidation stage, in which the plasticised surfaces are pressed together and cooled. In industrial settings, the process is implemented on multi-head welding machines, allowing multiple corners to be produced within a single cycle [15–16].

Excess plasticised PVC forced out of the joint during welding, is technologically and qualitatively significant. On the one hand, it indicates sufficient plasticisation. On the other hand, it affects aesthetics and necessitates subsequent finishing. For this reason, modern technological solutions aim to improve control of weld geometry and to reduce post-processing, while preserving the strength requirements for corners [15–16]. In this context, the expelled material may be described as the weld bead formed at the joint edges.

The quality of corner welds in PVC-U window profiles is influenced by multiple interdependent parameters. Core variables include heated-plate temperature, heating time, meaning the duration of contact between profile ends and the plate, transition time, meaning the interval between plate withdrawal and application of pressure, consolidation time, and the applied force during the joining and cooling phase. In older equipment, force control and head motion were often implemented pneumatically, which limited precision in both force and positional control. In newer welding machines, servo drives are increasingly used to provide electrically controlled motion and consolidation force, thereby improving cycle repeatability [12], [16].

The need for strict parameter control arises from the narrow processing window of PVC. If insufficient energy is delivered to the joint, plasticisation is inadequate and the weld is weak. If excessive energy is delivered, through overly high temperature or prolonged heating, the risk of thermal degradation in the weld zone increases. This may manifest as impaired mechanical performance and a colour change in the joint region. In production practice, control is achieved through machine parameter management combined with corner strength testing and visual weld criteria [15–16], [18].

Requirements for PVC-U profiles intended for windows and doors, as well as requirements for testing welded corners, are defined in standards. PN-EN 12608-1 concerns classification of PVC-U profiles and material requirements for the product, whereas PN-EN 514 describes methods for determining the strength of welded corners and T-joints. Incorporating standard references into the process description clarifies quality criteria and supports justification of process-control procedures [18], [85].

In practice, PVC-U window profiles occur in at least two relevant structural variants. These are conventional profiles reinforced with a steel section and profiles reinforced with a glass-fibre-based composite. Steel reinforcement is a long-established and well-characterised solution that increases the stiffness of frame and sash members. From the standpoint of corner welding, steel does not participate directly in weld formation. The reinforcement is instead treated as a structural element within the profile limbs [17].

The development of profiles with glass-fibre composites is driven by the need to improve thermal performance and reduce thermal bridging and mass relative to steel. However, introducing composite inserts alters the welding problem. Depending on composite type, the reinforcement may be located closer to the weld zone and its thermal response may differ from that of PVC. Under such conditions, it becomes critical to secure PVC weld quality without simultaneously generating defects at the PVC–composite interface. Studies indicate that preparation of profile ends and the feed and consolidation parameters can materially affect joint strength [12–14].

A distinct class comprises thermoplastic-matrix composite reinforcements that may, in principle, be welded together with PVC in hot-plate processes. If both PVC and the thermoplastic matrix of the composite are plasticised within the weld region, more continuous load transfer across the corner may be achievable. The literature reports concepts and test results for PVC profiles reinforced with pultruded thermoplastic elements, indicating potential for improved window thermal performance and highlighting the need to refine welding technology for multi-material systems [11].

At this point, a key technological challenge arises. If the objective is to co-plasticise a region encompassing both PVC and the composite reinforcement, increasing temperature or extending heating time to achieve sufficient plasticity in the reinforcement elevates the risk of PVC degradation in the weld zone. This implies that, for PVC window profiles with composite reinforcements, solutions must balance reinforcement geometry at the corner, welding-cycle parameters, and the profile-end preparation strategy. The aim is to avoid deterioration of PVC-U weld quality while still exploiting the potential benefits of the composite [12–13], [11].

2.4. Summary of the Literature

Window joinery is assuming an increasingly prominent role in contemporary construction, as it materially affects both building energy performance and occupant comfort. The evolution from simple glazing to highly engineered products has been driven by escalating requirements for thermal insulation, acoustic performance, and airtightness, which are associated, among other factors, with tighter energy regulations and ongoing urbanisation [4–5]. As a result, the window has become part of an integrated building-energy strategy, and its in-service performance depends not only on the product itself, but also on correct installation and interaction with the adjacent building envelope [6]. Over recent decades, the window market has developed rapidly, and multi-chamber solutions, including PVC-U systems, have become widespread by combining relatively low thermal conductivity with the industrial feasibility of manufacturing complex cross-sections [8]. At the same time, window design inevitably involves trade-offs between thermal insulation, structural stiffness, durability, and the technological constraints of manufacturing both profiles and joints [9]. Despite technological progress, window systems still face substantive challenges. Improving frame insulation often requires low-conductivity materials that typically offer lower stiffness and therefore require

reinforcement [9–10]. In PVC-U profiles, load-bearing capacity is commonly achieved by introducing steel reinforcements, which addresses strength requirements while creating thermal bridges and a thermally and mechanically non-uniform system response [10]. These constraints motivate the search for alternative material solutions, including composites, and for further process improvements. Consequently, PVC window profiles have become a focus of intensive scientific analysis. The literature includes numerous reviews and research studies addressing optimisation of window materials and designs [8], alongside detailed investigations into corner failure load and the quality of welded joints [16–17]. Increasingly, publications also examine innovative approaches to improving window performance, which underlines the currency and importance of this research domain.

Joints in PVC-U profiles are predominantly produced by hot-plate butt welding. The process relies on plasticising the mating profile faces through partial polymer melting and then consolidating them under pressure. After cooling, a weld is formed that provides the required strength and tightness [15–16]. The formation of a durable joint is governed by diffusion and interpenetration of polymer chains within the molten zone, followed by reconstruction of the material microstructure during solidification. PVC welding is therefore employed wherever a continuous, high-integrity joint is required and is difficult to achieve using alternative methods, such as adhesive bonding or mechanical fasteners, which are often less efficient or more challenging to control in production [184]. In PVC window manufacture, hot-plate butt welding remains the dominant route because it is fast and repeatable and allows precise control of key parameters, including plate temperature, heating time, and consolidation time and pressure, which together determine weld quality [15–16]. Experimental evidence confirms that the welding regime directly affects corner failure load and joint reliability. Even minor parameter deviations can reduce either the load-bearing performance or the tightness of the joint [16–17]. For this reason, standardised weld-quality criteria have been established, including corner failure load testing [18], [85].

The specific characteristics of window profiles, namely multi-chamber cross-sections of polymer parts and 90° corner joints, impose practical limitations on alternative joining techniques. Welding methods widely reported for thermoplastics, such as ultrasonic or vibration friction welding, are of limited applicability to PVC-U window profiles. This follows from the difficulty of ensuring uniform energy input across a massive profile and from challenges in controlling motion and the molten weld bead in a corner with complex geometry. Manual techniques, including hot-gas welding, are in turn too time-consuming and do not provide the repeatability required for mass production [184–185]. Consequently, the sector standard is butt welding using heated plates, most often implemented on multi-head welding machines that can join all frame corners within a single cycle [15–16]. This method supports a continuous weld through the profile thickness and delivers high corner tightness and strength. A further advantage is that the process is fully automatable, provided the technological regime is maintained with high precision. Other joining routes are used only occasionally. Mechanical fasteners and adhesives are typically limited to specialist applications, such as refurbishments or atypical assemblies, where conventional welding is not feasible or not justified.

The current state of knowledge emphasises the need to optimise welding parameters to achieve the best joint. Key variables, including heated-plate temperature, heating time, meaning the duration of profile contact with the plate, consolidation pressure, and cooling time, govern the degree of PVC plasticisation and the resulting weld bead size. Excessive heating time or overly high temperature can promote overheating and material degradation

within the weld zone, which may manifest as discolouration or increased brittleness of the joint. Conversely, insufficient time or low temperature can lead to incomplete surface melting and a reduced weld strength. Accordingly, numerous comparative studies have sought to define optimal processing windows [16–17], [127–128], [136], [184]. Conventional PVC-U profiles contain internal steel reinforcements that markedly increase the stiffness of frames and sashes. However, steel does not fuse with the polymer during welding. The steel section serves a structural function but does not participate in weld formation at the corner [17]. While steel reinforcement provides load-bearing capacity, its high thermal conductivity and lack of integration with the weld leave scope for thermo-mechanical optimisation. In response, glass-fibre-based composite reinforcements have been developed to reduce thermal bridging and window mass. Introducing composite inserts, however, alters the joining process. Depending on composition and geometry, a composite insert may be positioned closer to the weld zone and can respond to temperature differently from the surrounding PVC [11]. This makes it critical to achieve high-quality PVC welding without defects at the PVC–composite interface. Studies indicate that appropriate end preparation, including machining of the composite at the profile ends, combined with adjusted welding parameters, including time, head feed, and consolidation pressure, is decisive for maintaining corner failure load in composite-reinforced profiles [12–14]. In one comparative study, a conventional steel-reinforced window was evaluated against an assembly with a composite reinforcement. The pultruded thermoplastic insert reduced the sash heat-transfer coefficient by approximately 12% and the frame value by approximately 13% relative to the steel variant. In the same study, the corner joint failure load for the composite solution, co-welded with the profile, was about twice that of the conventional steel-reinforced design [11]. These findings support efforts to reduce steel content in profile reinforcement and indicate a clear direction for further development. Overall, the literature provides a detailed characterisation of PVC-U welding, identifies the parameters that control weld quality, and reports early implementations of reinforcement concepts that couple improved insulation with maintained or improved structural performance.

Despite substantial progress in understanding PVC profile joining, the literature also highlights persistent knowledge gaps and issues requiring further research. A key challenge is to assess weld durability under real service conditions. Standard corner tests are typically conducted under controlled laboratory conditions, most often at room temperature and on unaged specimens. This does not fully represent long-term window service, where the product is exposed to variable wind loading, cyclic operation, and environmental action. Comprehensive data remain limited on how welded joints behave after years of exposure to thermal ageing, ultraviolet radiation, moisture, or freezing conditions. Accelerated ageing studies indicate that, already at moderately elevated temperatures on the order of 60–80 °C, chemical changes can initiate in PVC-U, including the formation of conjugated polyenes associated with yellowing, before a clear loss of strength becomes evident [134]. This implies that a material may temporarily retain load-bearing capacity while undergoing gradual structural changes that later facilitate further degradation. Interpreting such behaviour requires concurrent mechanical and chemical assessment. It is not always straightforward to separate purely viscoelastic effects, including PVC softening near the glass-transition region, from chemical degradation processes [122], [126–128], [137]. The influence of material structure and temperature on joint performance therefore remains an important research area. Different PVC formulations, particularly those with differing stabiliser systems, can exhibit materially different thermal resistance. Moreover, weld microstructure, including the extent of the molten zone and the presence of pores or under-heated regions, can affect crack initiation under load. The literature therefore recommends multi-factor ageing approaches in which

temperature, exposure time, environment, including moisture and oxygen availability, and formulation are treated as jointly controlling the degradation rate [127–128], [137]. Only such integrated analysis can indicate whether an observed loss of performance is dominated by reversible thermal effects, such as proximity to Tg, or by progressive dehydrochlorination and related degradation pathways [127–128].

A further issue concerns PVC degradation during welding and subsequent service. PVC is known to be sensitive to overheating. Above approximately 135 °C, dehydrochlorination can initiate, generating unsaturated sequences and associated discolouration [127–128], [133]. During welding, where local temperatures can exceed 200 °C, degradation risk is therefore non-negligible, particularly under extended heating times. Potential manifestations include browning of the weld zone, emission of irritant volatiles, including HCl and organic acids, and reduced impact resistance of the joint. Although thermal stabilisers are incorporated into PVC formulations to retard such processes, the literature still does not fully resolve how short-duration but intense thermal exposure during welding affects long-term weld durability. In addition, service conditions can further influence joint integrity. Daily thermal cycling can impose repeated expansion and contraction, which may progressively weaken the joint through thermal fatigue processes in and around the weld. Water ingress into microgaps followed by freezing can also induce local stresses. These ageing mechanisms remain insufficiently quantified for PVC window joints and therefore represent a material research gap.

Recent publications place particular emphasis on the co-welding of PVC profiles with composite reinforcements. Thermoplastic-matrix composite inserts may, in principle, soften and weld together with PVC, enabling a more continuous and integrated load path through the corner [11]. Realising this potential, however, is technologically challenging. Achieving adequate plasticisation of both PVC and the reinforcement in the weld region may require either higher temperature or extended heating time compared with standard PVC-only cycles. This strategy, however, increases the risk of PVC degradation. PVC may begin to deteriorate before the composite reaches sufficient plasticity for effective joining [11]. At present, the literature does not yet provide a single, consolidated design framework for weld-zone engineering in multi-material systems. Further work is needed to optimise reinforcement geometry and welding parameters to reduce temperature non-uniformity within the joint, avoid extended welding cycles, and prevent interfacial defects.

Therefore, while the literature provides a substantial foundation for joining PVC window profiles, key research questions remain. These relate to long-term weld durability under realistic service conditions, the influence of environmental factors, including temperature, moisture, and UV radiation, on progressive joint degradation, and the integration of advanced composite reinforcements within welding processes. Future research should prioritise weld monitoring during production, the refinement of weld-quality assessment methods in finished windows, and the development of process concepts that enable efficient and safe co-welding of dissimilar materials. Only a comprehensive approach that integrates polymer chemistry, mechanics of materials, and civil engineering requirements is likely to unlock the full performance potential of modern window joinery while ensuring reliability and durability.

3. Formulation of the Research Problem

3.1. Research Hypothesis of the Dissertation

On the basis of a review of the literature on joining technologies for window profiles, it may be concluded that the fusion welding of unplasticised poly(vinyl chloride) (PVC-U) profiles has been extensively examined with regard to material formulation optimisation, the specification of general welding process parameters, and the evaluation of corner-weld strength. Moreover, they have examined the relationship between welding temperature and joint strength. Nevertheless, the available studies have predominantly addressed profiles without reinforcement or profiles reinforced with conventional steel inserts [16–18], [79], [85], [184], [186-187]. The international literature lacks analyses concerned with the possibility of comprehensively optimising the welding technology for unplasticised PVC window profiles reinforced with glass-fibre composite inserts in a manner that simultaneously accounts for the influence of all criteria relating to the complete set of process parameters, i.e. insert milling depth, welding-head travel speed, welding temperature and melt time, on corner strength, frame dimensional accuracy and changes in the physicochemical structure of the material within the joint region. In particular, there is a shortage of studies that cover the full range of investigated milling depths of the composite reinforcing insert in combination with welding-head travel speeds and that provide a comprehensive analysis of the effects of welding temperature and melt time, considered jointly in relation to strength, dimensional, and overall weld-quality criteria.

Both the review of the literature related to the investigated problem and the author's preliminary exploratory studies have formed the basis for the formulation of the following research hypothesis:

"the welding technology for unplasticised poly(vinyl chloride) window profiles reinforced with glass-fibre composite inserts can be optimised by an appropriate selection of insert milling depth, welding-head travel speed, welding temperature and time, so as to obtain welds whose failure loads exceed the admissible requirements, that maintain the permissible dimensional tolerances of the frames, exhibit a proper geometry and continuity of the weld bead and show no evidence of thermal degradation of the material in the joint region, while simultaneously shortening the process duration and reducing the energy consumption of the welding operation."

This hypothesis assumes that a close coupling between the results of strength tests on window corners and the results of mechanical, thermal, structural and spectroscopic investigations of specimens taken from the base materials and from the welds will make it possible to unambiguously delineate a practical process window for the welding parameters that can be implemented under industrial conditions.

3.2. Objectives and Scope of the Study

Window profiles made of unplasticised PVC are among the most important polymer-based products used in construction because they combine favourable service performance with the ability to form complex multi-chamber sections by extrusion and a comparatively favourable life-cycle environmental balance [79], [186–187]. Achieving the required mechanical properties, weathering resistance, and long-term durability depends on the appropriate selection of PVC formulation, additives, stabilisers, and processing parameters [79], [186]. At

the same time, the need to reduce hazardous emissions and ensure recyclability imposes additional constraints on both material formulation and profile design and manufacture [186–187].

Corner welding is a key technological operation in window manufacture and one of the principal joining methods for thermoplastics, requiring control of the thermal and rheological state in the joint region [184]. For unplasticised PVC profiles, even small variations in hot-plate temperature, melt time, or surface preparation can substantially affect corner strength, dimensional accuracy, tightness, and weld appearance [16]. Relevant standards define profile requirements, testing methods, and the minimum performance required for welded corners, while analytical and experimental studies show that failure force also depends on cross-sectional geometry, stiffening, and wall-thickness distribution [17–18], [85].

Studies [10], [188–190] indicate that conventional steel inserts provide the stiffness and load-bearing capacity required in PVC profiles, but also constitute a major source of thermal bridges. The geometry and thermal design of the reinforcement zone strongly influence frame heat transfer and linear thermal bridges [188], [190], which justifies the search for alternatives such as composite reinforcements. At the same time, complete-window tests and advanced material modelling show that insert geometry, stiffness, and stress distribution are critical to structural performance [188], [189]. This makes it necessary to examine the welding of PVC-U profiles with composite reinforcements not only in terms of corner strength, but also in relation to material behaviour in the joint region.

At present, the international literature does not provide a quantitative experimental assessment of the full set of welding parameters for unplasticised PVC window profiles reinforced with glass-fibre composite inserts. In particular, no study jointly considers insert milling depth, welding-head travel speed, welding temperature, and melt time with respect to corner strength, frame dimensional tolerances, and physicochemical changes in the joint region. Nor is there a coherent, cross-validated dataset linking weld performance in the PVC-U profile–glass-fibre composite insert system to the corresponding microstructural and physicochemical signatures [e.g., hardness, thermal transitions, spectroscopy, and microscopy]. This state of the art determined the scientific and utilitarian objective of the dissertation.

The scientific objective of the research, in turn, was

“to identify and characterise the relationships between the welding process parameters and the mechanical and structural properties of the welded window-profile corners, as well as the changes in the physicochemical structure of the material within the joint region.”

The principal objective of the present work was

“to establish parameter-selection guidelines for corner welding of unplasticised PVC window profiles reinforced with glass-fibre composite inserts across the studied ranges of insert milling depth, welding-head traverse speed, welding temperature, and melt time, ensuring jointly adequate corner load capacity and dimensional accuracy, while preserving a sound joint-zone structure and reducing welding cycle time and energy demand.”

Five specific sub-objectives of the study:

- to establish the baseline material state of the investigated unplasticised PVC profile and the glass-fibre composite insert through integrated mechanical, thermal, structural, and spectroscopic characterization,
- to examine how the full investigated range of insert milling depths governs weld-core formation and material distribution within the joint, and to quantify weld failure forces for the considered parameter sets,
- to determine the effect of welding-head travel speed on weld-bead geometry and symmetry, and to quantify the associated dimensional deviations of the welded frames
- to identify, within the investigated welding-temperature range, the minimum admissible melt times at which weld-quality requirements remain satisfied,
- to detect and interpret any indications of thermally driven material degradation in the joint region.

Three criteria indicating the achievement of the sub-objectives:

- a coherent, cross-correlated evidence base that links mechanical response and frame dimensional accuracy to thermal, structural, and spectroscopic signatures measured for the base materials and the weld region,
- a practically delimited process window for the welding parameters (insert milling depth, welding-head travel speed, welding temperature, and melt time) that simultaneously meets corner load-bearing requirements, dimensional-accuracy constraints, and joint-integrity expectations,
- technologically implementable recommendations for industrial corner welding of unplasticised PVC window profiles reinforced with composite inserts, grounded in the integrated interpretation of the mechanical, dimensional, thermal, structural, and spectroscopic results.

The scope of this work includes:

- the work addresses six-chamber unplasticised PVC window profiles reinforced with glass-fibre-based composite inserts used in window systems, selected in view of current PVC profile standard requirements and the practical constraints of the available laboratory infrastructure,
- the investigation encompasses 90° welded window-frame corners produced on a four-head welding machine under conditions intended to be representative of industrial practice,
- the welding programme covers systematic variation of the key process variables considered in the study: composite-insert milling depth, welding-head travel speed, welding temperature, and melt time, while maintaining controlled manufacturing and handling conditions for the profiles and corners,
- mechanical assessment within the scope includes standard-aligned compressive corner bending tests on welded corners, complemented by mechanical characterisation of the base materials via impact testing and static tensile and bending testing,
- geometrical and process-quality assessment within the scope includes measurement of welded-frame dimensional deviations, alongside observational evaluation of weld-bead geometry (including symmetry and continuity) and surface features indicative of process stability,

- materials characterisation within the scope encompasses hardness and composite fibre-content determination, thermal characterisation via softening/deflection-related temperature measurements and calorimetric-type analyses, and spectroscopic evaluation of chemical-structure signatures for specimens extracted from both base materials and the weld region,
- structural and microstructural characterisation within the scope includes microscopic examination of representative specimens and weld cross-sections to support interpretation of material-state changes localised to the joint region.

3.3. Tasks for Experimental Implementation

1. Specification and preparation of the object of study:
- selection of unplasticised PVC window profiles with a six-chamber cross-section and glass-fibre-based composite inserts is to be undertaken so as to reflect current PVC profile requirements and the practical constraints of the available laboratory infrastructure,
- Preparation of profile segments and insert variants is to be conducted under controlled conditions of identification, traceability, and conditioning, so that all subsequent manufacturing and testing stages remain comparable.

2. Manufacture of representative welded corners:
- configuration of a four-head welding machine, supported by ancillary preparation equipment including a cut-off saw, an automated milling machine, and a CNC machining centre, is to be carried out so as to produce 90° window-frame corners under process conditions intended to be representative of industrial practice,
- setup of tooling and fixtures is to be undertaken to ensure repeatable alignment, clamping, and handling of the profiles and corners throughout the welding campaign.

3. Execution of a structured welding programme with systematic parameter variation:
- implementation of a staged test matrix is to be undertaken in order to vary composite-insert milling depth across the investigated range while holding the remaining parameters constant within each dedicated series,
- variation of welding-head travel speed is to be performed in subsequent series for selected milling-depth variants defined in the preceding stage,
- variation of melt time at fixed welding temperatures and milling variants, together with complementary variation of welding temperature in defined combinations with melt time, is to be carried out in further experimental series,
- recording of manufacturing metadata for each parameter set is to be performed in a form suitable for subsequent cross-referencing with mechanical, dimensional, and materials-characterisation datasets.

4. Mechanical testing of welded corners and base materials:
- performance of standard-aligned compressive corner bending tests on welded corners is to be undertaken in order to obtain a consistent measure of mechanical performance for each parameter set,
- performance of impact tests and static tensile and bending tests on specimens extracted from the unplasticised PVC and the composite insert is to be undertaken in parallel so as to document the mechanical baseline of the constituent materials.

5. Geometrical and weld-quality evaluation:

- measurement of frame dimensional deviations relative to nominal dimensions is to be performed for each welding series using a consistent measurement protocol across machine axes,
- assessment of weld-bead geometry (symmetry) and continuity is to be carried out observationally, and documentation of macroscopic surface indicators of process instability, including colour shifts and cracking, is to be undertaken where present.

6. Thermal, physico-chemical, and spectroscopic characterization:

- performance of hardness testing and determination of glass-fibre content in the composite are to be undertaken for the base materials and for specimens taken from the weld region, using procedures consistent with the adopted laboratory practice,
- performance of softening- and deflection-related temperature measurements, together with heat-deflection-temperature testing, is to be undertaken and complemented by calorimetric evaluation using differential scanning calorimetry,
- performance of spectroscopic investigations on base-material and weld-region specimens is to be undertaken, including Fourier-transform infrared spectroscopy where consistent with the study plan.

7. Structural and microstructural examination of the joint region:

- preparation of representative specimens and weld cross-sections, together with their microscopic examination, is to be undertaken in order to document joint-region morphology, material distribution, and any parameter-linked structural features,
- curation of all microstructural records together with the corresponding processing and test metadata is to be undertaken so as to preserve a one-to-one linkage between observations and parameter sets.

Figure 3.1 illustrates the adopted research methodology.

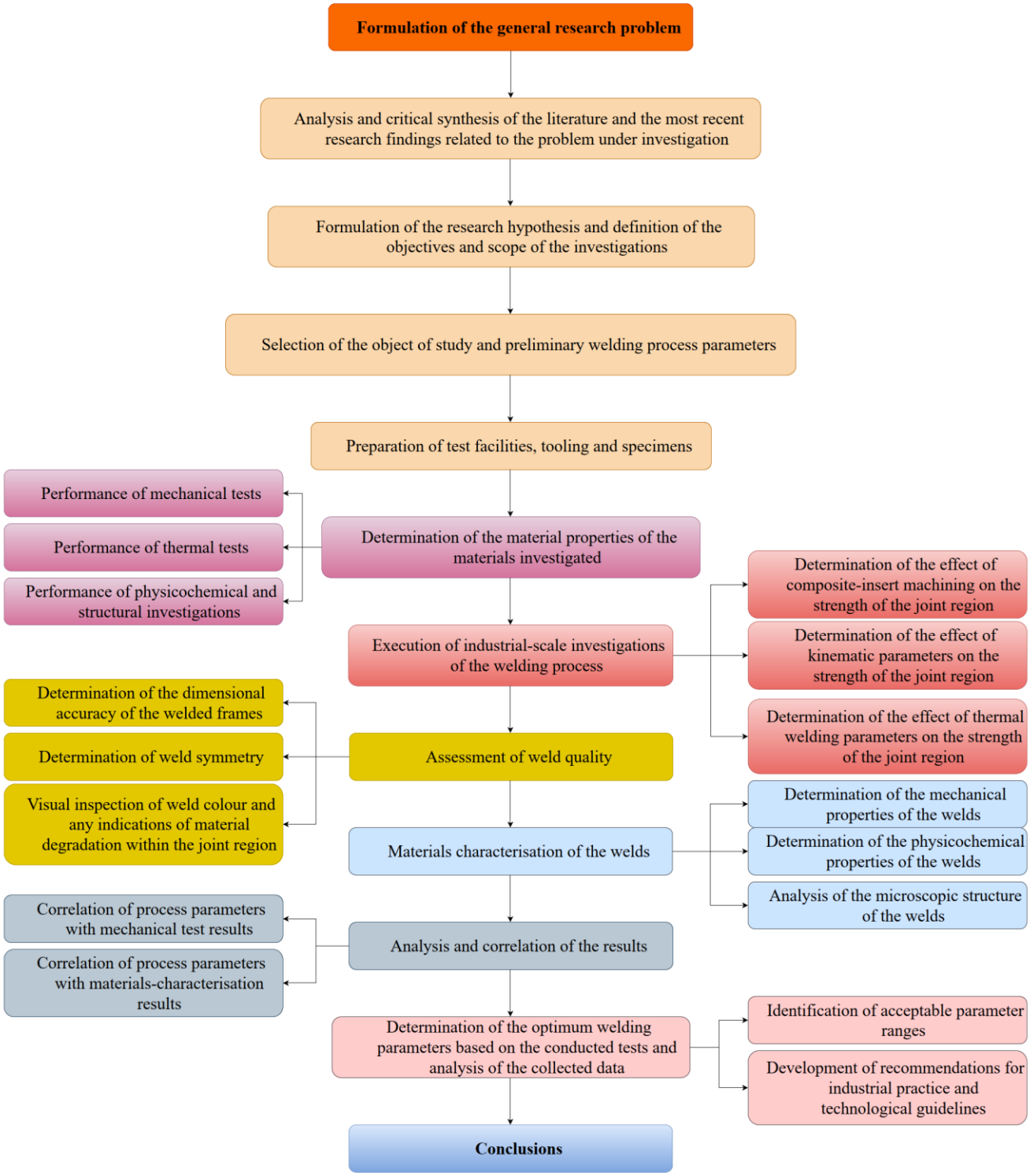

Fig. 3.1. Methodological workflow implemented in the present study. Source: Author's own work

4. Experimental Study

4.1. Fundamental Study of Constituent Materials

4.1.1. Experimental Methodology

The experimental campaign comprised a broad set of dedicated investigations. The material tests covered both specimens taken from the PVC profile and specimens from the composite used to reinforce the profile. The scope included impact resistance, tensile behaviour, flexural behaviour, heat deflection temperature (HDT), Rockwell hardness of PVC and composite specimens, the mass fraction of glass fibres in the composite, and Vicat softening temperature.

To prepare the PVC specimens, the composite specimens, and the welded-joint specimens, a six-chamber window profile was used (Fig. 4.1). The profile had a nominal depth of 70 mm, while the installation depth was 85 mm. The element was manufactured from rigid, unplasticised PVC (PVC-U). Owing to its multi-chamber architecture, the profile provides favourable thermal insulation and adequate stiffness, which explains its widespread adoption in contemporary window systems.

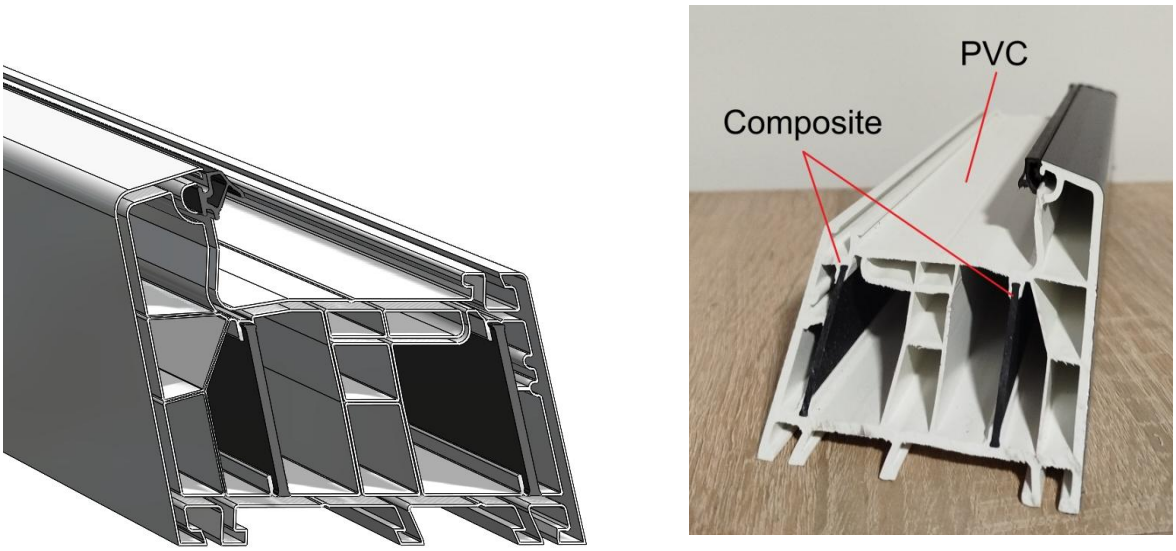

(a) (b)

Fig. 4.1. Model of the investigated profiles: (a) virtual model of the profile mitred at 45°, (b) model showing the composite reinforcing inserts within the profile [14]

According to the manufacturer, the key material properties of the investigated profile include a linear coefficient of thermal expansion of 7×10^{-5} K^{-1} (for −30 °C to 50 °C), a thermal conductivity of 0.16 W/(m·K), a Vicat softening temperature in the range 80–84 °C, a Charpy impact strength above 40 kJ/m², a flexural/tensile modulus in the range 2500–3000 N/mm², and a thermal stability time at 200 °C of 34–46 min [33].

The statistical analysis of the results was based on confidence intervals, assuming the prescribed number of specimens and a confidence level of 95%.

Impact testing of the rectangular PVC and composite specimens, both notched and unnotched, was conducted in accordance with PN-EN ISO 179-1:2023-11 (Fig. 4.2(a)). The tests were performed using a ZwickRoell Charpy HIT25P pendulum impact tester (Ulm, Germany) (Fig. 4.2(b)) at ambient temperature. A standard Charpy configuration was applied, measuring the energy required to fracture the specimen. The nominal impact velocity was 2.901 m/s, corresponding to the striker velocity at impact. The total mass of the pendulum system was 1.188 kg. Rectangular specimens with dimensions of 80 × 10 × 3 mm were tested. Five PVC specimens and five composite specimens were evaluated.

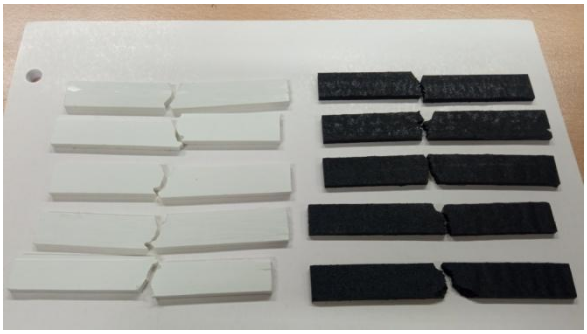

(a)

(b)

Fig. 4.2. Impact testing: (a) PVC and composite specimens, (b) test apparatus used in the study. Source: Author's own work

Static tensile testing of the rectangular PVC specimens and glass-fibre-reinforced composite specimens was carried out in accordance with PN-EN ISO 527-2:2025-12 (Fig. 4.3(a) and (b)). The measurements were performed at a crosshead speed of 50 mm/min under ambient conditions using a ZwickRoell Z010 universal testing machine (Ulm, Germany) (Fig. 4.3(c)). Ten rectangular PVC specimens and ten glass-fibre-reinforced composite specimens were tested, each with dimensions of 150 × 20 × 3 mm. The resulting stress–strain curves for the composites formed the basis for determining the mechanical properties, including the elastic modulus, tensile strength, strain at failure, and elongation at failure.

(a)

(b)

(c)

Fig. 4.3. Static tensile testing: (a) PVC specimens, (b) composite specimens, (c) test apparatus used in the study. Source: Author's own work

Flexural testing of rectangular PVC specimens and glass-fibre-reinforced composite specimens was performed in accordance with PN-EN ISO 178:2019-06 (Fig. 4.4(a)). Rectangular specimens with dimensions of 100 × 10 × 3 mm were used. Measurements were carried out at a crosshead speed of 5 mm/min for the PVC specimens and 20 mm/min for the composite specimens, using a ZwickRoell Z010 universal testing machine (Ulm, Germany) (Fig. 4.4(b)). Nine measurements were conducted for each material.

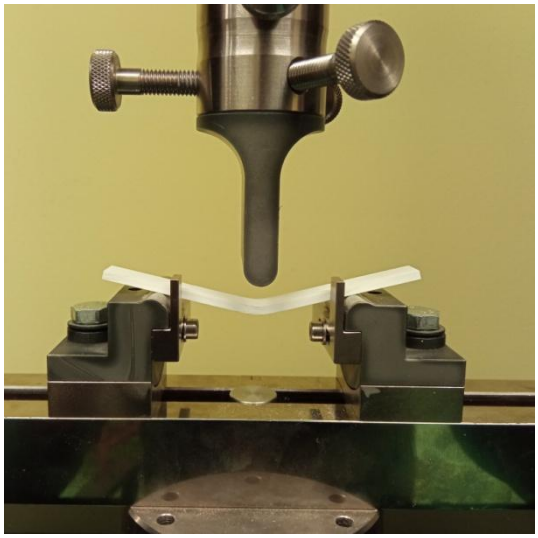

(a)

(b)

Fig. 4.4. Bending testing: (a) PVC specimens, (b) test apparatus used in the study. Source: Author's own work

Hardness testing of the PVC and composite specimens comprised Rockwell hardness measurements in accordance with PN-EN ISO 18265:2014-02. Five PVC specimens and five composite specimens, each measuring 80 × 10 × 3 mm, were tested (Fig. 4.5(a)). Each specimen was measured twice on each face. The tests were conducted using a KB Prüftechnik GmbH KB150R hardness tester (Hochdorf-Assenheim, Germany) (Fig. 4.5(b)).

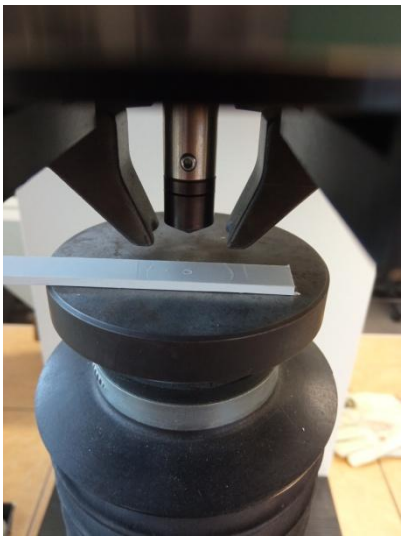

(a)

(b)

Fig. 4.5. Hardness testing: (a) PVC specimen, (b) test apparatus used in the study. Source: Author's own work

The mass fraction of glass fibres in the composite was determined using two composite specimens. The measurements were performed using a Nabertherm heat-treatment furnace (Nabertherm GmbH, Lilienthal/Bremen, Germany) (Fig. 4.6(a)) and an AXIS industrial balance. The procedure first involved weighing the crucibles into which cut composite specimens were placed. The crucibles with specimens were then weighed to determine the initial mass of the specimens. Subsequently, the specimens were conditioned in the furnace at 800 °C for 2 h (Fig. 4.6(b)). After removal from the furnace, the crucibles were reweighed together with the remaining specimen residue (Fig. 4.6(c)).

(a)

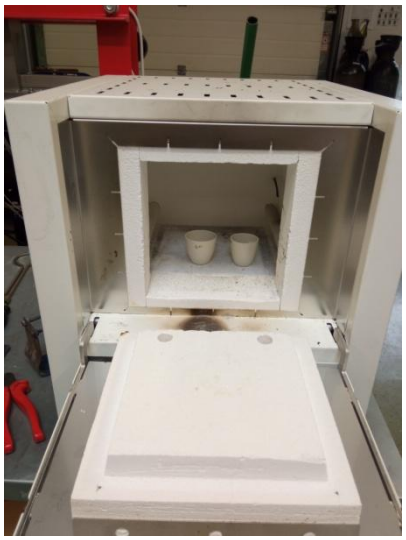

(b)

(c)

Fig. 4.6. Determination of the fibre-glass content in the composite: (a) test apparatus used in the study, (b) conditioning of the composites in a furnace, (c) weighing of the specimen with the crucible. Source: Author's own work

The Vicat softening temperature was determined for two PVC specimens using a Veb Thüringer Industriewerk drying cabinet, No. 633.10, type FWV (Rauenstein, German Democratic Republic). The unit is primarily intended for drying a range of materials under controlled conditions, where accurate temperature control and stable process parameters are essential. For the present measurements, the chamber was operated from an initial temperature of 20 °C, followed by a controlled heating rate of 50 °C/h in order to determine the softening temperature of the PVC specimens. The measurement was continued until the sensor indicated that the Vicat softening temperature had been exceeded.

Heat deflection temperature (HDT) measurements were carried out on two specimen sets: PVC taken from window profiles (n = 3) and the composite reinforcement (n = 3). Testing was performed using an HDT/VICAT TESTER RV-300C (TIME GROUP) (Fig. 4.7) in accordance with ISO 75, employing 0.45 kg weights and a heating rate of 50 °C/h. The specimens were placed flat on supports with a span of 64 mm and immersed in a methyl silicone oil bath equipped with a stirrer. HDT testing supports quality assurance by enabling deviations in material consistency to be identified during production. It also provides an indication of whether the material can meet end-use requirements without loss of dimensional stability.

Fig. 4.7. HDT test apparatus used in the study. Source: Author's own work

Chemical compounds were identified from their characteristic infrared signatures using Fourier transform infrared spectroscopy (FTIR). FTIR measurements were performed with a Jasco FT/IR-4600 spectrometer (TGS detector) equipped with an ATR PRO ONE accessory, using a 45° angle of incidence, a resolution of 4 cm^{-1}, and 60 or 40 co-added scans over approximately 4000–400 cm^{-1} (Fig. 4.8). The use of ATR implies that the recorded signal is strongly influenced by sample–crystal contact conditions, including applied pressure, surface roughness, and local topography, which is particularly relevant when comparing band intensities across spectra. Each specimen type exhibits a distinct physico-chemical absorption profile in the IR range, enabling its chemical composition to be inferred. The study comprised five PVC profile specimens and two specimens of the reinforcing composite, with four FTIR spectra recorded for each specimen. In addition, five weld types produced under different welding-parameter configurations were examined in accordance with Table 48, with at least two specimens analysed for each weld type.

(a)

(b)

(c) (d)

Fig. 4.8. FTIR analysis: (a) test setup, (b) sections of welded corners, (c) PVC profile specimen, (d) weld specimen. Source: Author's own work

4.1.2. Analysis of results

Following the impact tests, none of the unnotched PVC specimens fractured, although all exhibited deformation. This behaviour is consistent with the expected response of materials intended for window-profile applications. The maximum recorded force acting on a specimen was 14662.4 N. Since no fracture occurred, the impact strength could not be determined.

Figure 4.9 presents the key impact-resistance metric, namely the impact energy normalised by unit area.

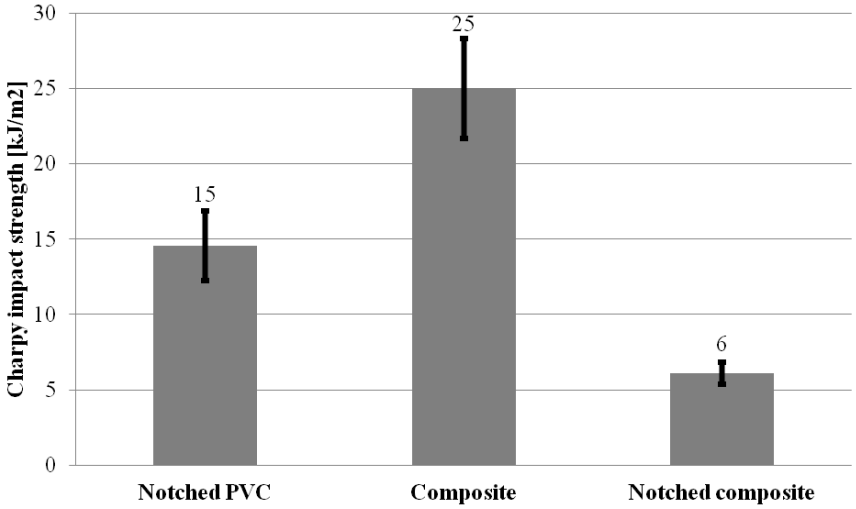

Fig. 4.9. Impact energy per unit area. Source: Author's own work

As shown in Fig. 4.9, the highest value, 25 kJ/m², was obtained for the unnotched composite, indicating superior impact resistance and more effective energy dissipation. The notched PVC achieved a moderate value of 15 kJ/m², whereas the notched composite exhibited the lowest value, 6 kJ/m².

Figure 4.10 shows the elastic modulus of the tested specimens, which quantifies material stiffness.

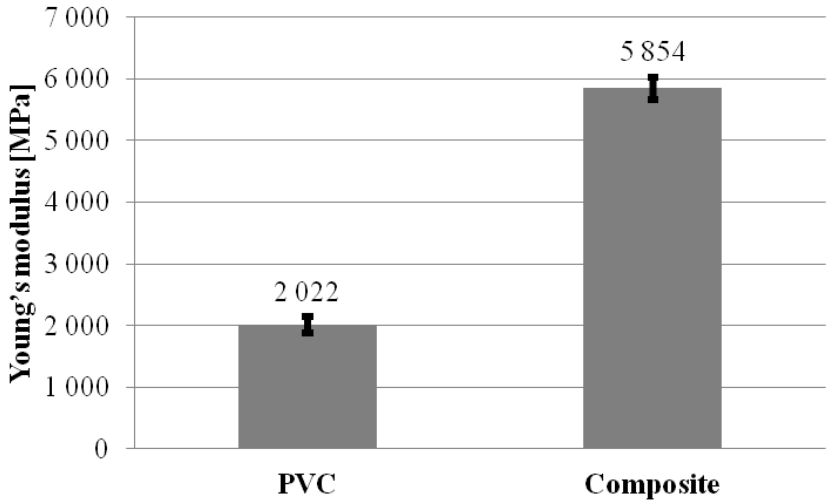

Fig. 4.10. Mean Young's modulus values for PVC specimens and glass-fibre-reinforced composite specimens. Source: Author's own work

Based on the data in Fig. 4.10, the higher modulus of the composite, 5854 MPa, indicates greater stiffness and superior resistance to elastic deformation than PVC, which exhibited a modulus of 2022 MPa. Accordingly, the composite shows a Young's modulus that is more than twice that of PVC.

Figure 4.11 presents the tensile strength values, Rm.

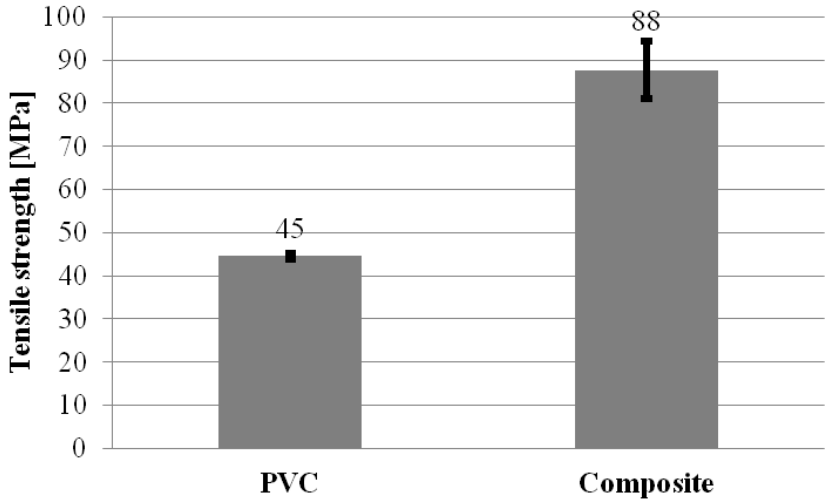

Fig. 4.11. Mean maximum stress prior to fracture for PVC and composite specimens. Source: Author's own work

As shown in Fig. 4.11, the composite attains a higher maximum stress of 88 MPa, attributable to the presence of glass fibres, compared with 45 MPa for PVC.

Figure 4.12 shows the mean strain values for the PVC and composite specimens at the maximum stress. This parameter reflects the material's capacity to deform at the point where the stress reaches its peak, immediately prior to fracture or another failure mode.

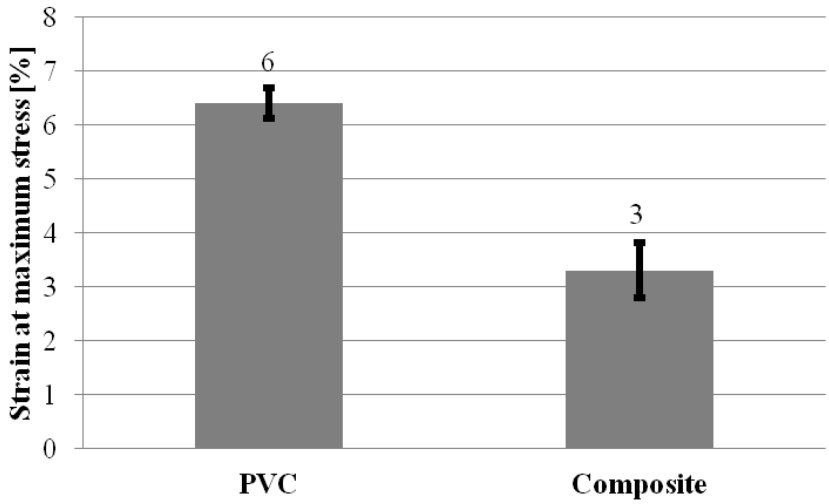

Fig. 4.12. Mean strain at maximum stress for PVC and composite specimens. Source: Author's own work

In Fig. 4.12, PVC exhibits approximately twice the strain at maximum stress (6%) compared with the composite (3%), indicating a greater propensity to deform before failure. Conversely, the composite, owing to the glass-fibre reinforcement, is stiffer but displays a reduced capacity for elastic and plastic deformation.

Figure 4.13 presents the mean values of the ultimate stress, Ru.

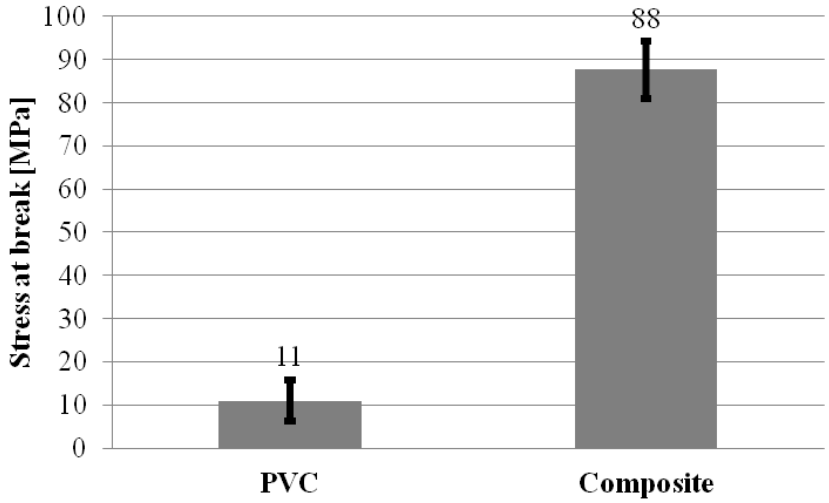

Fig. 4.13. Mean ultimate stress values for PVC and composite specimens, at which complete fracture or cracking occurs. Source: Author's own work

The results in Fig. 4.13 show that the ultimate stress, Ru, of PVC was markedly lower than that of the glass-fibre-reinforced composite. This means that PVC reached complete failure at a substantially lower stress level, with Ru equal to 11 MPa, whereas the composite sustained stresses up to 88 MPa. Considered together with the tensile strength results presented in Fig. 4.11, these findings indicate that the composite maintains a higher stress-bearing capacity both at maximum stress and at final rupture. By contrast, the data in Fig. 4.12 show that PVC exhibits a higher strain at maximum stress, which confirms its greater deformability before failure. This contrast demonstrates the fundamental difference between the two materials:

PVC is more deformable but fails at lower stress levels, whereas the glass-fibre-reinforced composite is stiffer, stronger, and capable of carrying substantially higher stresses up to final rupture.

Figure 4.14 presents the measured elongation at break for the tested specimens.

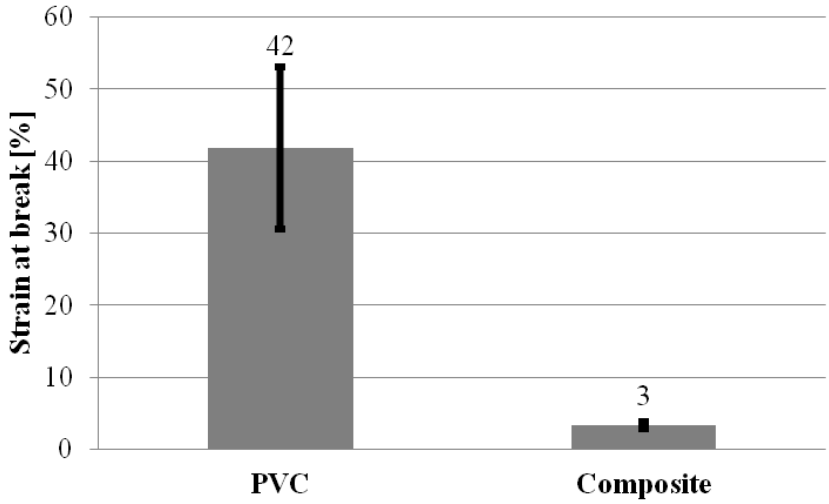

Fig. 4.14. Results of elongation-at-break measurements for PVC and composite specimens. Source: Author's own work

Analysis of Fig. 4.14 indicates that PVC exhibits a higher mean elongation at break, reaching 42%, which confirms its greater capacity to extend prior to complete rupture. In practical terms, this corresponds to higher ductility. By contrast, the glass-fibre-reinforced composite specimens show a much lower elongation at break of 3%, which is consistent with their greater stiffness.

Figures 4.15 and 4.16 show the strain responses of the PVC and composite specimens, including the elongation at specimen rupture immediately prior to the final loss of structural continuity.

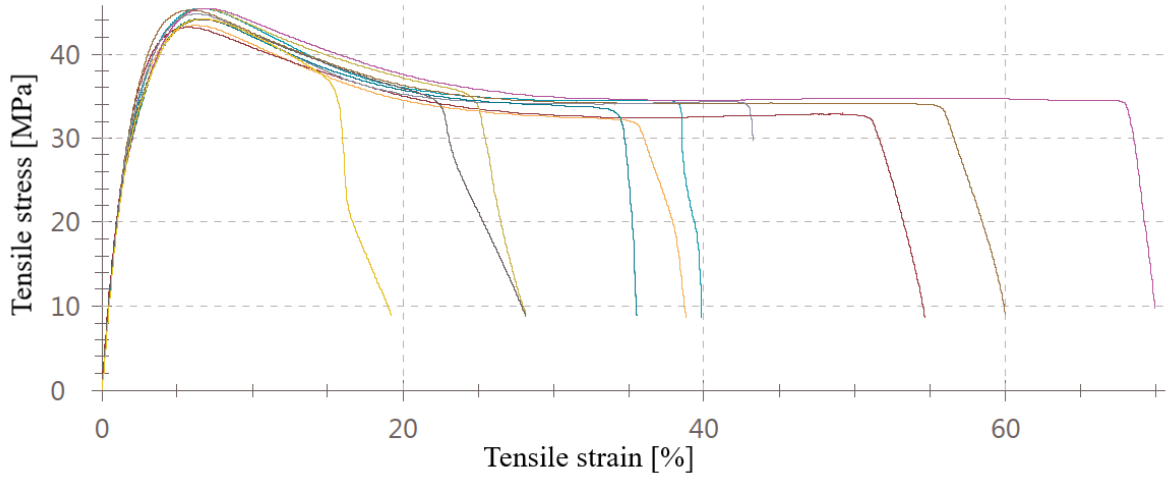

Fig. 4.15. Tensile stress–strain curves for PVC specimens. Source: Author's own work

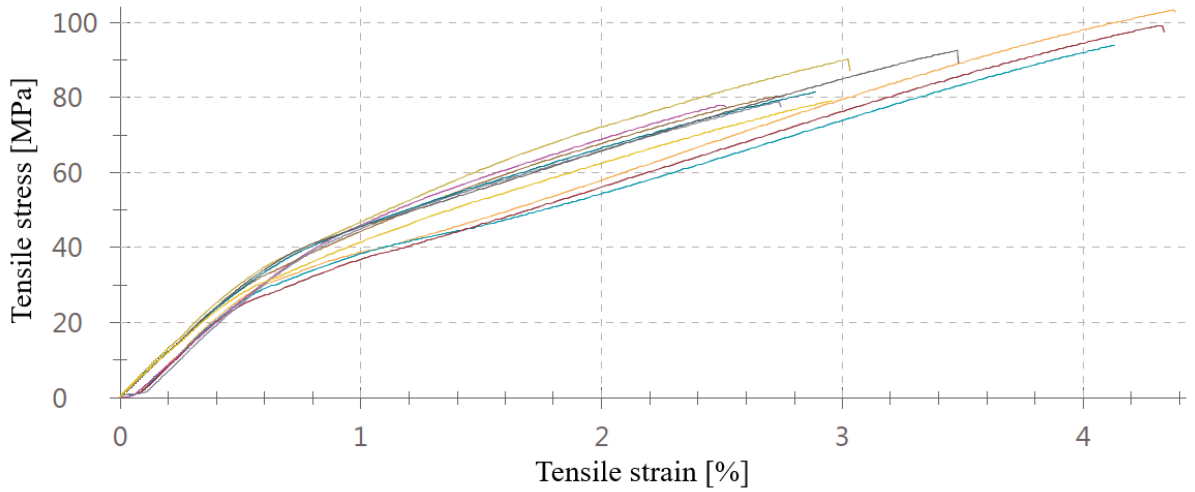

Fig. 4.16. Tensile stress–strain curves for glass-fibre-reinforced composite specimens. Source: Author's own work

The tensile curve for PVC (Fig. 4.15) indicates greater deformation than that of the composite. The onset of material discontinuity occurs at approximately 5–7% strain and corresponds to a stress of around 42 MPa. Complete rupture occurs at varying strains, typically above about 19%. Once damage initiates, subsequent separation proceeds differently for each specimen. For the glass-fibre-reinforced composite (Fig. 4.16), the corresponding strains are generally lower, which evidences a limited deformation capacity in the terminal stage and a characteristically abrupt fracture, governed by the dominant role of stiff fibres within the structure. The discrepancy between total elongation at break and the strain at the point of final rupture is substantially larger for PVC than for the composite, which further supports the more ductile character of PVC and its ability to undergo larger deformation prior to catastrophic rupture. In contrast, the composite, due to the presence of glass fibres, exhibits similar values for these parameters, leading to a rapid failure process. The phase of intensive damage can be identified at approximately 0.6% strain and a stress of around 30 MPa. As for PVC, this stage is broadly similar across all tested specimens. This contrast in failure behaviour aligns with the earlier findings for elastic modulus and maximum stress, underscoring the fundamental differences between the more ductile PVC and the stiffer, mechanically stronger composite.

Figure 4.17 presents the mean flexural modulus values for the PVC and composite specimens.

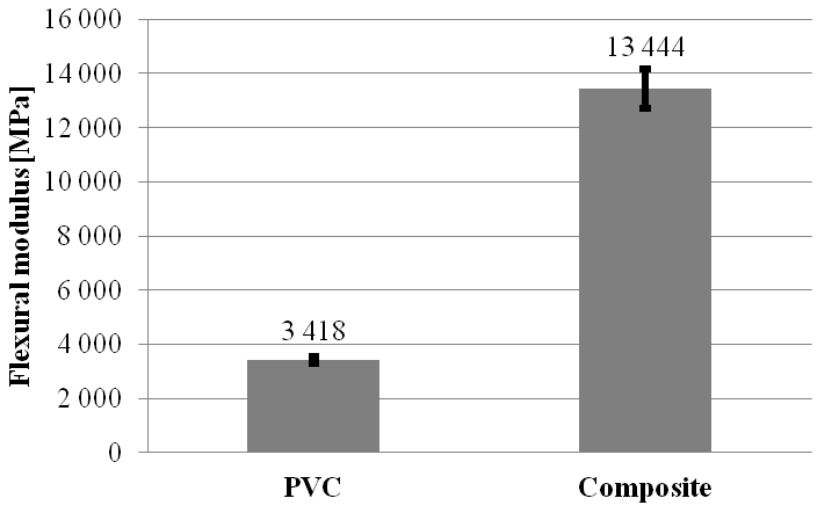

Fig. 4.17. Mean flexural modulus values for PVC and composite specimens. Source: Author's own work

The glass-fibre-reinforced composite exhibits a substantially higher flexural modulus of 13,444 MPa than PVC, which reached 3,418 MPa (Fig. 4.17). This indicates greater stiffness and enhanced resistance to deformation under bending loads. The presence of glass fibres therefore improves load transfer and raises mechanical performance, whereas PVC remains comparatively more compliant.

Figure 4.18 illustrates the mean compressive stress values generated during bending of the composite specimens.

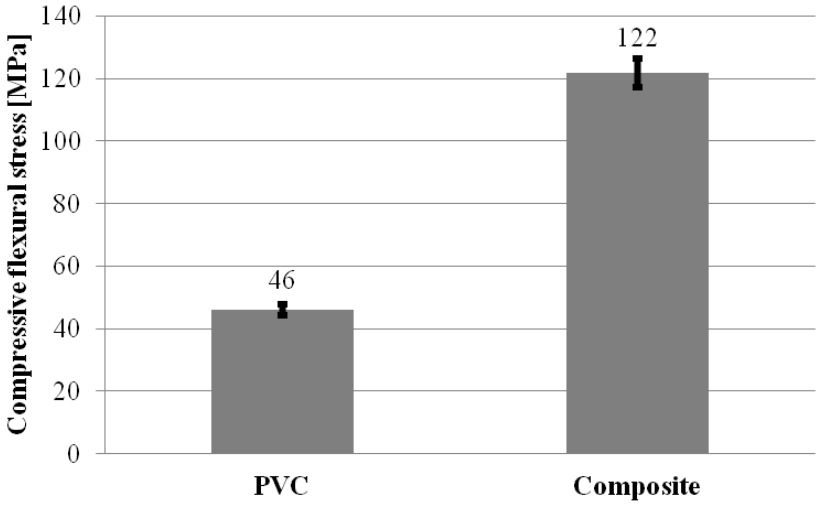

Fig. 4.18. Mean flexural compressive stress values for PVC and composite specimens. Source: Author's own work

The bending results (Fig. 4.18) show higher compressive stresses for the composite, reaching 122 MPa, which suggests that the material can sustain greater compressive loading before damage initiates than PVC. By contrast, PVC exhibited markedly lower stresses of approximately 46 MPa and is therefore more prone to cracking or permanent damage under comparable conditions. These data confirm that glass-fibre reinforcement increases not only

stiffness but also resistance to compressive stresses, making the composite well suited to applications governed by bending loads.

During the test programme, PVC specimens were also assessed by determining the force associated with a deformation equal to 2% of the initial specimen length, which yielded a mean value of 46 N. In addition, the maximum flexural stress was evaluated, defined as the highest stress sustained before the onset of cracking or irreversible deformation. For PVC, the mean value was 71 MPa. The strain at maximum flexural stress was also determined and averaged 4% for the PVC specimens.

The flexural stress as a function of strain for the PVC specimens is shown in Fig. 4.19.

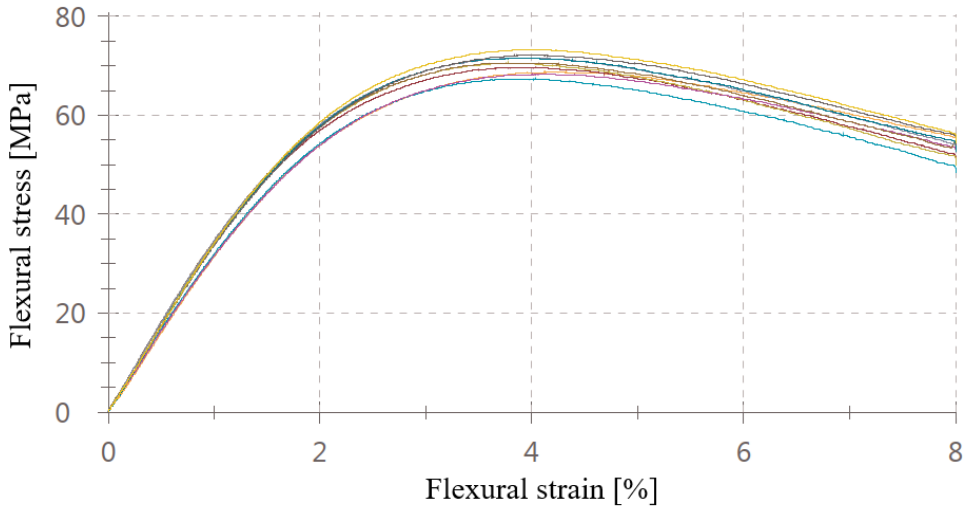

Fig. 4.19. Flexural stress–strain curves for PVC specimens. Source: Author's own work

For PVC, the results in Fig. 4.19 indicate a relatively high deformation capacity while retaining a degree of ductility. The characteristic curve shows an extended elasto-plastic regime in which stress increases progressively with strain. A maximum strain of 8% prior to cracking, observed consistently across the specimens, indicates both material uniformity and substantial compliance, despite the lower modulus compared with the composite. These findings also suggest that PVC can absorb more energy than the composite, because damage accumulates more gradually and the approach to final failure is less abrupt.

Figure 4.20 shows the flexural stress as a function of strain for the composite specimens.

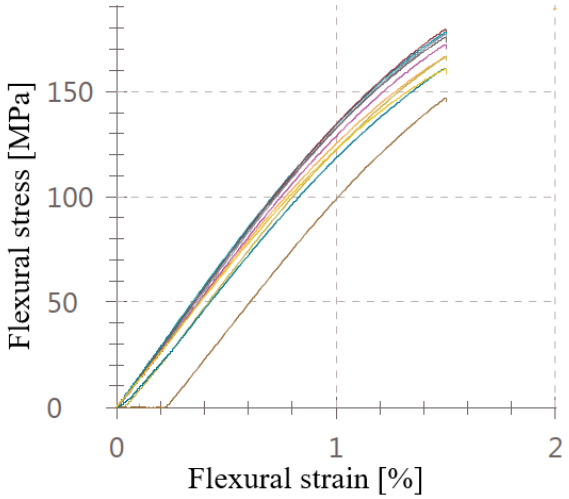

Fig. 4.20. Flexural stress–strain curves for glass-fibre-reinforced composite specimens. Source: Author's own work

As shown in Fig. 4.20, the glass-fibre-reinforced composite exhibits a very high stiffness, which inherently limits the attainable strain prior to cracking. The curves display a steep initial segment that remains close to linear almost until failure, which is consistent with a highly rigid response and rapid stress build-up under bending. The strain remains limited to approximately 1.5%, indicating that the energy absorbed prior to fracture is low. This confirms that the composite transfers loads efficiently, albeit at the expense of sustained deformation capacity, and aligns with the observed abrupt fracture mechanism of the tested specimens.

Figure 4.21 summarises the hardness measurements for the tested PVC and composite specimens.

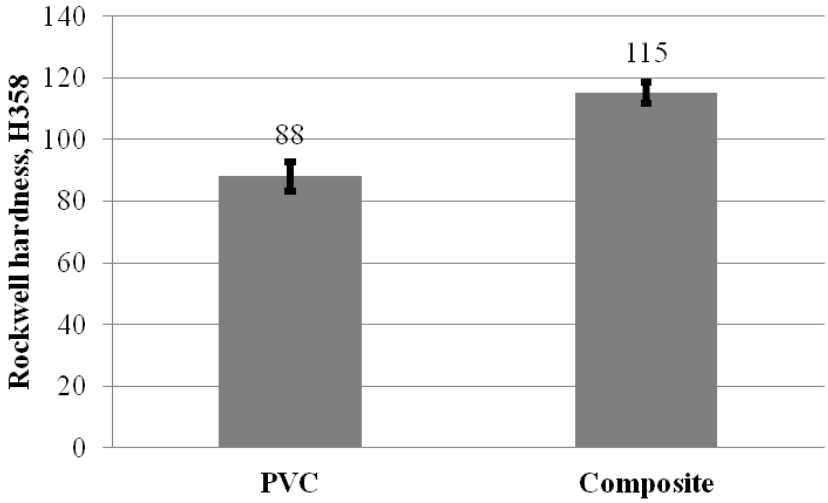

Fig. 4.21. Rockwell hardness test results for the tested PVC and composite specimens. Source: Author's own work

The mean hardness values obtained for the PVC and composite specimens differ, which indicates dissimilar resistance to indentation and local deformation in the two materials (Fig. 4.21). The limited scatter observed in both datasets suggests good material uniformity. The

higher mean hardness of the composite, reaching 115 N/mm² with stable readings, indicates greater deformation resistance than PVC, for which the mean hardness was approximately 88 N/mm².

In order to complement the mechanical characterisation of the composite insert, the glass-fibre content was also determined, as this parameter directly affects the stiffness, hardness, and overall reinforcement efficiency of the material. The measured glass-fibre contents of the two composite specimens, namely 52.41% and 52.08%, were closely aligned. This proximity indicates high measurement repeatability and consistent properties across the tested material. On this basis, the mean glass-fibre content for the two specimens can be taken as 52.25%. The results therefore suggest that the specimens exhibited near-identical reinforcement levels.

The Vicat softening temperature was 89 °C for the first PVC specimen and 90 °C for the second. The small difference primarily indicates a very similar chemical composition of the specimens. Such a deviation may reflect minor production variability or measurement resolution, which further supports the conclusion that the specimens are materially uniform. Moreover, values in the range 89–90 °C are typical for PVC used in window profiles. This implies that the tested specimens most likely originated from a standard-grade material commonly employed in this application.

According to the thermal resistance (HDT) results, the mean temperature for PVC was 73 °C, whereas the composite reached 202 °C. For PVC, this value is lower when set against the mean Vicat softening temperature of 90 °C. In the patent application WO2009053959A2, an unplasticised PVC product incorporating a thermosetting system was reported to exhibit an HDT above 65 °C, while an unplasticised PVC with an epoxy-based interpenetrating network achieved an HDT above 75 °C. Study [136] also addressed HDT, analysing unplasticised PVC with three stabilisation systems, namely lead-stabilised, calcium–zinc-stabilised, and an organic heavy-metal-free stabiliser. The reported values were 76 °C, 75 °C, and 74.5 °C, respectively. Against this background, the measured HDT for the PVC profile specimens can be regarded as expected and broadly comparable to literature values. A higher HDT indicates improved resistance to heat-induced deflection under the specified mechanical load. However, these results do not, on their own, define the maximum permissible service temperature of the final product.

Figure 4.22 provides a consolidated comparison of FTIR-ATR spectra for five PVC profile specimens, whereas Figures 4.23–4.27 present the spectra individually with characteristic absorption bands highlighted. Across Figures 4.22–4.27, the spectra show a high degree of concordance in absorption profiles for all five specimens, which supports the chemical consistency of the profile material at the sampled locations. Each spectrum contains the characteristic set of bands associated with C–H stretching and with the fingerprint region, and peak positions differ only marginally, typically by a few wavenumbers. Such small shifts are common in ATR series and usually reflect variations in contact conditions or local surface structure rather than a change in functional group identity.

The band observed between 2850 and 3000 cm^{-1} corresponds to C–H stretching vibrations in aliphatic groups, which is consistent with the characteristic absorption window for saturated hydrocarbons. In the high-wavenumber region, each specimen shows two dominant aliphatic C–H stretching bands near 2920 cm^{-1}, specifically 2916.81–2919.70 cm^{-1}, and near 2851 cm^{-1}, specifically 2850.27–2851.24 cm^{-1}. This confirms the presence of an organic polymer backbone. In addition, two spectra (Figs. 4.23 and 4.24) show a weak band near 3690

cm^{-1}, specifically 3689.16–3693.98 cm^{-1}, which falls within the O–H stretching range of 3500–3700 cm^{-1}. Because this signal is not reproduced across all specimens, the most defensible interpretation is a variable surface contribution, such as adsorbed moisture or local surface contamination, rather than a systematic difference in the bulk formulation.

In the carbonyl region, bands are observed between 1730 and 1741 cm^{-1}. The maxima occur at 1730.8 cm^{-1} for the first specimen, 1729.83 cm^{-1} for the second, 1739.48 cm^{-1} for the fourth, and 1741.41 cm^{-1} for the fifth, consistent with C=O vibrations. The absence of a reported peak for the third specimen should be interpreted in light of the peak-picking routine, which typically lists only maxima exceeding a predefined threshold. In practice, a carbonyl band may still be present but weaker or less distinct against the baseline. Such a distribution is typical of industrial materials, in which the carbonyl signal can originate from formulation constituents, for example ester-type additives, or from mild surface-related changes. Given the overall spectral consistency, this does not constitute evidence that any specimen represents a materially different substrate.

Within the fingerprint region, where numerous closely spaced bands provide a material-specific signature, all specimens exhibit a repeatable set of features between approximately 1500 and 400 cm^{-1}, which together form a distinctive spectral profile. A strong band near 1420–1421 cm^{-1} is particularly stable, specifically 1420.32–1421.28 cm^{-1}, alongside bands near 1329–1331 cm^{-1}, 1245–1249 cm^{-1}, and 1095–1096 cm^{-1}. Below 1000 cm^{-1}, repeatable maxima occur near 961–964 cm^{-1} and at about 874.6 cm^{-1}. In the 700–600 cm^{-1} interval, bands appear near 683–686 cm^{-1} and 609–611 cm^{-1}, which fall within the C–Cl stretching window of 600–800 cm^{-1}. This lower-fingerprint pattern is consistent with PVC and provides the strongest basis for concluding that all profile specimens represent the same material type.

Among the less frequent features, a band at 1796.37 cm^{-1} appears in the first, second, and fourth specimens, and a single band at 2518.58 cm^{-1} appears in the first specimen. Because these signals do not occur consistently across the entire set, the most methodologically cautious approach is to treat them as potentially dependent on peak detection settings, baseline behaviour, or local ATR contact conditions. Given their low reproducibility within the series, they do not provide a robust basis for inferring distinct chemical compositions among the specimens.

Overall, the FTIR-ATR results for the five PVC profile specimens indicate chemical consistency across the series. The dominant C–H stretching bands and the stable fingerprint pattern, including the characteristic bands between 600 and 800 cm^{-1} associated with C–Cl vibrations, are coherent for all specimens. The observed differences primarily concern the presence or intensity of surface-related O–H features and the weaker, less consistently reported signals in the carbonyl region. In ATR geometry, such variability is compatible with the influence of sample contact, local surface heterogeneity, and contributions from formulation additives, while providing no evidence for a change in material identity between specimens.

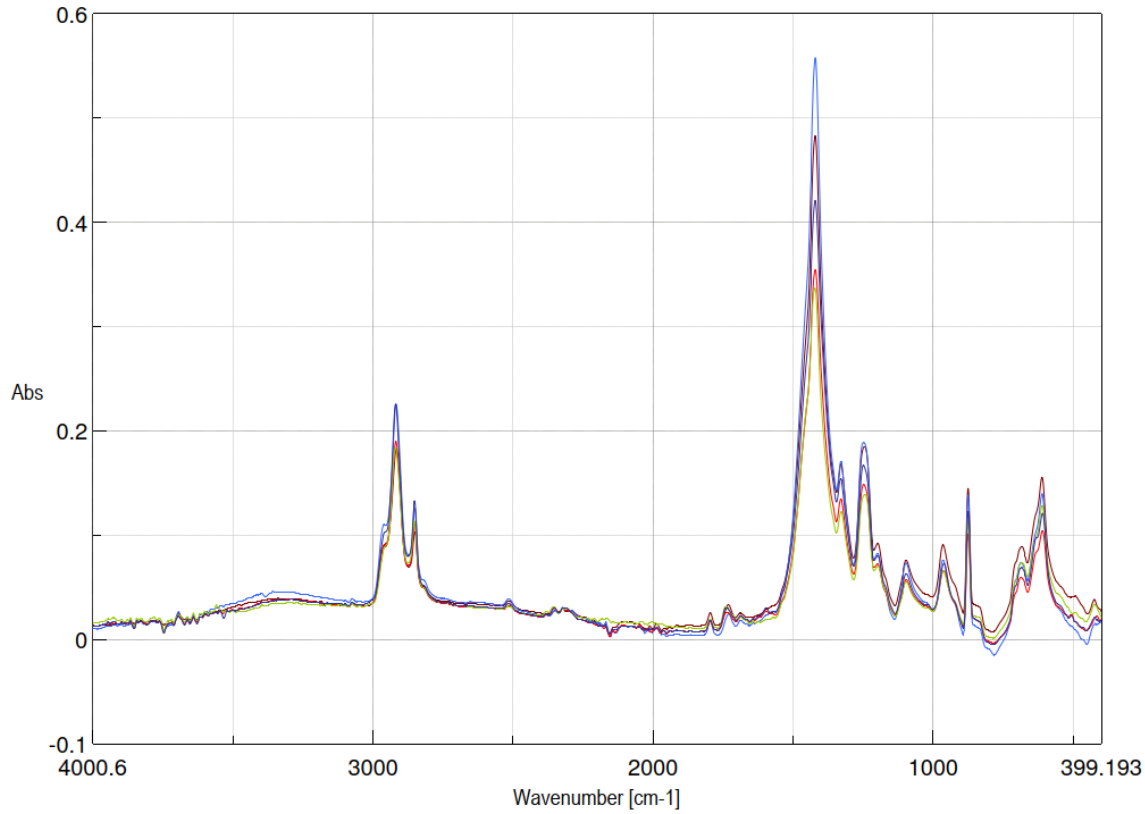

Fig. 4.22. Comparison of FTIR-ATR spectra of PVC profile specimens. Source: Author's own work

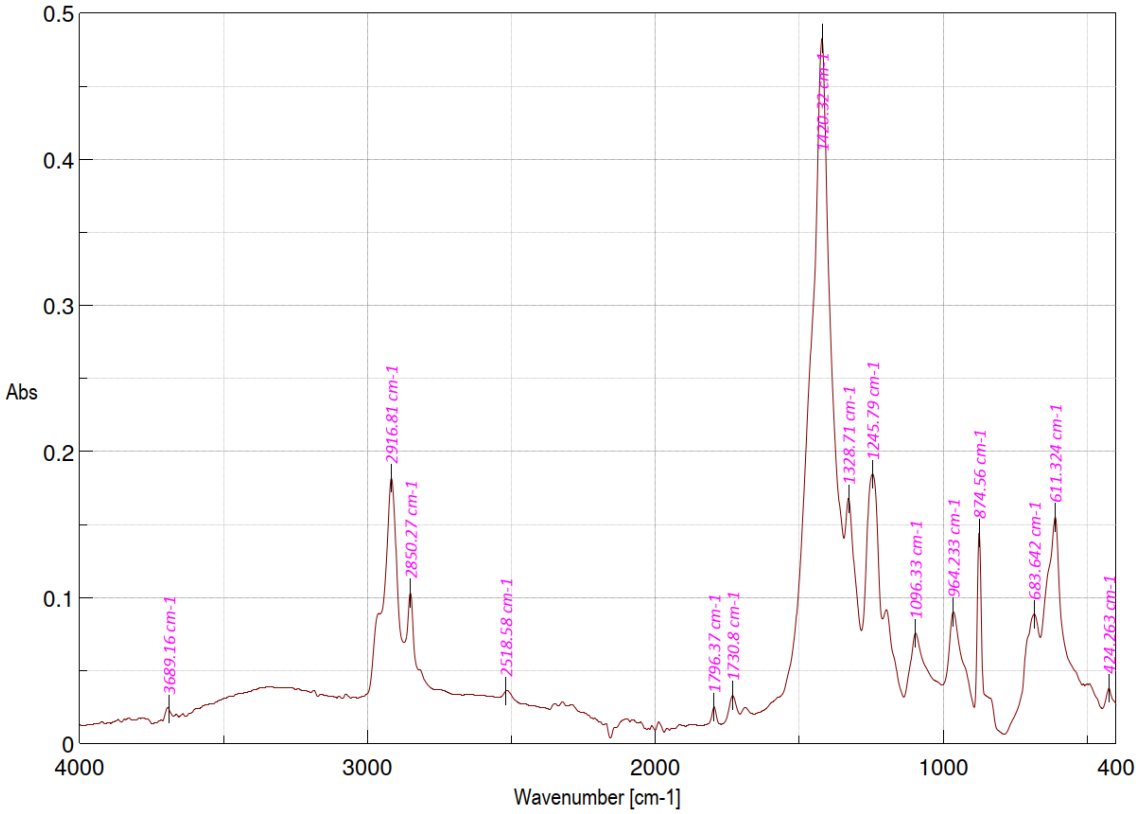

Fig. 4.23. Spectrum of the first PVC profile specimen. Source: Author's own work

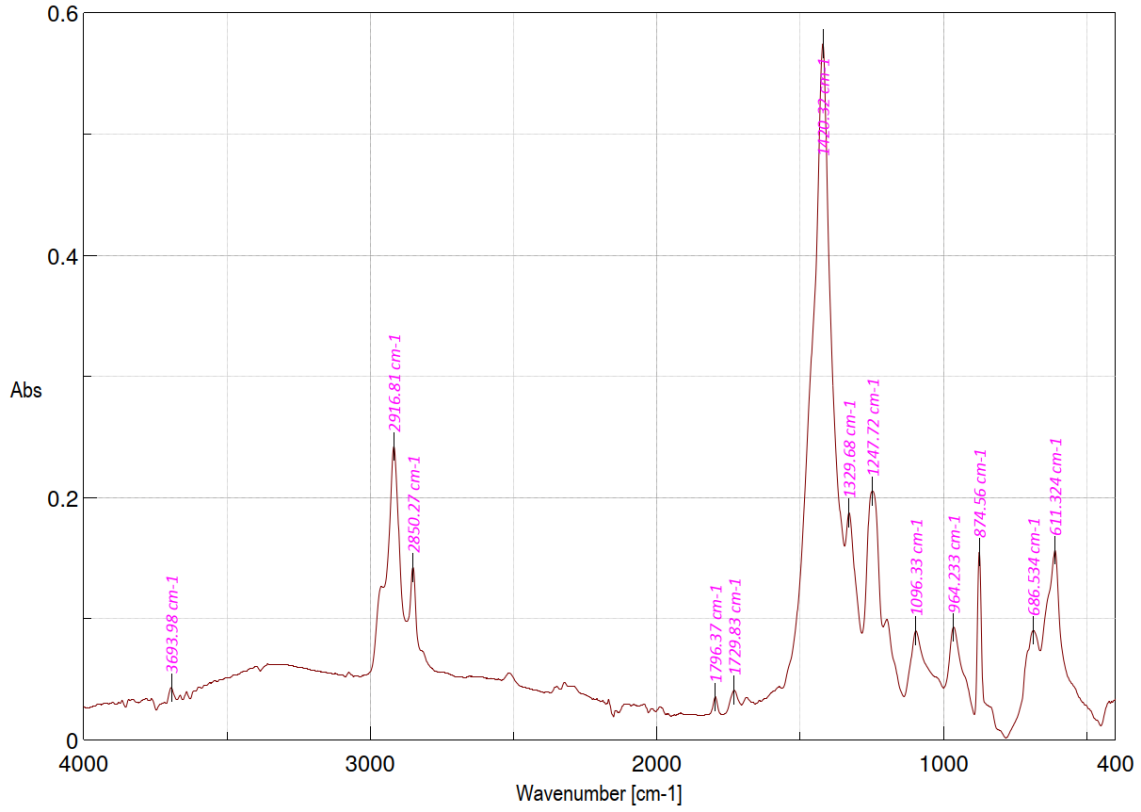

Fig. 4.24. Spectrum of the second PVC profile specimen. Source: Author's own work

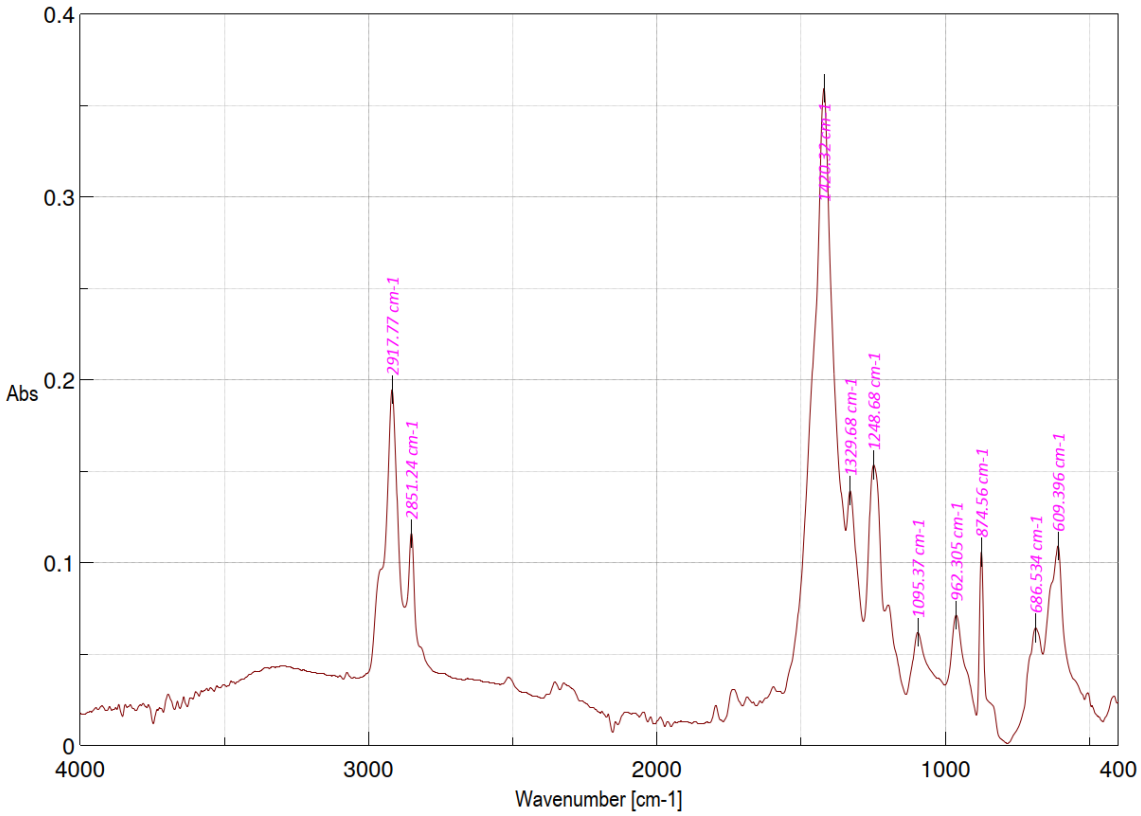

Fig. 4.25. Spectrum of the third PVC profile specimen. Source: Author's own work

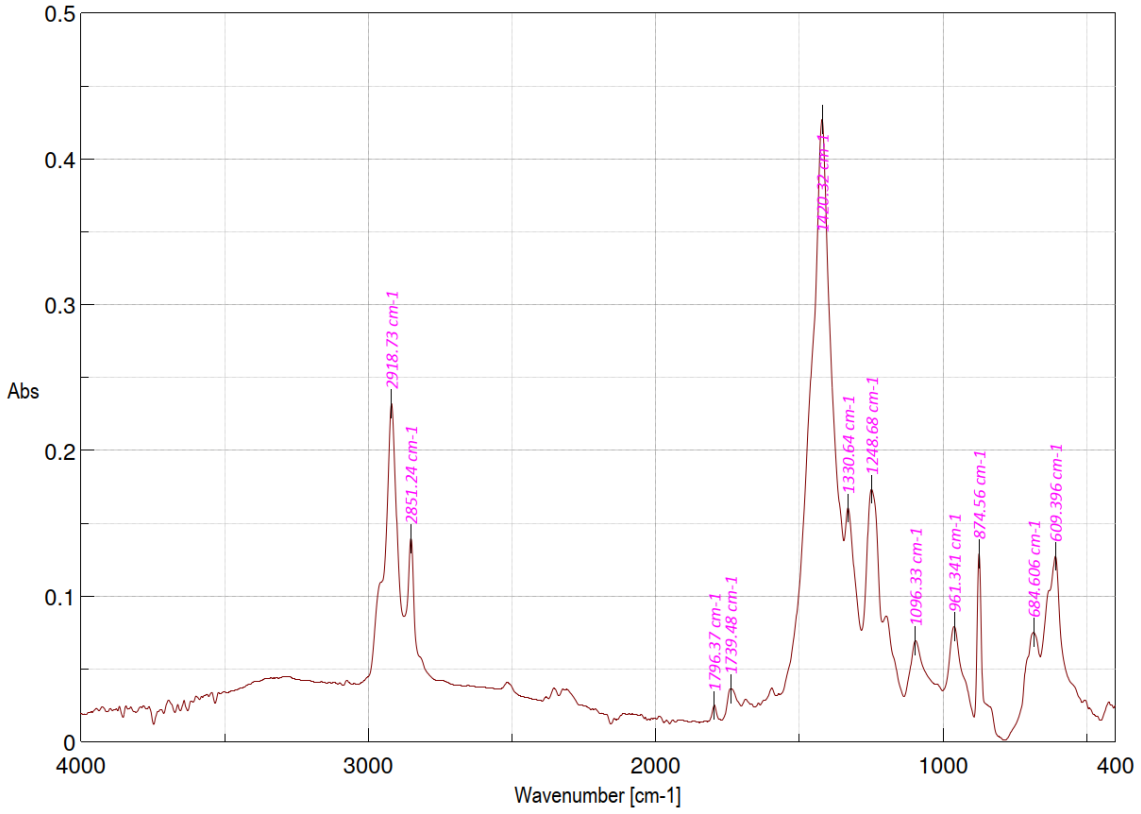

Fig. 4.26. Spectrum of the fourth PVC profile specimen. Source: Author's own work

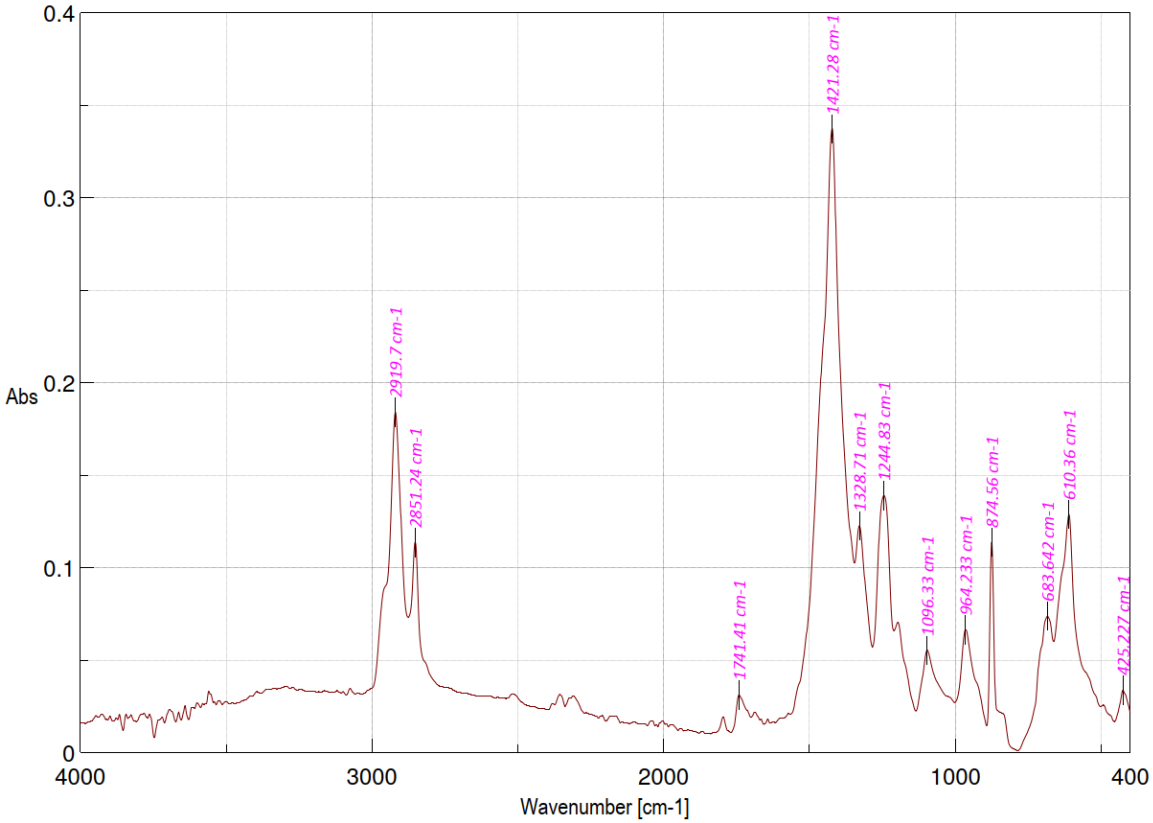

Fig. 4.27. Spectrum of the fifth PVC profile specimen. Source: Author's own work

Figure 4.28 compares the spectrum of the first PVC profile specimen with a reference spectrum for poly(vinyl chloride). From Fig. 4.28, it can be inferred that the profile specimen

exhibits very close agreement with the PVC reference spectrum, most notably within the fingerprint region, approximately 1500–600 cm^{-1}, which is the most discriminative domain for polymer identification. The principal maxima within this region coincide. The profile specimen shows peaks, among others, at about 1420 cm^{-1}, 1329 cm^{-1}, 1246 cm^{-1}, 1096 cm^{-1}, 964 cm^{-1}, and 684 cm^{-1}, whereas the reference spectrum displays very similar positions at about 1428 cm^{-1}, 1330 cm^{-1}, 1254 cm^{-1}, 1096 cm^{-1}, 964 cm^{-1}, and 682 cm^{-1}. This convergence in both peak positions and the overall fingerprint pattern provides practical evidence that the profile material is chemically consistent with PVC as the dominant polymer matrix.

Agreement is also evident within the C–H stretching region. The profile specimen exhibits bands at about 2917 cm^{-1} and 2850 cm^{-1}, whereas the library reference reports bands in this zone at around 2910 cm^{-1} and 2968 cm^{-1}. Minor differences in peak position and relative intensity are expected, because the profile spectrum was acquired in ATR mode, which is strongly influenced by specimen–crystal contact. By contrast, library spectra are often recorded using different geometries, such as transmission, which can alter band shapes and apparent intensities without changing the underlying material identification.

The most consequential differences between the profile spectrum and the reference relate to auxiliary bands that do not constitute the core fingerprint signature and may arise from industrial formulation constituents or ATR surface effects. Specifically, the profile specimen shows a band at 1730.8 cm^{-1} attributed to C=O vibrations, as well as weaker signals near 1796 cm^{-1} and near 3689 cm^{-1} associated with O–H stretching, which are not reported as peaks in the reference spectrum.

On this basis, the investigated profile can be identified primarily as poly(vinyl chloride), which forms the matrix, whereas the presence of carbonyl and hydroxyl signals may indicate contributions from additives, for example ester-type components, or other minor constituents. This does not challenge the identification of PVC as the principal material, because the decisive fingerprint bands remain consistent with the reference.

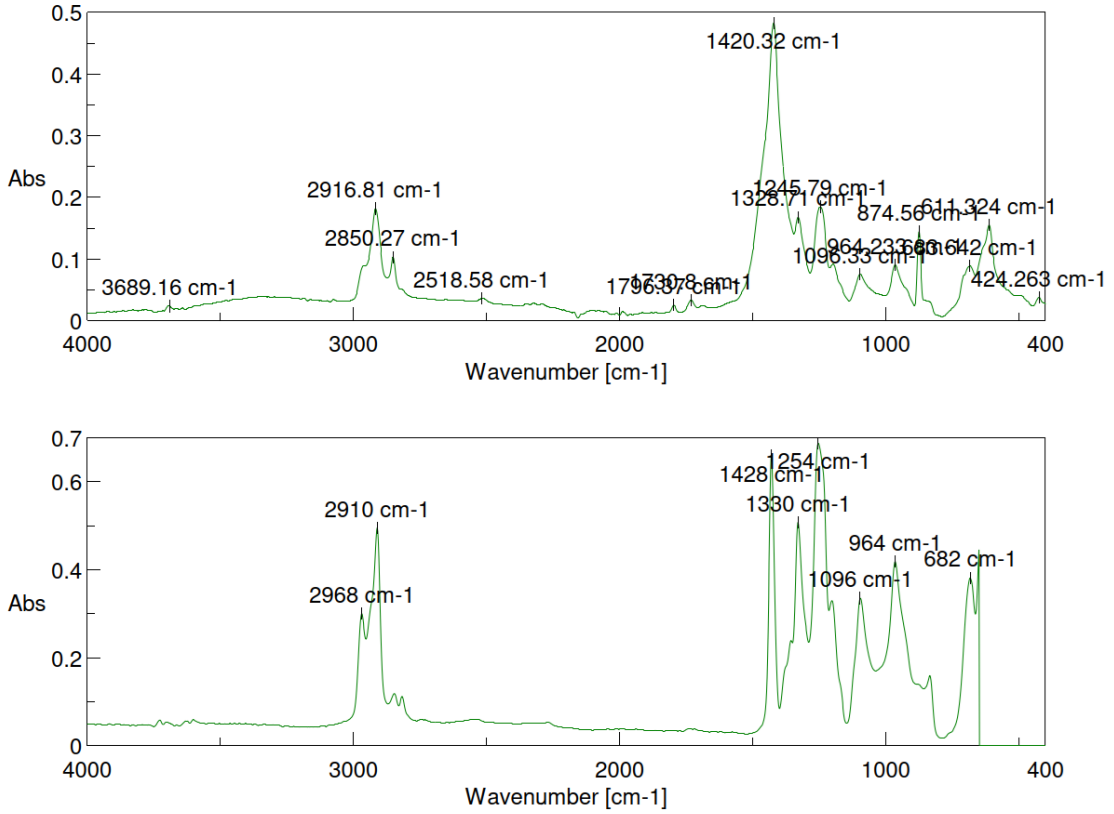

Fig. 4.28. Comparative spectra of the first PVC profile specimen (upper) and a reference poly(vinyl chloride) spectrum (lower). Source: Author's own work

Figure 4.29 presents an aggregated comparison of FTIR-ATR spectra for two glass-fibre-reinforced composite specimens used as reinforcement in PVC window profiles, whereas Figures 4.30 and 4.31 show the spectra individually with characteristic absorption bands marked. The comparison in Fig. 4.29 indicates that both composites share essentially the same spectral backbone. Bands associated with C–H vibrations and the fingerprint region below 1500 cm^{-1} dominate, and the principal maxima occur at closely matching positions. Both spectra also show a strong band near 1708–1709 cm^{-1}, which lies within the carbonyl window of 1650–1750 cm^{-1}. This feature suggests the presence of carbonyl-containing constituents, such as a resinous component, a modifier, or oxidation-related products, thereby distinguishing the composite from neat PVC, which is primarily characterised by bands associated with a chloro-organic matrix.

Within the 2850–3000 cm^{-1} interval, aliphatic C–H stretching bands are observed. The first specimen, shown in Fig. 4.30, displays a full set of three bands at 2959.23 cm^{-1}, 2921.63 cm^{-1}, and 2852.2 cm^{-1}, whereas the second specimen, shown in Fig. 4.31, exhibits a pronounced maximum near 2920.66 cm^{-1}. In practical terms, both materials contain a dominant aliphatic, organic component, while the difference in the number of detected peaks is more plausibly associated with detection thresholds and intensity variations inherent to ATR than with a substantive change in chemical composition.

Within the fingerprint region, the two composites are highly concordant. Shared bands include those near 1454–1455 cm^{-1}, 1407.78 cm^{-1}, 1245.79 cm^{-1}, 1097–1098 cm^{-1}, 1015–1016 cm^{-1}, 871.667 cm^{-1}, and 723.175 cm^{-1}. Bands in the approximate range of 1050–1430 cm^{-1} may be associated with C–O vibrations, whereas the 600–800 cm^{-1} interval can coincide with C–Cl vibrations. However, the presence of a single band near 723 cm^{-1} is not, on its

own, sufficient evidence for C–Cl bonds, because similar positions may also arise from other hydrocarbon vibrations or composite constituents. Accordingly, any inference regarding chlorine should be grounded in the full characteristic band pattern rather than in one isolated maximum within a broad interval.

The differences between the two specimens, shown in Figs. 4.30 and 4.31, are localised and predominantly concern bands present only in the first specimen (Fig. 4.30), namely those near 1504.2 cm^{-1} and 934.342 cm^{-1}, alongside additional C–H bands near 2959 cm^{-1} and 2852 cm^{-1}. Because the second specimen (Fig. 4.31) retains the remaining bands in the same spectral regions, it can be inferred that both composites are chemically very similar. The first specimen may therefore reflect a slightly different surface contribution from the constituent responsible for the bands near 1504 cm^{-1} and 934 cm^{-1}, or it may simply have been acquired under conditions that yielded a different peak-picking outcome.

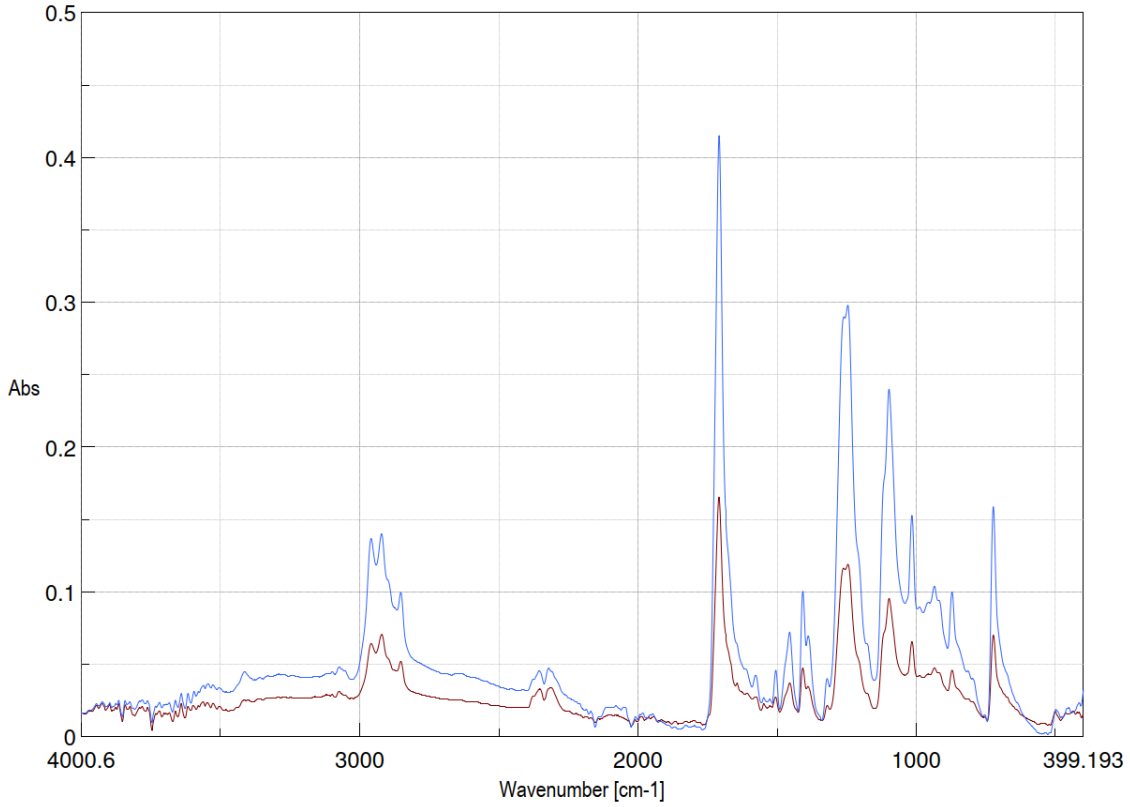

Fig. 4.29. Comparison of FTIR-ATR spectra of composite profile specimens. Source: Author's own work

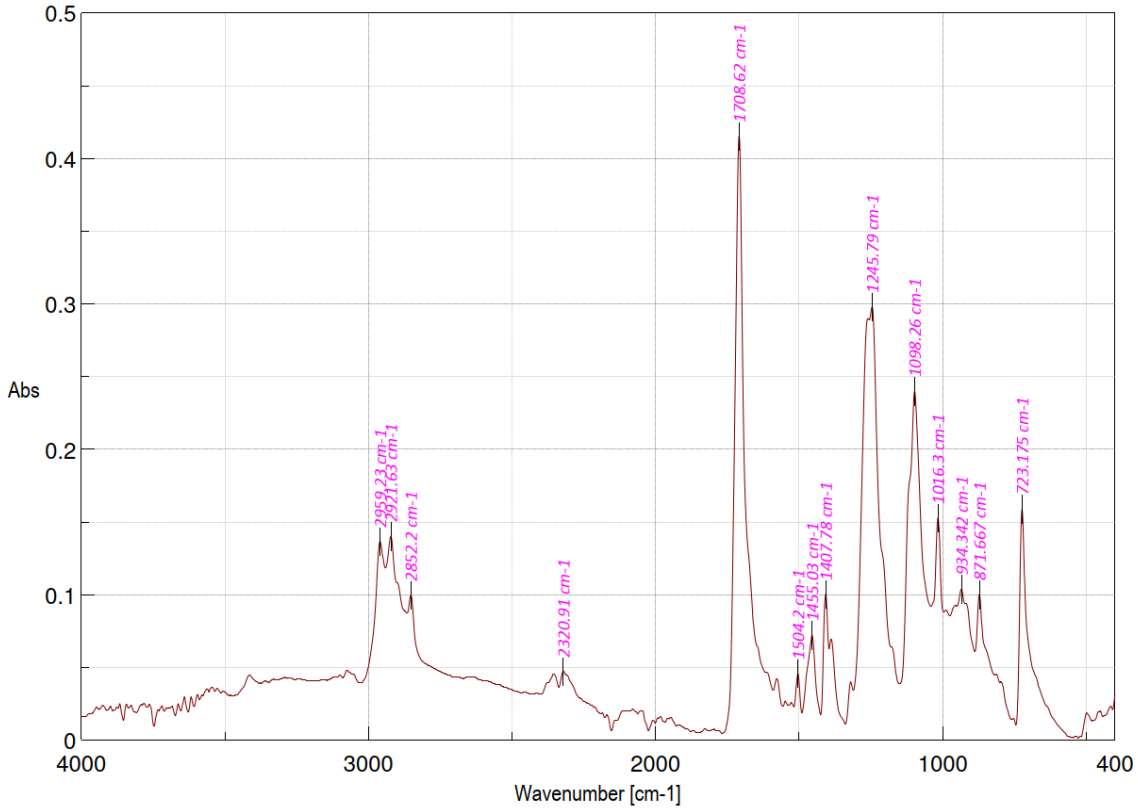

Fig. 4.30. Spectrum of the first composite profile specimen. Source: Author's own work

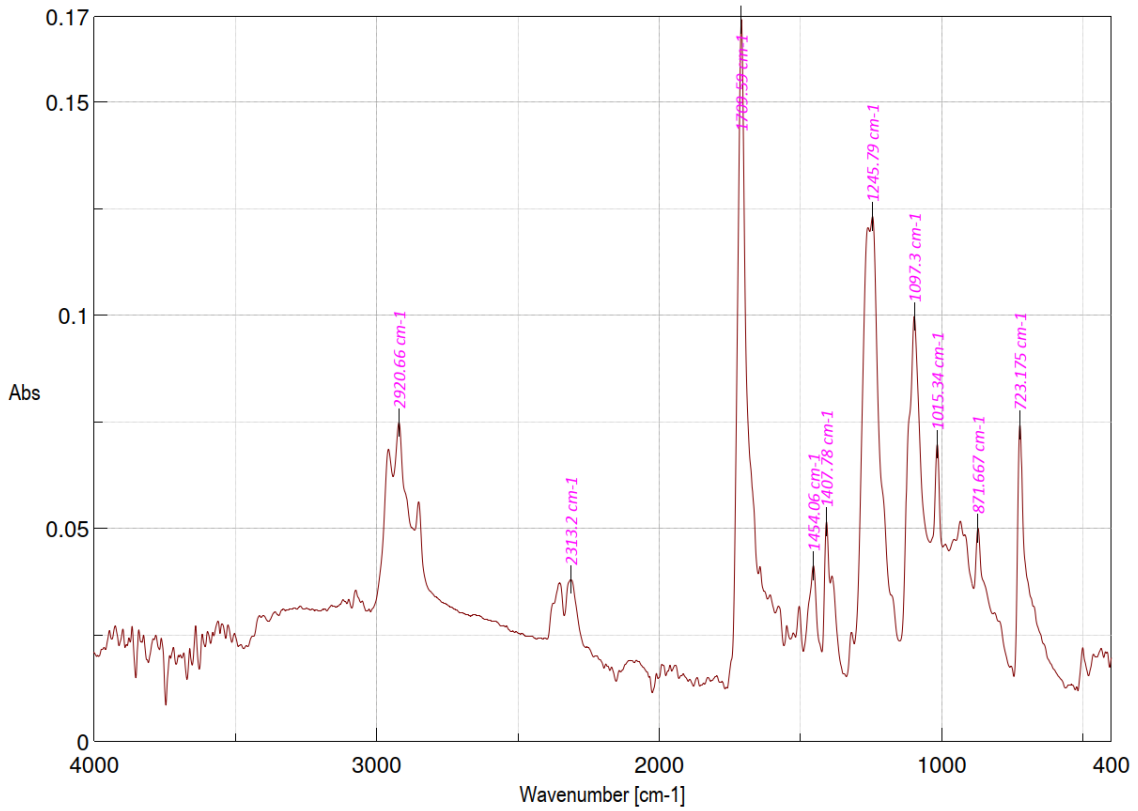

Fig. 4.31. Spectrum of the second composite profile specimen. Source: Author's own work

Figure 4.32 compares the spectrum of the first composite specimen with a reference spectrum for polyester. The correspondence is particularly pronounced in polyester-diagnostic

regions, namely the strong carbonyl band associated with C=O vibrations and the fingerprint region, approximately 1500–600 cm^{-1}, where the band pattern is most discriminative for polymer identification. The composite specimen exhibits a very intense peak at 1708.62 cm^{-1}, while the polyester reference shows an analogous strong band at about 1722 cm^{-1}. Both lie within the carbonyl window of 1650–1750 cm^{-1} and constitute a characteristic marker for ester functionalities.

Within the fingerprint region, numerous near-matching band pairs are observed, which strengthens the inference of chemical similarity. For the composite specimen, peaks can be identified at about 1504.2 cm^{-1}, 1455.03 cm^{-1}, 1407.78 cm^{-1}, 1245.79 cm^{-1}, 1098.26 cm^{-1}, 1016.3 cm^{-1}, 871.667 cm^{-1}, and 723.175 cm^{-1}. The polyester reference shows corresponding bands at about 1506 cm^{-1}, 1456 cm^{-1}, 1410 cm^{-1}, 1244 cm^{-1}, 1100 cm^{-1}, 1018 cm^{-1}, 874 cm^{-1}, and 728 cm^{-1}. Agreement at this level, with differences of only a few cm^{-1}, is typical when an industrial specimen is compared against a library spectrum. At the same time, it provides practical identification evidence that the investigated composite retains the characteristic polyester band pattern.

In the aliphatic C–H stretching zone, from 2850 cm^{-1} to 3000 cm^{-1}, the composite specimen shows bands at 2959.23 cm^{-1}, 2921.63 cm^{-1}, and 2852.2 cm^{-1}, whereas the polyester reference reports a band near 2964 cm^{-1}. Differences in the number of detected bands and their relative intensities in this region are expected, because reference spectra are commonly acquired in transmission, whereas the present measurements were recorded by ATR under laboratory conditions. In ATR, band intensities depend strongly on specimen–crystal contact and the near-surface layer. For this reason, material identification should be driven primarily by concordance in the positions of key bands rather than by an exact match in peak heights.

The remaining discrepancies between the composite spectrum and the reference are local and can be attributed to the composite formulation, in which additional constituents may be present, including fillers, curing-related species, or other modifiers. They may also reflect measurement conditions. The composite specimen shows an O–H band at 3421.1 cm^{-1}, while the reference indicates a band near 3434 cm^{-1}. In composites, this can be associated with surface moisture or with constituents containing hydroxyl groups. The specimen also displays a band at 2320.91 cm^{-1}, which very frequently corresponds to atmospheric CO_2 contributions and is therefore typically treated as background rather than as a material-specific band.

At the same time, the polyester reference contains additional bands, including those near 792 cm^{-1}, 972 cm^{-1}, 1340 cm^{-1}, 1372 cm^{-1}, and 500 cm^{-1}, which the peak-picking routine did not report for the composite specimen. This does not undermine the identification, because automated reports may omit bands due to detection thresholds, band overlap, or different baseline characteristics. Moreover, in composite materials the polymer signal can be altered by fillers and surface structure. The decisive point is that the composite spectrum contains a strong carbonyl C=O band in the region around 1700–1730 cm^{-1}, which is typical for polyester materials and is likewise present in the reference spectrum. In addition, the fingerprint region, approximately 1500–600 cm^{-1}, includes a band set consistent with C–O vibrations, including ester-associated contributions often described as C–O–C, alongside skeletal C–C vibrations. The fact that these key bands occur at closely matching positions in cm^{-1} provides qualitative confirmation that the investigated composite has a matrix chemically consistent with polyester.

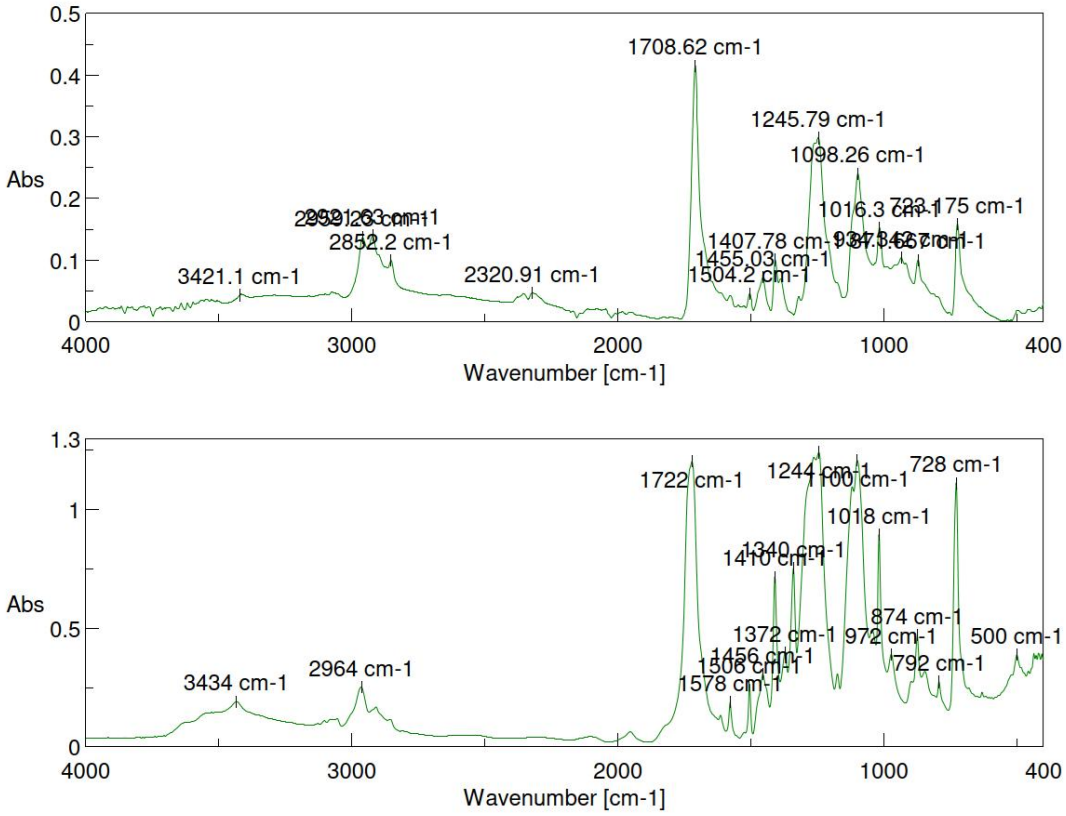

Fig. 4.32. Comparative spectra of the first composite profile specimen (upper) and a reference polyester spectrum (lower). Source: Author's own work

The study focused on a multi-criteria assessment of how incorporating composite reinforcement into PVC window solutions affects the mechanical and thermal performance of the material system. A comparative approach was adopted, in which the base PVC-U material was evaluated against the composite intended to serve as reinforcement.

The determined mass fraction of glass fibre in the composite material was approximately 52%. In tensile testing, PVC-U exhibited a Young's modulus of approximately 2 GPa, a tensile strength of 45 MPa, and an elongation at break of 42%, which confirms the ductile character of the base material. These values are consistent in order of magnitude with literature data for PVC-U, where, at ambient temperature, a tensile strength of approximately 52 MPa and an elastic modulus of about 3 GPa have been reported, alongside a pronounced temperature dependence of the properties. The modest differences in modulus and strength can reasonably be associated with formulation differences, including the content of fillers and stabilisers, specimen geometry, and processing regime, all of which can materially affect the elasto-plastic response of PVC-U [191].

The composite exhibited a response characteristic of fibre reinforcement. The Young's modulus was approximately 5.85 GPa and the tensile strength 88 MPa, while elongation decreased to 3%. This indicates that a greater share of the load is carried by the reinforcement and that the capacity for stress relaxation within the matrix is reduced. This behaviour is beneficial where profile deflections must be minimised, yet it reduces the available strain reserve prior to crack initiation. Etcheverry and Barbosa reported a comparable order of magnitude for glass-fibre composites with high reinforcement levels, for which the elastic modulus reached approximately 8.1–8.9 GPa and the tensile strength approximately 102–105 MPa [192]. The values obtained here are lower, which is consistent with the strong

dependence of composite properties on fibre fraction, fibre orientation, wet-out quality, interfacial adhesion, and matrix type.

An analogous trend was observed in bending tests. For PVC-U, the flexural modulus was approximately 3.4 GPa and the flexural strength 46 MPa, whereas for the composite the respective values were approximately 13.4 GPa and 122 MPa. This corresponds to an almost fourfold increase in stiffness and a more than 2.5-fold increase in bending load capacity for the composite relative to PVC, which directly supports reduced deflections of elements subjected to wind loads and the weight of insulating glazing units. At the same time, the impact results indicate increased notch sensitivity. In the unnotched configuration, PVC-U did not fail, while the composite reached approximately 25 kJ/m². In the notched configuration, the values were 15 kJ/m² for PVC-U and 6 kJ/m² for the composite. This pattern is typical of fibre-reinforced composites, where fibres enhance stiffness and strength, yet stress concentrators promote earlier crack initiation and reduce the contribution of matrix plasticity to energy dissipation [192].

In thermal testing, PVC-U exhibited an HDT of approximately 73 °C, which is broadly consistent with the range reported for rigid PVC formulations, typically around 74.5–76 °C depending on the Pb/CaZn/organic stabilisation system [136]. The Vicat softening temperature remained within approximately 89–90 °C, which suggests that the onset of macroscopic softening occurs at a similar temperature level for the tested material set. The critical distinction instead concerns stiffness retention under sustained load, which is captured by the HDT metric. In this context, it is relevant that PVC can exhibit accelerated degradation under combined elevated temperature and humidity, which reinforces the need for careful thermal management of exterior components [134]. By contrast, the composite reached an HDT of 202 °C, which indicates a markedly larger margin of dimensional stability under the applied test conditions and a reduced propensity for creep and permanent deformation in locally heated regions. This result is directionally consistent with reports on window solutions in which pultruded composite reinforcements improve mechanical performance and reduce thermal bridging relative to steel-based designs [11].

Overall, the results indicate that the observed differences between PVC-U and the composite arise directly from the load-transfer mechanism. Fibre reinforcement increases modulus and strength, thereby improving stiffness-driven performance criteria, but it also reduces deformation capacity and increases notch sensitivity. This, in turn, implies that stress concentrators should be minimised through detail design and manufacturing control. At the same time, the magnitude of the measured parameters and the direction of change are consistent with literature data for PVC-U and glass-fibre-reinforced composites, which strengthens the credibility of the findings and supports their relevance to the structural analysis of window-profile solutions [136], [191–192].

4.2. Fundamental Study of Welded Joints

4.2.1. Experimental Methodology

Having established the distinct mechanical and thermal responses of PVC-U and the glass-fibre-reinforced composite insert, the next stage of the investigation translated these material-level findings into a process-oriented assessment of welded profile corners, with particular emphasis on how insert preparation and welding parameters affect joint strength.

The pilot study was divided into successive stages of strength tests addressing:

a) application of the initial parameter set – preliminary tests,
b) the milling parameter for the glass-fibre-reinforced composite,
c) the welding-head travel speed parameter,
d) the melting-time parameter,
e) the melting-temperature parameter.

Each stage followed the same workflow, executed in the order listed below:

a) inspection of the test apparatus and tooling to identify any faults or defects,
b) verification of the conformity and quality of the profiles and test materials,
c) profile cutting,
d) milling of the gasket and the glass-fibre-reinforced composite insert,
e) marking of the cut profiles to enable subsequent verification of weld symmetry,
f) profile welding,
g) description of the welded frames and preparation of process documentation,
h) post-weld finishing of the joints, including removal of the weld bead,
i) verification of weld symmetry,
j) sectioning of the welded frames into individual corners (specimens),
k) measurement of weld failure loads,
l) preparation of documentation and specimen descriptions after completion of the measurements.

The principal test material was a six-chamber profile with an installation depth of 85 mm and a width of 70 mm. In accordance with the definition in [85], the width of the profile was taken as the largest dimension measured in the glazing-plane direction, perpendicular to the longitudinal axis of the profile. A tolerance compliant with the standard, namely ±0.5 mm, was adopted. Likewise, the profile depth was defined as the dimension measured normal to the glazing plane, between the front and rear end visible faces of the profile [85], again with a tolerance of ±0.5 mm. The installation depth and profile height were verified using a calibrated calliper and a tape measure. The six-chamber geometry was confirmed by visual inspection. Profiles were accepted for testing only if their wall thickness satisfied class B requirements in [85]. This corresponds to a minimum of 2.5 mm for walls on visible surfaces and a minimum of 2.0 mm for walls on non-visible surfaces. The standard does not specify a minimum internal wall thickness, and this parameter was therefore not measured. Wall thickness was measured with a calliper to an accuracy of 0.1 mm at no fewer than three locations, and the mean value was taken as the result, as prescribed in [85]. In addition, straightness of the main profile was verified as required by [85], where straightness is defined as a deviation of the longitudinal axis from a straight line not exceeding 1 mm per 1 m of length. Measurements were performed on segments intended for testing. Sections of 1000 mm were placed on a flat, clean surface, and a feeler gauge with a resolution of 0.05 mm was used to determine the maximum gap between the profile and the surface. The maximum value was recorded, and segments exceeding 1 mm were rejected. The study accounted for the presence of a weldable TPE (thermoplastic elastomer) gasket co-extruded with the profile, meaning that it constituted an integral part of the section. Profiles reinforced with a glass-fibre composite were required to contain two composite inserts, and their number was confirmed by visual inspection. The investigation predominantly employed profiles that were white on both the interior and exterior sides. Owing to material availability, profiles with a foil lamination in a different colour were also permitted in isolated cases. Based on current knowledge and industrial experience relating to PVC technology and the manufacture of PVC profiles, material differences were not recordedin the obtained weld failure loads, for instance

in compression-bending corner tests, across profiles of different colours or with different laminates and lacquers used in routine production. Profile colour was verified in two steps. First, manufacturer documentation was checked. Second, the laminate structure was compared using the manufacturer's authorised reference swatches.

Given the material-property requirements of PVC profiles during cutting and welding, the temperature of profiles stored prior to processing, under ambient conditions, was maintained at not less than 18 °C. This temperature was verified using sensors positioned directly adjacent to the profiles. If profiles had been stored at a lower temperature, they were conditioned before processing. In line with commonly accepted practice, it was assumed throughout the study that cold profiles require approximately 1 h for their temperature to increase by 1 °C until reaching 18 °C. Storage conditions were selected to preserve profile geometry and to eliminate the risk of bending or twisting. Accordingly, profiles were arranged so that they rested on the substrate along their full surface area and were stored on racks with supports, in shape-stabilising containers, or in dedicated trolleys with partitions, which also reduced the likelihood of mechanical damage. Profiles were additionally kept away from radiant heat sources and heaters. Storage behind transparent panels or outdoors was not permitted, and the material was protected from moisture and direct sunlight. Profiles packaged in PE (polyethylene) film were ventilated by opening the end faces of the packaging. Where profiles were stacked, the stack height did not exceed 0.5 m, and a board was used as the supporting base. Profiles were segregated from impregnation agents and other chemical substances. Individual profiles were removed only longitudinally. After cutting, the elements were stored so as to protect the ends from dust, contamination, and mechanical damage. Cut profiles were welded on the same day as cutting.

Profile cutting was performed using a DS 150 – Gamma automatic double-head mitre saw supplied by WEGOMA Polska (WEGOMA Weiss Fensterbau Maschinen GmbH, Bietigheim, Germany) (Fig. 4.33). Cutting was carried out in automatic mode. Prior to each run, the heads were calibrated, enabling dimensional accuracy to within tenths of a millimetre. The profile was clamped in two planes, vertical and horizontal, which reduced the risk of angular and dimensional deviations. The cutting tool parameters were as follows: a carbide-tipped circular blade, 550 mm in diameter and 4.2 mm thick, with 120 teeth of flat-trapezoidal geometry, operating at 3000 rpm with a feed rate of 45 mm/s. Because cut quality directly governs subsequent weld quality, particular attention was paid to ensuring that the cut surface was straight and clean, namely free from oil, grease, water, and other contaminants. Profile elements were cut to the required length and angle. Segments were mitred at 45°, and the overall external edge length of a single segment after cutting was set to at least 726 mm. Any local dimensional deviations across measurement points were identified using calibrated set squares and a calibrated tape measure. Post-cut inspection covered the mitre angle, overall dimension, and surface condition, including any colour change. Yellowing of the profile was treated as an indicator of an excessively low cutting speed or blade wear. It was also observed that blades used to cut profiles incorporating a glass-fibre-reinforced composite insert wear more rapidly, with yellowing being a characteristic manifestation of this effect. In the present study, cut surfaces remained clean and free of yellowing, since even local contamination could materially impair weld integrity. Cleanliness was maintained by storing the cut segments on purpose-designed profile trolleys with compartmentalised bays. Dimensional processing parameters were approved numerically at the machine in accordance with the machining programme. The saw blades employed were intended and dedicated for PVC profiles. Before each cutting procedure, blades were checked for the presence of the sintered-carbide cutting edges, and cutting accuracy was verified on a preceding trial specimen. The

feed rate was estimated from time-measurement trials. The maximum available feed speed on the machine was adopted, set via the pneumatic regulator of the reduction unit. During cutting, stable profile fixation in the 0° plane, without tilt, was critical. The widest profile face was used as the reference surface. The profile was secured by two clamping systems, vertical and horizontal, because stabilisation in only one plane, as is typical of older saw designs, increases the likelihood of profile torsion and an incorrect mitre angle. Such an error can result in a nominally correct overall length but different longitudinal dimensions at the external face, internal face, and along the neutral axis. This, in turn, reduces the volume of material available for welding and markedly increases the risk of material deficit, that is, loss of material continuity after welding. Owing to the profile geometry, the section was positioned on the saw with the high rebate facing the machine. In addition, consistent with the assumptions adopted by many machine manufacturers, a welding allowance of 3 mm per welded face was applied for each segment. An insufficient allowance would result in inadequate material to form the weld bead and would therefore weaken the joint, whereas an excessive allowance could trigger a welding-machine error due to dimensional non-conformance with the programmed target, preventing initiation of the welding cycle.

Fig. 4.33. Automatic double-head saw. Source: Author's own work

Milling of the gasket and the profile-reinforcing composite insert was performed using a DFM-202/4 automatic twin-spindle milling machine (URBAN Polska Sp. z o.o., Żary, Poland) (Fig. 4.34(a)). For the purposes of this study, a proprietary composite-milling programme was developed and implemented. The machine enabled machining to be programmed with decimal-level precision. The trials employed an 80 mm diameter slitting cutter with a sintered-carbide cutting edge (insert width 12 mm), operated at 18000 rpm with a feed rate of 20 mm/s. Profiles were stabilised in the machine by pneumatic clamps in two planes, which ensured process repeatability (Fig. 4.34(b)). To maintain consistent cutting quality, the tool condition and machining uniformity were checked before each milling procedure. Uniformity was defined as a constant cutting depth along the full length of the machined region (Fig. 4.34(c)). Verification was performed using a calibrated calliper. Only specimens meeting the quality criteria were admitted to further testing, namely those without material tear-out and without surplus welded gasket material. This assessment was carried out by visual inspection. The milling depth in the material was, however, intentionally varied in accordance with the experimental design. Excessive milling depth weakened the weld and reduced its capacity to transfer loads and stresses. Conversely, insufficient milling impeded the ability to obtain a welded frame to the programmed dimensions (Fig. 4.34(d)). The

selection of an 80 mm slitting cutter as the primary tool was preceded by trials with alternative tools, including an HSSE end mill, Ø 5 mm, a VHM end mill, Ø 5 mm, with a chip breaker, and a smaller carbide-tipped slitting cutter of 40 mm diameter (insert width 4 mm, maximum spindle speed 18000 rpm) (Fig. 4.34(e)). The end mills did not satisfy the primary requirement, namely cutting quality, because the gasket was not removed uniformly. As a consequence of non-uniform or overly shallow machining, gasket residues remained. These residues subsequently welded, rubbed against the laminate, damaged the profile, and led to complete stripping of the foil. In contrast, overly deep gasket milling weakened the weld and produced material tear-out. The 40 mm slitting cutter was functionally adequate, but it was less efficient than the largest tool diameter permissible for this machine. This follows from the mechanics of cutting. At the same programmed depth of cut, the larger diameter, together with a wider cutting insert, provided greater cutting width along the longitudinal axis. It also enabled a shorter programmed tool path for the larger cutter. By contrast, the smaller diameter reduced the effective cutting width on the composite and gasket, which resulted in partial material removal, necessitated re-machining of uncut regions, and extended the operation time. In addition, for technological reasons, specifically torque constraints, and for safety considerations, the approach speed of the cutter into the material (50 mm/s) was not increased to compensate for the smaller tool diameter. Such an adjustment would increase the risk of machine damage.

The initial phase of the experimental programme investigated the effect of milling the profile's composite reinforcement on weld strength and joint integrity. Accordingly, the study considered the following milling-depth conditions: no milling, 6.0 mm, 3.0 mm, 2.0 mm, 1.5 mm, 1.0 mm, and 0.5 mm. Throughout this series, the process parameters were held constant at a welding temperature of 264 °C, a melting time of 30 s, and a welding-head feed rate of 0.25 mm/s.

(a)

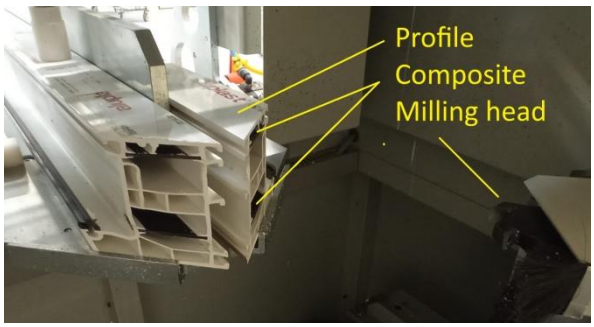

(b)

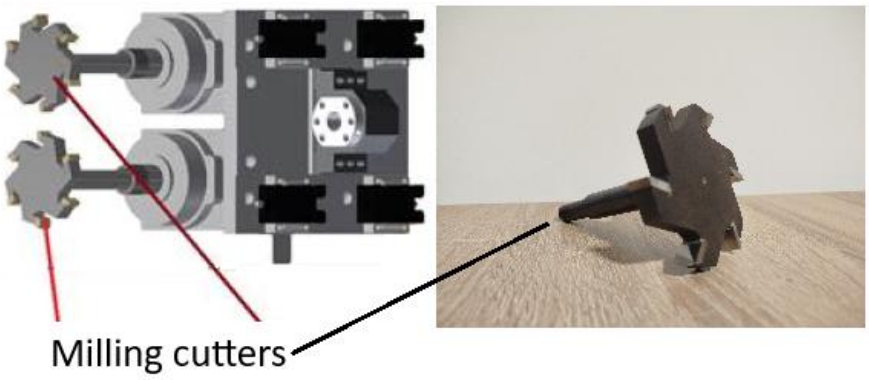

(c)

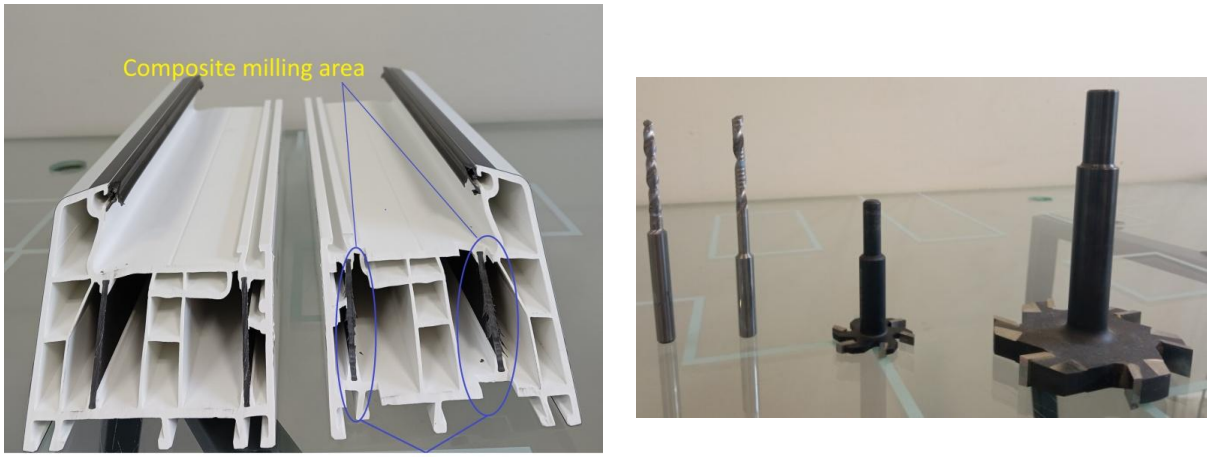

(d) (e)

Fig. 4.34. Profile milling: (a) test stand, (b) profile with a milling head for composites and gaskets, (c) visualisation of circular saw blades on the milling heads, (d) profiles with composite inserts with the milling area indicated, (e) types of tools used in the tests [14]

Within the research programme, which included verification of weld-joint symmetry, a dedicated proprietary tool (Fig. 4.35) was employed [193]. Specifically, the tool is a gauge in the form of a purpose-designed plate compatible with PVC window profiles mitred at 45°. It was used to apply reference markings to the cut profiles, enabling subsequent verification of joint symmetry after the fusion process. Electronically controlled machines are most commonly used in series production. In particular, four-head fusion machines operate under automatic control, although the operator sets and supervises the key process parameters. Nevertheless, post-fusion deviations in joint symmetry are frequently observed, which results in incomplete joints. Such nonconformities may arise from inappropriate process settings, inaccurate or incomplete mechanical adjustment of the fusion-head assemblies, material defects in the profiles, or incorrect profile positioning at the fusion heads. These factors directly impair the efficiency and precision of joint formation and therefore govern the process outcome, producing asymmetrical, low-quality joints. Asymmetrical joints do not transfer loads correctly, so the window assembly fails to maintain the required rectangular or square geometry and consequently does not meet its intended dimensions. In practice, this prevents the use of the specified glazing unit and precludes correct frame–sash assembly, thereby rendering the product unusable. One established approach to evaluating the quality of joints produced by window-profile fusion is destructive load testing. This standardised

procedure, specified in [18], applies an increasing load to the joint until failure, thereby identifying the critical value. Its principal limitation is inherent: the test irreversibly destroys both the joint and the parent material. Moreover, it does not address joint symmetry. An alternative is visual inspection, which assesses the colour and morphology of the joint, typically through observation of the weld bead. When fusion parameters are appropriately selected, they should not induce material degradation or depolymerisation. Consequently, the PVC bead should remain white. Although the bead geometry can be appraised visually, it should be noted that organoleptic assessment has limited precision, and determining joint symmetry by sight alone is of limited reliability. To enable accurate assessment of joint symmetry, a dedicated template was proposed for marking PVC window profiles mitred at 45° (Figs. 4.35 and 4.36) [193]. The template may be manufactured from an aluminium alloy, steel, composite, or any other material with a hardness exceeding 50 HRC. Its functionality depends primarily on its geometry, i.e., the specified shape and dimensions. Owing to its symmetrical design, the gauge allows profiles to be marked at both ends, while its overall dimensions and form enable adaptation to window profiles across systems. The gauge measures 140 × 100 × 23 mm and incorporates symmetrical recesses, 7 mm in depth, on both sides. These features impart a T-shaped cross-section to one of the longer side walls (1), whereas the opposite wall (2) includes a spline (3) with a 45°-inclined notch (4) aligned with side wall (1).

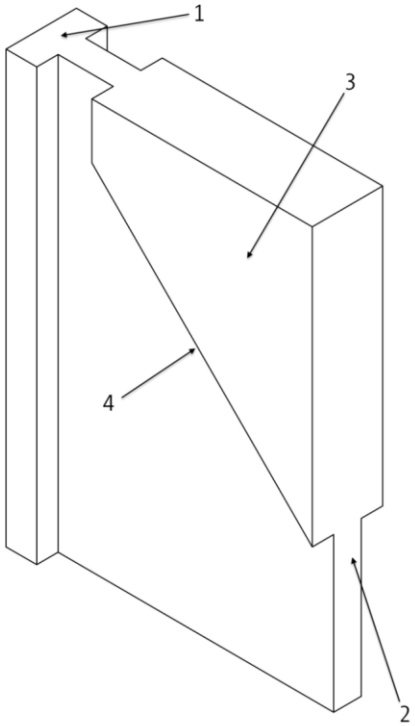

Fig. 4.35. Illustration of the measuring template [193]

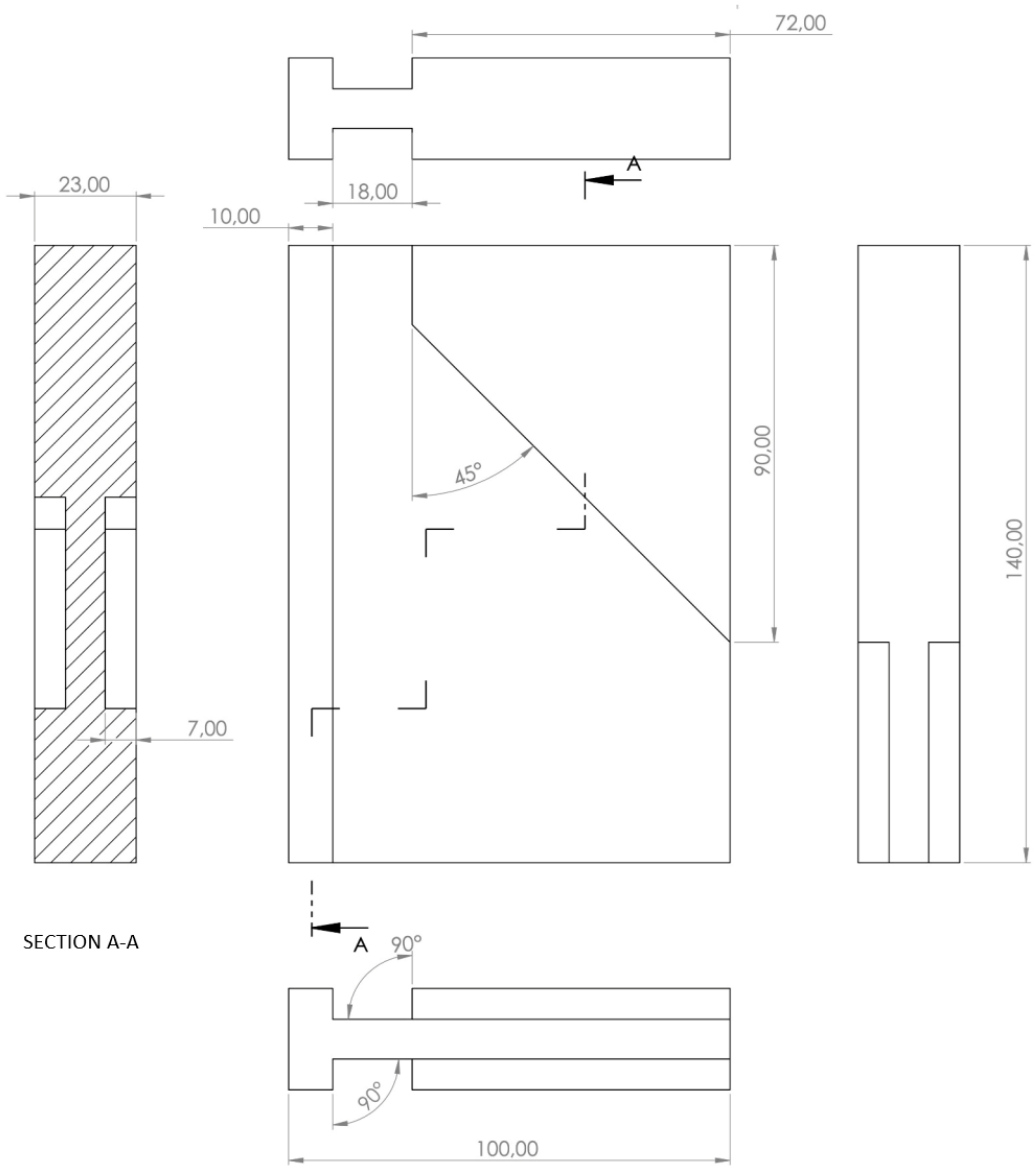

Fig. 4.36. Geometric representation of the inspection tool [193]

The template-based marking procedure began with placing the profile section on a flat surface, with the contact surface oriented upwards (Fig. 4.37(a)). This was followed by cutting both profile faces at an angle of 45° and sliding the gauge along the mitred butt surface until resistance was encountered, which indicated that the template had been securely seated in a defined position relative to the profile (Fig. 4.37(b)). Owing to the template geometry, contour, and dimensions, only one mounting position was possible, thereby eliminating ambiguity during positioning. The marking stage consisted of drawing a horizontal reference line at the junction between the template and the rebate surface of the profile using a fine-tip marking tool (Fig. 4.37(c)). The same marking operation was performed on all joint sections at both profile ends. After fusion welding, the distances between the outer edges of the moulded weld buttresses and the reference marker were measured with a calliper (Fig. 4.37(d)). These measurements were then used to verify the symmetry of the welded joint.

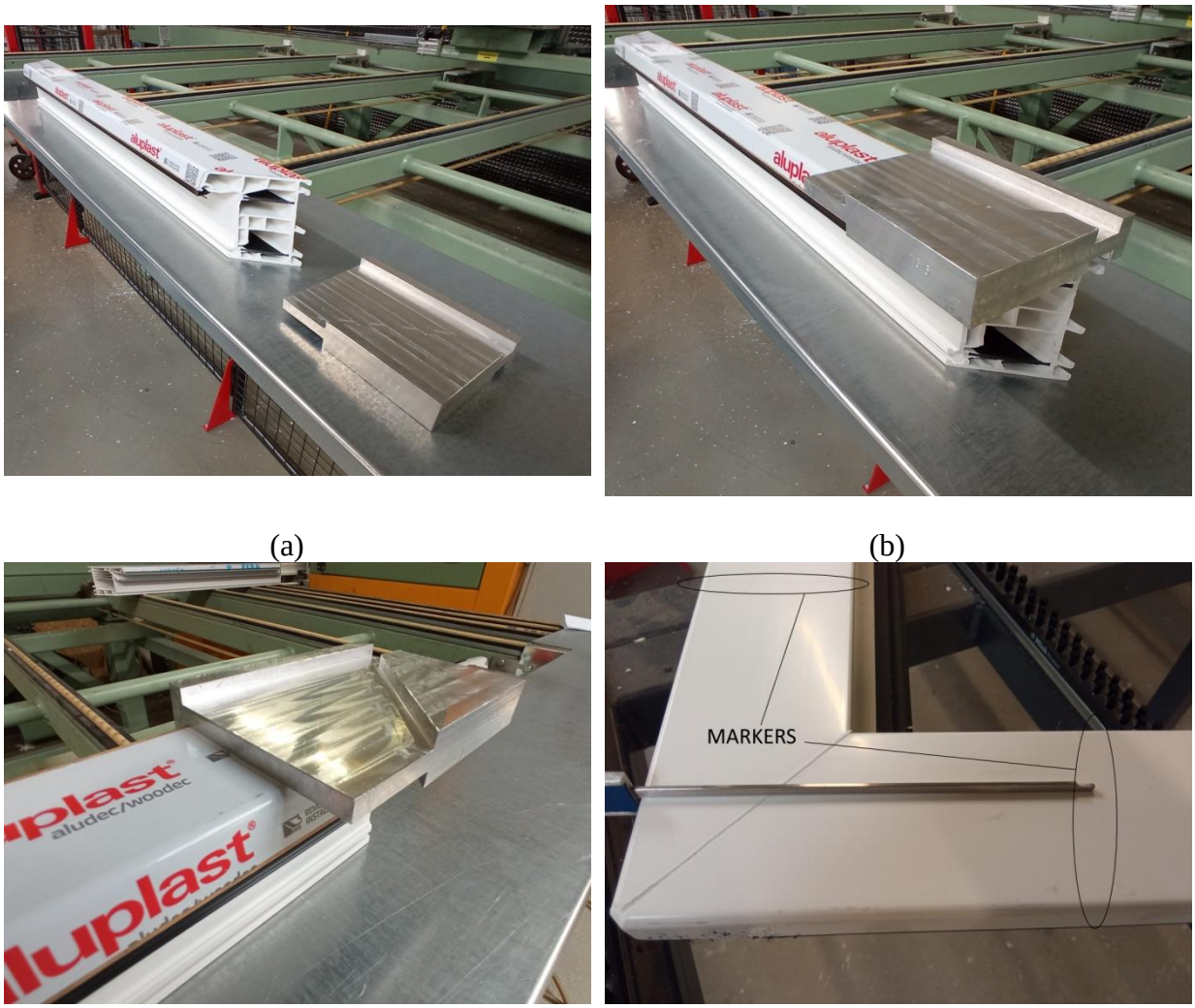

(a) (b)

(c) (d)

Fig. 4.37. Marking profiles for verifying joint symmetry: (a)–(d) subsequent stages. Source: Author's own work

The welding cycle was performed on a WSA 4RH/LH automatic four-head welder (WEGOMA Polska; WEGOMA Weiss Fensterbau Maschinen GmbH, Bietigheim, Germany) (Fig. 4.38(a)). Post-weld cleaning was carried out using an automatic corner-cleaning unit, WPCNC2/4, from the same manufacturer (Fig. 4.38(b)). Prior to welding, the profiles were stored in a compartmentalised trolley and inspected for contamination. Specimens exhibiting dirt were rejected, since the presence of grease, swarf, moisture, or other contaminants on the faying surfaces increases the risk of a weakened joint or an outright welding failure. Immediately before processing, the prepared segments were labelled with the welding-head number, enabling unequivocal identification of the corner origin. Corner assembly was implemented as butt welding, namely plasticisation on the heating element followed by consolidation under servomotor control. The process was managed to prevent any lateral offset of the welded end faces. In accordance with the experimental procedure, each welded frame had dimensions of at least 720 × 720 mm. Welding time was defined as the sum of the melting time (variable) and the joining time, while temperature and time values were treated as author-defined parameters and as variables within the procedure. The initial settings comprised a melting time of 30 s, a welding temperature of 264 °C, and a head feed rate of 0.25 mm/s. Before each weld, the temperature of the heating plates was verified using a

handheld sensor. In parallel, the condition of the plates and the PTFE film was inspected. Adhered residues such as swarf were removed using a linen cloth, soft paper, or another non-synthetic fabric, and the PTFE layer was cleaned regularly and replaced if damaged. In addition, after each weld, residues from the composite matrix were removed from the PTFE surface, including by wiping with a hard oak-wood scraper in the form of a paddle. Process stability also required control of the profile-to-plate stand-off distance prior to welding, which was set to 0.2 mm and confirmed using a calibrated feeler gauge. This value was retained as the minimum fully safe clearance, given profile dimensional tolerances and the risk of collision with the heating plate, while acknowledging that the profile approach time is included in the welding time. Increasing the stand-off would therefore reduce the effective thermal exposure. A minimum profile ambient temperature of 18 °C was also adopted, because failure to maintain this condition would promote residual stresses that may later manifest as cracking or weld failure. Hall temperature was monitored by sensors. In line with machine and window-manufacturer practice, a 3 mm welding allowance per side was used, together with the machine software's fixed partition of dimensional reduction into a component associated with actual melting (2.3 mm) and a component attributed to heat conduction into the bulk (0.7 mm). This ratio could not be modified by the operator without changes to the source code. The melting speed was controlled by the servodrive via electrical head feed, in accordance with the experimental procedure. A servodrive sensor error was unacceptable during welding. Any overloads were recorded in the documentation, since they may arise, for example, from out-of-tolerance and excessively long segments, failure to maintain the mitre angle, or incorrect parameter settings. In the present study, such events did not occur due to the preceding verification steps. After welding and prior to corner cleaning, the frame was allowed to cool fully for at least 4 min. This stage was not accelerated using compressed air or by placing the frame on a cold floor, in order to avoid inducing uncontrolled residual stresses. In addition to weld symmetry, weld quality was assessed visually. A weld bead exhibiting a creamy appearance, a glossy surface, and slight roughness was considered acceptable. Yellowish or brown discoloration was interpreted as an indication of incipient thermal burning due to excessive temperature or an overly long melting time, which was unacceptable. Before CNC processing, photographic documentation and qualitative visual inspection of the specimens were performed. The welding procedure can be described as an ordered sequence of technological operations (Fig. 4.38(c)). First, the machine was prepared by installing the appropriate tooling, namely adapters matched to the profile type, and by setting the parameters, including welding temperature, melting time, and head feed rate. The profiles were then placed on the adapters and positioned against the centraliser. Subsequently, the centraliser was retracted and the heating plates were lowered to the working position. Plasticisation was achieved by pressing the profile ends against the plates under the set melting time, melting speed, and prescribed melting distance. During this stage, the profile was compressed at a defined speed, reducing the dimension by 2.3 mm per side. The profile was then held against the plate until the melting time elapsed, which allowed heat to penetrate into the bulk. This thermal reserve was exploited during joining. After separating the profile ends from the plates by head retraction and lifting the heating plates, the heads advanced towards one another, bringing the heated cross-sections into contact and reducing the dimension by a further 0.7 mm per side to reach the final geometry. After completion of joining, the frame was left to cool in accordance with the assumptions.

(a)

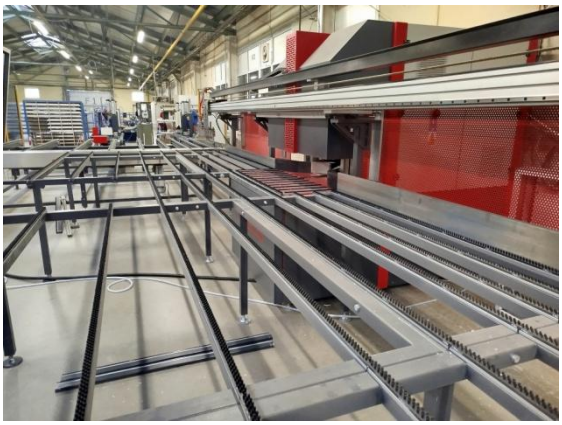

(b)

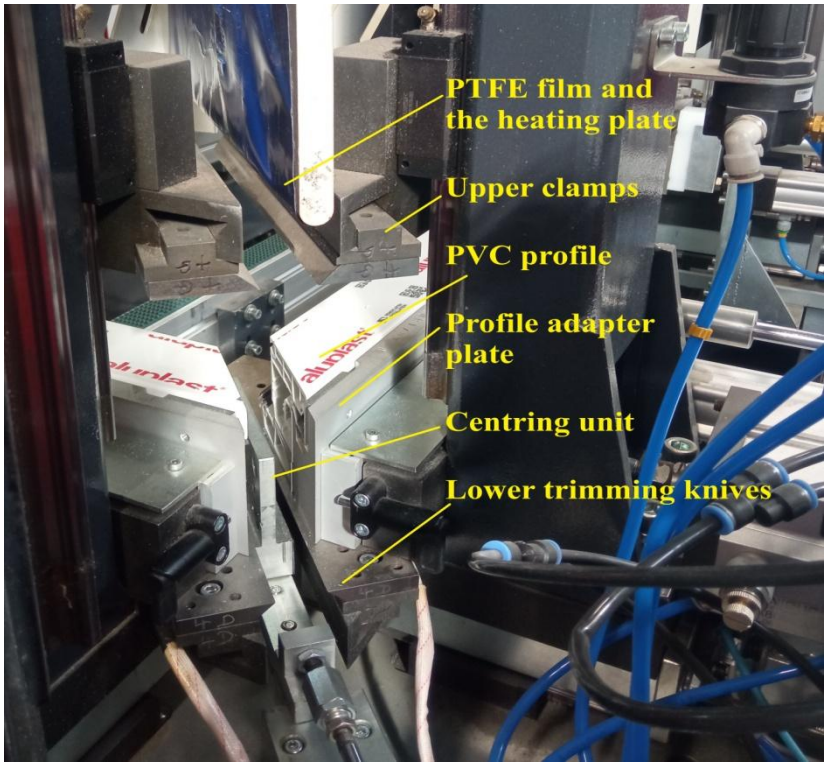

(c)

Fig. 4.38. Machines involved in the welding process: (a) welding machine, (b) CNC unit, (c) selected components of the welding head [14]

One of the welding-process parameters was the welding-head feed rate. Based on machine-manufacturer recommendations, an initial value of 0.25 mm/s was adopted. Since feed rate was treated as a variable, the programme also assessed weld quality and corner failure loads for alternative values of this parameter. When developing the methodology for different head-speed variants, the study drew on conclusions from pilot trials performed at the baseline settings of 264 °C, 30 s, and 0.25 mm/s, combined with varied milling depth of the composite reinforcement. Analysis using 0.5 mm milling-depth increments did not reveal unambiguous differences in failure load. This indicated that, within the investigated range, milling depth was not the decisive factor. Consequently, the milling depth corresponding to the 0.5 mm increment was adopted as the reference condition for selecting alternative head feed rates, higher and lower, which, unlike the milling increment, were expected to exert a more pronounced influence on weld quality and strength. A welding allowance of 3 mm per

component was applied, consistent with industrial practice. Accordingly, the two joined components provided a total of 6 mm of material intended for formation of the weld bead and the effective joint. This allowance encompassed two stages of melting. In the first stage, the profile was plasticised on the heating plate to a depth of 2.3 mm. This was the active phase, in which the welding heads pressed the profile against the plates at the prescribed feed rate. Under the adopted settings, this corresponded to the first part of the melting time and lasted 12 s (measured). After reaching 2.3 mm, the pressing action ceased, and the remaining melting depth of 0.7 mm developed passively through heat conduction from the plate into the profile during the remaining melting time, namely 18 s out of the nominal 30 s, thereby softening the material. This partition of the 3 mm allowance into an active component (2.3 mm) and a passive component (0.7 mm) enabled the actual, head-motion-controlled melting depth to be linked directly to the head feed rate. It was also assumed that a technologically meaningful milling depth of the composite, affecting failure loads, was at least 0.5 mm, which was considered in the subsequent selection of parameter variants. To establish the relationship, the distribution of velocities acting on the profile was first defined (Fig. 4.39). P1 denotes the physical head feed rate, as set and controlled by the operator. It acts normal to the positioned profile. The baseline value of P1 was 0.25 mm/s. P2 denotes the resultant velocity component derived from P1 and the 45° mitre angle. This is the effective velocity between the 45° cut surface of the profile and the heating plate.

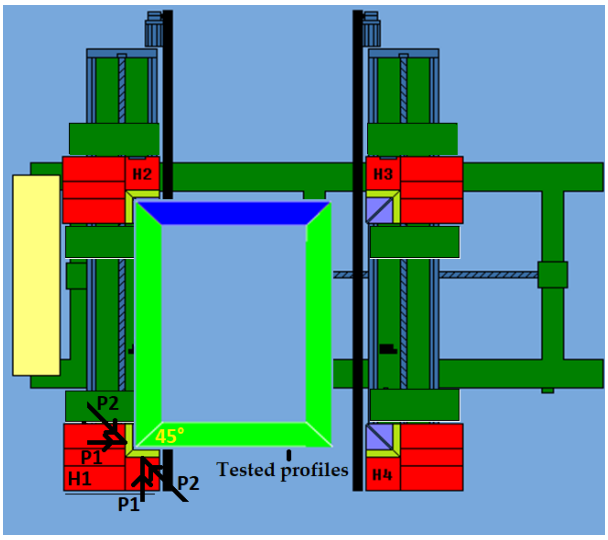

Fig. 4.39. Schematic of the H1 welding-head feed rate during welding: P1 – commanded physical feed rate (set and controlled), P2 – effective feed rate resulting from the 45° mitre geometry (projection of P1), H1, H2, H3, H4 – welding heads [12]

Because the profile end faces were cut at 45° relative to the longitudinal axis, and given their orientation with respect to the heating plate and the associated resolution of motion, P2 represented the passive, effective feed rate at the faying surface. Conversely, from the operator's perspective, the programmable parameter during the trials was P1, that is, the active head feed rate. Accordingly, for a prescribed active melting distance of 2.3 mm, the passive, effective velocity P2 was the quantity of primary technological significance. Determination of P2 therefore required identification of the relationship between P1 and P2. This relationship is given in Equation (1).

$$P2 = P1 \cdot \cos 45^{\circ} = 0.25 \frac{\text{mm}}{\text{s}} \cdot 0.71 = 0.18 \frac{\text{mm}}{\text{s}} \quad (1)$$

To determine the change in welding-head feed rate, the 0.5 mm melt length was divided by the effective melting time of the profile. The measured head-advance time was 12 s. It should be noted, however, that for safety reasons the profile is initially positioned at a defined stand-off distance from the heating plate when the plates are lowered. This distance is fixed in the standard process, although it may be adjusted in specific cases. The smaller the stand-off, the longer the effective melting time. In the present study, the stand-off measured with a feeler gauge was 0.2 mm. With P2 set to 0.18 mm/s, it was assumed that approximately the first second of head motion was expended on closing this stand-off, i.e., bringing the profile into contact with the heating plates. Accordingly, the effective melting time was taken as 11 s. On this basis, the welding-head feed-rate change P2 was determined using Equation (2).

$$\Delta P2 = 0.5\ \text{mm} : 11\ \text{s} = 0.045\,\frac{\text{mm}}{\text{s}} \tag{2}$$

However, it should be noted that P1 is the parameter that can be programmed into the machine. Accordingly, the corresponding value of P1 was determined using Equation (3).

$$\Delta P1 = \Delta P2 : \cos 45^{\circ} = 0.045\,\frac{\text{mm}}{\text{s}} : 0.707 = 0.06\,\frac{\text{mm}}{\text{s}} \tag{3}$$

Consequently, to obtain an additional or reduced profile melt length of 0.5 mm at a welding-head travel time of 12 s, the head feed rate must be increased or decreased by at least 0.06 mm/s, respectively. Therefore, the alternative welding-head feed rates were set to 0.19 mm/s and 0.31 mm/s.

Accordingly, the options in the Table 9 were adopted for this study.

Table 9. Summary matrix of the test variants, where D denotes the milling depth of the composite reinforcement [mm] and P denotes the welding-head feed rate [mm/s] [12]

	D →		
P ↓	D=0.0 P=0.19	D=0.5 P=0.19	D=1.0 P=0.19
	D=0.0 P=0.25	D=0.5 P=0.25	D=1.0 P=0.25
	D=0.0 P=0.31	D=0.5 P=0.31	D=1.0 P=0.31

On the basis of the weld-strength results obtained for varying composite-milling depths and welding-head feed rates, further parameter variants were developed for subsequent verification. The variants aimed at welding-time optimisation are summarised in Table 10, whereas the variants addressing temperature changes are reported in Table 11.

Table 10. Parameter set for investigating reduced melting time [14]

		Set melting time [s]				
		21	22	23	24	25
Milling depth of the composite [mm]	0.0		X			
	0.5		X			
	1.0	X	X	X	X	X

Table 11. Set of parameters for testing changes in welding temperature [202]

		Welding temperature [°C]								
		247	248	249	250	256	263	270	271	280
Melting time [s]	21							X	X	X
	22						X			
	30	X	X	X	X	X				

Because finished products used in practice are routinely deburred for aesthetic reasons, and because the present work was application-oriented, all welds were post-processed after welding using grooving, trimming, and other CNC operations consistent with standard commercial practice. Removal of weld beads from visible surfaces was performed mechanically using an automatic CNC cleaning unit. In this procedure, the knives produced a visible groove along the weld line on the white side, whereas on the coloured side no groove was machined and the operation was limited to bevel trimming of the bead on the upper portion of the profile. To minimise material removal, the groove depth was kept as small as practicable and was approximately 0.4 mm on the white side and 0 mm on the coloured side. In parallel, internal and external corners were cleaned by machining operations including milling, drilling, and trimming, using a tool set comprising, inter alia, upper and lower cutters (plain and grooving), a cutting disc, upper and lower internal cutters, and upper and lower drills. Since bead trimming, understood as removal of the excess material extruded during welding, provides an aesthetic benefit yet may also weaken the joint, the cleaning cycle was numerically programmed and applied identically to all specimens. Any deviation in the cleaning process could therefore bias the assessment of weld quality and strength. Accordingly, specimens were rejected whenever an abnormal cleaning run was suspected.

To prepare specimens for destructive testing, the welded frames had to be cut after CNC post-processing. The cut was made perpendicular to the profile cross-section in order to divide the frame into two symmetric halves, without cutting along the weld line (Figs. 4.40(a) and (b)). Subsequently, the remaining U-shaped section was trimmed on an automatic saw to obtain weld arms with a length of 343 mm while maintaining the 45° angle (Fig. 4.40(c)). The required weld-arm length was determined through calculations based on the geometric relationships of the investigated profile, in accordance with Eqs. (4)–(9).

$$a = 400 \pm 2 \text{ mm} \tag{4}$$

$$L_n = \frac{400}{\sqrt{2}} = 283 \text{ mm} \tag{5}$$

$$e = 40 \text{ mm} \tag{6}$$

$$L_i = L_n - 2e = 283 - 2 * 40 = 203 \text{ mm} \tag{7}$$

$$A = 70 \text{ mm} \tag{8}$$

$$L_z = L_n + 2(A - e) = 283 + 2(70 - 40) = 343 \text{ mm} \tag{9}$$

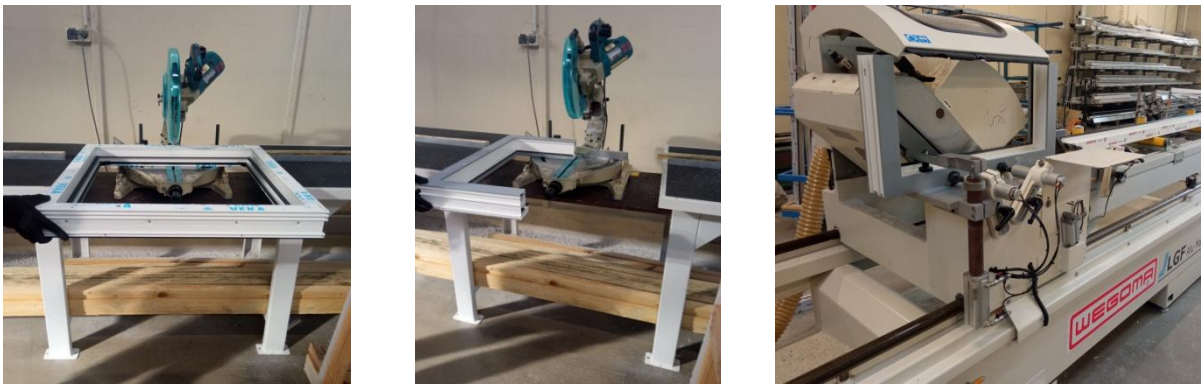

(a) (b) (c)

Fig. 4.40. Sectioning of welded mouldings into test specimens: (a)–(c) individual stages. Source: Author's own work

Compressive bending tests were conducted to determine the failure load, defined as the load at which a loss of strength occurs. Where no such drop was observed, the failure load was taken as the load causing specimen fracture, in accordance with the standard. (keep your local reference as [18] in the thesis text). To ensure representativeness, at least three window frames were tested for each variant, yielding a minimum of twelve corner specimens. For each test type and variant, at least three specimens produced on each welding head were qualified. The minimum acceptable failure load for the welds was set to 2760 N, in line with the profile manufacturer's recommendations. Specimens were conditioned immediately prior to testing at 23 ± 5 °C for at least 2 h, and the tests were performed within the same temperature range. Each specimen comprised a welded 90 ± 1° corner, with arms cut to 45 ± 1°, such that the neutral axes of the end cross-sections were positioned vertically above the trolley rotation axes, approximately in the region of the main chamber centreline. The load was recorded using an LN2000 corner-cracking device (PPHU DELTA, Ksawerów, Poland), measured directly at the breaking punch with digital display of the instantaneous value and recording of the maximum value (Fig. 4.41). The machine operated over a range of 2–20 kN and featured a load indicator with zero adjustment and a peak-hold function. The punch feed rate was constant at 50 ± 5 mm/min, ensured by the worm gearbox and trapezoidal screw. The reading resolution for failure load was 10 N, and the metrological status was confirmed by a calibration certificate from an accredited laboratory. Compliance with the standard requirement of ±3% measurement accuracy was designated for verification in the subsequent step. Destructive stress was not calculated, since this would require geometric and material data for the profile that are proprietary to the manufacturer.

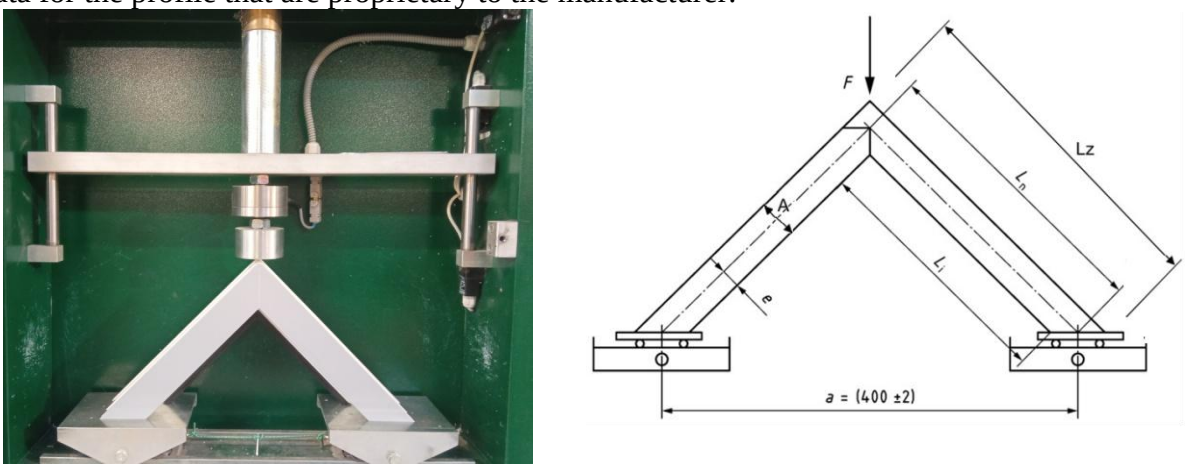

(a) (b)

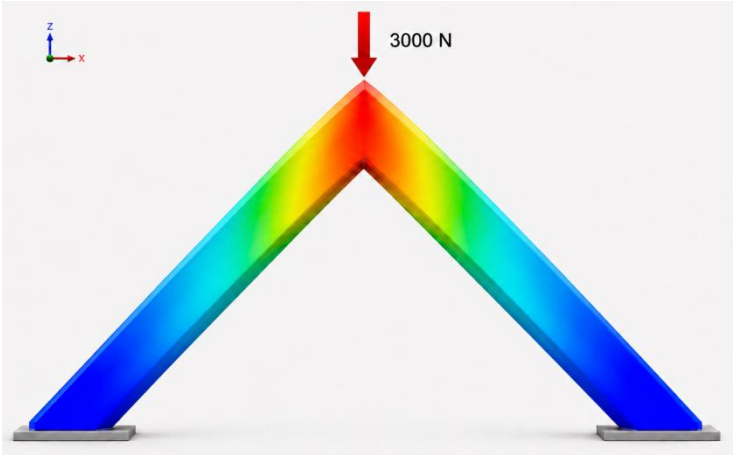

(c)

Fig. 4.41. Failure load measurements: (a) testing machine, (b) specimen geometry schematic, F – punch load, Lz, Ln, Li, A, e – dimensional parameters, (c) example of the stress distribution in a specimen under a load of 3000 N, modelled using the finite element method [13]

In accordance with the standard [18], the accuracy of failure-load measurements should be ±3%. This requirement is critical because it directly governs the credibility of the recorded failure loads and the acceptability of the test results. Input data were taken from the calibration certificate of the device and from EA-4/02 M:2022, adopting an expanded uncertainty at an approximate 95% coverage probability with an expansion factor k = 2. The calculation used the coefficient values listed in Table 12.

Table 12. The data required to calculate the measurement accuracy of the failure loads

True value [kN]	Reading corrected for relative indication error [%]	Measurement uncertainty [%]
3	–0.46	0.51
5	–0.49	0.65

The relative indication error quantifies the extent to which the instrument systematically overestimates or underestimates the reading. A negative sign indicates underestimation of the true value. Therefore, the corresponding correction is applied by adding the percentage value to the instrument reading. Next, the lower and upper bounds are obtained by subtracting and adding, respectively, the measurement uncertainty to the corrected value, thereby defining the final interval. Finally, the limiting relative errors are calculated by comparing each interval bound with the original (uncorrected) reading.

4.2.2. Analysis of Results

The first strand of the experimental programme examined how milling the composite reinforcement within the profile influences weld strength and weld integrity. To this end, the following milling-depth variants were adopted: no milling, 6.0 mm, 3.0 mm, 2.0 mm, 1.5 mm, 1.0 mm, and 0.5 mm. The process parameters held constant were a welding temperature of 264 °C, a melting time of 30 s, and a welding-head feed rate of 0.25 mm/s.

Table 13 specifies dimensional deviations for welds in the variant without composite milling.

Table 13. Results of reconnaissance tests on the dimensional deviations of the welded PVC mould [13]

Sample No.	1	2	3	4	5	6
Dimensional deviations from nominal size in the X; Y axes [mm]	1; 1	0; 1	1; 0	1; 0	0; 1	0; 1

The test results indicate that dimensional deviations from the nominal dimension do not exceed 1 mm along any axis of the welding machine. Accordingly, with respect to the target dimensions, the welded assembly can be regarded as dimensionally compliant.

Figure 4.42 presents the mean failure load obtained in the exploratory tests for each specimen. For each specimen, the reported value represents the average across all welding heads. The results show no material differences between the individual test runs, which is consistent with good test repeatability. All specimens exceeded the 3000 N failure-load threshold, and two also surpassed 3500 N. Consequently, the results were comfortably above the minimum failure load of 2760 N adopted for the present tests.

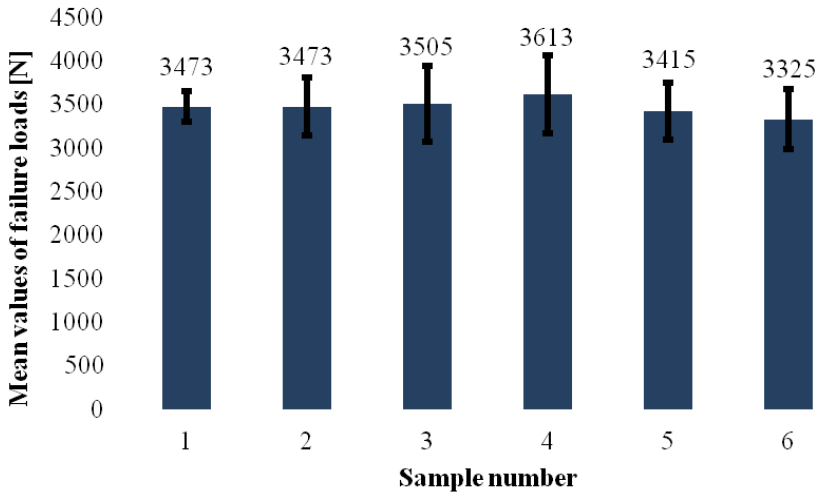

Fig. 4.42. Mean failure loads of the individual test specimens without composite milling [13]

Figure 4.43 presents the mean failure loads obtained in the exploratory tests for each of the four welding heads. For each head, the reported value is the mean of all tests conducted on that head. The results show no material differences between the heads. The highest mean value was recorded for the second head, whereas the lowest was observed for the first head. Consistent with the specimen-level results, the mean failure load for each head exceeded 3000 N.

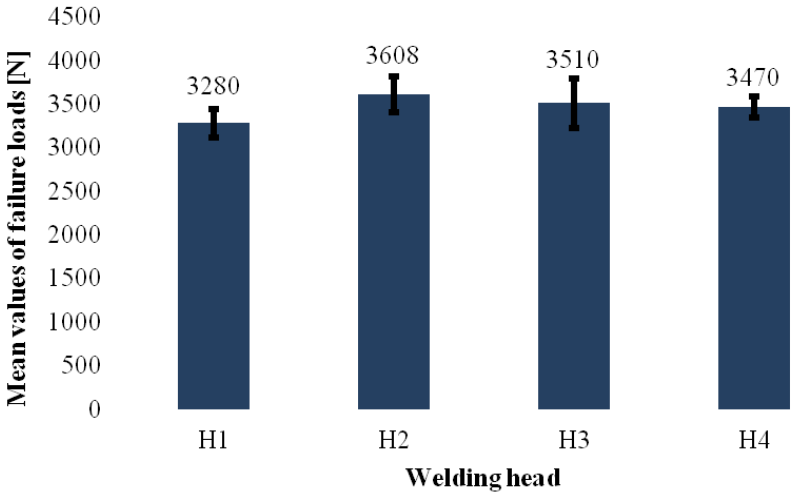

Fig. 4.43. Mean failure loads for the individual welding heads for test specimens without composite milling [13]

Figure 4.44 illustrates the welds produced for two representative specimens from the exploratory tests. A white weld bead was observed for all specimens. This observation is consistent with the selection of a welding temperature that does not induce visible thermal degradation of the poly(vinyl chloride). In all cases, material continuity across the joint was maintained, and a discernible weld line was present. The weld bead corresponds to a re-solidified flow of molten profile material formed during the welding cycle. Weld symmetry was also assessed, with no evidence of profile misalignment during welding.

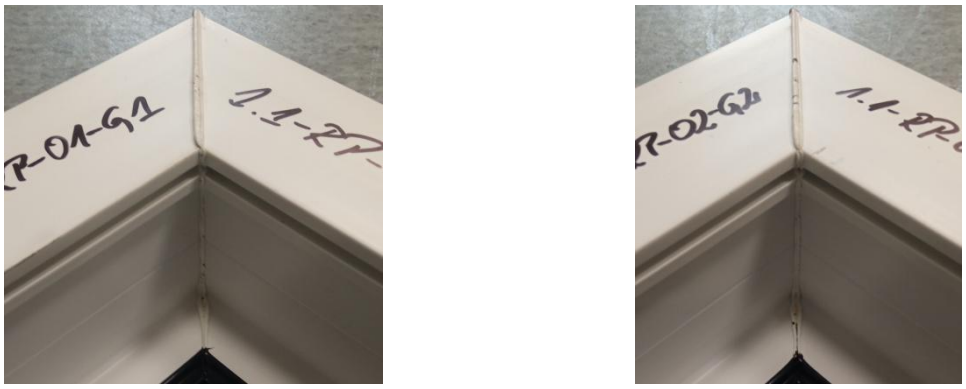

(a) (b)

Fig. 4.44. Representative welds from the reconnaissance tests: (a) specimen welded using the first head, (b) specimen welded using the second head [13]

Table 14 summarises the validation of failure loads for the variant without composite milling, conducted in accordance with the adopted methodology.

Table 14. Validation of failure loads for the variant without composite milling. Source: Author's own work

Specimen No.	True value [N]	Reading corrected for relative indication terror [N]	Upper limit including measurement uncertainty [N]	Lower limit including measurement uncertainty [N]	Compliance with the ±3% measurement accuracy requirement
1.1-RP-01-G1	3330	3345	3362	3328	YES
1.1-RP-01-G2	3540	3556	3574	3538	YES
1.1-RP-01-G3	3450	3466	3484	3448	YES
1.1-RP-01-G4	3570	3586	3605	3568	YES
1.1-RP-02-G1	3310	3325	3342	3308	YES
1.1-RP-02-G2	3310	3325	3342	3308	YES
1.1-RP-02-G3	3750	3767	3786	3748	YES
1.1-RP-02-G4	3520	3536	3554	3518	YES
1.1-RP-03-G1	3210	3225	3241	3208	YES
1.1-RP-03-G2	3760	3777	3797	3758	YES
1.1-RP-03-G3	3720	3737	3756	3718	YES
1.1-RP-03-G4	3330	3345	3362	3328	YES
1.1-RP-04-G1	3230	3245	3261	3228	YES
1.1-RP-04-G2	3880	3898	3918	3878	YES
1.1-RP-04-G3	3750	3767	3786	3748	YES
1.1-RP-04-G4	3590	3607	3625	3588	YES
1.1-RP-05-G1	3530	3546	3564	3528	YES
1.1-RP-05-G2	3630	3647	3665	3628	YES
1.1-RP-05-G3	3170	3185	3201	3168	YES
1.1-RP-05-G4	3330	3345	3362	3328	YES
1.1-RP-06-G1	3070	3084	3100	3068	YES
1.1-RP-06-G2	3530	3546	3564	3528	YES
1.1-RP-06-G3	3220	3235	3251	3218	YES
1.1-RP-06-G4	3480	3496	3514	3478	YES

Based on the data in Table 14, the upper limiting relative error was determined as 0.97%, whereas the lower limiting relative error was −0.05%. These results confirm compliance with the ±3% measurement accuracy requirement for failure load measurements.

Table 15 specifies dimensional deviations for welds in the composite milling variant to a depth of 6 mm.

Table 15. Weld dimensional deviations at 6 mm milling depth [13]

Sample No.	1	2	3
Dimensional deviations from nominal size in the X; Y axes [mm]	0; 0	−1; −1	0; 0

The analyses indicated that dimensional deviations along each welding-machine axis did not exceed 1 mm relative to the nominal dimension. Accordingly, the welded assembly met the intended dimensional target.

Figure 4.45 presents the mean failure loads of the individual specimens produced with composite milling to a depth of 6 mm. None of the specimens reached a mean failure load of 3000 N. Moreover, two of the three specimens remained below the adopted limit value of 2760 N.

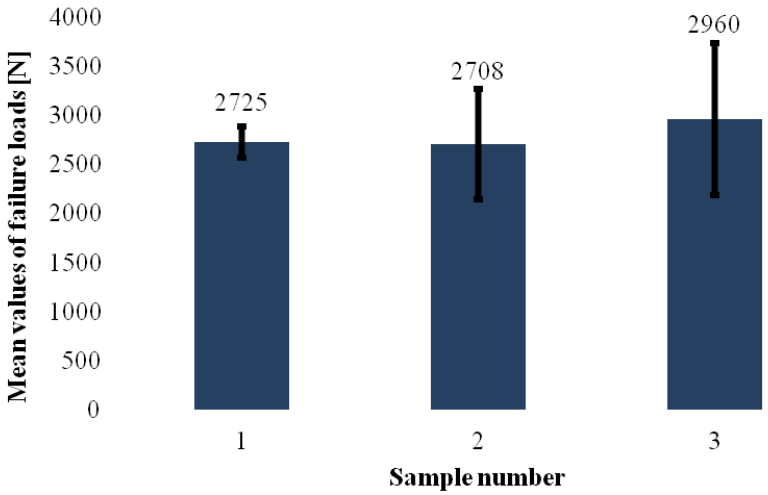

Fig. 4.45. Mean failure loads of the individual test specimens produced with composite milling to a depth of 6 mm [13]

Figure 4.46 illustrates representative welds obtained for two specimens produced with the composite milled to a depth of 6 mm. A white weld bead was observed for all specimens, which is consistent with the selected welding temperature. Material continuity across the joint was not preserved, and interrupted weld seams with localised discontinuities were evident in each specimen. This pattern is consistent with an excessive milling depth of the composite reinforcement. Weld symmetry was also assessed, and no evidence of profile displacement was identified during welding. Nonetheless, the discontinuous joint formation precludes acceptance of this parameter set within the assumed process window.

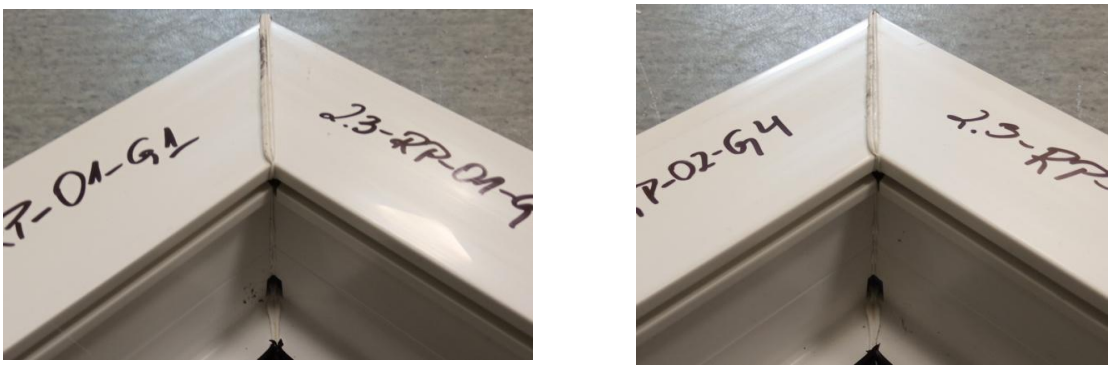

(a) (b)

Fig. 4.46. Selected welds from test specimens produced with composite milling to a depth of 6 mm: (a) welded using head 1, (b) welded using head 4 [13]

The third case studied was milling the composite at a depth of 3 mm. Table 16 reports the dimensional deviations of welds for the composite-milling variant at a milling depth of 3 mm.

Table 16. Dimensional weld deviations for 3 mm milling [13]

Sample No.	1	2	3
Dimensional deviations from nominal size in the X; Y axes [mm]	0; 0	−1; −1	−1; −1

The results indicate that dimensional deviations from the nominal dimension do not exceed 1 mm along any axis of the welding machine. Accordingly, the welded assembly can be regarded as dimensionally compliant.

Figure 4.47 presents the mean failure loads of the individual specimens produced with composite milling to a depth of 3 mm. The results show no material differences between the specimens. Only one specimen exceeded a mean failure load of 3000 N, whereas the remaining two did not surpass 2900 N.

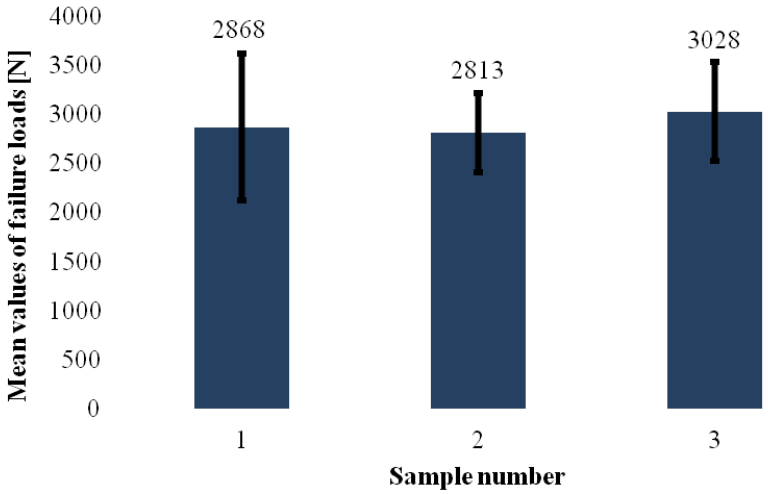

Fig. 4.47. Mean failure loads of the individual test specimens produced with composite milling to a depth of 3 mm [13]

Figure 4.48 illustrates representative welds obtained for two specimens produced with composite milling to a depth of 3 mm. A white weld bead was again observed for all specimens, which is consistent with the adopted welding temperature. Material continuity across the joint was not preserved, and localised, spot-like interruptions of the weld seam were evident in each specimen. This pattern is consistent with an excessive milling depth of the composite reinforcement. Weld symmetry was also assessed, and no evidence of profile displacement was identified during welding. Nonetheless, the discontinuous joint formation precludes acceptance of this parameter set within the assumed process window.

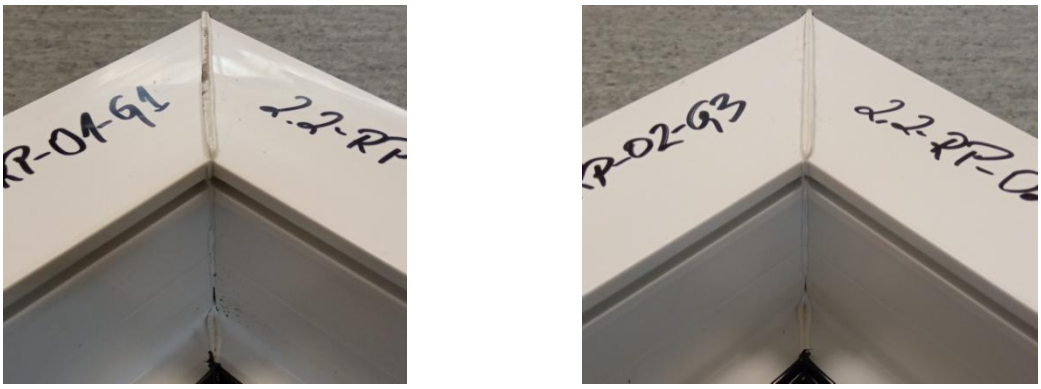

(a) (b)

Fig. 4.48. Selected welds from test specimens produced with composite milling to a depth of 3 mm: (a) welded using head 1, (b) welded using head 3 [13]

Table 17 summarises weld dimensional deviations corresponding to the composite milling variant with a 2 mm milling depth.

Table 17. Weld dimensional deviation results at 2 mm [13]

Sample No.	1	2	3	4	5	6
Dimensional deviations from nominal size in the X; Y axes [mm]	0; 0	0; 0	0; 1	1; 1	0; 0	0; 1

The test results indicate that deviations from the nominal dimension do not exceed 1 mm along any axis of the welding machine. Accordingly, the welded assembly can be regarded as dimensionally compliant.

Figure 4.49 presents the mean failure loads of the individual specimens produced with composite milling to a depth of 2 mm. The results show no material differences between the specimens. Five of the six specimens achieved mean failure loads exceeding 3000 N. By contrast, specimen 1 welded on head H2 yielded a failure load of 1430 N, which constituted a pronounced outlier relative to the remaining observations. A Dixon test was therefore applied to assess whether this value should be excluded. The analysis supported rejection of this single result.

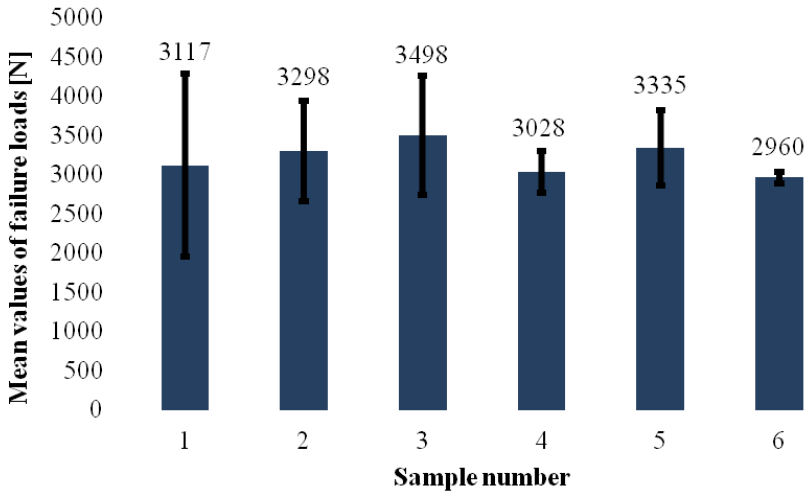

Fig. 4.49. Mean failure loads of the individual test specimens produced with composite milling to a depth of 2 mm [13]

Figure 4.50 illustrates representative welds obtained for two specimens produced with the composite milled to a depth of 2 mm. A white weld bead was observed for all specimens, which is consistent with a welding temperature that does not produce visible thermal degradation of the PVC profile. Material continuity across the joint was not preserved, particularly in the corner regions, and localised interruptions of the weld seam were evident in each specimen. This pattern is consistent with an excessive milling depth of the composite reinforcement. Weld symmetry was also assessed, and no evidence of profile displacement was identified during welding. Nonetheless, the observed discontinuities preclude acceptance of this parameter set within the assumed process window.

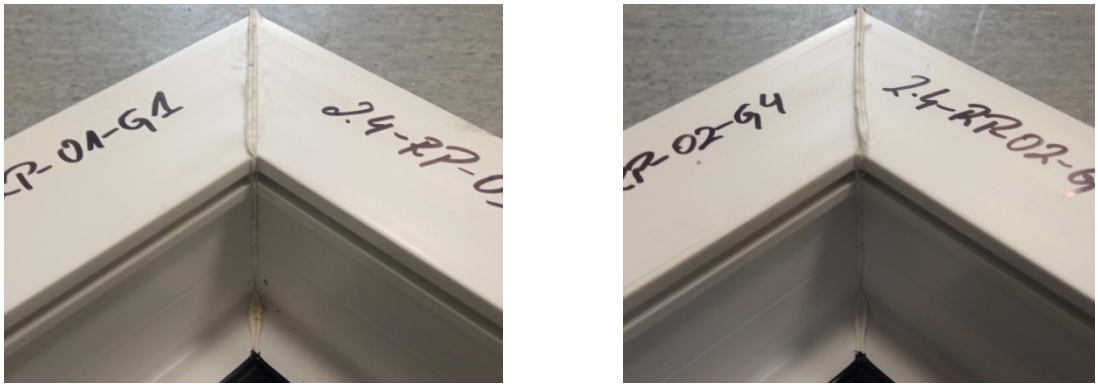

(a) (b)

Fig. 4.50. Selected welds from test specimens produced with composite milling to a depth of 2 mm: (a) welded using head 1, (b) welded using head 4 [13]

Table 18 presents the dimensional deviation results for welds in the composite-milling case, milled to 1.5 mm.

Table 18. Weld dimensional deviations for milling to 1.5 mm [13]

Sample No.	1	2	3
Dimensional deviations from nominal size in the X; Y axes [mm]	1; 1	1; 1	0; 1

The test results indicate that the dimensional deviations along the welding-machine axes remain within 1 mm of the nominal dimension. Accordingly, the welded assembly can be regarded as dimensionally compliant.

Figure 4.51 compares the failure load values obtained with composite milling to a depth of 1.5 mm. The highest value was recorded for specimen 3. The remaining specimens yielded values with no material deviation from the maximum value of 3400 N.

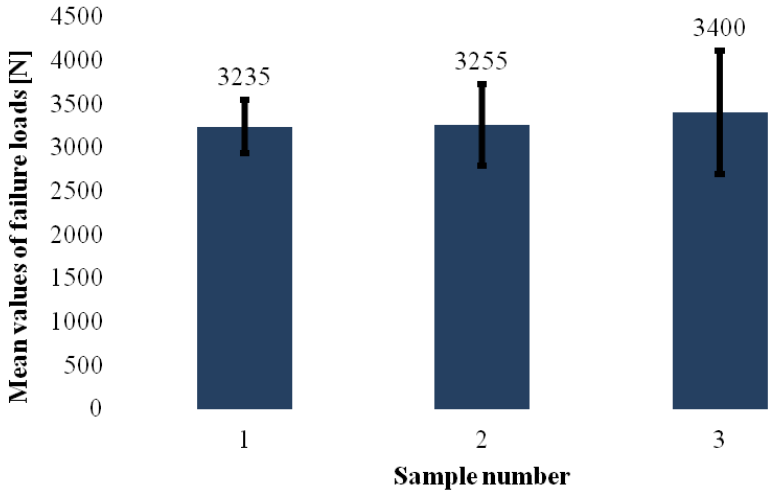

Fig. 4.51. Mean failure loads of the individual test specimens produced with composite milling to a depth of 1.5 mm [13]

Figure 4.52 illustrates representative welds obtained for two specimens produced with composite milling to a depth of 1.5 mm. A white weld bead was observed for all specimens, which is consistent with a welding temperature that does not produce visible thermal degradation of the PVC profile. Material continuity across the joint was not preserved, particularly in the corner regions, and localised interruptions of the weld seam were evident in most specimens. This pattern is consistent with an excessive milling depth of the composite reinforcement. Weld symmetry was also assessed, and no evidence of profile displacement was identified during welding. Nonetheless, the discontinuities observed in the majority of specimens preclude qualitative acceptance of this parameter set within the assumed process window.

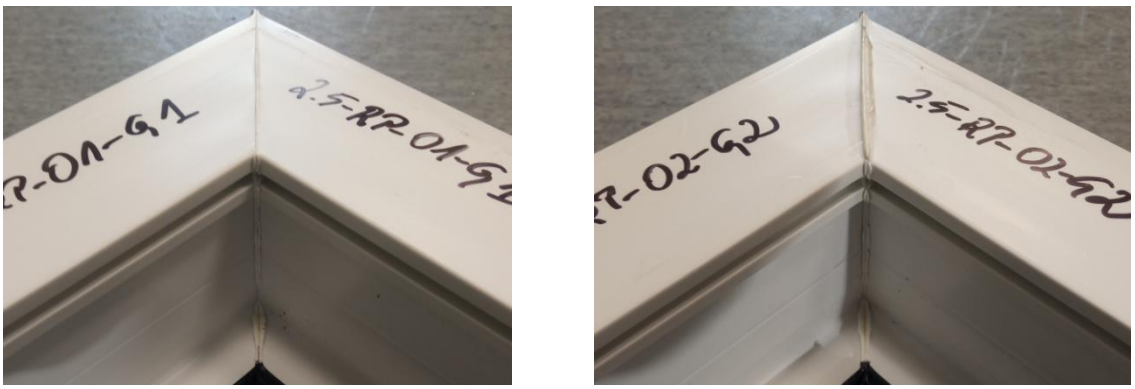

(a) (b)

Fig. 4.52. Selected welds from test specimens produced with composite milling to a depth of 1.5 mm: (a) welded using head 1, (b) welded using head 2 [13]

Table 19 details the weld dimensional deviations obtained for the composite milling variant at 1 mm depth.

Table 19. Dimensional deviations of welds at 1 mm depth [13]

Sample No.	1	2	3	4	5	6
Dimensional deviations from nominal size in the X; Y axes [mm]	1; 1	1; 1	1; 1	0; 1	0; 0	0; 0

The test results indicate that dimensional deviations from the nominal values remain below 1 mm along all axes of the welding machine. Accordingly, the welded assembly can be regarded as dimensionally compliant with the intended geometry.

Figure 4.53 compares the failure load values obtained with composite milling to a depth of 1 mm. All specimens exceeded 3000 N, and all except specimen 4 also surpassed 3500 N. No material differences were observed among the failure load values for the specimens included in this comparison.

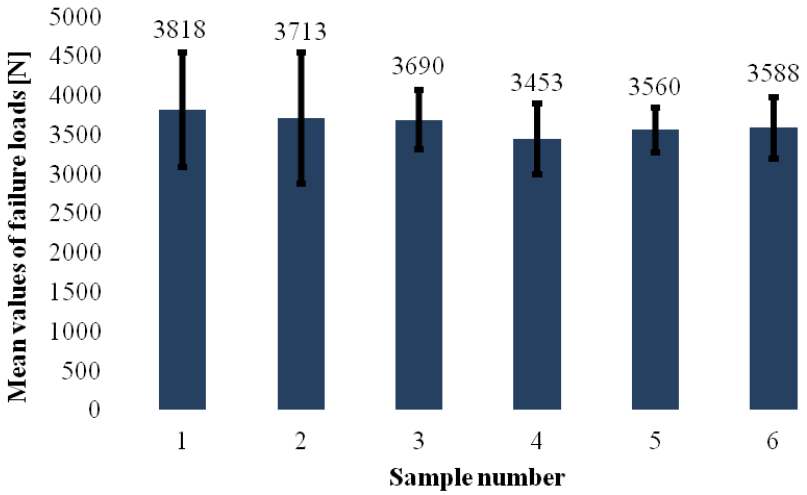

Fig. 4.53. Mean failure loads of the individual test specimens produced with composite milling to a depth of 1 mm [13]

Figure 4.54 illustrates representative welds obtained for two specimens produced with composite milling to a depth of 1 mm. A white weld bead was observed for all specimens, which is consistent with the selected welding temperature and the absence of visible thermal degradation of the PVC profile. In this case, material continuity across the joint was preserved, and a discernible weld seam was present in each specimen. Weld symmetry was also assessed, and no evidence of profile displacement was identified during welding.

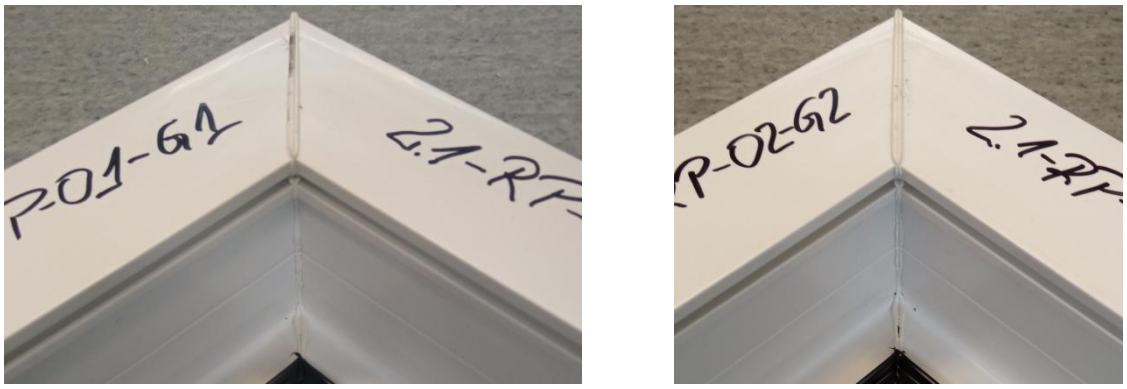

(a) (b)

Fig. 4.54. Selected welds from test specimens produced with composite milling to a depth of 1 mm: (a) welded using head 1, (b) welded using head 2 [13]

Table 20 tabulates the dimensional deviations measured for welds in the composite milling variant with milling depth set to 0.5 mm.

Table 20. Dimensional weld deviation data for 0.5 mm depth [13]

Sample No.	1	2	3
Dimensional deviations from nominal size in the X; Y axes [mm]	1; 1	1; 1	0; 1

The measurements indicate that the maximum dimensional deviations from the nominal values do not exceed 1 mm along the welding-machine axes. Accordingly, the welded assembly can be regarded as meeting the intended dimensional requirements.

Figure 4.55 presents the mean failure loads of the individual specimens produced with composite milling to a depth of 0.5 mm. The results show no material differences between the specimens. All three specimens exceeded 3400 N.

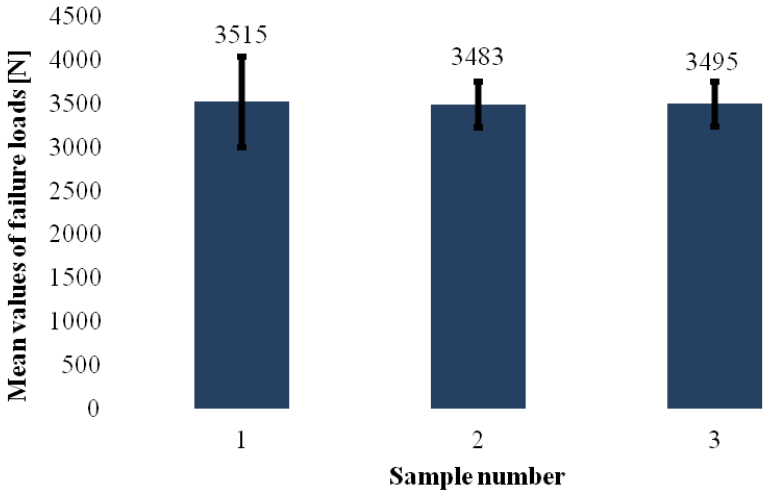

Fig. 4.55. Mean failure loads of the individual test specimens produced with composite milling to a depth of 0.5 mm [13]

Figure 4.56 illustrates representative welds obtained for two specimens produced with composite milling to a depth of 0.5 mm. A white weld bead was observed for all specimens, as expected. This observation is consistent with selection of a welding temperature that does not produce visible thermal degradation of the PVC profile. Material continuity across the joint was preserved, and a discernible weld seam was present in each specimen. Weld symmetry was also assessed, and no evidence of profile displacement was identified during welding.

(a) (b)

Fig. 4.56. Selected welds from test specimens produced with composite milling to a depth of 0.5 mm: (a) welded using head 1, (b) welded using head 3 [13]

Figure 4.57 summarises the mean failure loads of the specimen sets grouped by composite-insert milling depth. The highest mean failure load was recorded for specimens milled to 1.0 mm, whereas the lowest was observed for milling to 6.0 mm. Across the 0.0–1.0 mm range, the mean failure load increased modestly and peaked at 1.0 mm, although differences between the 0.0 mm, 0.5 mm, and 1.0 mm sets were not pronounced. Beyond 1.0 mm, the mean values decreased, with a pronounced drop between the 1.0 mm and 1.5 mm conditions. The 1.5 mm set exhibited a markedly lower mean failure load, and the divergence became more evident when compared with the deeper-milling sets. For milling depths of 1.5 mm and greater, discontinuities within the weld region were observed and a discernible weld seam was not apparent, which is consistent with excessive milling of the composite reinforcement.

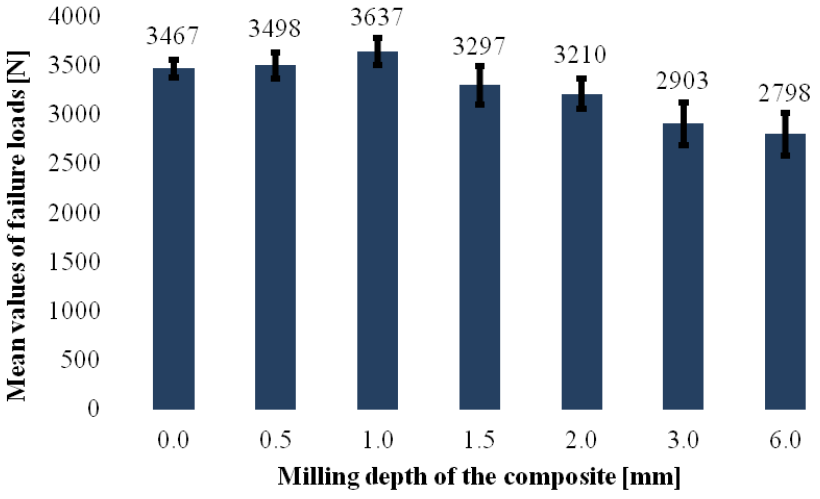

Fig. 4.57. Mean failure loads for specimen sets grouped by composite milling depth [13]

The subsequent phase of the study examined the effect of welding-head feed rate on weld strength and weld integrity. As the 0.25 mm/s condition had already been evaluated in the composite-milling programme, this stage considered only 0.19 mm/s and 0.31 mm/s (Table 9).

The first case study assessed weld failure loads at a welding-head feed rate of 0.31 mm/s, with the composite reinforcement milled to a depth of 1 mm. Table 21 reports the resulting dimensional deviations in mould length and width after welding relative to the nominal values, resolved by the individual machine axes.

Table 21. Dimensional deviations of the welded molds for a set welding head speed of 0.31 mm/s when milling the composite reinforcement to a depth of 1 mm [12]

Sample No.	1	2	3
Dimensional deviations from nominal size in the X; Y axes [mm]	1; 1	1; 1	1; 1

The results presented in Table 21 indicate that the discrepancy between the target dimensions and the post-weld dimensions does not exceed 1 mm. Accordingly, the mould can be regarded as meeting the adopted dimensional tolerance of 1 mm.

Figure 4.58 presents the mean failure loads for the specimen sets produced at a welding-head feed rate of 0.31 mm/s, with the glass-fibre-reinforced composite milled to a depth of 1 mm. The results show no material differences between the mean values. Two specimen sets exceeded the 3000 N failure-load threshold, and a further set surpassed 2950 N.

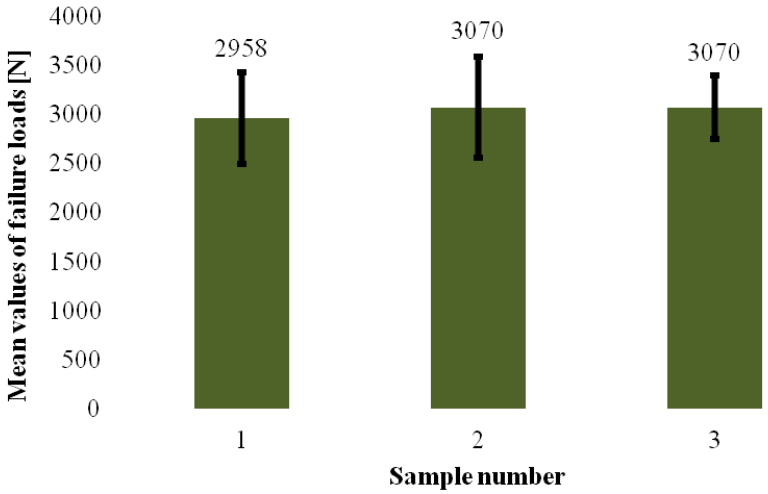

Fig. 4.58. Mean failure loads for specimen sets produced at a welding-head feed rate of 0.31 mm/s with composite-reinforcement milling to a depth of 1 mm [12]

Figure 4.59 illustrates representative welds obtained for two specimens produced at a welding-head feed rate of 0.31 mm/s with the glass-fibre-reinforced composite milled to a depth of 1 mm. A clearly defined weld bead was present, which is consistent with material continuity across the joint and is likely to contribute to the recorded failure loads. The weld bead exhibited a white coloration, which is consistent with an appropriate temperature setting. Excessive welding temperatures may increase the likelihood of PVC depolymerisation, which typically manifests as darkening of the weld region.

(a) (b)

Fig. 4.59. Representative welds from the test specimens: (a) welded using head 2, (b) welded using head 4 [12]

The second case study assessed weld failure loads at a welding-head feed rate of 0.19 mm/s, with the composite reinforcement milled to a depth of 1 mm. Table 22 reports the resulting dimensional deviations in mould length and width after welding relative to the nominal values, resolved by the individual machine axes.

Table 22. Dimensional deviations of the welded molds for a set welding head speed of 0.19 mm/s when milling the composite reinforcement to a depth of 1 mm [12]

Sample No.	1	2	3
Dimensional deviations from nominal size in the X; Y axes [mm]	1; 1	1; 1	1; 1

The results reported in Table 22 indicate that the discrepancy between the target dimensions and the post-weld dimensions does not exceed 1 mm. Accordingly, the adopted dimensional tolerance of 1 mm can be regarded as satisfied.

Figure 4.60 presents the mean failure loads for the specimen sets produced at a welding-head feed rate of 0.19 mm/s, with the glass-fibre-reinforced composite milled to a depth of 1 mm. The results show no material differences between the mean values. Two specimen sets exceeded the 3100 N failure-load threshold, and one set surpassed 3050 N.

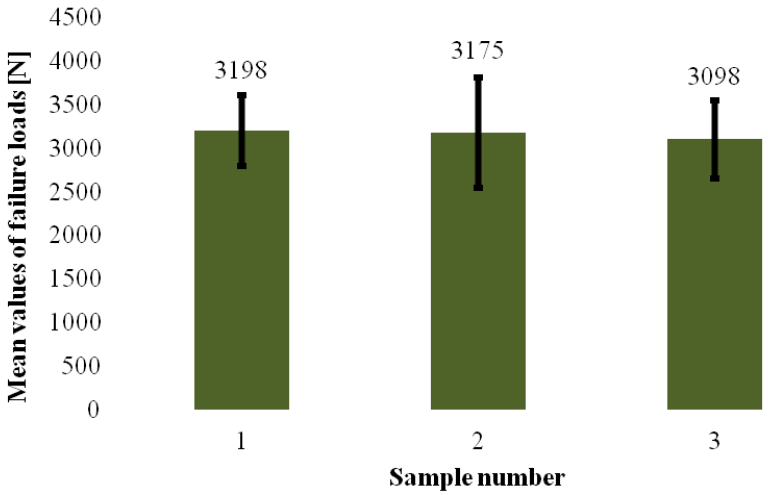

Fig. 4.60. Mean failure loads for specimen sets produced at a welding-head feed rate of 0.19 mm/s with composite-reinforcement milling to a depth of 1 mm [12]

Figure 4.61 illustrates representative welds obtained for two specimens produced at a welding-head feed rate of 0.19 mm/s with the glass-fibre-reinforced composite milled to a depth of 1 mm. Weld symmetry was assessed, and no evidence of profile displacement was identified during welding. A discernible weld seam was present, which is consistent with material continuity across the joint and is likely to contribute to weld strength. In turn, weld strength governs the measured failure load. The weld bead exhibited a white coloration, which is consistent with an appropriate temperature setting.

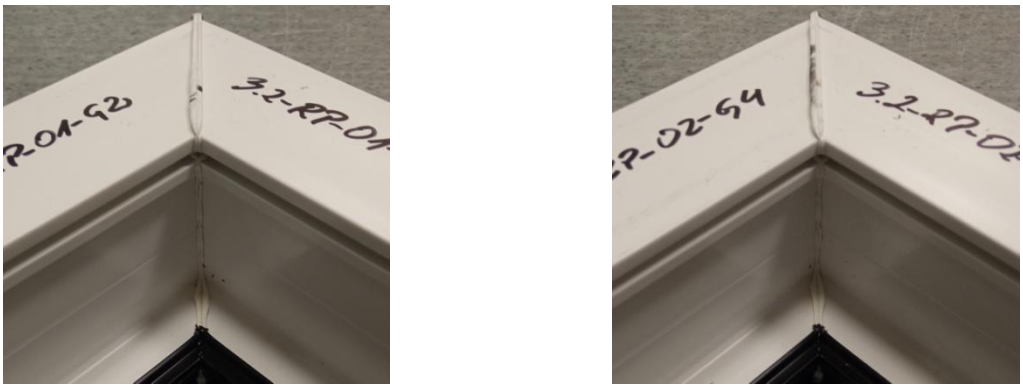

(a) (b)

Fig. 4.61. Representative welds from the reconnaissance tests: (a) welded using head 2, (b) welded using head 4 [12]

The third case study assessed weld failure loads at a welding-head feed rate of 0.31 mm/s, with the composite reinforcement milled to a depth of 0.5 mm. Table 23 reports the resulting dimensional deviations in mould length and width after welding relative to the nominal values, resolved by each machine axis.

Table 23. Dimensional deviations of welded molds for a set welding head speed of 0.31 mm/s when milling the composite reinforcement to a depth of 0.5 mm [12]

Sample No.	1	2	3
Dimensional deviations from nominal size in the X; Y axes [mm]	1; 1	0; 1	1; 1

The results reported in Table 23 indicate that the discrepancy between the target dimensions and the post-weld dimensions does not exceed 1 mm. Accordingly, the adopted dimensional tolerance of 1 mm can be regarded as satisfied.

Figure 4.62 presents the mean failure loads for the specimen sets produced at a welding-head feed rate of 0.31 mm/s, with the glass-fibre-reinforced composite milled to a depth of 0.5 mm. The mean values were comparable across all sets. All sets recorded mean failure loads exceeding 2800 N, and the third set also surpassed 3000 N.

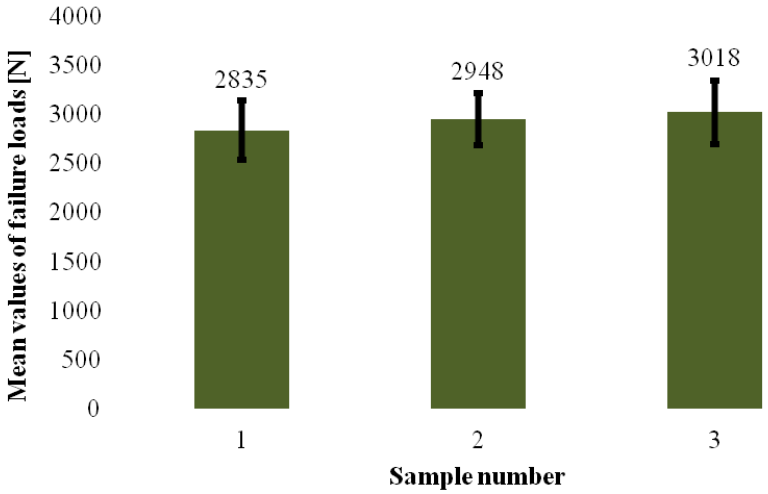

Fig. 4.62. Mean failure loads for specimen sets produced at a welding-head feed rate of 0.31 mm/s with composite-reinforcement milling to a depth of 0.5 mm [12]

Figure 4.63 illustrates representative welds obtained for two specimens produced at a welding-head feed rate of 0.31 mm/s with the glass-fibre-reinforced composite milled to a depth of 0.5 mm. Weld symmetry was assessed, and the joints appeared to be well aligned, with no evidence of profile displacement. A discernible weld seam was present, which is consistent with material continuity across the joint. In addition, a white weld bead was observed, which is consistent with an appropriate temperature setting.

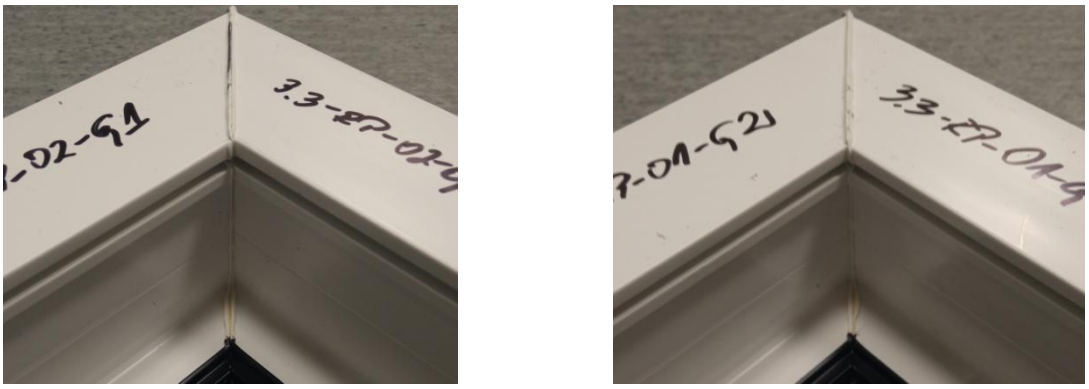

(a) (b)

Fig. 4.63. Representative welds from the reconnaissance tests: (a) welded using head 1, (b) welded using head 2 [12]

The fourth case study assessed weld failure loads at a welding-head feed rate of 0.19 mm/s, with the composite reinforcement milled to a depth of 0.5 mm. Table 24 reports the resulting dimensional deviations in mould length and width after welding relative to the nominal values, resolved by each machine axis.

Table 24. Dimensional deviations of welded molds for a set welding head speed of 0.19 mm/s when milling the composite reinforcement to a depth of 0.5 mm [12]

Sample No.	1	2	3
Dimensional deviations from nominal size in the X; Y axes [mm]	0; 1	0; 1	0; 0

The results reported in Table 24 indicate that the discrepancy between the target dimensions and the post-weld dimensions does not exceed 1 mm. Accordingly, the adopted dimensional tolerance of 1 mm can be regarded as satisfied.

Figure 4.64 presents the mean failure loads for the specimen sets produced at a welding-head feed rate of 0.19 mm/s, with the glass-fibre-reinforced composite milled to a depth of 0.5 mm. The mean values were comparable across all sets, with no material differences observed. All three sets recorded mean failure loads exceeding 3100 N.

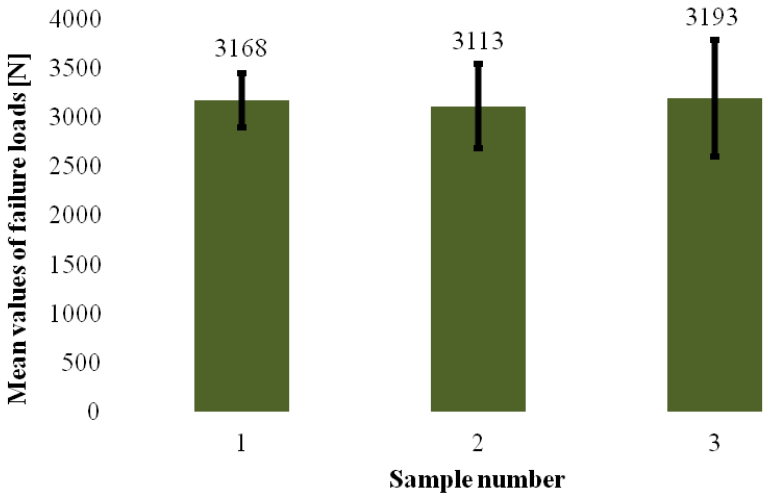

Fig. 4.64. Mean failure loads for specimen sets produced at a welding-head feed rate of 0.19 mm/s with composite-reinforcement milling to a depth of 0.5 mm [12]

Figure 4.65 illustrates representative welds obtained for two specimens produced at a welding-head feed rate of 0.19 mm/s with the glass-fibre-reinforced composite milled to a depth of 0.5 mm. Weld symmetry was assessed, and the joints appeared to be well aligned, with no evidence of profile displacement. A discernible weld seam was present, which is consistent with material continuity across the joint. The weld region also exhibited a white coloration, which is consistent with an appropriate temperature setting.

(a) (b)

Fig. 4.65. Representative welds from the reconnaissance tests: (a) welded using head 2, (b) welded using head 4 [12]

The fifth case study assessed weld failure loads at a welding-head feed rate of 0.31 mm/s, with the composite reinforcement left unmilled. Table 25 reports the resulting dimensional deviations in mould length and width after welding relative to the nominal values, resolved by each machine axis.

Table 25. Dimensional deviations of the welded molds for the set welding head speed of 0.31 mm/s without milling the composite reinforcement [12]

Sample No.	1	2	3
Dimensional deviations from nominal size in the X; Y axes [mm]	0; 0	0; 0	0; 0

The results reported in Table 25 indicate that the discrepancy between the target dimensions and the post-weld dimensions does not exceed 1 mm. Accordingly, the adopted dimensional tolerance of 1 mm can be regarded as satisfied.

Figure 4.66 presents the mean failure loads for the specimen sets produced at a welding-head feed rate of 0.31 mm/s with the glass-fibre-reinforced composite left unmilled. The mean values were comparable across all sets, with no material differences observed. All three sets recorded mean failure loads exceeding 3000 N, and two sets also surpassed 3100 N.

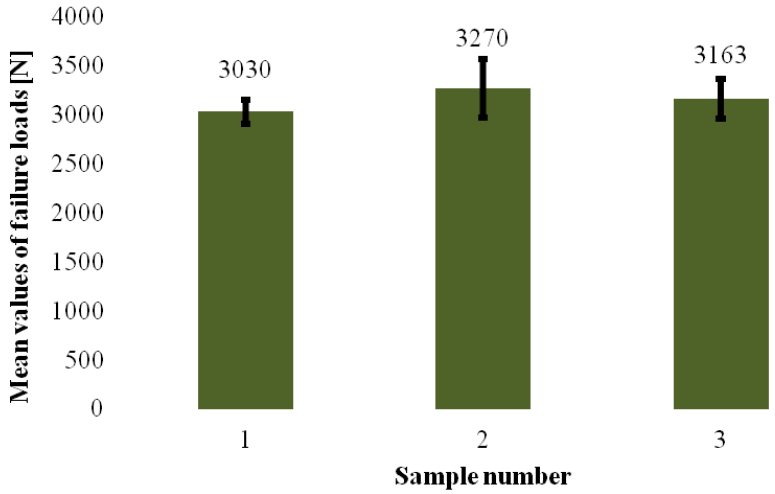

Fig. 4.66. Mean failure loads for specimen sets produced at a welding-head feed rate of 0.31 mm/s with the composite reinforcement left unmilled [12]

Figure 4.67 illustrates representative welds obtained for two specimens produced at a welding-head feed rate of 0.31 mm/s with the glass-fibre-reinforced composite left unmilled. Weld symmetry was assessed, and the joints appeared to be well aligned, with no evidence of profile displacement. A discernible weld seam was present, which is consistent with material continuity across the joint. In addition, a white weld bead was observed, which is consistent with an appropriate temperature setting.

(a) (b)

Fig. 4.67. Representative welds from the reconnaissance tests: (a) welded using head 1, (b) welded using head 3 [12]

The sixth case study assessed weld failure loads at a welding-head feed rate of 0.19 mm/s, with the composite reinforcement left unmilled. Table 26 reports the resulting dimensional deviations in mould length and width after welding relative to the nominal values, resolved by each machine axis.

Table 26. Dimensional deviations of welded molds for a set welding head speed of 0.19 mm/s without milling the composite reinforcement [12]

Sample No.	1	2	3
Dimensional deviations from nominal size in the X; Y axes [mm]	0; 1	0; 0	0; 1

Consistent with the preceding test variants, the results reported in Table 26 indicate that the discrepancy between the target dimensions and the post-weld dimensions remains within 1 mm. Accordingly, the adopted dimensional tolerance of 1 mm can be regarded as satisfied.

Figure 4.68 presents the mean failure loads for the specimen sets produced at a welding-head feed rate of 0.19 mm/s with the glass-fibre-reinforced composite left unmilled. The mean values were comparable across all sets, with no material differences observed. All sets recorded mean failure loads exceeding 3000 N, and one set also surpassed 3300 N.

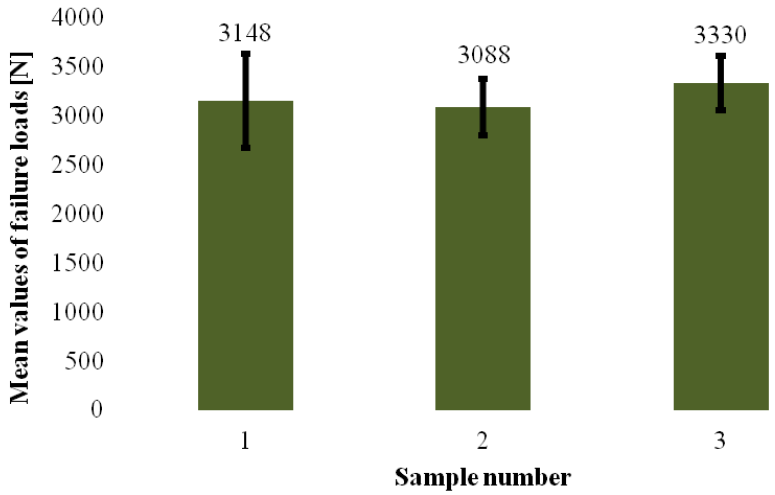

Fig. 4.68. Mean failure loads for specimen sets produced at a welding-head feed rate of 0.19 mm/s with the composite reinforcement left unmilled [12]

Figure 4.69 illustrates representative welds obtained for two specimens produced at a welding-head feed rate of 0.19 mm/s with the glass-fibre-reinforced composite left unmilled. Weld symmetry was assessed, and the joints appeared to be well aligned, with no evidence of profile displacement. A discernible weld seam was present, which is consistent with material continuity across the joint, and a white weld bead was observed, which is consistent with an appropriate temperature setting.

(a) (b)

Fig. 4.69. Representative welds from the reconnaissance tests: (a) welded using head 1, (b) welded using head 4 [12]

Figure 4.70 summarises the mean weld failure loads as a function of composite milling depth (0.5 mm and 1.0 mm) and the unmilled condition. The comparison also incorporates welding-head feed rates of 0.19 mm/s, 0.25 mm/s, and 0.31 mm/s.

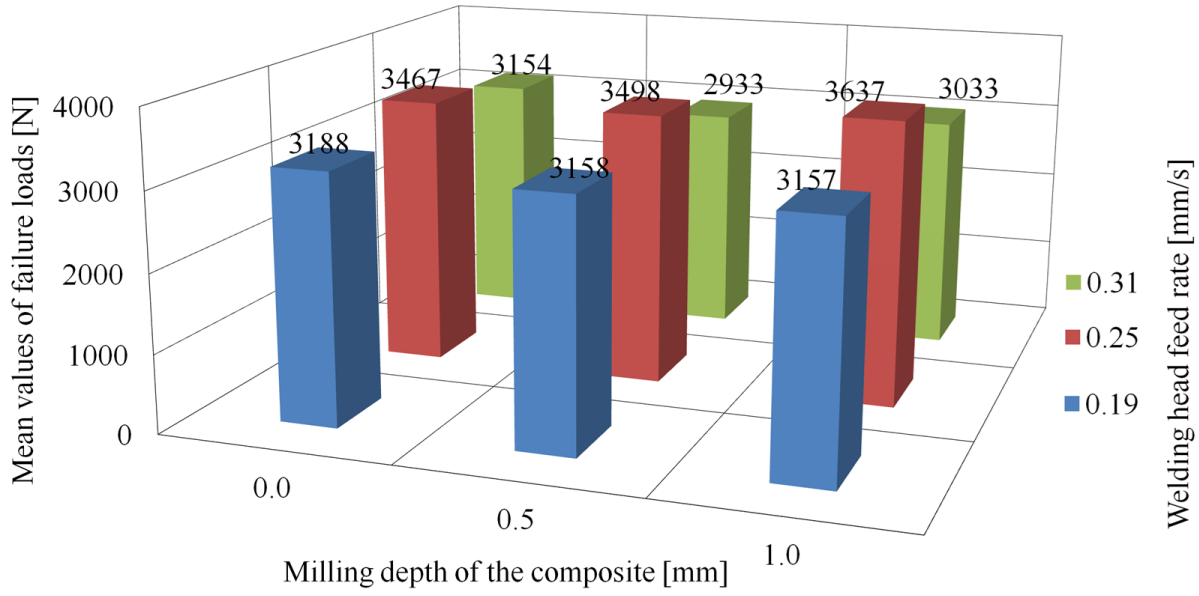

Fig. 4.70. Summary of mean failure loads for specimen sets as a function of composite-reinforcement milling depth and welding-head feed rate [12]

For a composite milling depth of 1 mm, the mean failure load varied with welding-head feed rate. The lowest mean values were recorded at 0.31 mm/s (3033 N) and 0.19 mm/s (3157 N). The highest mean failure load was obtained at 0.25 mm/s (3637 N), which was markedly higher than the values recorded at the other feed rates. Figure 4.70 also reports mean failure loads for welds produced with composite-reinforcement milling to a depth of 0.5 mm. The mean values again depended on welding-head feed rate, with the lowest values recorded at 0.31 mm/s (2933 N) and 0.19 mm/s (3158 N). The highest mean failure load was observed at 0.25 mm/s (3498 N). Notably, this value was lower than the corresponding mean at 1 mm milling depth for the same feed rate. For the unmilled condition, Figure 4.70 indicates that the mean failure load also varied with welding-head feed rate. The lowest mean values were again recorded at 0.31 mm/s (3154 N) and 0.19 mm/s (3188 N). The highest mean failure load occurred at 0.25 mm/s (3467 N). Among the 0.25 mm/s conditions, this value was the lowest across the three milling variants, although it remained higher than the mean values obtained at the other tested feed rates. Inspection of Figure 4.70 suggests that a welding-head feed rate of 0.25 mm/s provides the most favourable mean failure-load response within the investigated range. On this basis, the remaining comparison concerns the milling-depth variants at this feed rate, namely the unmilled condition, milling to 0.5 mm, and milling to 1.0 mm. The lowest mean failure load was recorded for the unmilled set (3467 N), followed by the 0.5 mm condition (3498 N), while the 1.0 mm condition yielded the highest mean value (3637 N). Nonetheless, the differences between these means are modest, and the available evidence does not allow a definitive ranking of milling depth in terms of peak performance and repeatability.

Overall, the analysis indicates that welding-head feed rate is among the principal process parameters governing weld failure loads in hot-plate welding. Within the investigated range, a feed rate of 0.25 mm/s yielded the highest mean failure loads and was clearly differentiated from the 0.19 mm/s and 0.31 mm/s conditions under the adopted settings of 264 °C and a melting time of 30 s, which is consistent with the disparate thermophysical behaviour of PVC and the glass-fibre-reinforced composite reinforcement. Visual inspection further suggests that 264 °C is appropriate for the PVC matrix, although it remains insufficient to plasticise the composite reinforcement. At the higher feed rate of 0.31 mm/s, the reinforcement is likely to

oppose head motion more strongly, which can hinder intimate contact formation and compromise joint quality, thereby reducing the measured failure load. Conversely, at 0.19 mm/s the thermal input may be applied for longer than required, increasing the likelihood of inefficient heat utilisation and non-ideal melt-flow conditions, which can likewise limit the development of a robust joint. Notwithstanding the clear preference for 0.25 mm/s within the feed-rate study, this conclusion cannot be directly extrapolated to the effect of composite milling depth, whether unmilled or milled to 0.5 mm or 1.0 mm, because the resulting failure-load values are closely clustered and do not permit an unambiguous identification of an optimal milling-depth variant under this criterion.

Accordingly, within the investigated range, a welding-head feed rate of 0.25 mm/s was identified as the most favourable condition and was adopted as the reference value for the subsequent stages of the experimental programme.

In the subsequent phase of the study, the effect of reducing the melting time on weld strength and integrity was evaluated. Since earlier results indicated that a welding-head feed rate of 0.25 mm/s was the most favourable, the parameter set listed in Table 10 was adopted for this part of the investigation.

The first case examined assessed weld failure loads at a melting time of 25 s. The composite reinforcement was milled to a depth of 1.0 mm, the welding temperature was set to 264 °C, and the welding-head feed rate was 0.25 mm/s. Table 27 reports the post-weld dimensional deviations in mould length and width relative to the nominal dimensions along each machine axis.

Table 27. Dimensional deviations of welded moulds for a given melting time of 25 s when milling the composite reinforcement to a depth of 1 mm [14]

Sample No.	1	2	3	4	5	6
Dimensional deviations from nominal size in the X; Y axes [mm]	1; 1	0; 1	1; 1	1; 1	1; 1	1; 1

The results in Table 27 indicate that the difference between the set dimension and the post-weld dimension did not exceed 1 mm. This outcome is consistent with the assumed dimensional tolerance of 1 mm. The tests also indicated that the weld remained symmetric.

Figure 4.71 presents the mean failure loads for specimen sets produced at a melting time of 25 s, with the glass-fibre-reinforced composite milled to a depth of 1.0 mm. The mean values were comparable across the sets, and all exceeded 3300 N. The highest recorded mean failure load was 3678 N, while the lowest was 3310 N, both comfortably above the target threshold of 2760 N.

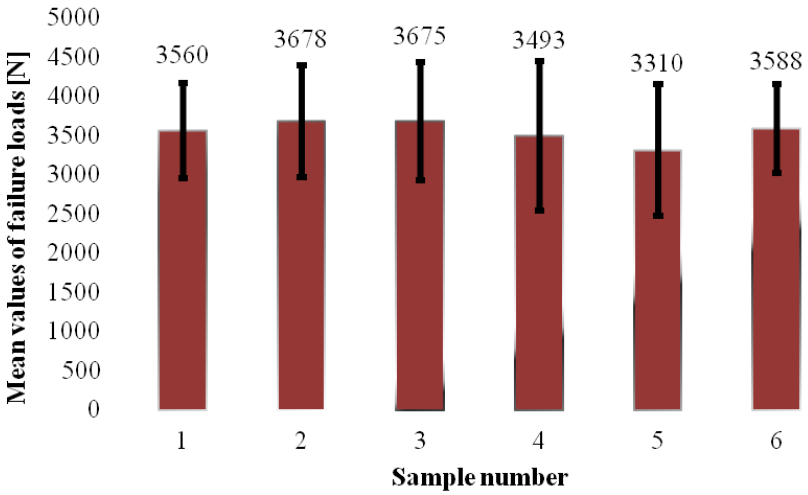

Fig. 4.71. Mean failure loads for specimen sets at a melting time of 25 s, with the composite reinforcement milled to a depth of 1.0 mm. Source: Author's own work

Figure 4.72 shows representative welds from two specimens produced at a melting time of 25 s, with the glass-fibre-reinforced composite milled to a depth of 1.0 mm. A continuous weld bead indicated adequate material continuity across the interface, which is consistent with the measured failure load levels. The pale, uniform bead colour was consistent with an appropriate temperature setting. By contrast, excessive process temperature may induce thermal degradation of the PVC profile, which is typically manifested by darkening of the weld region.

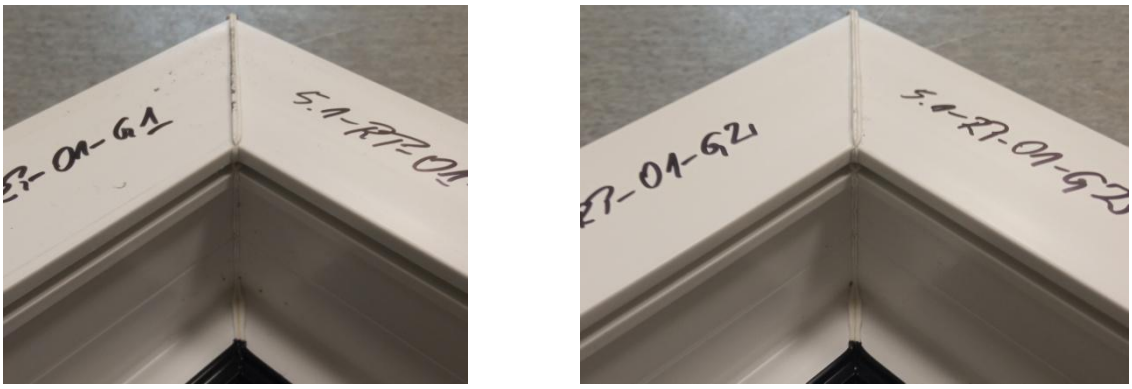

(a) (b)

Fig. 4.72. Representative welds from preliminary specimens: (a) first welding head, (b) second welding head. Source: Author's own work

The second case examined assessed weld failure loads at a melting time of 24 s. The composite reinforcement was milled to a depth of 1.0 mm, the welding temperature was set to 264 °C, and the welding-head feed rate was 0.25 mm/s. Table 28 summarises the post-weld dimensional deviations in mould length and width relative to the nominal dimensions along each machine axis.

Table 28. Dimensional deviations of welded moulds for a given melting time of 24 s when milling the composite reinforcement to a depth of 1 mm [14]

Sample No.	1	2	3	4	5	6
Dimensional deviations from nominal size in the X; Y axes [mm]	1; 1	1; 1	1; 1	1; 1	1; 1	1; 1

Table 28 indicates that the difference between the specified dimension and the post-weld dimension did not exceed 1 mm, which is consistent with the assumed dimensional tolerance of 1 mm. The results also indicated that the weld remained symmetric.

Figure 4.73 presents the mean failure loads for specimen sets produced at a melting time of 24 s, with the glass-fibre-reinforced composite milled to a depth of 1.0 mm. Although the fourth set achieved a mean failure load of 3260 N and the fifth set reached 3740 N, the inter-set differences in the mean values remained limited. All specimen sets exceeded 3200 N, and four sets achieved mean levels above 3400 N.

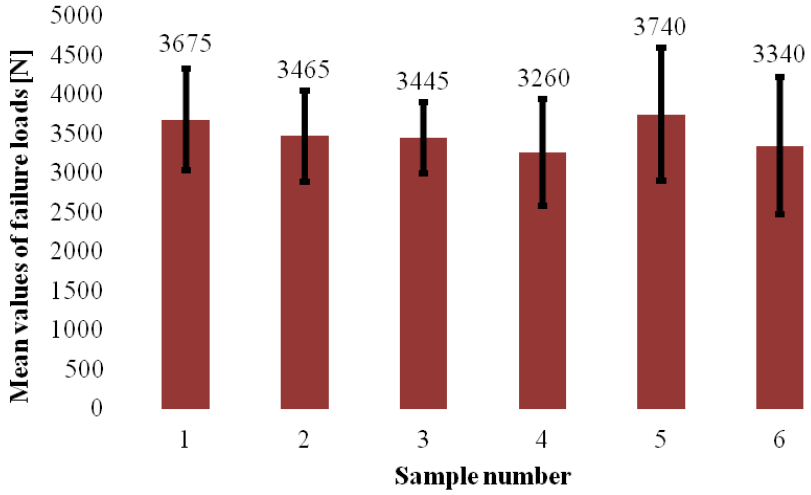

Fig. 4.73. Mean failure loads for specimen sets at a melting time of 24 s, with the composite reinforcement milled to a depth of 1.0 mm. Source: Author's own work

Figure 4.74 shows representative welds from two specimens produced at a melting time of 24 s, with the glass-fibre-reinforced composite milled to a depth of 1.0 mm. A visible and continuous weld bead suggested that material continuity across the interface was maintained, which is consistent with the measured failure load levels. The light bead colour was consistent with an appropriate process temperature setting. If the optimum welding temperature is exceeded, there is an increased risk of thermal degradation of the PVC profile, which may be manifested by darkening of the weld region.

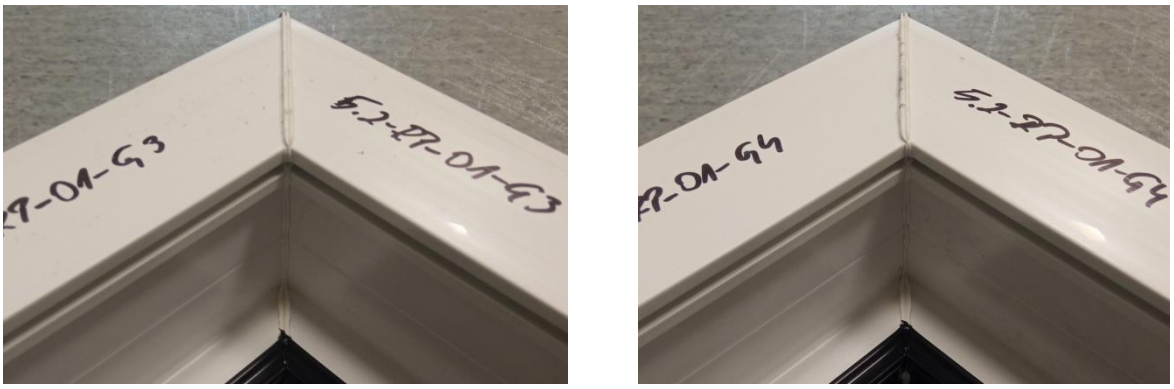

(a) (b)

Fig. 4.74. Representative welds from preliminary specimens: (a) third welding head, (b) fourth welding head. Source: Author's own work

The third case examined assessed weld failure loads at a melting time of 23 s. The composite reinforcement was milled to a depth of 1.0 mm, the welding temperature was set to 264 °C, and the welding-head feed rate was 0.25 mm/s. Table 29 reports the post-weld dimensional deviations in mould length and width relative to the nominal dimensions along each machine axis.

Table 29. Dimensional deviations of welded moulds for a given melting time of 23 s when milling the composite reinforcement to a depth of 1 mm [14]

Sample No.	1	2	3	4	5	6
Dimensional deviations from nominal size in the X; Y axes [mm]	1; 1	0; 1	1; 1	1; 1	1; 1	0; 1

Table 29 indicates that the difference between the set dimension and the post-weld dimension did not exceed 1 mm, which is consistent with the assumed dimensional tolerance of 1 mm. The results also indicated that the weld remained symmetric.

Figure 4.75 presents the mean failure loads for specimen sets produced at a melting time of 23 s, with the glass-fibre-reinforced composite milled to a depth of 1.0 mm. The mean values were closely clustered across the sets, with three sets between 3400 N and 3450 N. The highest mean failure load was recorded for the second set at 3540 N, whereas the sixth set yielded the lowest value at 3193 N.

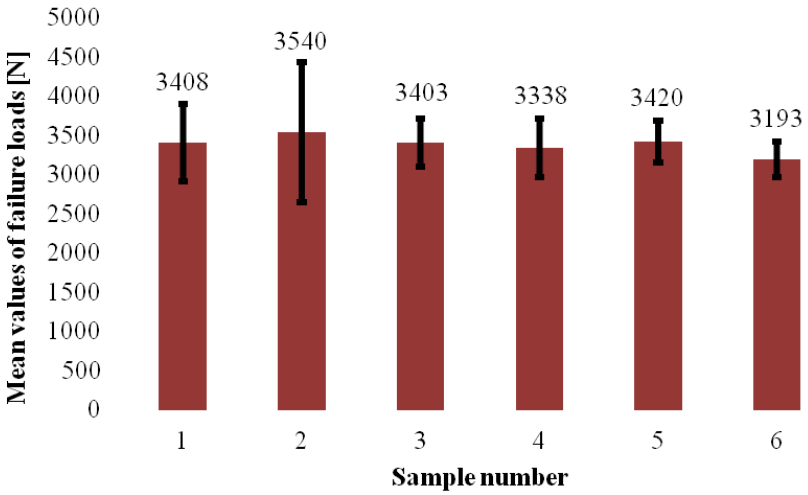

Fig. 4.75. Mean failure loads for specimen sets at a melting time of 23 s, with the composite reinforcement milled to a depth of 1.0 mm. Source: Author's own work

Figure 4.76 shows representative welds from two specimens produced at a melting time of 23 s, with the glass-fibre-reinforced composite milled to a depth of 1.0 mm. A visible and continuous weld bead suggested that material continuity across the interface was maintained, which is consistent with the measured failure load levels. The light bead colour was consistent with an appropriate process temperature setting. Excessive welding temperature may induce thermal degradation of the PVC profile, which may be manifested by darkening of the weld region.

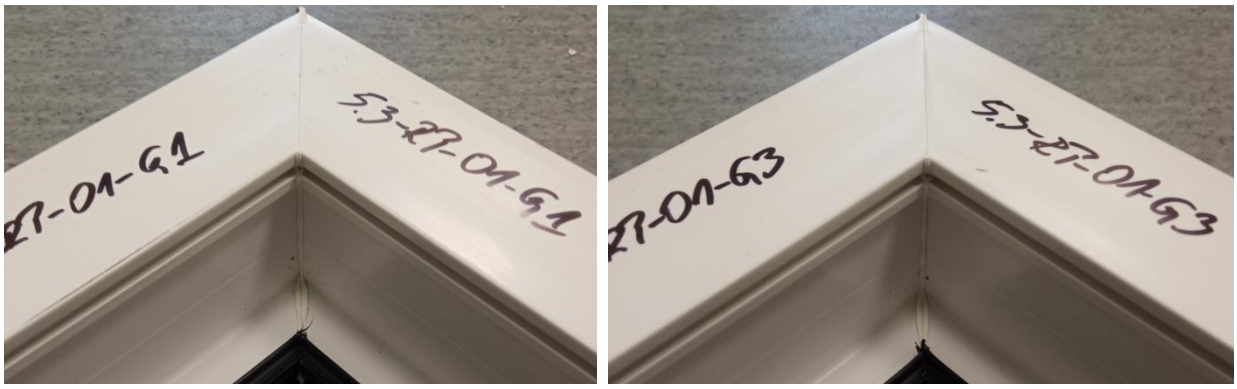

(a) (b)

Fig. 4.76. Representative welds from preliminary specimens: (a) first welding head, (b) third welding head. Source: Author's own work

The fourth case examined assessed weld failure loads at a melting time of 22 s. The composite reinforcement was milled to a depth of 1.0 mm, the welding temperature was set to 264 °C, and the welding-head feed rate was 0.25 mm/s. Table 30 reports the post-weld dimensional deviations in mould length and width relative to the nominal dimensions along each machine axis.

Table 30. Dimensional deviations of welded moulds for a given melting time of 22 s when milling the composite reinforcement to a depth of 1 mm [14]

Sample No.	1	2	3	4	5	6
Dimensional deviations from nominal size in the X; Y axes [mm]	1; 1	1; 1	1; 1	1; 1	1; 1	0; 1

Table 30 indicates that the difference between the target dimension and the post-weld dimension did not exceed 1 mm, which is consistent with the assumed dimensional tolerance of 1 mm. The tests also indicated that the weld remained symmetric.

Figure 4.77 presents the mean failure loads for specimen sets produced at a melting time of 22 s, with the glass-fibre-reinforced composite milled to a depth of 1.0 mm. All specimen sets exceeded 3100 N in terms of mean failure load. The second set exceeded 3500 N, while four of the six sets achieved mean values above 3400 N. Overall, the inter-set differences in the mean failure load were limited.

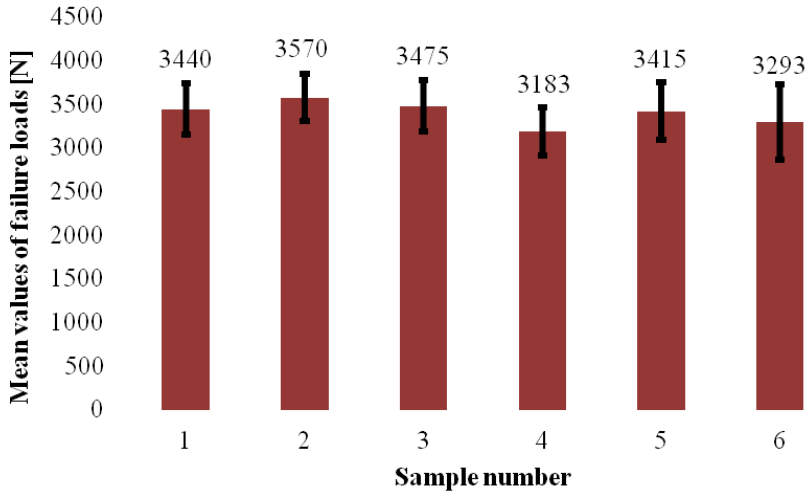

Fig. 4.77. Mean failure loads for specimen sets at a melting time of 22 s, with the composite reinforcement milled to a depth of 1.0 mm. Source: Author's own work

Figure 4.78 shows representative welds from two specimens produced at a melting time of 22 s, with the glass-fibre-reinforced composite milled to a depth of 1.0 mm. A distinct weld seam suggested that material continuity across the interface was maintained, which is consistent with the measured failure load levels. The pale weld bead colour was consistent with an appropriate welding temperature. By contrast, excessive process temperature may cause thermal degradation of the PVC, which may be manifested by darkening of the weld region.

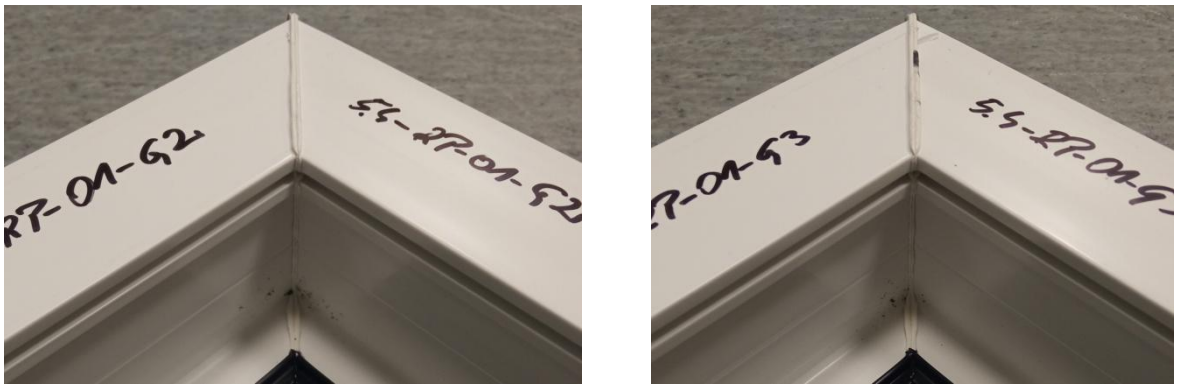

(a) (b)

Fig. 4.78. Representative welds from preliminary specimens: (a) second welding head, (b) third welding head [14]

The fifth case study assessed weld failure loads at a melting time of 21 s. The composite reinforcement was milled to a depth of 1.0 mm, the welding temperature was set to 264 °C, and the welding-head feed rate was 0.25 mm/s. Table 31 summarises the post-weld dimensional deviations in mould length and width relative to the nominal dimensions along each machine axis.

Table 31. Dimensional deviations of welded moulds for a given melting time of 21 s when milling the composite reinforcement to a depth of 1 mm [14]

Sample No.	1	2	3	4	5	6
Dimensional deviations from nominal size in the X; Y axes [mm]	2; 2	2; 2	2; 2	2; 2	2; 2	2; 2

Table 31 shows that, for each welded mould, the deviation between the set dimension and the post-weld dimension was 2 mm, which exceeds the 1 mm dimensional tolerance. This outcome suggests that a melting time of 21 s was insufficient, as indicated by the elevated loads registered by the machine during heating-head actuation. The increased resistance of the profile likely impeded proper consolidation, thereby preventing the mould from reaching the target dimensions and leading to an absence of the required weld symmetry.

Figure 4.79 presents the mean failure loads for specimen sets produced at a melting time of 21 s, with the glass-fibre-reinforced composite milled to a depth of 1.0 mm. All specimen sets exceeded 3200 N in terms of mean failure load. The fourth set yielded the highest mean value at 3713 N, and no set exhibited a materially different mean failure load from the others.

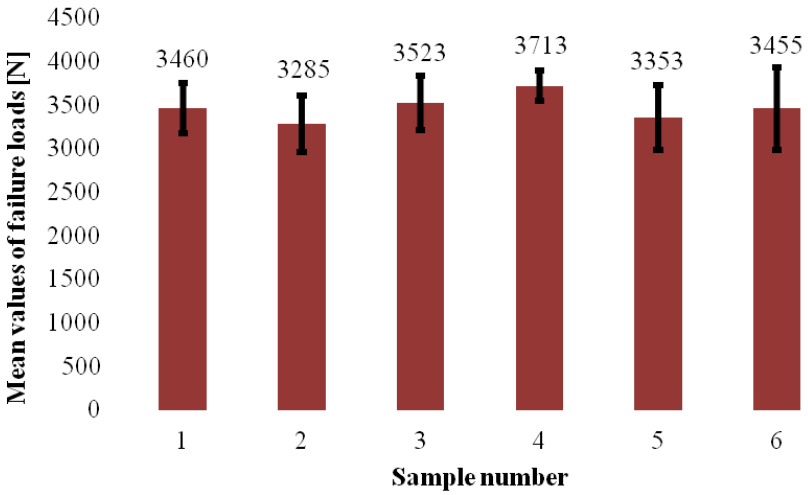

Fig. 4.79. Mean failure loads for specimen sets at a melting time of 21 s, with the composite reinforcement milled to a depth of 1.0 mm. Source: Author's own work

Figure 4.80 shows representative welds from two specimens produced at a melting time of 21 s, with the glass-fibre-reinforced composite milled to a depth of 1.0 mm. A visible weld bead suggested material continuity across the interface, which is conducive to attaining adequate failure load. The bright bead colour was consistent with an appropriate temperature setting. However, the dimensional nonconformity reported in Table 31 and the loss of weld symmetry call into question joint quality and may compromise subsequent assembly of the welded moulds.

(a) (b)

Fig. 4.80. Representative welds from preliminary specimens: (a) first welding head, (b) fourth welding head [14]

The sixth case examined weld failure loads at a melting time of 22 s. The composite reinforcement was milled to a depth of 0.5 mm, the welding temperature was set to 264 °C, and the welding-head feed rate was 0.25 mm/s. Table 32 reports the post-weld dimensional deviations in mould length and width relative to the nominal dimensions along each machine axis.

Table 32. Dimensional deviations of welded moulds for a given melting time of 22 s when milling the composite reinforcement to a depth of 0.5 mm [14]

Sample No.	1	2	3
Dimensional deviations from nominal size in the X; Y axes [mm]	2; 2	1; 2	1; 2

As shown in Table 32, each welded mould exhibited a dimensional deviation of at least 2 mm along one axis, which exceeds the permissible tolerance of 1 mm. This outcome indicates that the melting time was insufficient under the prevailing conditions. In this variant, the milling depth was reduced to 0.5 mm, which increased the effective engagement of the composite reinforcement relative to the 1.0 mm milling condition. Consequently, material resistance was encountered earlier during the melting stage, and overload of the welding-head actuators was again observed. Notably, extending the melting time by 1 s relative to the 22 s, 1.0 mm variant did not offset the adverse effect of reducing the milling depth to 0.5 mm. The additional 1 s is introduced at the end of the melting phase, whereas the early-stage interaction is governed primarily by milling depth and welding-head feed rate, because the heating platens reach the composite sooner when the reinforcement is less recessed. Within the previously identified optimum feed rate of 0.25 mm/s, the applied milling depth therefore degraded weld quality. As a result, the required mould geometry could not be achieved, and a loss of weld symmetry was also observed.

Figure 4.81 presents the mean failure loads for specimen sets produced at a melting time of 22 s, with the glass-fibre-reinforced composite milled to a depth of 0.5 mm. All specimen sets exceeded 3100 N in terms of mean failure load. The highest recorded mean value was 3380 N, while the lowest was 3185 N. The spread between sets remained limited.

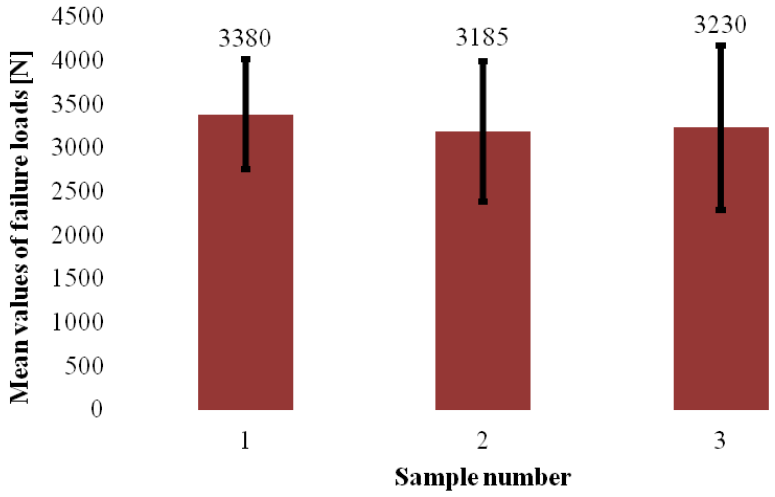

Fig. 4.81. Mean failure loads for specimen sets at a melting time of 22 s, with the composite reinforcement milled to a depth of 0.5 mm. Source: Author's own work

Figure 4.82 shows representative welds from two specimens produced at a melting time of 22 s, with the glass-fibre-reinforced composite milled to a depth of 0.5 mm. The weld bead exhibited a pale, uniform appearance, which is consistent with an appropriate temperature setting. However, weld symmetry assessment indicated a defect, and this observation aligns with the dimensional nonconformities identified in the post-weld tolerance measurements.

(a) (b)

Fig. 4.82. Representative welds from preliminary specimens: (a) first welding head, (b) second welding head. Source: Author's own work

The seventh case examined weld failure loads at a melting time of 22 s, with the composite reinforcement left unmilled. The welding temperature was set to 264 °C, and the welding-head feed rate was 0.25 mm/s. Table 33 reports the post-weld dimensional deviations in mould length and width relative to the nominal dimensions along each machine axis.

Table 33. Dimensional deviations of welded moulds for a given melting time of 22 s without milling of the composite reinforcement [14]

Sample No.	1	2	3
Dimensional deviations from nominal size in the X; Y axes [mm]	2; 2	2; 2	2; 2

Table 33 indicates that each welded mould deviated from the nominal dimension, with a 2 mm offset recorded on every axis. This exceeds the allowable dimensional tolerance of 1 mm. The results therefore suggest that a melting time of 22 s was insufficient under the prevailing process conditions. Omitting milling of the composite reinforcement likely increased resistance to welding-head motion. Under such resistance, the reduced melting time was inadequate to enable correct weld formation during the heating and joining stages.

Figure 4.83 presents the mean failure loads for specimen sets produced at a melting time of 22 s, with the glass-fibre-reinforced composite left unmilled. All specimen sets exceeded 2800 N in terms of mean failure load. The first set yielded the highest mean value at 3120 N, whereas the second set produced the lowest at 2845 N. Overall, the mean values were closely clustered.

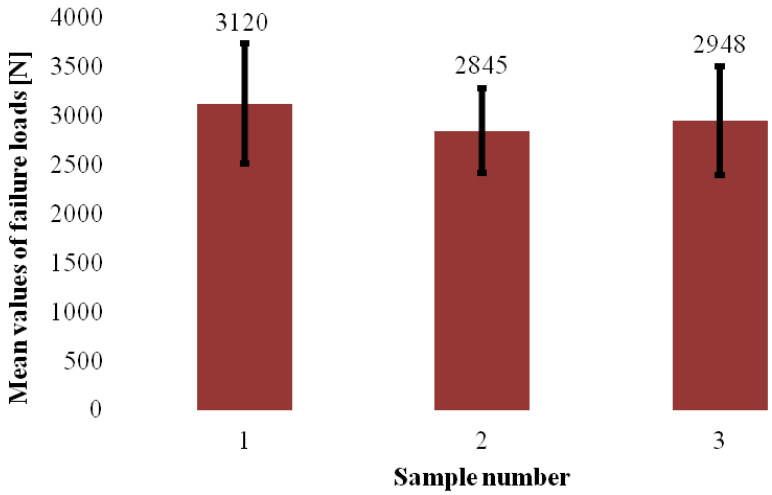

Fig. 4.83. Mean failure loads for specimen sets at a melting time of 22 s, without milling of the glass-fibre-reinforced composite reinforcement. Source: Author's own work

Figure 4.84 shows representative welds from two specimens produced at a melting time of 22 s, without milling of the glass-fibre-reinforced composite. A distinct weld seam with a pale, uniform appearance was consistent with an appropriate welding temperature setting. However, weld symmetry assessment indicated a defect, and this observation was corroborated by the post-weld dimensional tolerance evaluation of the moulds. Overload of the welding-head actuators was also observed under these conditions, which further calls into question the integrity and repeatability of the joints produced.

(a) (b)

Fig. 4.84. Representative welds from preliminary specimens: (a) second welding head, (b) third welding head. Source: Author's own work

Figure 4.85 compares mean failure loads across specimen sets produced at different melting times, with the glass-fibre-reinforced composite milled to a depth of 1.0 mm. All sets achieved mean failure loads of at least 3300 N, which is well above the target minimum of 2760 N. The highest mean value was recorded at a melting time of 25 s (3550 N), whereas the lowest was observed at 23 s (3383 N). Although the 23 s mean was marginally below those obtained at 22 s and 21 s, the results indicate no materially significant differences in mean failure load across the 21–25 s window.

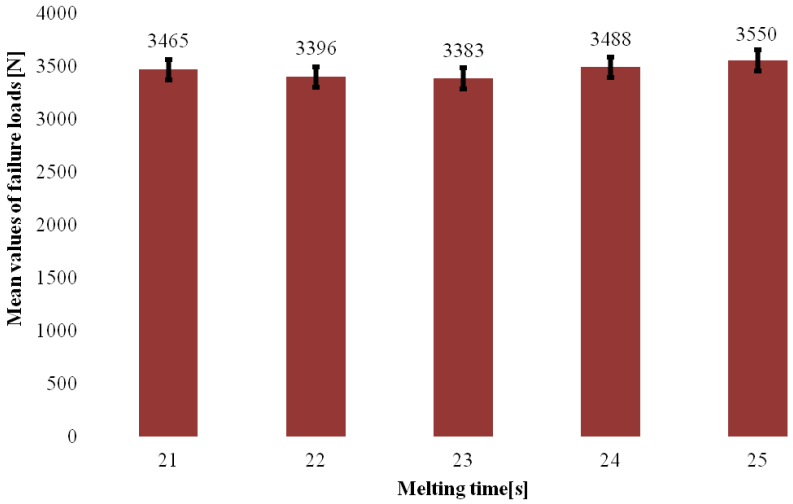

Fig. 4.85. Comparison of mean failure loads for specimen sets as a function of melting time, for a glass-fibre-reinforced composite milling depth of 1.0 mm [14]

Nevertheless, mean failure load alone does not capture all relevant distinctions between the specimen sets. Table 34 summarises selected acceptance checks, including attainment of the target final dimensions, preservation of weld symmetry, and compliance with the failure load requirement for each weld. Under these criteria, only specimen sets produced at melting times of 22–25 s met the acceptance requirements, whereas the 21 s condition did not. Accordingly, for a milling depth of 1.0 mm, the minimum melting time that satisfies both strength and quality requirements is 22 s.

Table 34. Summary of selected weld quality results for a composite milling depth of 1 mm [14]

Melting time [s]	25	24	23	22	21
Compliance with the expected value of minimum fracture loads on individual welds	Yes	Yes	Yes	Yes	Yes
Dimensional conformity, symmetry of welds	Yes	Yes	Yes	Yes	No

Figure 4.86 compares mean failure loads for specimen sets produced at a melting time of 22 s, for glass-fibre-reinforced composite milling depths of 1.0 mm, 0.5 mm, and 0 mm. All sets achieved mean failure loads of at least 2900 N. The highest mean value was obtained at a milling depth of 1.0 mm (3396 N), whereas the lowest was recorded for the unmilled condition. A clear monotonic trend is evident across the three variants, with mean failure load increasing as milling depth increases. The separation between the 1.0 mm and unmilled conditions is pronounced, whereas the difference between 1.0 mm and 0.5 mm is comparatively limited.

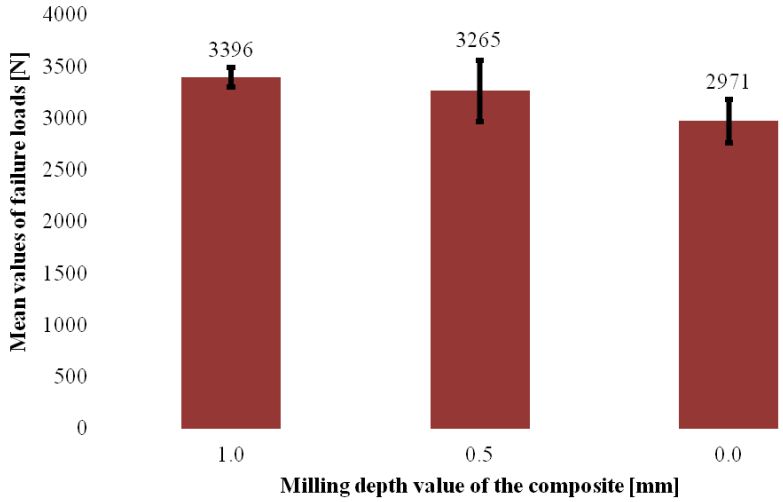

Fig. 4.86. Comparison of mean failure loads for specimen sets at a melting time of 22 s, for different milling depths of the glass-fibre-reinforced composite [14]

Nevertheless, mean failure load alone does not determine overall process acceptability. Table 35 provides the combined verification results, covering dimensional compliance, weld symmetry, and satisfaction of the failure-load requirement for each weld. Under this combined criterion set, only the 1.0 mm milling condition met all requirements. The 0.5 mm and unmilled conditions did not satisfy the joint strength and quality expectations. Accordingly, at a melting time of 22 s, milling the glass-fibre-reinforced composite reinforcement to a depth of 1.0 mm is the only configuration that meets both strength and quality criteria in full.

Table 35. Summary of selected weld quality results for a given welding time of 22 s and different milling depths of the composite [14]

Milling depth of composite reinforcement [mm]	1.0	0.5	0.0
Compliance with the expected value of minimum fracture loads on individual welds	Yes	No	No
Dimensional conformity, symmetry of welds	Yes	No	No

The preliminary optimisation established that, at a welding temperature of 264 °C and a welding-head feed rate of 0.25 mm/s, a composite-insert milling depth of 1.0 mm was the only configuration that concurrently satisfied the strength, dimensional, and weld-symmetry requirements. Reducing the melting time to 22 s did not compromise either the required failure-load level or the post-weld quality criteria, whereas a further reduction to 21 s, as well as decreasing or omitting insert milling, resulted in unacceptable dimensional and/or symmetry deviations. Accordingly, the parameter set comprising a welding temperature of 264 °C, a welding-head feed rate of 0.25 mm/s, a melting time of 22 s, and a composite-insert milling depth of 1.0 mm was adopted as the reference condition for the subsequent experimental stage.

In the subsequent phase, the effect of welding temperature on joint strength and weld integrity was evaluated. Based on earlier results indicating threshold welding times of 21 s and 22 s, these durations were incorporated into the test matrix alongside a 30 s reference condition. A broad temperature window of 247–280 °C was applied to capture potentially

material-relevant changes in behaviour and their implications for joint quality. The investigated variants are summarised in Table 11.

The first case considered involved assessing the failure loads of welds at a preset melting temperature of 256 °C, a melting time of 30 s, milling of the composite reinforcement to a depth of 1 mm, and a welding-head traverse speed of 0.25 mm/s. Table 36 presents the dimensional deviations in the post-weld moulding length and width relative to the nominal dimensions, resolved along the individual machine axes.

Table 36. Dimensional deviations of welded moulds for a given melting temperature of 256 °C and a melting time of 30 s. Source: Author's own work

Sample No.	1	2	3
Dimensional deviations from nominal size in the X; Y axes [mm]	1; 1	1; 1	1; 1

The results reported in Table 36 indicate that the difference between the target dimension and the value obtained after welding remained within 1 mm. This confirms compliance with the adopted dimensional tolerance of 1 mm. Weld symmetry was also confirmed during the tests.

Figure 4.87 presents the mean failure loads for specimen sets tested at a preset melting temperature of 256 °C and a melting time of 30 s. No statistically meaningful differences are evident between the individual mean values. All specimen sets achieved at least 3400 N. The highest recorded mean failure load was 3675 N, which substantially exceeded the anticipated mean failure-load level.

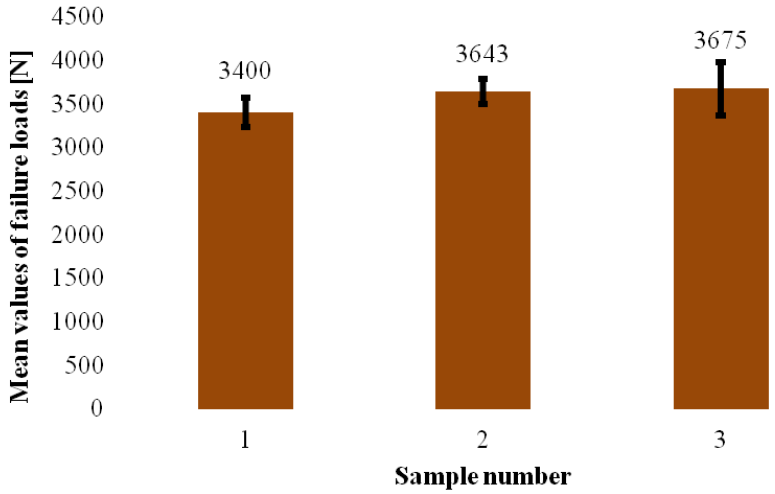

Fig. 4.87. Mean failure loads for specimen sets at a preset melting temperature of 256 °C and a melting time of 30 s. Source: Author's own work

Figure 4.88 shows two welds produced on two different specimens at a preset welding temperature of 256 °C and a melting time of 30 s. The presence of a clearly formed weld bead indicates continuity of the joined material, which is consistent with the measured failure loads. The light, white appearance of the weld bead confirms that the process temperature remained below the onset of thermal degradation of the PVC profile. Excessive process temperature could lead to local scorching of the PVC, typically manifested as a darkened weld region.

(a)

(b)

Fig. 4.88. Representative welds from the preliminary trials: (a) first head, (b) second head. Source: Author's own work

The second case considered involved assessing weld failure loads at a preset melting temperature of 250 °C, a melting time of 30 s, milling of the composite reinforcement to a depth of 1 mm, and a welding-head traverse speed of 0.25 mm/s. Table 37 reports the dimensional deviations in post-weld assembly length and width relative to the nominal dimensions, resolved along the individual machine axes.

Table 37. Dimensional deviations of welded moulds for a given melting temperature of 250 °C and a melting time of 30 s. Source: Author's own work

Sample No.	1	2	3
Dimensional deviations from nominal size in the X; Y axes [mm]	1; 1	1; 1	1; 1

As shown in Table 37, the post-weld dimensions deviated from the target values by no more than 1 mm, which confirms that a 1 mm dimensional tolerance was maintained. The tests also confirmed weld symmetry.

Figure 4.89 presents the mean failure loads for specimen sets tested at a preset melting temperature of 250 °C and a melting time of 30 s. All specimen sets reached at least 3200 N, which exceeds the anticipated mean failure-load level. The highest recorded mean value was 3755 N, whereas the lowest was 3213 N. Although a difference was observed between the first and second sets, no clear separation was evident between the second and third sets, or between the first and third sets. Given the confirmed weld symmetry and the dimensional compliance of the welded assembly, the observed difference is of limited practical significance. One plausible contributing factor may be an insufficient process temperature.

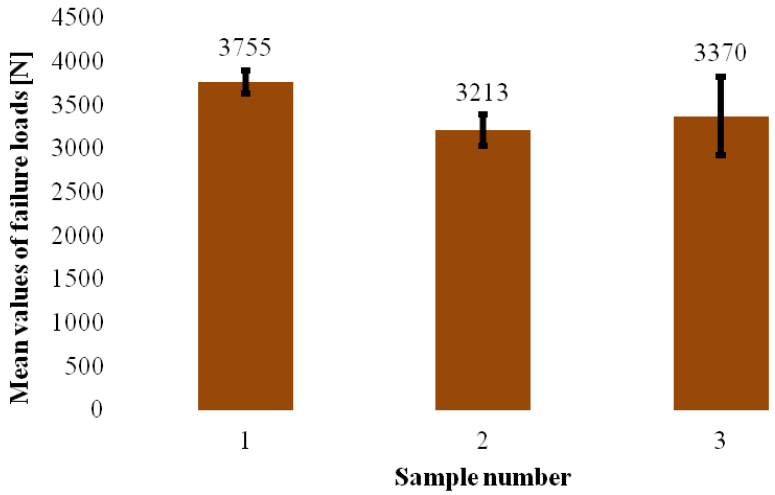

Fig. 4.89. Mean failure loads for specimen sets at a preset melting temperature of 250 °C and a melting time of 30 s. Source: Author's own work

Figure 4.90 shows two representative welds produced on two different specimens at a preset welding temperature of 250 °C and a melting time of 30 s. A clearly discernible weld bead indicated continuity of the joined material, which is consistent with the measured failure loads. The light, white appearance of the weld bead further indicates that the process temperature remained appropriate, avoiding thermal degradation of the profile. Excessive temperature could cause local scorching of the PVC, typically manifested as a darkened weld region.

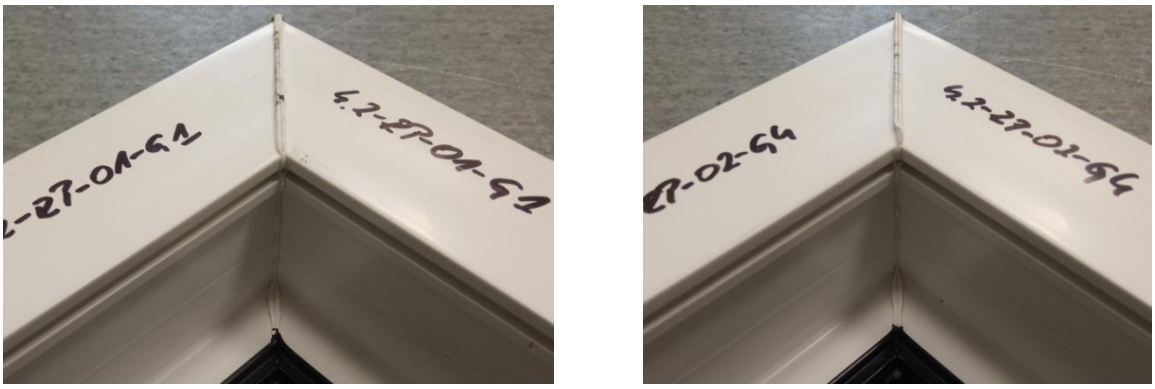

(a) (b)

Fig. 4.90. Representative welds from the preliminary trials: (a) first head, (b) fourth head. Source: Author's own work

The third case considered involved assessing weld failure loads at a preset melting temperature of 249 °C, a melting time of 30 s, milling of the composite reinforcement to a depth of 1 mm, and a welding-head traverse speed of 0.25 mm/s. Table 38 reports the dimensional deviations in post-weld assembly length and width relative to the nominal dimensions, resolved along the individual machine axes.

Table 38. Dimensional deviations of welded moulds for a given melting temperature of 249 °C and a melting time of 30 s. Source: Author's own work

Sample No.	1	2	3
Dimensional deviations from nominal size in the X; Y axes [mm]	1; 1	1; 1	1; 1

Analysis of the data in Table 38 shows that the deviation between the design and final dimensions did not exceed 1 mm, confirming compliance with the specified dimensional tolerance of 1 mm. Weld symmetry was also demonstrated during the tests.

Figure 4.91 presents the mean failure loads for specimen sets tested at a preset melting temperature of 249 °C and a melting time of 30 s. The results indicate no practically meaningful differences between the mean failure loads of the sets included in the comparison. All specimen sets exceeded 3300 N. The highest recorded mean value was 3568 N, whereas the lowest was 3310 N.

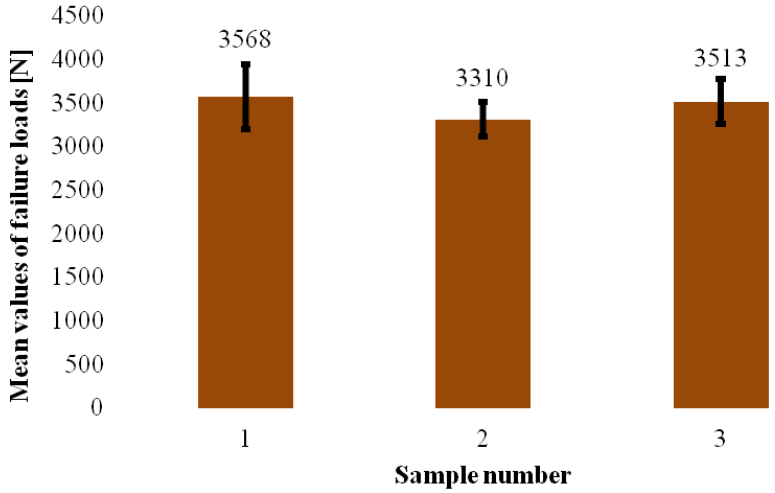

Fig. 4.91. Mean failure loads for specimen sets at a preset melting temperature of 249 °C and a melting time of 30 s. Source: Author's own work

Figure 4.92 shows two welds produced on two different specimens at a preset welding temperature of 249 °C and a melting time of 30 s. The presence of a clearly formed weld bead indicates intact material continuity, which is consistent with the measured failure loads. The bright, white appearance of the weld bead further indicates that the process temperature did not reach levels associated with thermal degradation of the profile. Exceeding this threshold could lead to local scorching of the PVC, typically manifested as a darkened weld region, which was not observed. The dark deposit visible in the images is attributable to residual matrix material from the composite reinforcement.

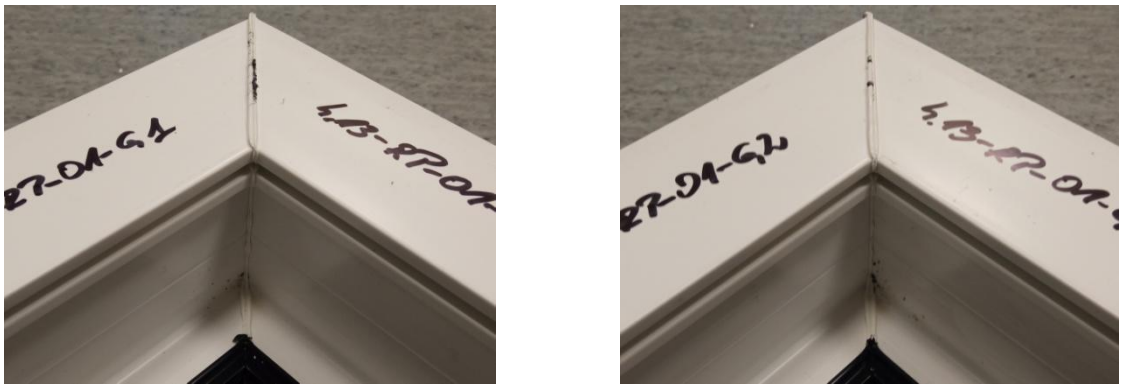

(a) (b)

Fig. 4.92. Representative welds from the preliminary trials: (a) first head, (b) second head. Source: Author's own work

The fourth case considered involved assessing weld failure loads at a preset melting temperature of 248 °C, a melting time of 30 s, milling of the composite reinforcement to a depth of 1 mm, and a welding-head traverse speed of 0.25 mm/s. Table 39 reports the dimensional deviations in the post-weld moulding length and width relative to the nominal dimensions, resolved along the individual machine axes.

Table 39. Dimensional deviations of welded moulds for a given melting temperature of 248 °C and a melting time of 30 s. Source: Author's own work

Sample No.	1	2	3
Dimensional deviations from nominal size in the X; Y axes [mm]	1; 1	1; 1	1; 1

According to Table 39, the discrepancy between the planned and post-weld dimensions was at most 1 mm, confirming compliance with the required dimensional tolerance of 1 mm. Weld symmetry was additionally confirmed during the tests.

Figure 4.93 presents the mean failure loads for specimen sets tested at a preset melting temperature of 248 °C and a melting time of 30 s. The results indicate no practically meaningful differences between the mean failure loads. All specimen sets exceeded 3300 N. The highest recorded mean value was 3675 N, whereas the lowest was 3308 N.

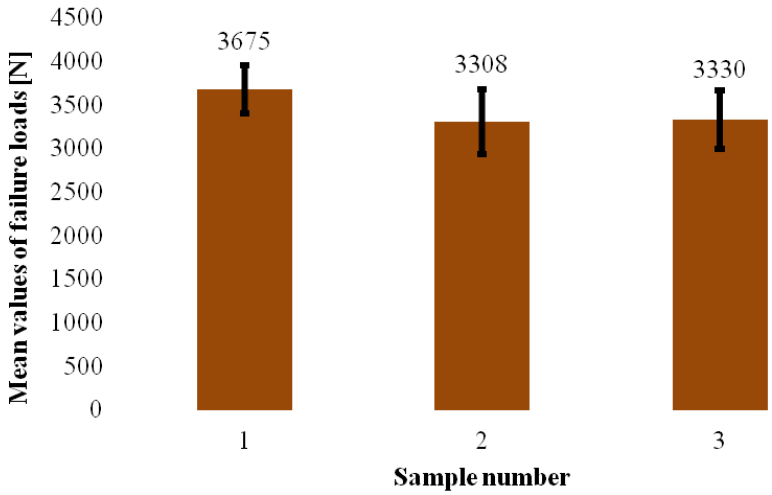

Fig. 4.93. Mean failure loads for specimen sets at a preset melting temperature of 248 °C and a melting time of 30 s. Source: Author's own work

Figure 4.94 shows two welds produced on two different specimens at a preset welding temperature of 248 °C and a melting time of 30 s. The clearly defined weld bead visible in the images suggests preserved material integrity, which is consistent with the mean failure-load levels. The light colour of the weld bead indicates an appropriate temperature that did not promote profile degradation. Excessive temperature could cause local scorching of the PVC, typically manifested as a darker weld bead.

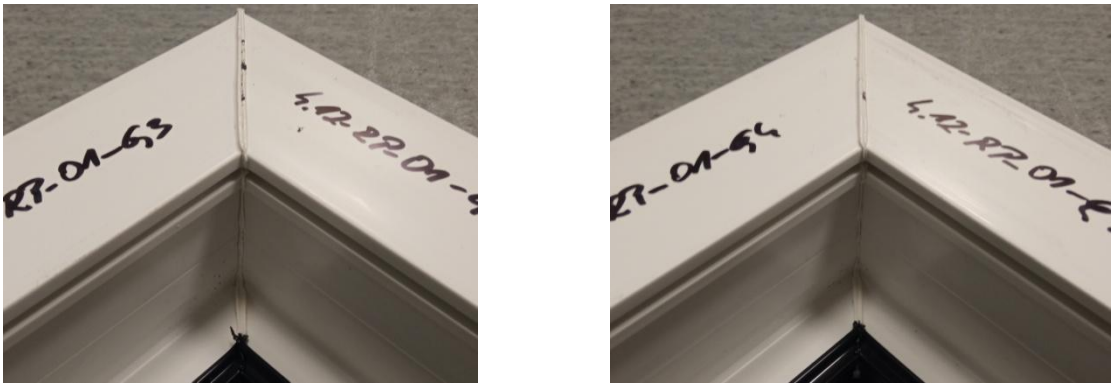

(a) (b)

Fig. 4.94. Representative welds from the preliminary trials: (a) third head, (b) fourth head. Source: Author's own work

The fifth case considered involved assessing weld failure loads at a preset melting temperature of 247 °C, a melting time of 30 s, milling of the composite reinforcement to a depth of 1 mm, and a welding-head traverse speed of 0.25 mm/s. Table 40 reports the dimensional deviations in post-weld assembly length and width relative to the nominal dimensions, resolved along the individual machine axes.

Table 40. Dimensional deviations of welded moulds for a given melting temperature of 247 °C and a melting time of 30 s. Source: Author's own work

Sample No.	1	2	3
Dimensional deviations from nominal size in the X; Y axes [mm]	1; 1	1; 1	2; 2

Referring to Table 40, the deviation between the target dimension and the post-weld value for the third specimen set exceeded 1 mm. Consequently, these specimens did not satisfy the tolerance requirement associated with the dimensional allowance. In addition, weld symmetry was not maintained, as confirmed during the tests. This may be attributable to an insufficient temperature to melt the assemblies to the specified geometry. The incompletely melted PVC profile appears to have resisted the welding-head actuators, resulting in overload conditions observed during testing.

Figure 4.95 presents the mean failure loads for specimen sets tested at a preset melting temperature of 247 °C and a melting time of 30 s. The mean failure-load values did not differ materialny. However, pronounced differences in scatter were observed between the specimen sets. All analysed sets exceeded 3200 N. The highest recorded mean value was 3665 N, whereas the lowest was 3278 N.

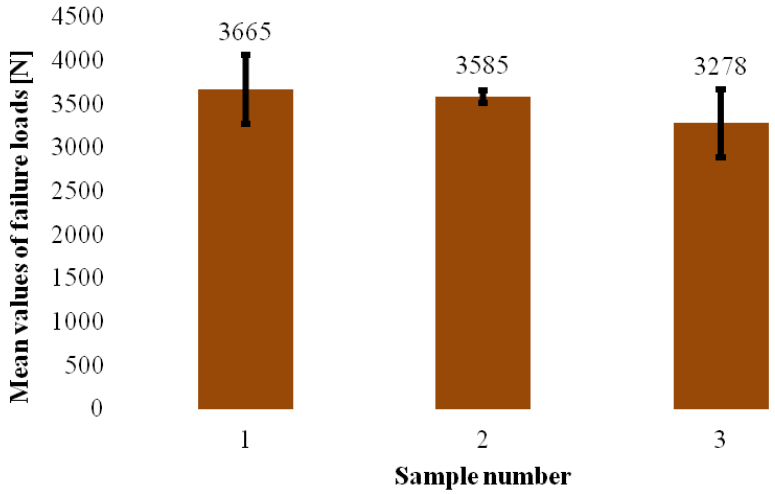

Fig. 4.95. Mean failure loads for specimen sets at a preset melting temperature of 247 °C and a melting time of 30 s. Source: Author's own work

Figure 4.96 shows two welds produced on two different specimens at a welding temperature of 247 °C and a melting time of 30 s. The weld bead indicates continuity of the joined material. The low process temperature is consistent with the absence of thermal degradation of the profile.

(a) (b)

Fig. 4.96. Representative welds from the preliminary trials: (a) first head, (b) fourth head. Source: Author's own work

The sixth case considered involved assessing weld failure loads at a preset melting temperature of 263 °C, a melting time of 22 s, milling of the composite reinforcement to a depth of 1 mm, and a welding-head traverse speed of 0.25 mm/s. Table 41 reports the dimensional deviations in post-weld moulding length and width relative to the nominal dimensions, resolved along the individual machine axes.

Table 41. Dimensional deviations of welded moulds for a given melting temperature of 263 °C and a melting time of 22 s. Source: Author's own work

Sample No.	1	2	3	4	5	6
Dimensional deviations from nominal size in the X; Y axes [mm]	1; 1	2; 2	2; 2	1; 1	2; 2	1; 1

An examination of Table 41 shows that the deviation between the target dimension and the post-weld value exceeded 1 mm for the second, third, and fifth specimen sets. Dimensional deviations of 2 mm indicate noncompliance with the tolerance requirement. These specimen sets also failed to maintain weld symmetry, as confirmed during the tests. This may reflect an insufficient temperature to achieve full melting to the target geometry within the prescribed melting time. Such incomplete melting could increase resistance to head motion and may have contributed to actuator overload events, which were observed in almost all investigated specimen sets.

Figure 4.97 presents the mean failure loads for specimen sets tested at a preset melting temperature of 263 °C and a melting time of 22 s. All specimen sets achieved mean failure loads of at least 3100 N. The mean values show no clear separation between sets, which is consistent with the substantial scatter. Machine fault events during welding and the lack of weld symmetry point to an unstable joint-formation process, which renders the resulting welds unsuitable for acceptance under the adopted criteria. The highest recorded mean value was 3758 N, whereas the lowest was 3100 N. It is also noteworthy that a single specimen from the first head in the first set exhibited a failure load of 2710 N, which falls below the expected level.

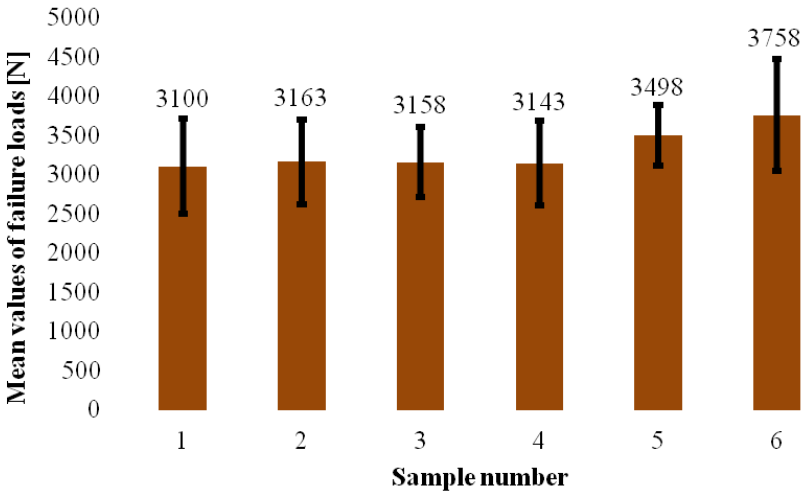

Fig. 4.97. Mean failure loads for specimen sets at a preset melting temperature of 263 °C and a melting time of 22 s. Source: Author's own work

Figure 4.98 shows two welds produced on two different specimens at a preset welding temperature of 263 °C and a melting time of 22 s. The presence of a clearly formed weld bead is consistent with continuity of the joined material and the measured failure-load levels. The white weld bead suggests an appropriate thermal input that did not promote profile degradation. Excessive heat input could lead to local scorching of the PVC, which typically manifests as a darkened weld bead.

(a) (b)

Fig. 4.98. Representative welds from the preliminary trials: (a) second head, (b) fourth head. Source: Author's own work

The seventh case considered involved assessing weld failure loads at a preset melting temperature of 280 °C, a melting time of 21 s, milling of the composite reinforcement to a depth of 1 mm, and a welding-head traverse speed of 0.25 mm/s. Table 42 reports the dimensional deviations in post-weld moulding length and width relative to the nominal dimensions, resolved along the individual machine axes.

Table 42. Dimensional deviations of welded moulds for a given melting temperature of 280 °C and a melting time of 21 s. Source: Author's own work

Sample No.	1	2	3
Dimensional deviations from nominal size in the X; Y axes [mm]	1; 1	0; 1	0; 1

Based on Table 42, the discrepancy between the post-weld and target dimensions did not exceed 1 mm. The welded mouldings were therefore consistent with the intended final geometry. Weld inspection also confirmed symmetry. Despite reducing the welding time from 30 s to 21 s, the process proceeded smoothly. No actuator overload events were recorded. This outcome is plausibly attributable to the increased temperature from 264 °C to 280 °C, which likely compensated for the shorter melting time.

Figure 4.99 presents the mean failure loads for specimen sets tested at a preset melting temperature of 280 °C and a melting time of 21 s. All specimen sets achieved mean failure loads of at least 3400 N. The mean values were closely clustered across the investigated sets. The highest recorded mean failure load was 3588 N, whereas the lowest mean value was 3435 N.

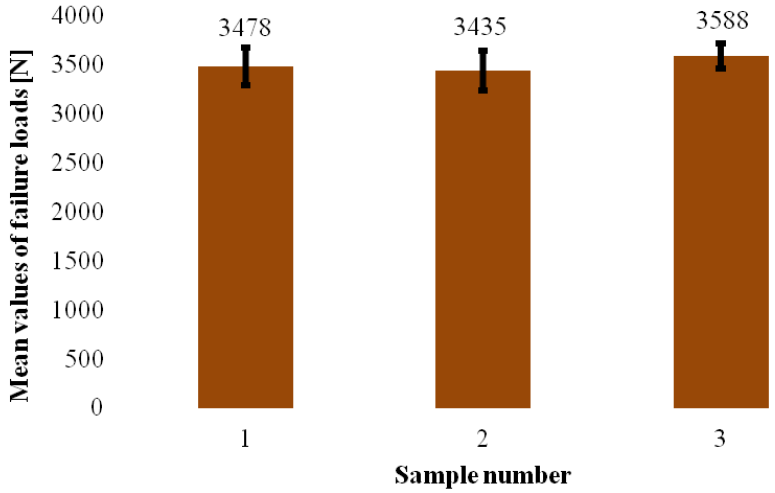

Fig. 4.99. Mean failure loads for specimen sets at a preset melting temperature of 280 °C and a melting time of 21 s. Source: Author's own work

Figure 4.100 shows two welds produced on two different specimens at a preset welding temperature of 280 °C and a melting time of 21 s. The presence of a discernible weld bead indicates continuity of the joined material, which is consistent with achieving the required mean failure-load level. Yellow discolouration of the weld bead was observed. This was expected given that 280 °C substantially exceeds the 264 °C reference condition. Such yellowing after welding is not permissible under the adopted acceptance criteria. Since the welding time was reduced from 30 s to 21 s, the most plausible cause of the yellowing is excessive temperature leading to thermal degradation of the profile. No actuator overload events were observed at this setting, which is consistent with increased softening at elevated temperature. Overall, temperature appears to have been the dominant parameter governing process behaviour under these conditions.

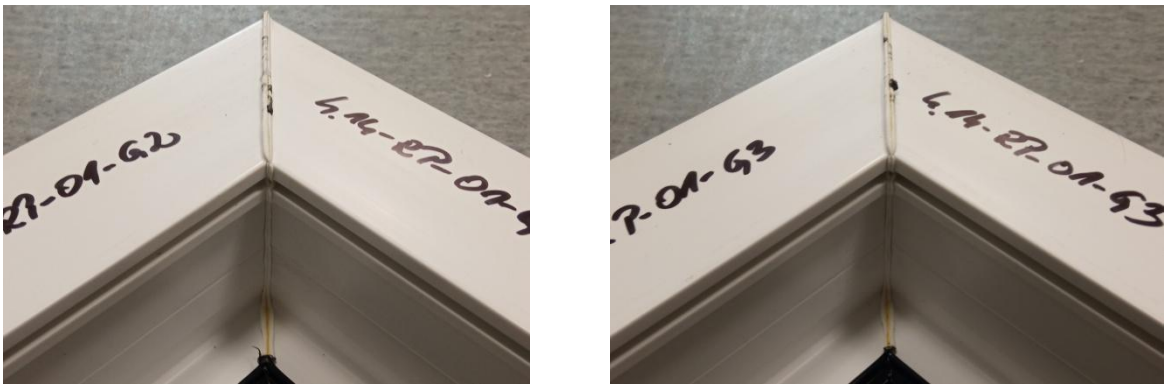

(a) (b)

Fig. 4.100. Representative welds from the preliminary trials: (a) second head, (b) third head [202]

The eighth case considered involved assessing weld failure loads at a preset melting temperature of 271 °C, a melting time of 21 s, milling of the composite reinforcement to a depth of 1 mm, and a welding-head traverse speed of 0.25 mm/s. Table 43 reports the dimensional deviations in post-weld moulding length and width relative to the nominal dimensions, resolved along the individual machine axes.

Table 43. Dimensional deviations of welded moulds for a given melting temperature of 271 °C and a melting time of 21 s. Source: Author's own work

Sample No.	1	2	3
Dimensional deviations from nominal size in the X; Y axes [mm]	1; 1	1; 1	1; 1

Considering Table 43, the discrepancy between the target dimension and the value obtained after mould heating did not exceed 1 mm. The final geometry was therefore consistent with expectations. Weld inspection confirmed symmetry. Despite reducing the welding time from 30 s to 21 s, the process proceeded without disturbance. No actuator overload events were recorded. The smooth process behaviour is plausibly attributable to increasing the temperature from 264 °C to 271 °C.

Figure 4.101 presents the mean failure loads for specimen sets tested at a preset melting temperature of 271 °C and a melting time of 21 s. The analysis indicates that all specimen sets achieved mean failure loads within 3400–3500 N. The mean values were closely clustered across the investigated sets. The highest recorded mean value was 3498 N, whereas the lowest mean value was 3400 N.

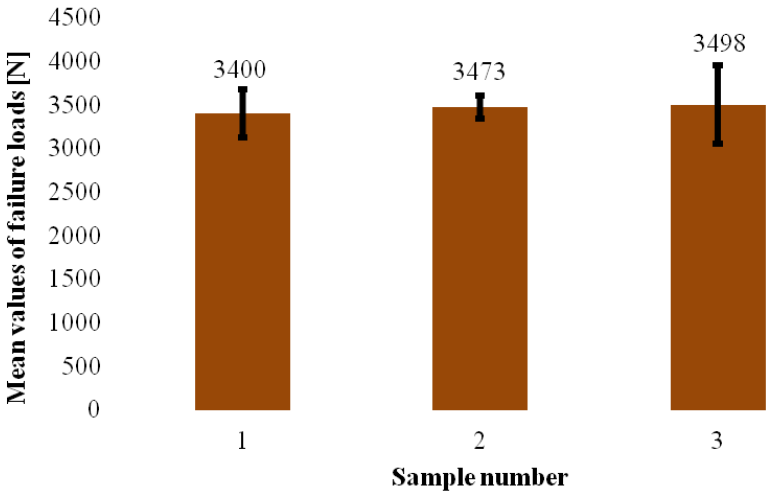

Fig. 4.101. Mean failure loads for specimen sets at a preset melting temperature of 271 °C and a melting time of 21 s. Source: Author's own work

Figure 4.102 shows two welds produced on two different specimens at a preset welding temperature of 271 °C and a melting time of 21 s. The presence of a discernible weld bead indicates continuity of the joined material, which is consistent with achieving the required mean failure-load levels. Yellow discolouration of the weld bead was confirmed. This outcome was anticipated because 271 °C substantially exceeds the nominal reference of 264 °C. Yellowing after welding is not acceptable under the adopted acceptance criteria. Given the shortened welding time from 30 s to 21 s, the yellowing is most plausibly associated with excessive temperature and incipient thermal degradation of the profile. No actuator overload was observed, which is consistent with increased softening at elevated temperature. Temperature therefore appears to have been the dominant parameter governing process behaviour under these conditions.

(a) (b)

Fig. 4.102. Representative welds from the preliminary trials: (a) second head, (b) third head. Source: Author's own work

The ninth case considered involved assessing weld failure loads at a preset melting temperature of 270 °C, a melting time of 21 s, milling of the composite reinforcement to a depth of 1 mm, and a welding-head traverse speed of 0.25 mm/s. Table 44 reports the dimensional deviations in post-weld moulding length and width relative to the nominal dimensions, resolved along the individual machine axes.

Table 44. Dimensional deviations of welded moulds for a given melting temperature of 270 °C and a melting time of 21 s. Source: Author's own work

Sample No.	1	2	3
Dimensional deviations from nominal size in the X; Y axes [mm]	2; 2	2; 2	2; 2

Based on Table 44, a substantial discrepancy was observed between the target dimension and the value obtained after welding. In each specimen set, the final dimension exceeded the target by more than 2 mm, and thus did not meet the expected outcome. Weld inspection did not confirm symmetry. The welding time was reduced from 30 s to 21 s, while the temperature was increased from 264 °C to 270 °C. Despite the higher temperature, actuator overload of the welding heads was observed during the trials. This suggests that, under the present conditions, 270 °C combined with a melting time of 21 s represents a limiting operating point for the welding process.

Figure 4.103 presents the mean failure loads for specimen sets tested at a preset melting temperature of 270 °C and a melting time of 21 s. The results indicate that all specimen sets achieved mean failure loads in the range of 3000–3600 N. The mean values were broadly comparable across the investigated sets. The highest recorded mean value was 3538 N, whereas the lowest mean value was 3035 N.

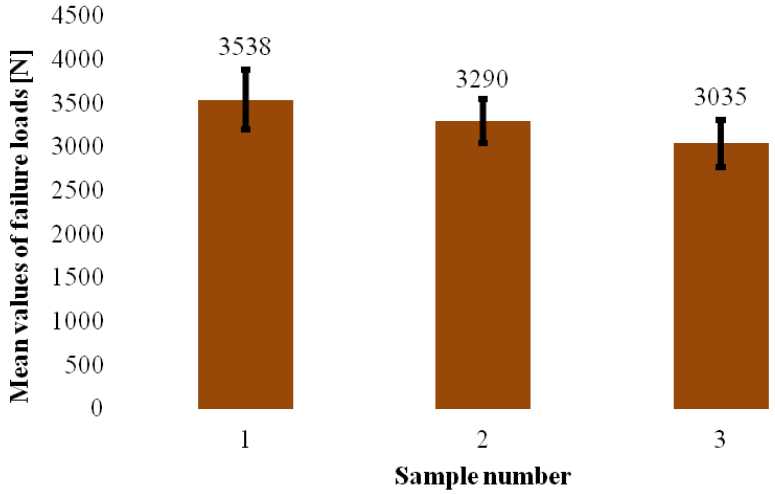

Fig. 4.103. Mean failure loads for specimen sets at a preset melting temperature of 270 °C and a melting time of 21 s. Source: Author's own work

Figure 4.104 shows two welds produced on two different specimens at a preset welding temperature of 270 °C and a melting time of 21 s. The presence of a discernible weld bead indicates continuity of the joined material. Yellow discolouration of the weld bead was also observed, which was anticipated because 270 °C exceeds the 264 °C reference condition by a considerable margin. Yellowing after welding is not acceptable under the adopted acceptance criteria. Given the reduced welding time from 30 s to 21 s, the yellowing is most plausibly associated with excessive temperature and incipient thermal degradation of the profile. Actuator overload was also recorded, which further supports the view that temperature was a governing parameter under these conditions.

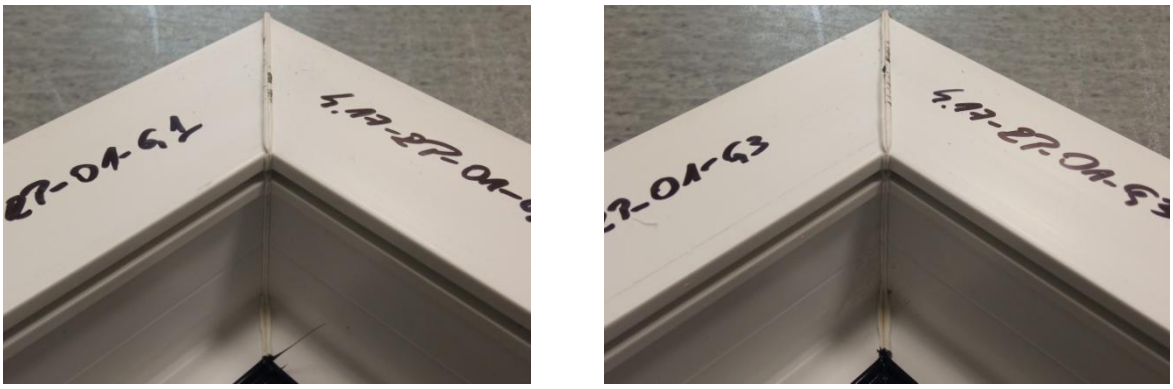

(a) (b)

Fig. 4.104. Representative welds from the preliminary trials: (a) first head, (b) third head. Source: Author's own work

Table 45 summarises selected weld-quality outcomes for the investigated temperature levels at a melting time of 30 s, a composite-reinforcement milling depth of 1 mm, and a welding-head traverse speed of 0.25 mm/s.

Table 45. Summary of selected weld quality results for individual temperature values at a welding time of 30 s [202]

Welding temperature [°C]	256	250	249	248	247
Compliance with the expected value of minimum fracture loads on individual welds	Yes	Yes	Yes	Yes	Yes
Dimensional conformity, symmetry of welds	Yes	Yes	Yes	Yes	No
White weld-bead appearance	Yes	Yes	Yes	Yes	Yes

Inspection of Table 45 indicates that all specimen sets met the expected strength and quality criteria at 248 °C, with a melting time of 30 s, a milling depth of 1 mm, and a welding-head traverse speed of 0.25 mm/s. Under these conditions, 248 °C therefore represents the lowest temperature at which the adopted acceptance criteria were satisfied. At 247 °C, dimensional conformity of the welded mouldings was not achieved, and weld symmetry could not be confirmed. This outcome is consistent with insufficient thermal input at 247 °C for stable joint formation in the present configuration. Table 46 summarises weld-quality outcomes for selected temperature levels at a melting time of 22 s, a composite-reinforcement milling depth of 1 mm, and a welding-head traverse speed of 0.25 mm/s.

Table 46. Summary of selected weld quality results for individual temperature values at a welding time of 22 s [202]

Welding temperature [°C]	264	263
Compliance with the expected value of minimum fracture loads on individual welds	Yes	No
Dimensional conformity, symmetry of welds	Yes	No
White weld-bead appearance	Yes	Yes

On the basis of Table 46, and for a milling depth of 1 mm and a welding-head traverse speed of 0.25 mm/s, 264 °C appears to be the threshold temperature required to maintain acceptable weld quality at the minimum melting time of 22 s. Within the investigated parameter window, this value can be treated as the minimum temperature compatible with stable process execution. At 263 °C, actuator overload of the welding heads was observed, together with dimensional nonconformance of the post-weld mouldings and the absence of weld symmetry.

Table 47 summarises weld-quality outcomes for selected temperature levels at a melting time of 21 s, a composite-reinforcement milling depth of 1 mm, and a welding-head traverse speed of 0.25 mm/s.

Table 47. Summary of selected weld quality results for individual temperature values at a welding time of 21 s [202]

Welding temperature [°C]	280	271	270
Compliance with the expected value of minimum fracture loads on individual welds	Yes	Yes	No
Dimensional conformity, symmetry of welds	Yes	Yes	No
White weld-bead appearance	No	No	No

Consideration of Table 47 suggests that reducing the melting time below the 22 s threshold, combined with welding temperatures of 270 °C or higher, adversely affected weld quality. The results do not support the hypothesis that further time reduction below 22 s can be compensated solely by increasing welding temperature under the present conditions. At 280 °C, actuator overload was not recorded, which is consistent with enhanced softening at elevated temperature. However, profile degradation was indicated by yellow weld beads, which are not acceptable under the adopted criteria. A comparable outcome was observed at 271 °C. A further reduction to 270 °C, intended to identify a limit for yellow weld-bead formation while maintaining a melting time of 21 s, did not yield a favourable result. Yellow weld beads persisted, and actuator overload events were also recorded at 270 °C. Collectively, these findings indicate that, at a melting time of 21 s, raising welding temperature is not an effective strategy for recovering weld quality and process repeatability within the investigated setup.

The experiments demonstrated a pronounced dependence of weld quality on the welding parameters applied to PVC profiles reinforced with a glass-fibre composite. Joint quality was assessed in terms of weld symmetry, weld continuity, weld colour, and failure load analysis. Testing of the reference series (with no composite milling) confirmed both the geometric stability of the system, with dimensional deviations not exceeding 1 mm, and the validity of the measurement chain, as evidenced by compliance with the required ±3% accuracy. In addition, the mean failure load exceeded 3400 N. Subsequent stages examined the effects of composite-reinforcement milling depth, welding-head feed rate during the melting stage, melting time, and welding temperature on weld quality and strength. This experimental structure aligns with the process-oriented approach reported for polymer welding, in which thermal and kinematic parameters are treated as jointly governing joint integrity and load-bearing performance [184], [194].

For the composite-insert milling stage, the following variants were applied: 0 mm (no milling), 0.5 mm, 1.0 mm, 1.5 mm, 2.0 mm, 3.0 mm, and 6.0 mm, while keeping the settings

constant at 264 °C, 30 s, and 0.25 mm/s. In the unmilled condition, all series exceeded 3000 N, and two series exceeded 3500 N, while preserving weld continuity, weld symmetry, and a white weld bead. For 0.5 mm milling, repeatable results above 3400 N were obtained, with continuity of the joint maintained. The 1.0 mm variant exhibited the most favourable strength response profile, as all series exceeded 3000 N and, except for one case, also exceeded 3500 N, while weld continuity was preserved. Beyond 1.0 mm, a qualitative process boundary became apparent. At 1.5 mm, despite failure loads reaching approximately 3400 N, local weld discontinuities were observed, which disqualified this variant on quality grounds. At 2.0 mm, a single extreme result of 1430 N was recorded and rejected using Dixon's test, and substantial differences between welding heads were also identified, with mean values of approximately 2840 N for head H1 versus approximately 3450 N for head H4. Weld discontinuity was again observed, indicating unstable joint formation. At 3.0 mm, only one series exceeded 3000 N, while the remaining series did not exceed 2900 N, with concurrent weld interruptions. The poorest response occurred at 6.0 mm, where no series reached 3000 N, and two out of three series fell below the expected level. Consequently, the 0 mm, 0.5 mm, and 1.0 mm variants were retained for further work, whereas milling depths above 1.0 mm were rejected as qualitatively unacceptable. This trend is consistent with reports indicating that co-weldable thermoplastic reinforcements can maintain or improve corner load capacity, provided that geometric losses are not introduced in the joint region that would hinder full filling and consolidation of the molten PVC [11].

The influence of welding-head feed rate was evaluated for three values, 0.19 mm/s, 0.25 mm/s, and 0.31 mm/s, in combination with three milling variants: 0 mm, 0.5 mm, and 1.0 mm. For 1.0 mm milling, the mean failure loads were clearly differentiated as 3033 N (0.31 mm/s), 3157 N (0.19 mm/s), and 3637 N (0.25 mm/s). Similarly, for 0.5 mm milling the corresponding values were 2933 N (0.31 mm/s), 3158 N (0.19 mm/s), and 3498 N (0.25 mm/s), while for the unmilled variant they were 3154 N (0.31 mm/s), 3188 N (0.19 mm/s), and 3467 N (0.25 mm/s). Across the investigated range, 0.25 mm/s delivered the highest mean failure loads and the most favourable balance between load capacity and weld stability, and was therefore adopted as the reference setting for subsequent stages. In interpretative terms, an excessive feed rate (0.31 mm/s) may have limited the time available for contact formation and consolidation of the plasticised layer in the presence of reinforcement, whereas an overly low feed rate (0.19 mm/s) may have promoted non-optimal flow conditions of molten PVC in the weld-bead region. This dependence accords with the literature, where kinematic parameters are considered decisive, alongside thermal settings, for strength development in hot-plate welding of thermoplastics [184], [194].

The melting-time analysis was conducted at fixed settings of 264 °C, 0.25 mm/s, and 1.0 mm milling, for melting times of 25 s, 24 s, 23 s, 22 s, and 21 s. Mean failure loads remained within the expected range for correctly produced welds, that is, above 2760 N. Clear discrimination between variants emerged only when geometric and qualitative criteria were applied. For 22–25 s, dimensional tolerance was maintained within 1 mm and weld symmetry was preserved. By contrast, at 21 s, systematic deviations of approximately 2 mm and a loss of symmetry were recorded, indicating insufficient plasticisation and an increased resistance to head motion. Accordingly, under the combined strength and quality criteria at 1.0 mm milling, 22 s was identified as the minimum melting time. An additional comparison at 22 s across milling variants of 1.0 mm, 0.5 mm, and 0 mm showed that, although mean failure loads exceeded 2900 N, only 1.0 mm simultaneously satisfied the load-capacity requirement for all welds and the qualitative criteria. For 0.5 mm and 0 mm, dimensional deviations above 1 mm, lack of weld symmetry, and individual failure loads below the expected level were

observed, specifically 2380 N and 2480 N for 0.5 mm milling, and 2460 N and 2510 N without milling of the composite insert. This confirms the necessity of milling the composite insert when short melting times of 22 s are applied (Fig. 4.105). These findings remain consistent with observations for PVC welds, where the plasticisation time governs not only the level of failure loads but also repeatability and the failure mechanism along the weld line [17].

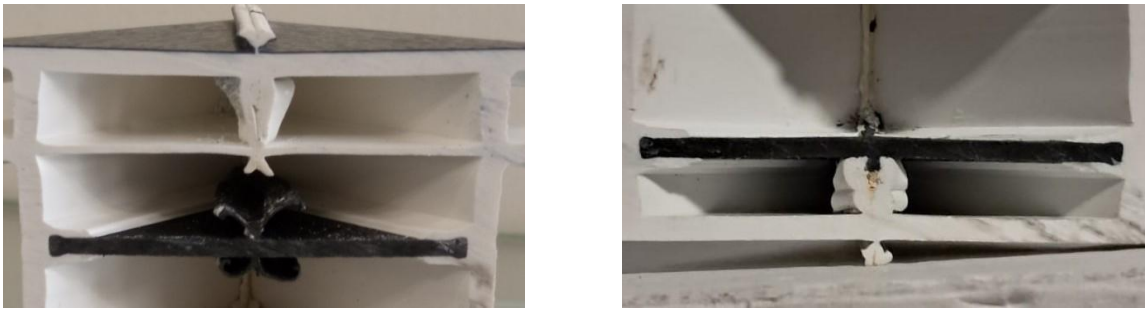

(a) (b)

Fig. 4.105. Cross-section of the welded profile showing the composite insert arrangement: (a) variant without composite milling, (b) milling of the composite insert to a depth of 1 mm. Source: Author's own work

In the temperature study, a broad window of 247–280 °C was explored, while simultaneously evaluating weld-bead colour, weld continuity, and machine overload events associated with the welding heads. At a melting time of 30 s, a milling depth of 1.0 mm, and a welding-head feed rate of 0.25 mm/s, temperatures of 256–248 °C enabled acceptable weld geometry, with form deviations below 1 mm, and preserved weld symmetry. Mean failure loads remained in the range of approximately 3200–3400 N, with a white weld bead. However, as the temperature decreased from 250 °C to 248 °C, a pronounced scatter in the mean failure loads across welding heads emerged, indicating a narrowing process-stability margin. At 247 °C, dimensional non-compliance was already observed, with 2 mm deviations, loss of symmetry, and recurrent overloads culminating in a machine error. This supports treating 247 °C as too low for repeatable cycle execution in the investigated configuration. Under the shortened melting time of 22 s, 264 °C was compared as the reference against 263 °C. At 263 °C, frequent 2 mm deviations, loss of symmetry, and repeated overloads were recorded, even though mean failure loads were occasionally high. This series also included failure loads below the expected threshold, specifically 2710 N. These observations indicate that, at the minimum melting time of 22 s, 264 °C constitutes the threshold required for process stability. Attempts to reduce the melting time further to 21 s were compensated by increasing the temperature to 270–280 °C. Although the 271–280 °C range eliminated head overloads and produced acceptable geometry, yellowing of the weld bead appeared, which was interpreted as evidence of unacceptable thermal exposure within the joint region. At 270 °C, head overloads persisted alongside dimensional non-compliance, loss of weld symmetry, and yellowing of the welds (Fig. 4.106). Collectively, these results confirm that raising the welding temperature above the reference level of 264 °C is not an effective strategy for compensating a shorter melting time, because temperature begins to govern joint quality through weld-bead discolouration and reduced joint stability. This direction is consistent with [11], where welding temperature enables simultaneous plasticisation of PVC and a thermoplastic reinforcement, allowing both to be welded in a single operation and thereby increasing corner load capacity. However, larger material losses due to milling hinder full filling of the joint zone by molten PVC and therefore constrain this effect.

Fig. 4.106. Cross-sections of welds produced at 270 °C (left profile) and 264 °C (right profile). Source: Author's own work

The parameter–response relationships between the mean failure load and the two principal thermal variables of the welding process, namely welding temperature and melting time, were quantified using regression analysis. Figure 107(a) shows the relationship between welding temperature and the average breaking load of welded joints, whilst Figure 107b shows the relationship between melting time and the average breaking load of welded joint.

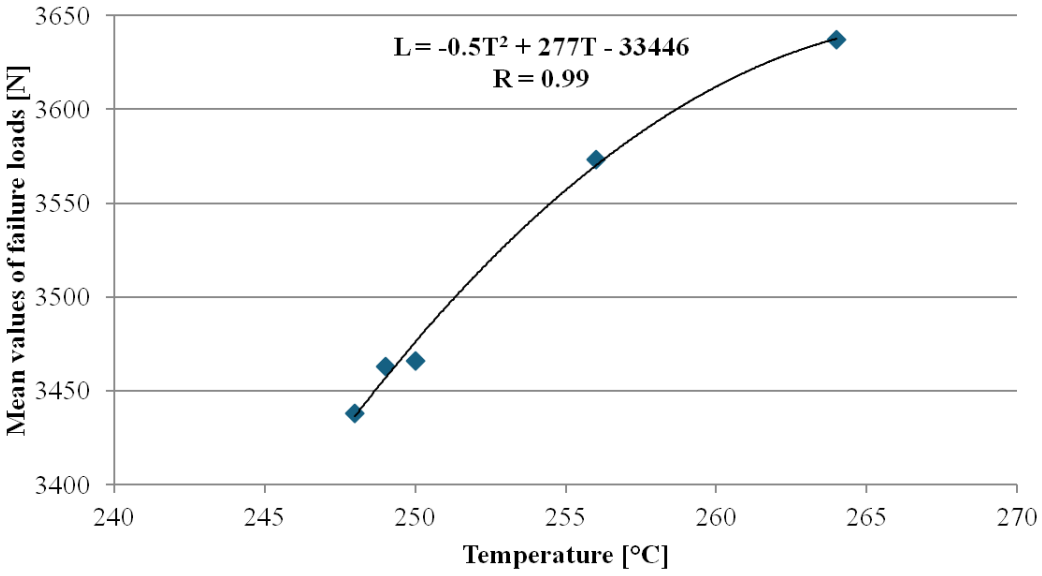

(a)

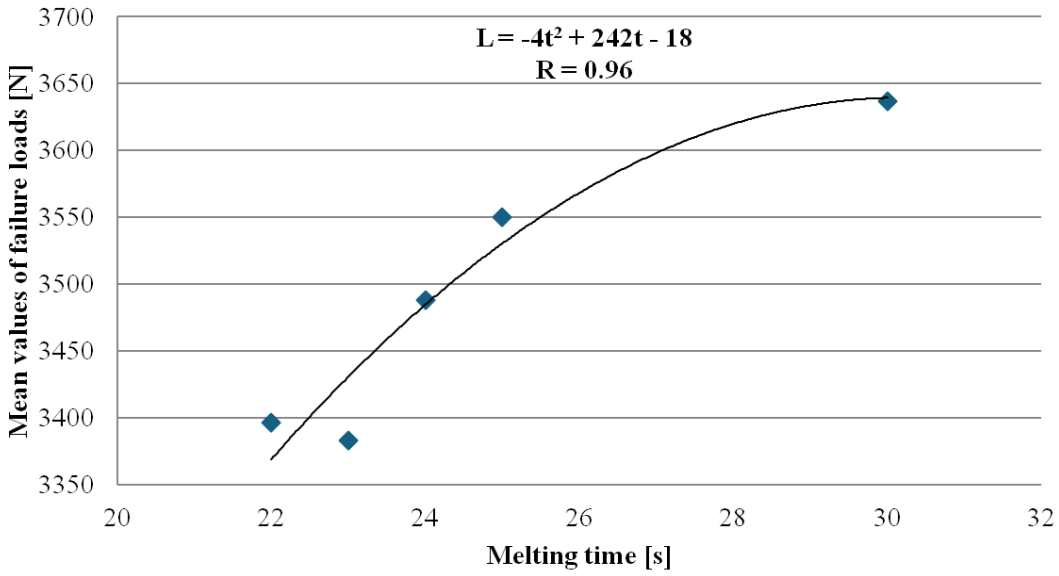

(b)

Fig. 107. Polynomial approximation of the mean failure load of welded joints as a function of process parameters: (a) welding temperature, (b) melting time. Source: Author's own work

As shown in Figure 107, the regression analysis revealed an exceptionally strong association between the mean failure load and both welding temperature and melting time. The correlation coefficient was 0.99 for the relationship between failure load and welding temperature, and 0.96 for the relationship between failure load and melting time. These values indicate a very close correspondence between the fitted response and the experimental data.

The use of a second-order polynomial model made it possible not only to describe the relationship between the welding parameters and the failure load, but also to estimate theoretical threshold values derived from the adopted force-based criterion. It should be emphasised that the measurement points used to construct the models did not represent single observations, but mean failure-load values determined from a large number of specimens. For both the melting-time analysis and the welding-temperature analysis, at least 60 specimens were considered separately. After substituting the limiting failure-load value of 2760 N into the equations, the minimum load-bearing level of the joint was estimated to be attainable at approximately 226.7 °C and at approximately 15.4 s. These values should be interpreted as the outcome of extrapolative prediction related solely to the strength criterion, rather than as a complete boundary of technological process acceptability.

The results indicate that, from the perspective of failure load alone, the investigated joints retain a substantial load-bearing reserve relative to the minimum level of 2760 N. The actual process boundaries, namely 264 °C and 22 s, therefore result from the combined consideration of the quantitative strength criterion and the qualitative assessment of the weld zone. This means that the polynomial model can be used to predict threshold values with respect to failure load, while the final acceptance of welding parameters must also account for qualitative factors, including proper weld formation, material condition and process stability.

On the basis of the experimental programme, the optimal process window for welding a PVC profile reinforced with a glass-fibre composite comprises a welding temperature of 264 °C, a melting time of 22 s, a welding-head feed rate of 0.25 mm/s, and a composite milling

depth of 1.0 mm. The melting time of 22 s should therefore be regarded as an optimum only within this defined parameter regime, with the welding temperature maintained at 264 °C.

4.3. Confirmatory Study of Welded Joints

4.3.1. Experimental Methodology

Hardness testing of the welded-joint specimens was carried out using the Rockwell method in accordance with PN-EN ISO 18265:2014-02 for five weld variants (Fig. 4.108(a)). Each variant, corresponding to a defined set of process parameters, was assessed on three specimens. Measurements were taken at two locations on each side of the corner, namely two points per side of the weld, giving a total of 12 measurements per weld type. Testing was performed using a KB Prüftechnik GmbH KB150R hardness tester (Hochdorf-Assenheim, Germany) (Fig. 4.108(b)). The analysed welding-parameter variants are summarised in Table 48.

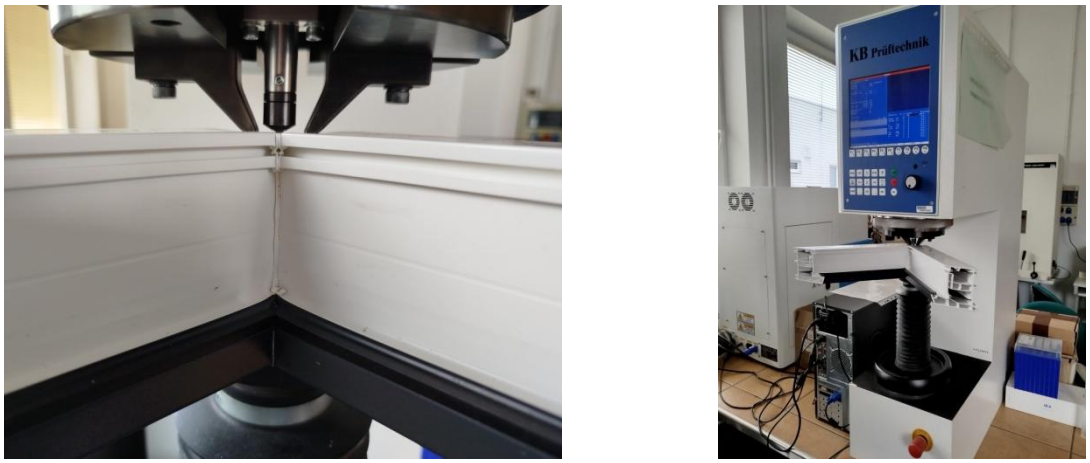

(a) (b)

Fig. 4.108. Hardness testing: (a) weld specimen, (b) test apparatus used. Source: Author's own work

Table 48. Selected weld variants obtained under different process parameters, with a constant welding-head feed rate of 0.25 mm/s. Source: Author's own work

Parameter	(a)	(b)	(c)	(d)	(e)
Welding temperature [°C]	256	263	264	264	270
Melting time [s]	30	22	22	30	21
Composite milling depth [mm]	1.0	1.0	1.0	0.0	1.0

Microscopic examination of the welds was performed using an Opta-Tech SK-series stereomicroscope (Fig. 4.109). The instrument is suitable for three-dimensional observation of small objects under reflected light, transmitted light, or both simultaneously. Observations were conducted with WF10×/20 eyepieces over a magnification range of 7×–45×. The zoom setting for each image was selected according to the weld region under assessment. Microscopy was undertaken for the five weld variants listed in Table 48.

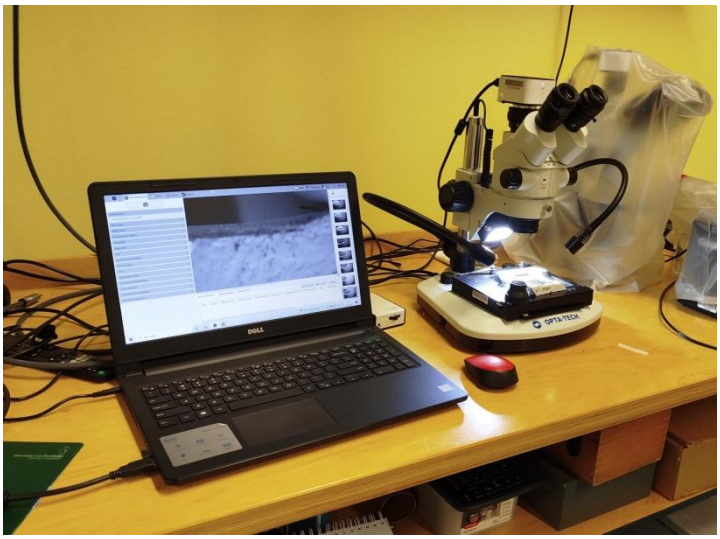

Fig. 4.109. Microscopic examination of welds. Source: Author's own work

Information on the structure of polymeric materials can be obtained, among other techniques, from differential scanning calorimetry (DSC) performed in a heating–cooling–heating sequence. The second heating was used to impose a defined thermal history on the materials under investigation. A 10.00 ± 0.20 mg specimen was weighed using a RADWAG XA52/2X laboratory balance with a 0.01 mg resolution and placed in an aluminium pan (Fig. 4.110). DSC measurements were conducted using a Netzsch DSC 204F1 Phoenix instrument. The glass-transition temperature, Tg, was determined at the inflection point corresponding to the maximum slope of the Cp step. Where this value was not available from the software output, Tg was taken as the midpoint temperature of the heat-capacity step (Tmid) during the second heating. Five weld variants produced under different processing conditions were examined in accordance with Table 48.

The DSC programme comprised the following steps, repeated twice:

a) heating from 20 °C to 130 °C at 10 °C/min under a nitrogen atmosphere,
b) isothermal hold at 130 °C for 10 min under a nitrogen atmosphere,
c) cooling from 130 °C to 20 °C at 10 °C/min under a nitrogen atmosphere,
d) isothermal hold at 20 °C for 10 min.

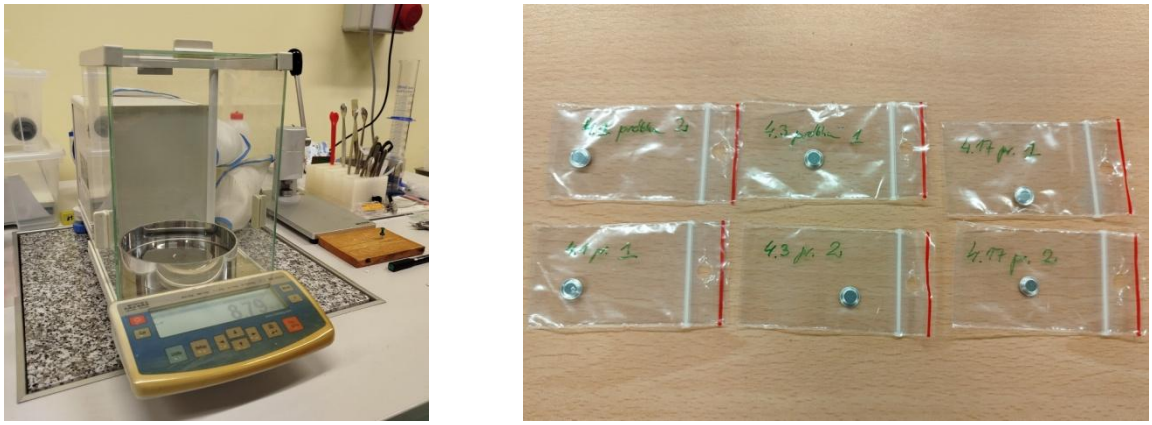

(a) (b)

Fig. 4.110. Preparation of specimens for DSC testing: (a) specimen weighing, (b) specimen labelling. Source: Author's own work

In this part of the study, the chemical stability of the weld material was assessed using the previously described FTIR-ATR procedure, with particular attention paid to the presence, disappearance, or intensity variation of diagnostic absorption bands.

4.3.2. Analysis of Results

Figure 4.111 summarises the hardness-measurement results for the investigated weld sets.

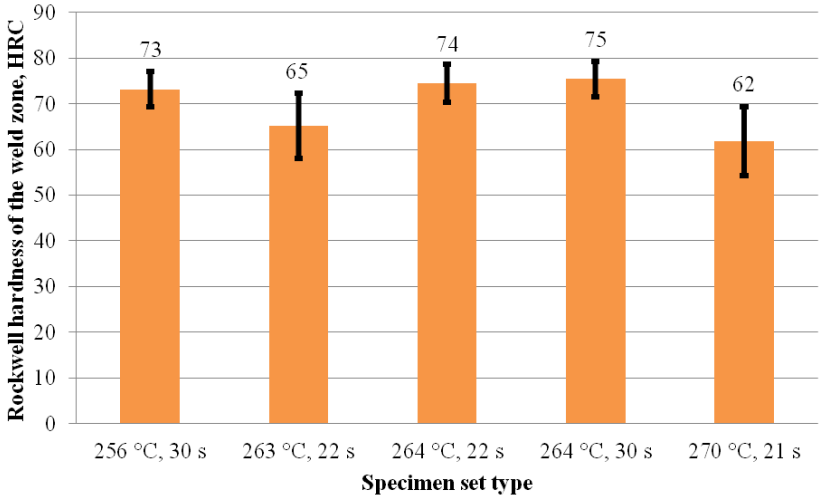

Fig. 4.111. Rockwell hardness measurements for the tested weld sets. Source: Author's own work

The plot indicates no material differences in weld hardness for melting temperatures in the range 256–264 °C, with mean values between 65 and 75 N/mm². Nevertheless, the analysis suggests that the use of higher welding temperatures, from approximately 270 °C, may result in lower weld hardness compared with the lower-temperature variants produced at 264 °C. Importantly, no meaningful difference in hardness was identified between the welds produced at 264 °C with melting times of 22 s and 30 s.

When the mean hardness values for the PVC specimens (Fig. 4.21) are compared with those of the welds, a pronounced disparity is evident. The mean hardness of PVC was 88 N/mm², whereas the closest and highest mean hardness among the weld sets was 75 N/mm² for 264 °C and 30 s, with the remaining weld-set means being lower. This pattern indicates a temperature-mediated effect on weld integrity, manifested as a reduction in the average hardness of the weld specimens.

Considering the 95% confidence intervals, the mean hardness of the welds is at least 4.7% lower than the mean hardness of the parent material. The smallest reduction was observed for welds produced at 264 °C and 30 s, 264 °C and 22 s, 256 °C and 30 s.

Figure 4.112 presents the relationship between the mean failure load of the welded joints and the measured Rockwell hardness of the weld zone.

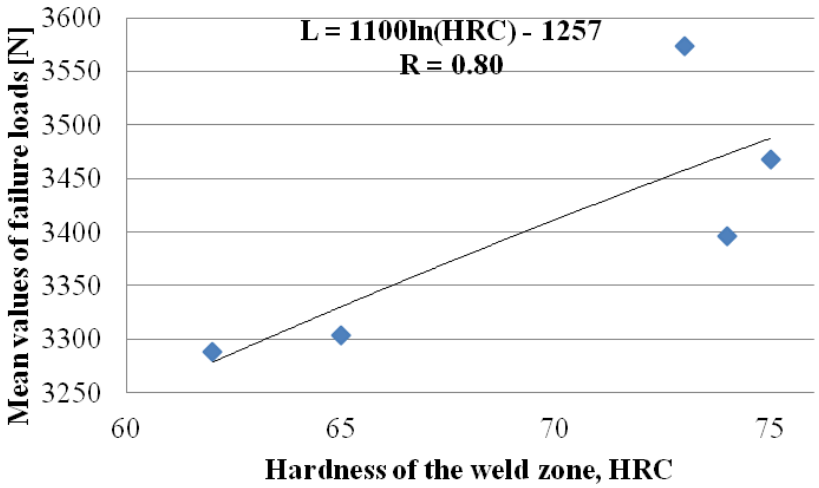

Fig. 4.112. Mean failure load of welded joints plotted against the measured Rockwell hardness of the weld zone. Source: Author's own work

The results indicate a positive tendency between the Rockwell hardness of the weld zone and the mean failure load of the welded joints. For each welding variant, hardness values were determined from 12 measurement points, comprising four measurements performed on each of three independent specimens, thereby improving the representativeness of the mean values adopted for the analysis. Nevertheless, this relationship should be interpreted as supportive rather than conclusive. The results suggest that the higher the weld zone hardness is obtained, the higher the breaking load can be expected. However, the load-bearing capacity of the joint is also governed by welding temperature, melting time and the overall quality of the weld zone.

Figure 4.113 presents the recorded images of the individual weld microstructures. Inspection of the microstructural images shows that the welds in Figs. 4.113(a)–(d) exhibit a white weld bead. The morphology is uneven and porous, yet no evidence of PVC degradation was identified. According to Table 48, these joints were produced within 256–264 °C, and their mean Rockwell hardness values (Fig. 4.111) ranged from 65 to 75 N/mm². This supports the conclusion that this temperature range is acceptable for welding PVC profiles. Moreover, the melting time did not exceed the standard 30 s, thereby limiting prolonged thermal exposure. A different response is evident for the weld shown in Fig. 4.113(e). The microscopy suggests PVC depolymerisation, expressed as a light-brown discolouration that extends beyond the outer bead and penetrates into the joint interior. In this case, Table 48 reports a welding temperature of 270 °C with a melting time of 21 s, while the mean hardness was 62 N/mm², markedly lower than for the 264 °C weld sets. This indicates that, despite the reduction in melting time from 30 s to 21 s, the elevated temperature induced irreversible degradation of the joint. Consequently, a welding temperature of 270 °C is clearly excessive and produced unambiguously adverse quality outcomes in the investigated weld.

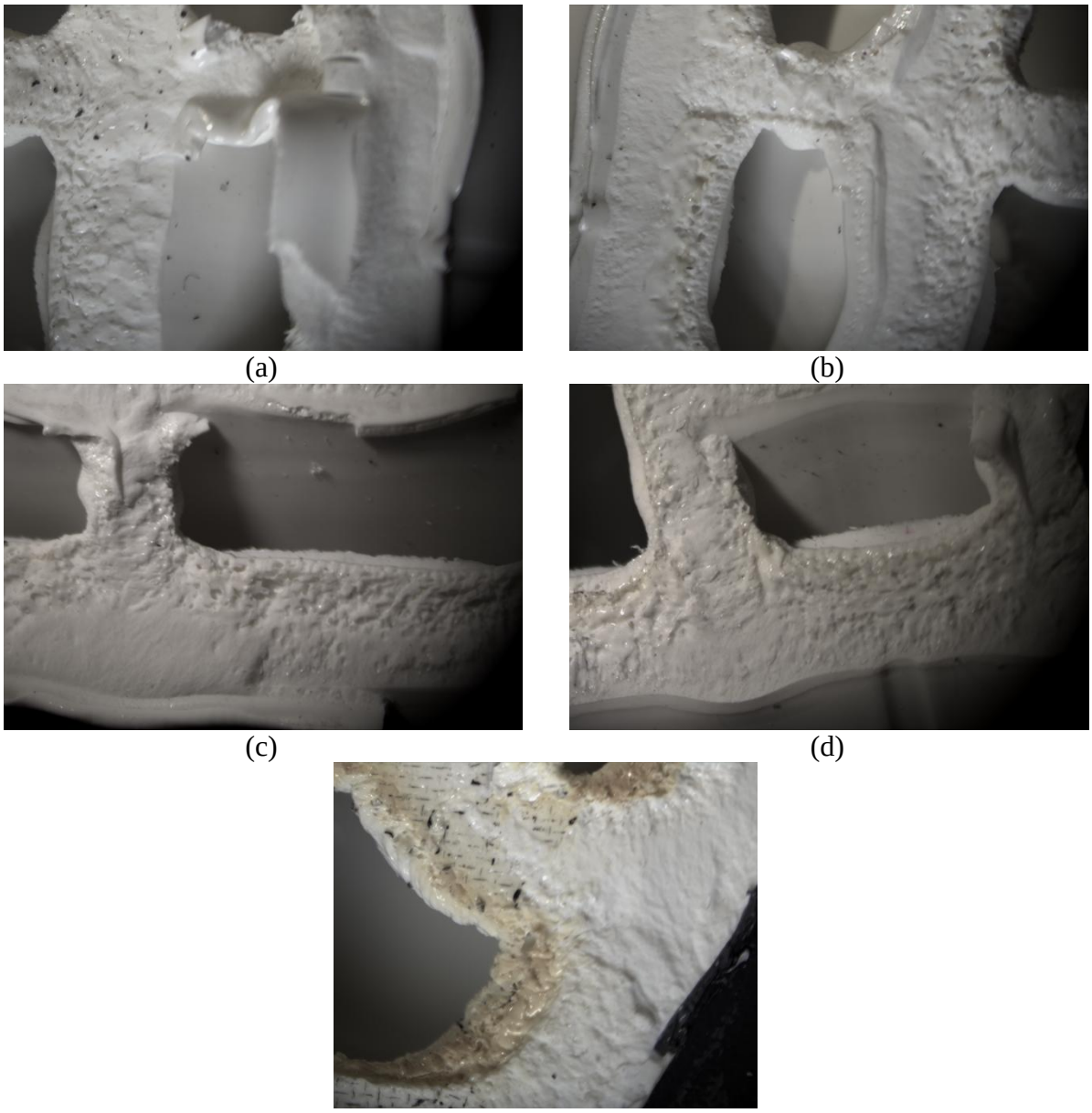

Fig. 4.113. Recorded images of weld structures for the individual welding-parameter variants (a) – (e), as specified in Table 48. Source: Author's own work

Figures 4.114 and 4.115 show DSC thermograms for PVC weld specimens produced at a welding temperature of 270 °C and a welding time of 21 s. In both thermograms, two thermal events were recorded within approximately 80–100 °C. No distinct, quantitatively resolved transition was observed at lower temperatures for any specimen in this series. In Fig. 4.114, the first event begins at about 88.4 °C, reaches a maximum at 89.8 °C, and ends at 92.2 °C. The second event starts at about 93.2 °C, peaks at 93.9 °C, and disappears at around 94.0 °C. Together, these features form a broad, bimodal glass-transition region. The lower component at around 90 °C can be treated as the dominant glass transition, whereas the narrower feature near 94 °C likely reflects a fraction of material exhibiting a slightly higher vitrification temperature. For the second specimen (Fig. 4.115), the maximum of the first event occurs at 86.1 °C and the event ends at 87.9 °C. The second event starts at about 93.7 °C, reaches a maximum at 94.6 °C, and ends at 94.5 °C. This yields a primary transition interval near 86–88 °C and a higher, narrow interval near 94–95 °C. In both specimens, the transition intensity is

sufficiently low that the software did not provide a reliable ΔCp value. The slope changes are therefore too subtle for a robust quantitative description. It can nonetheless be concluded that, under welding at 270 °C with a welding time of 21 s, the PVC welds show a clear glass-transition region around 86–90 °C and an additional narrow feature near 94 °C, accompanied by a comparatively small ΔCp. The low intensity implies limited mobilisation of segments in this temperature window, but it does not, on its own, justify inferences regarding the degree of gelation or the mechanical performance of the joint.

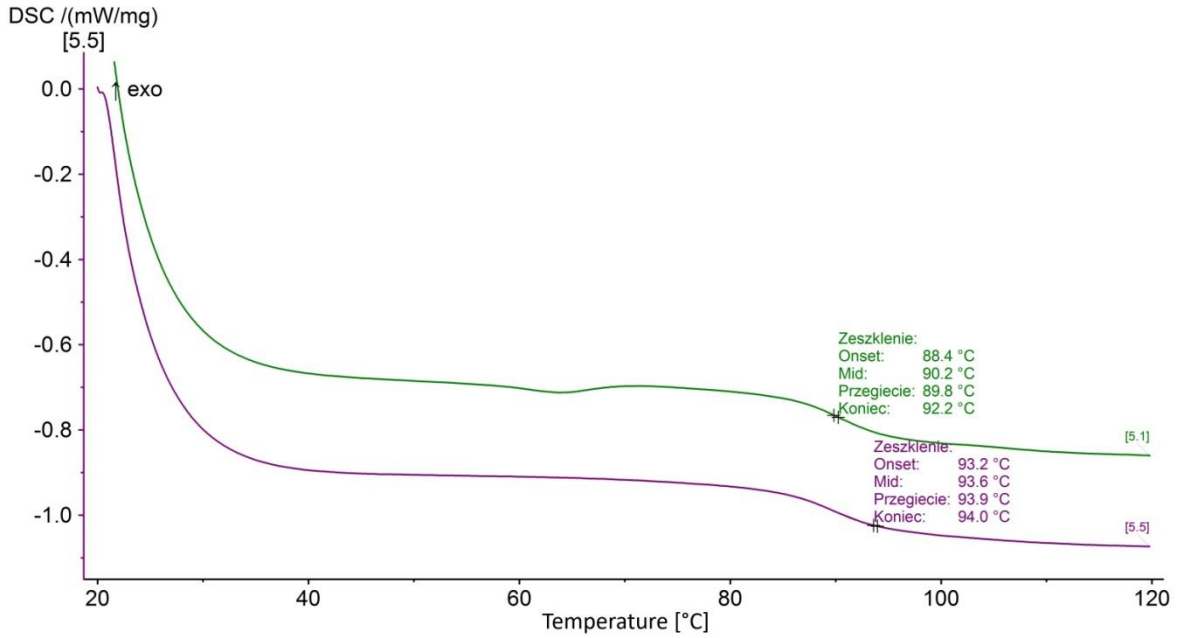

Fig. 4.114. Thermogram of the first PVC weld specimen produced at a welding temperature of 270 °C and a melting time of 21 s. Source: Author's own work

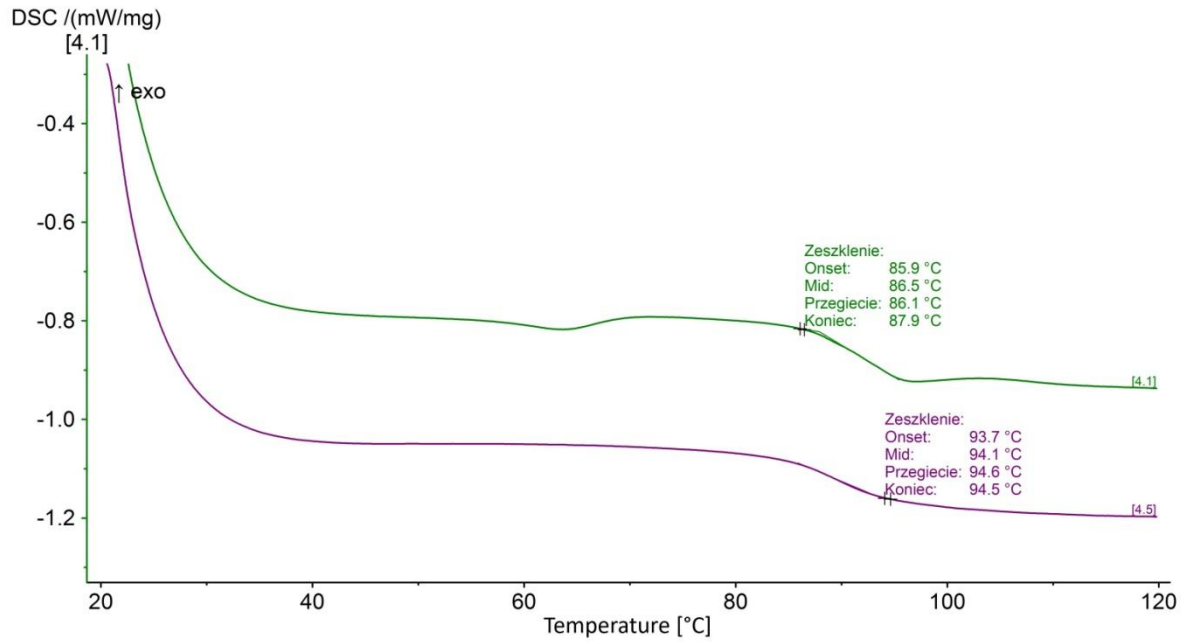

Fig. 4.115. Thermogram of the second PVC weld specimen produced at a welding temperature of 270 °C and a melting time of 21 s. Source: Author's own work

Figures 4.116–4.119 present DSC thermograms for PVC weld specimens produced at a welding temperature of 264 °C and a welding time of 30 s. Four measurements were performed for this condition. All specimens in this series show a distinct event at lower temperatures near 57–58 °C, with ΔCp of approximately 0.005–0.014 J/g·K. They also exhibit a dominant glass-transition region near 84–86 °C with comparatively high ΔCp of 0.19–0.33 J/g·K, together with additional weaker features across roughly 88–95 °C. These higher-temperature features can be interpreted as local domains experiencing different vitrification conditions. Figure 4.116 shows a low-temperature event at about 57.2–57.6 °C, with ΔCp of approximately 0.014 J/g·K. At higher temperatures, two closely spaced events appear at about 84.6 °C (ΔCp of approximately 0.189 J/g·K) and 85.1 °C (ΔCp of approximately 0.332 J/g·K). These two responses are more plausibly interpreted as a split of a broad glass transition into components with different segment mobility, rather than as fully independent Tg values. In Fig. 4.117, the low-temperature event occurs at about 57.5–58.3 °C with ΔCp of approximately 0.005 J/g·K. In the higher-temperature range, very weak effects are recorded around 88.6–88.9 °C, with ΔCp of approximately 0.013 and 0.001 J/g·K. Their very small magnitude indicates that only a minor fraction of the material participates in these local transitions, and differences of this order may approach the sensitivity limit of the method. In Fig. 4.118, a low-temperature event occurs within approximately 55–57 °C, with ΔCp of approximately 0.014 J/g·K. The higher-temperature region contains two events, with the dominant glass transition at about 85.9 °C (ΔCp of approximately 0.275 J/g·K) and a markedly weaker feature at about 94.0–94.4 °C (ΔCp of approximately 0.011 J/g·K). In Fig. 4.119, the low-temperature event appears at about 56–57 °C with ΔCp of approximately 0.010 J/g·K. Two higher-temperature events are visible, one at about 84.4 °C (ΔCp of approximately 0.315 J/g·K) and a second at about 86–87 °C (ΔCp of approximately 0.195 J/g·K). Overall, the dominant glass transition for PVC in this series falls within approximately 84–86 °C and is well developed, with ΔCp reaching above 0.3 J/g·K in several thermograms. The additional effects near 90–95 °C, together with very weak features near 88–89 °C, indicate heterogeneity within the amorphous phase. They do not, however, support the claim of three discrete Tg values. A more defensible description is a single, broad vitrification interval that is locally resolved into multiple components.

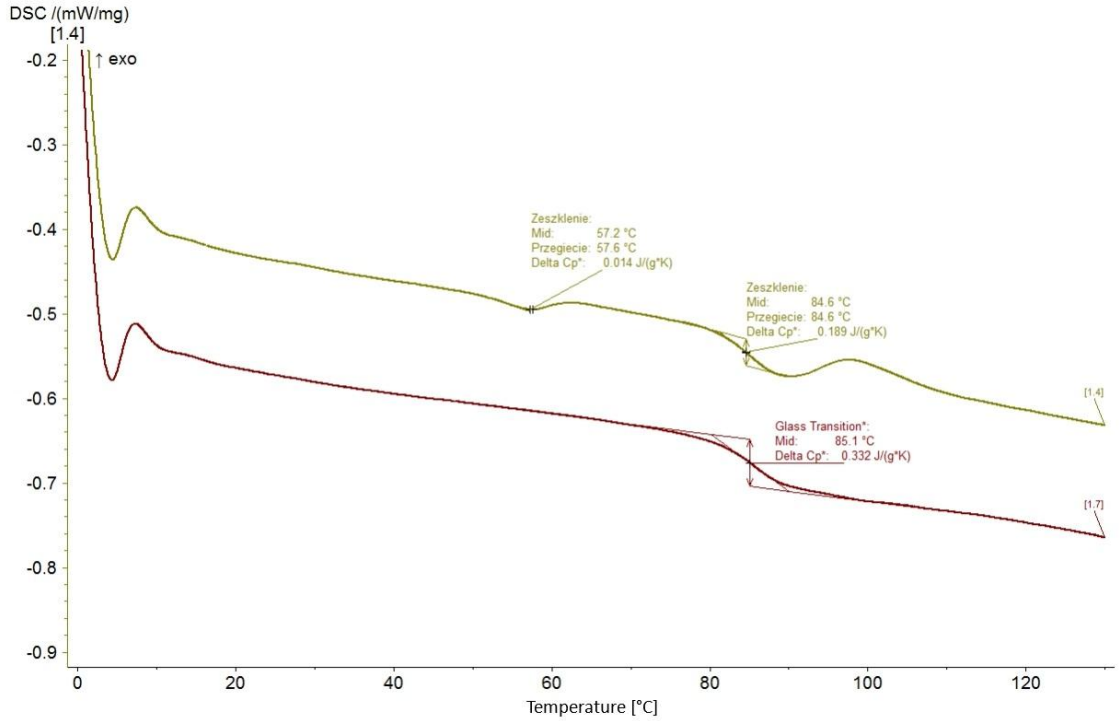

Fig. 4.116. Thermogram of the first PVC weld specimen produced at a welding temperature of 264 °C and a melting time of 30 s. Source: Author's own work

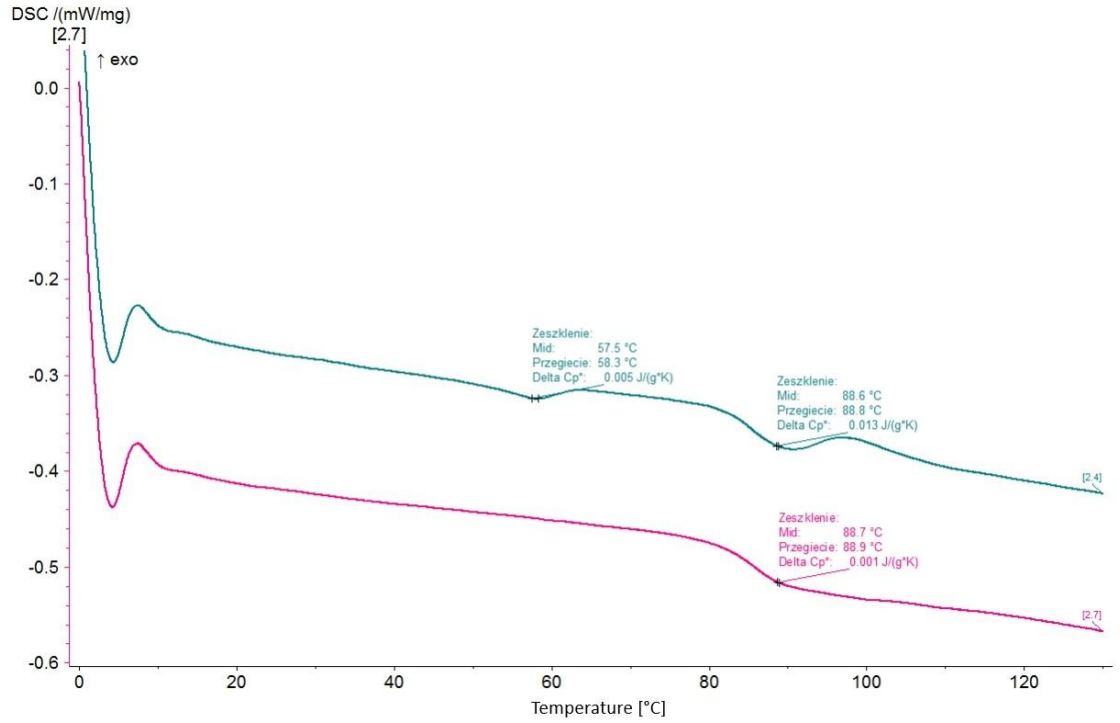

Fig. 4.117. Thermogram of the second PVC weld specimen produced at a welding temperature of 264 °C and a melting time of 30 s. Source: Author's own work

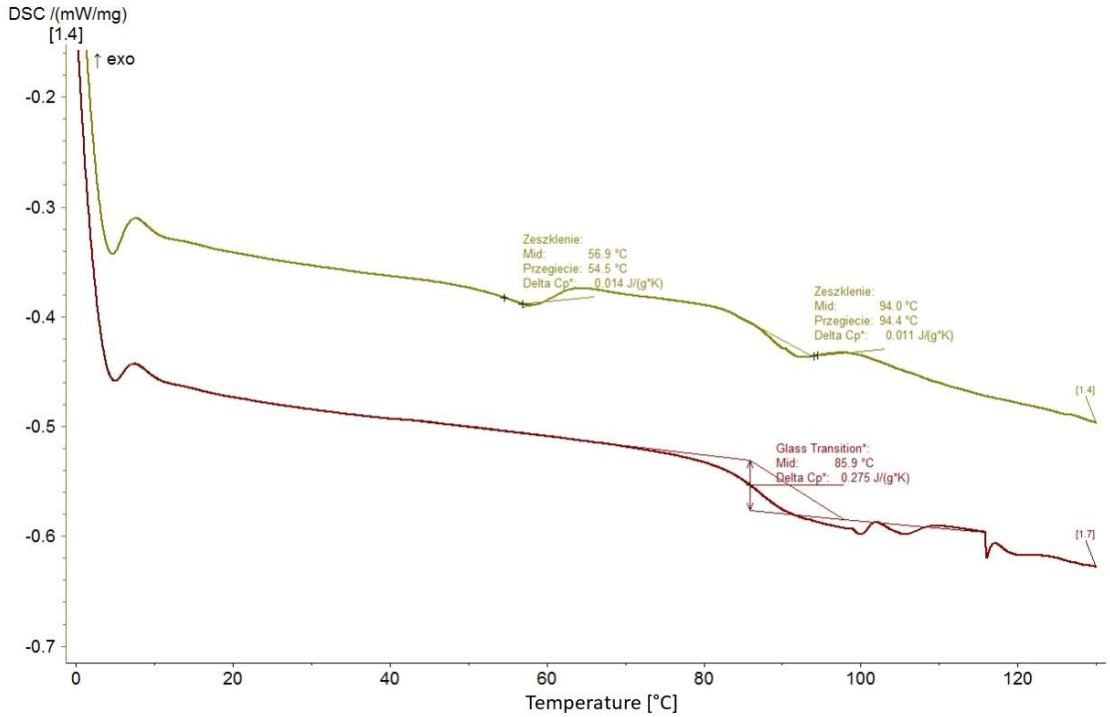

Fig. 4.118. Thermogram of the third PVC weld specimen produced at a welding temperature of 264 °C and a melting time of 30 s. Source: Author's own work

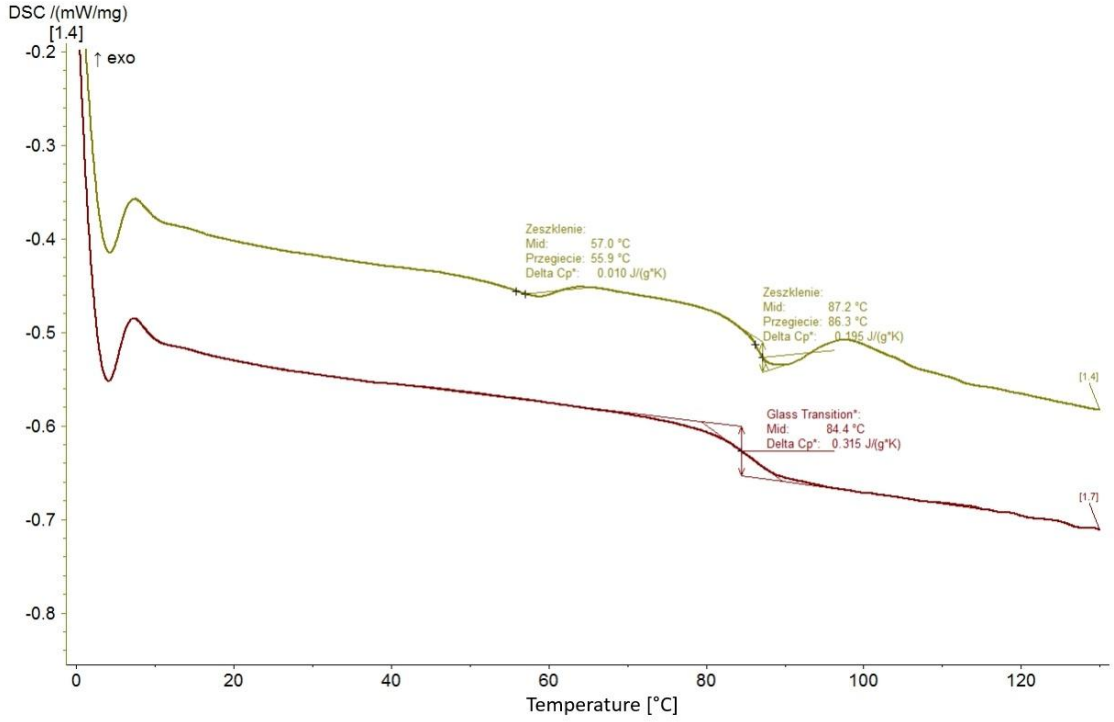

Fig. 4.119. Thermogram of the fourth PVC weld specimen produced at a welding temperature of 264 °C and a melting time of 30 s. Source: Author's own work

Figures 4.120–4.123 show DSC thermograms for four PVC weld specimens produced at a welding temperature of 264 °C and a welding time of 22 s. Their profiles closely resemble those obtained for welding at 264 °C with a welding time of 30 s. Across all specimens, a weak event appears near 57–59 °C, the dominant glass-transition region lies near 85–86 °C,

and further weaker transitions are observed between approximately 90 and 95 °C. In Fig. 4.120, the low-temperature event occurs near 56–57 °C with ΔCp of approximately 0.008 J/g·K. Two higher-temperature events are visible, with the stronger response at about 85.6 °C and ΔCp of approximately 0.323 J/g·K, and a weaker feature near 92.0–92.8 °C with ΔCp of approximately 0.027 J/g·K. In the next specimen (Fig. 4.121), the low-temperature event occurs near 58.0–58.5 °C with ΔCp of approximately 0.018 J/g·K. The dominant transition appears at about 84.8 °C with ΔCp of approximately 0.226 J/g·K, and an additional weak effect occurs near 90.6–91.7 °C with ΔCp of approximately 0.013 J/g·K. In Fig. 4.122, the low-temperature event is recorded at about 58.5–59.1 °C with ΔCp of approximately 0.015 J/g·K. The dominant high-temperature response occurs at about 85.6 °C with ΔCp of approximately 0.315 J/g·K, accompanied by a weaker feature near 93.2 °C with ΔCp of approximately 0.027 J/g·K. The fourth specimen (Fig. 4.123) shows a low-temperature event at about 58.8–59.5 °C with ΔCp of approximately 0.003 J/g·K. The dominant glass transition occurs at about 85.5 °C with ΔCp of approximately 0.287 J/g·K, while an additional weak transition spans roughly 90.8–95.6 °C with ΔCp of approximately 0.012 J/g·K. This series consistently reproduces three temperature regions: a weak sub-glass event near 57–59 °C, plausibly linked to locally more mobile segments or additives; a dominant glass transition near 85–86 °C with the highest ΔCp; and further weak features between about 90 and 95 °C that suggest domains with elevated vitrification temperatures. These observations support a broad, composite Tg region rather than three independent Tg values.

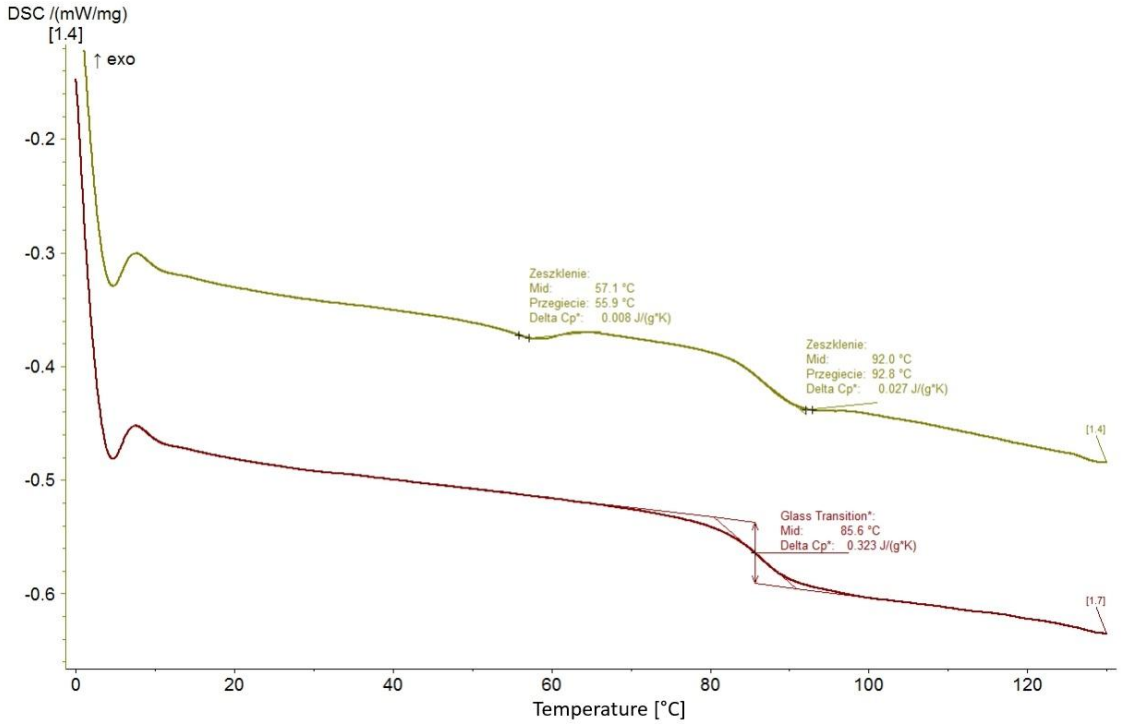

Fig. 4.120. Thermogram of the first PVC weld specimen produced at a welding temperature of 264 °C and a melting time of 22 s. Source: Author's own work

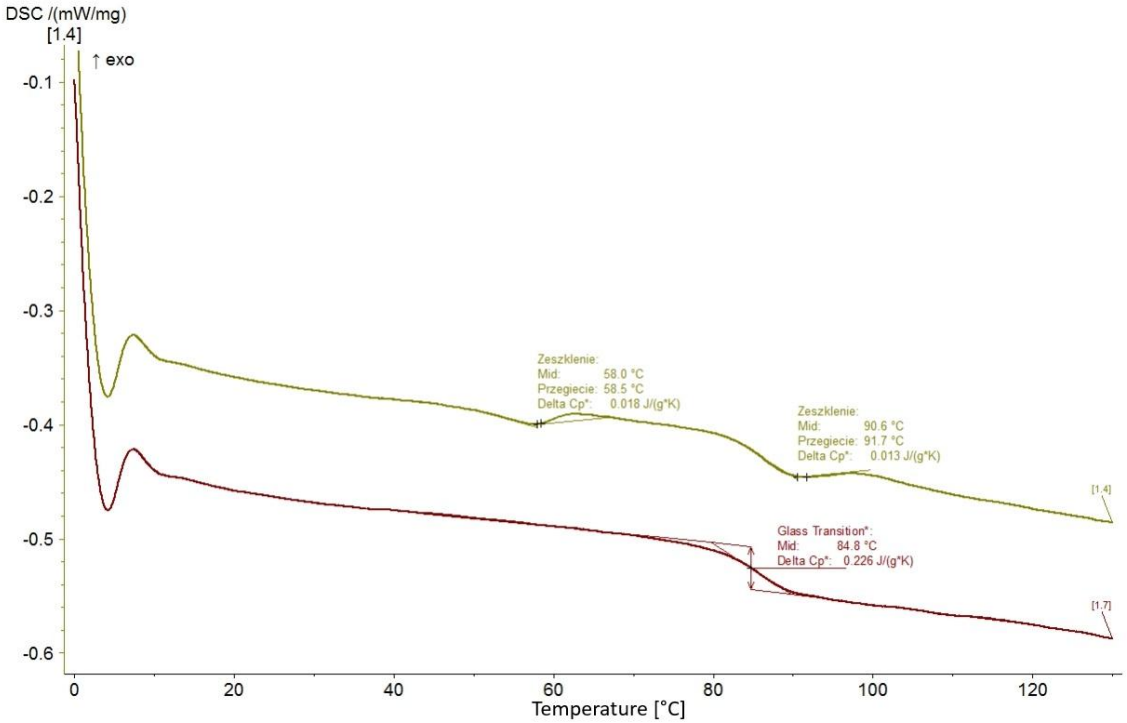

Fig. 4.121. Thermogram of the second PVC weld specimen produced at a welding temperature of 264 °C and a melting time of 22 s. Source: Author's own work

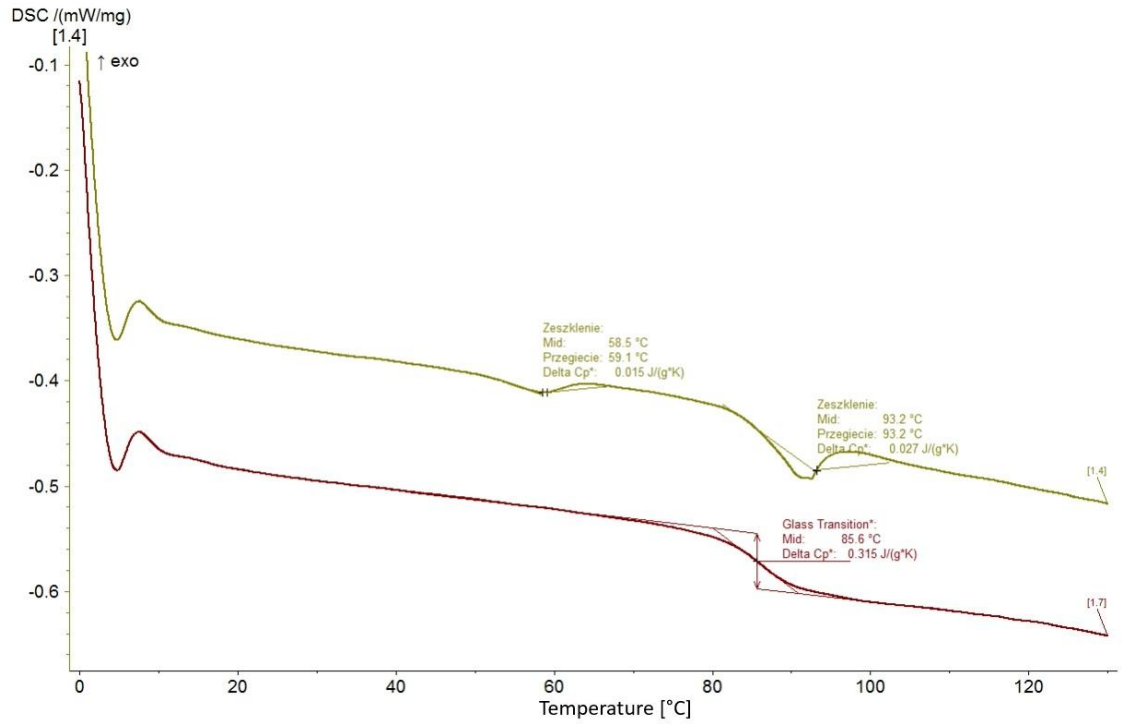

Fig. 4.122. Thermogram of the third PVC weld specimen produced at a welding temperature of 264 °C and a melting time of 22 s. Source: Author's own work

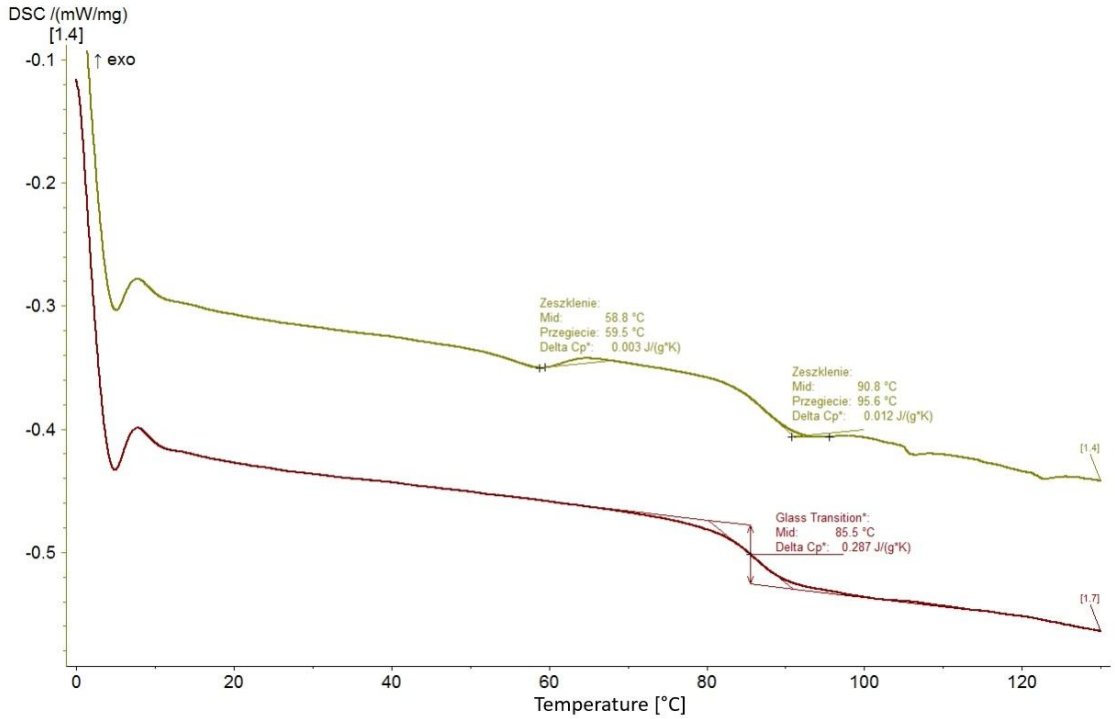

Fig. 4.123. Thermogram of the fourth PVC weld specimen produced at a welding temperature of 264 °C and a melting time of 22 s. Source: Author's own work

Figures 4.124 and 4.125 present DSC thermograms for two PVC weld specimens produced at a welding temperature of 263 °C and a welding time of 22 s. In contrast to the series obtained at a welding temperature of 264 °C, no low-temperature event near 57–59 °C was observed. Instead, both specimens exhibit two clearly separated transitions within approximately 90–95 °C. In Fig. 4.124, the first transition starts at about 90.5 °C, reaches a maximum at 92.3 °C, and ends at 93.4 °C. The second transition begins at around 94.0 °C, peaks at 94.5 °C, and terminates at about 94.3 °C. For the second specimen in this series (Fig. 4.125), the first transition begins at about 92.0 °C, shows an inflection at 92.8 °C, and ends at 93.6 °C. The second transition starts at around 93.8 °C and shows an inflection at 95.1 °C, with the end of the transition falling within a comparable interval. The absence of quantitative ΔCp values prevents a rigorous comparison of transition intensity with other series. Nevertheless, the clear separation of two high-temperature regions indicates pronounced heterogeneity within the amorphous phase in this temperature domain. The disappearance, or substantial attenuation, of the event near 57–59 °C may indicate that these welding conditions reduced the contribution of more mobile segments.

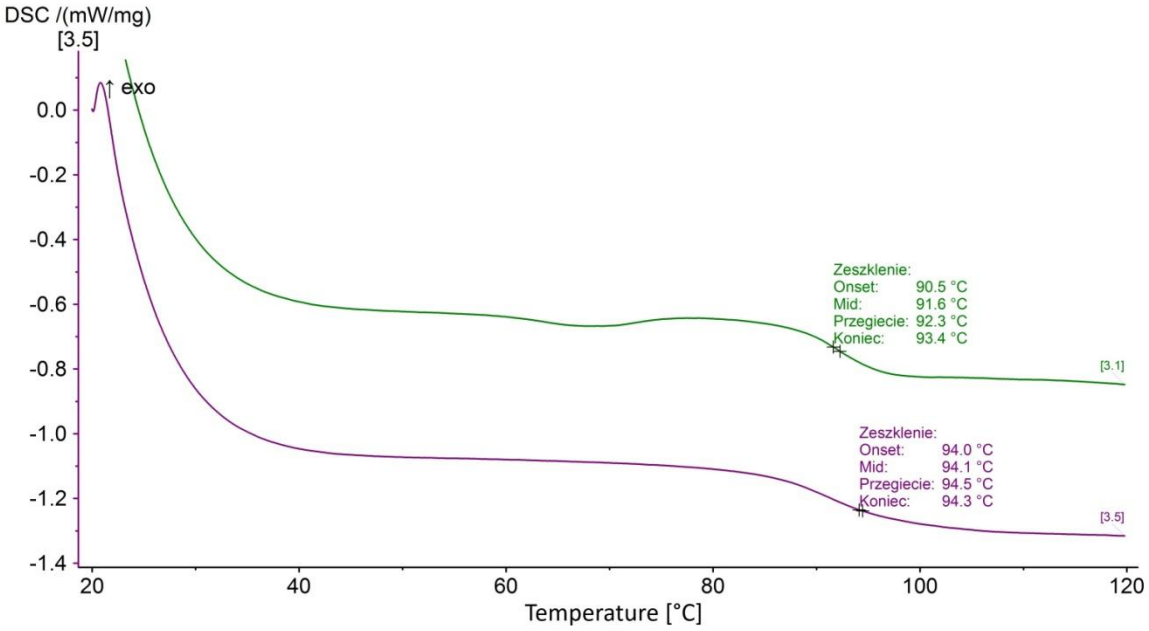

Fig. 4.124. Thermogram of the first PVC weld specimen produced at a welding temperature of 263 °C and a melting time of 22 s. Source: Author's own work

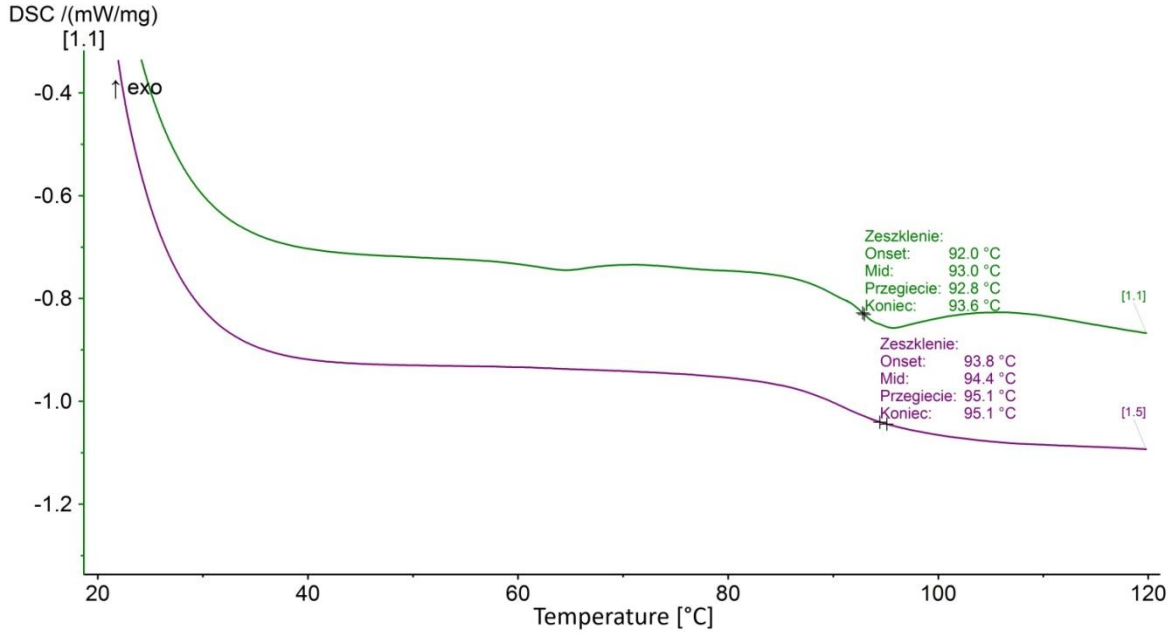

Fig. 4.125. Thermogram of the second PVC weld specimen produced at a welding temperature of 263 °C and a melting time of 22 s. Source: Author's own work

Figures 4.126 and 4.127 show DSC thermograms for two PVC weld specimens produced at a welding temperature of 256 °C and a welding time of 30 s. This was the lowest temperature examined, and the recorded traces display a distinctive profile. The transitions are concentrated within a relatively narrow interval of approximately 88–95 °C, without a pronounced dominant event near 84–86 °C. In Fig. 4.126, the first transition spans roughly 92–95 °C. A second transition occurs in a closely overlapping region, extending from about 92.8 °C to 94.6 °C, with an additional change noted near 91.0 °C. Given the proximity of Tmid and Tonset values, the thermogram qualitatively suggests two overlapping transitions

within a narrow high-temperature window. In Fig. 4.127, two transitions are again present with very similar ranges. The first extends from about 87.8 °C to 93.3 °C, with a maximum near 91.0 °C. The second spans approximately 87.9 °C to 92.0 °C, with a maximum near 90.4 °C. Because differences in position and width are minor, these effects can be interpreted as two mobility sub-domains within the same high-temperature glass-transition region. Overall, both specimens produced at a welding temperature of 256 °C and a welding time of 30 s indicate a glass transition concentrated within roughly 88–95 °C, with no strongly separated event near 84–86 °C and no clearly quantified low-temperature event near 57–59 °C. This pattern may be interpreted as a more uniform segmental mobility response across the analysed temperature range.

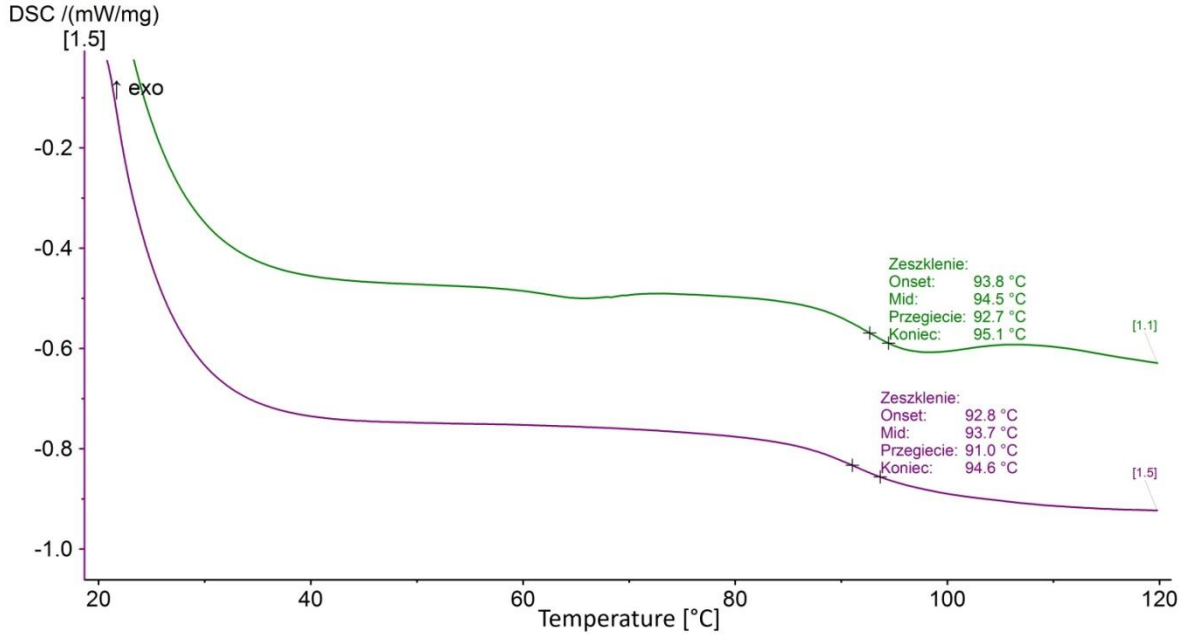

Fig. 4.126. Thermogram of the first PVC weld specimen produced at a welding temperature of 256 °C and a melting time of 30 s. Source: Author's own work

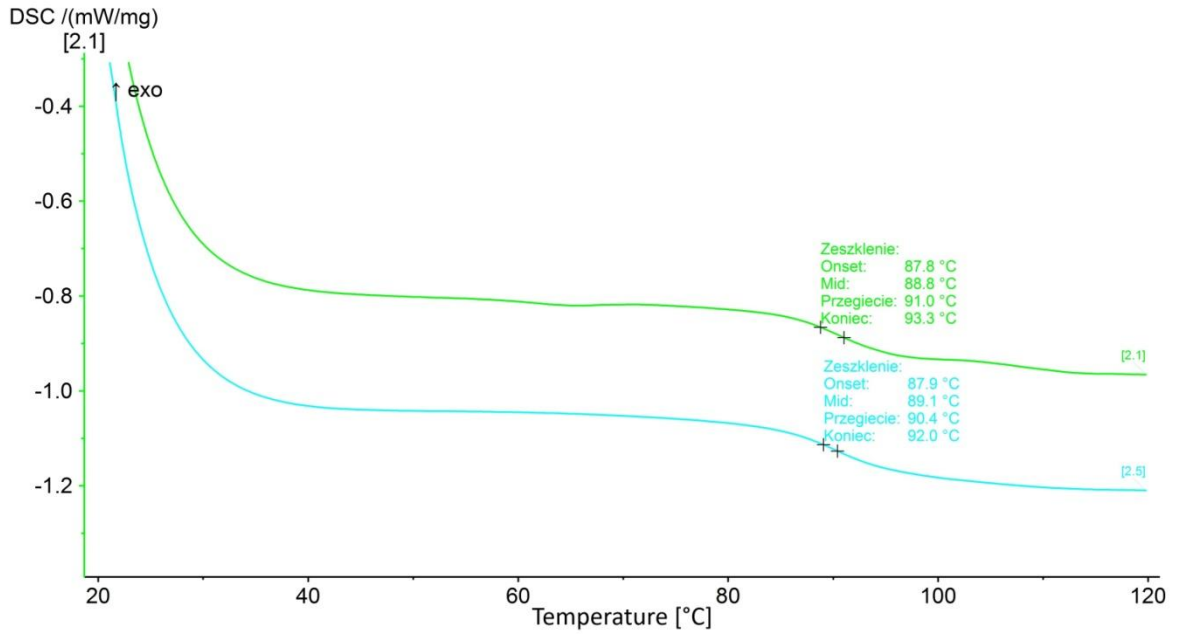

Fig. 4.127. Thermogram of the second PVC weld specimen produced at a welding temperature of 256 °C and a melting time of 30 s. Source: Author's own work

Table 49 presents the dominant glass-transition temperatures determined from DSC analysis for the analysed weld variants produced under different welding conditions.

Table 49. Dominant glass-transition temperatures determined from DSC analysis. Source: Author's own work

Weld condition	Dominant glass-transition temperature, Tg [°C]
270 °C / 21 s	86–90
264 °C / 30 s	84–86
264 °C / 22 s	85–86
263 °C / 22 s	92–93
256 °C / 30 s	88–95

The DSC results show that the welds produced at 264 °C, for both 22 s and 30 s, had a similar dominant Tg range of approximately 84–86 °C. This suggests that shortening the melting time from 30 s to 22 s at 264 °C did not noticeably change the thermal behaviour of the weld material. The variants produced at 263 °C / 22 s and 256 °C / 30 s showed higher Tg values than the welds produced at 264 °C / 22 s and 264 °C / 30 s. This indicates that these conditions produced a different thermal response of the weld material. For 270 °C / 21 s, the dominant Tg was approximately 86–90 °C, which also differs from the values obtained for the welds produced at 264 °C. This means that increasing the temperature to 270 °C while reducing the melting time to 21 s did not produce the same material response as welding at 264 °C for either 22 s or 30 s.

Figures 4.128 to 4.132 present FTIR-ATR spectra for weld specimens produced under different welding parameter configurations. Figure 4.133 compares the spectra obtained when welding was performed at 264 °C with a melting time of 22 s and when welding was performed at 264 °C with a melting time of 30 s over the range from about 4000 cm^{-1} to 400 cm^{-1}. For improved visibility of differences, the same comparison is additionally shown as magnified views over approximately 3731–2001 cm^{-1} in Fig. 4.134 and approximately 2230–464 cm^{-1} in Fig. 4.135.

In aggregate, all five weld spectra share a common core that is typical of the investigated material system. In the 2850–3000 cm^{-1} region, aliphatic C–H stretching vibrations are observed. A strong band within the fingerprint region recurs in each specimen at about 1421–1424 cm^{-1}, and further recurring maxima appear at approximately 874–875 cm^{-1} and 609–611 cm^{-1}. These bands fall within the 600–800 cm^{-1} interval that can be associated with C–Cl vibrations, as well as within the remaining fingerprint region below 1500 cm^{-1} where bands characteristic of the PVC matrix in the weld zone are expected. Accordingly, irrespective of the welding parameter variant, no step-change in chemical material type is observed, and any differences are local in nature.

The weld specimen produced at 264 °C with a melting time of 30 s shows a spectrum that is typical of PVC in the weld zone and comprises several characteristic bands. In the upper part of the spectrum, within 2850–3000 cm^{-1}, two distinct maxima occur at 2911.99 cm^{-1} and 2850.27 cm^{-1}, consistent with aliphatic C–H stretching vibrations originating from the organic

polymer matrix. In the mid-region, peaks appear at 2349.84 cm^{-1} and 2315.12 cm^{-1}. Such signals are frequently attributable to gaseous species in ambient air, most commonly CO_2, and are therefore generally treated as background rather than as intrinsic features of the polymer. Within the carbonyl window, from about 1650 cm^{-1} to 1750 cm^{-1}, a band is identified at 1733.69 cm^{-1}. Its presence indicates a contribution from carbonyl groups, which may arise from formulation additives, surface contamination, or local near-surface chemical changes. The spectrum alone does not permit an unambiguous assignment. The most discriminative domain for material identification is the fingerprint region below 1500 cm^{-1}. Here, a repeatable band set is observed at 1424.17 cm^{-1}, 1329.68 cm^{-1}, 1244.83 cm^{-1}, 1094.40 cm^{-1}, 965.198 cm^{-1}, 875.524 cm^{-1}, and 611.324 cm^{-1}, forming the characteristic absorption profile of the PVC matrix in the weld zone. Consistency of these bands across specimens provides the primary basis for concluding chemical similarity between the different welding variants. A very weak signal at 422.334 cm^{-1} appears only in this spectrum. Because it is not reproduced systematically in the other specimens, it should be treated as an artefact of spectral processing or ATR contact conditions, rather than as a robust indicator of compositional change.

The weld specimen produced at 264 °C with a melting time of 22 s exhibits a spectrum that closely matches the variant produced at 264 °C with a melting time of 30 s, indicating that the weld zone retains the same characteristic PVC band pattern. In the 2850–3000 cm^{-1} region, two distinct maxima occur at 2920.66 cm^{-1} and 2852.20 cm^{-1}, consistent with aliphatic C–H stretching vibrations and therefore with the organic polymer backbone. Peaks at 2349.84 cm^{-1} and 2312.23 cm^{-1} are also present and are typically associated with atmospheric species in the optical path, most commonly CO_2, and are therefore treated as background rather than as intrinsic chemical features of the specimen. Within the carbonyl window, from about 1650 cm^{-1} to 1750 cm^{-1}, a band is identified at 1742.37 cm^{-1}, attributable to C=O vibrations. As for the specimen produced with a melting time of 30 s, the occurrence of a signal in this region indicates a contribution from carbonyl groups that may arise from formulation additives or ATR surface effects. The critical point is that this band appears at a comparable wavenumber to that recorded for the 30 s variant. Interpretation is again driven primarily by the fingerprint region below 1500 cm^{-1}. For the specimen produced at 264 °C with a melting time of 22 s, a stable band set is observed at 1424.17 cm^{-1}, 1332.57 cm^{-1}, 1243.86 cm^{-1}, 1095.37 cm^{-1}, 965.198 cm^{-1}, 874.56 cm^{-1}, and 611.324 cm^{-1}, which reproduces the characteristic spectral signature of the material in the weld zone. Accordingly, when comparing the variants produced at 264 °C with melting times of 22 s and 30 s, the underlying chemical structure, understood as the set of diagnostic bands, remains unchanged. The differences are limited to minor shifts in selected maxima of only a few cm^{-1}, which is typical for ATR series and does not, in itself, evidence chemical change. In addition, the weak band near 422 cm^{-1}, previously observed only for the 30 s variant, is absent in the 22 s specimen. This does not affect the interpretation, because the decisive, reproducible fingerprint bands are conserved in both cases.

Figures 4.133 to 4.135 compare two key weld variants, namely the baseline condition in which welding was performed at 264 °C with a melting time of 30 s and the optimised condition in which welding was performed at 264 °C with a melting time of 22 s. Figure 4.133 overlays both spectra on a single axis, while Figs. 4.134 and 4.135 provide magnified views of the same curves over selected ranges to facilitate detection of subtle differences. The central finding is that the two spectra largely overlap, which indicates closely comparable chemistry within the weld zone. This conclusion follows from the presence of the same bands at the same positions, corresponding to the same functional groups, with no emergence of new bands and no disappearance of diagnostic bands that would imply either a material change or

a substantive chemical modification associated with reducing the melting time from 30 s to 22 s at 264 °C. In FTIR-ATR terms, both spectra comprise the same signal blocks, including hydrocarbon-related C–H bands at higher wavenumbers, a band within the carbonyl region, and the diagnostic fingerprint set below about 1500 cm^{-1} that is most decisive for identifying the PVC matrix in the weld zone. Any differences visible in the magnified plots are subtle and relate primarily to band intensities. Under ATR conditions, such intensity differences may reflect contact pressure, surface roughness, and local contact geometry rather than genuine compositional changes. Overall, the baseline and optimised weld variants are therefore chemically comparable by FTIR, and the selection of the optimised parameters can be justified on technological and mechanical grounds without evidence of a distinct, FTIR-detectable chemical change in the weld.

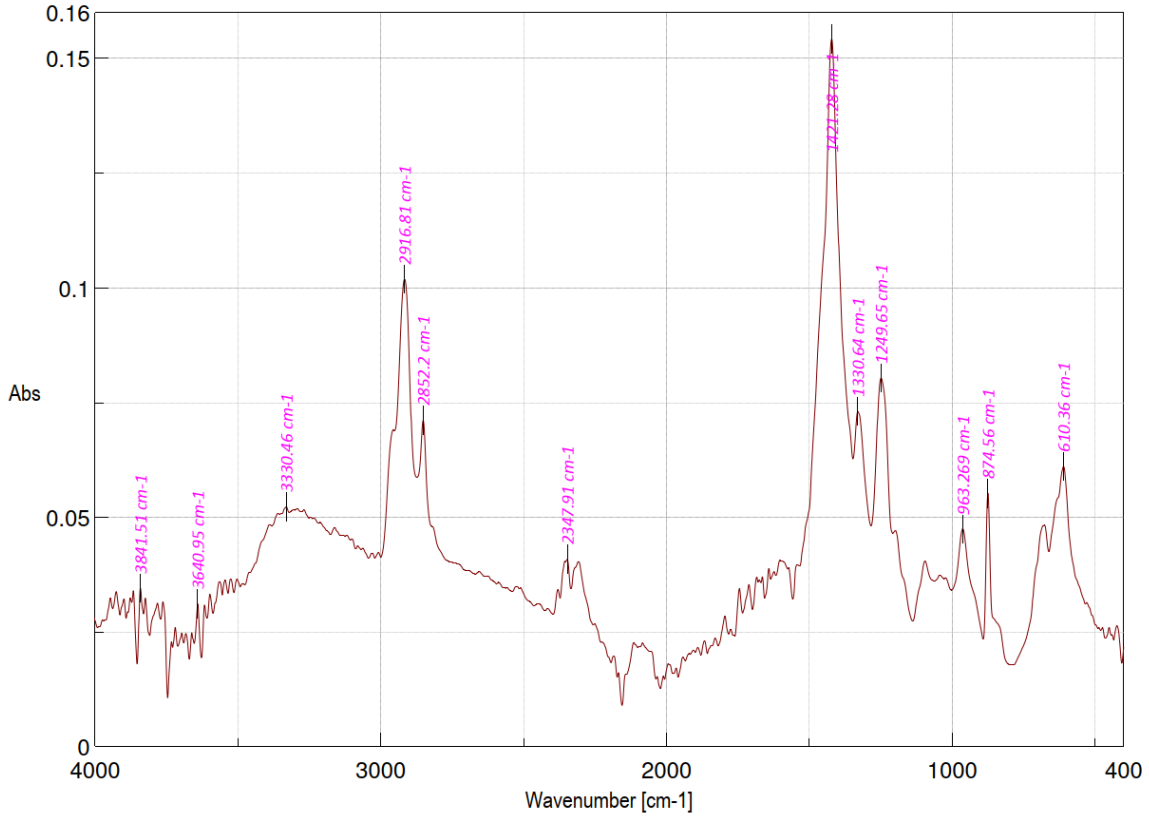

Fig. 4.128. Spectrum of a weld specimen produced at 270 °C for 21 s. Source: Author's own work

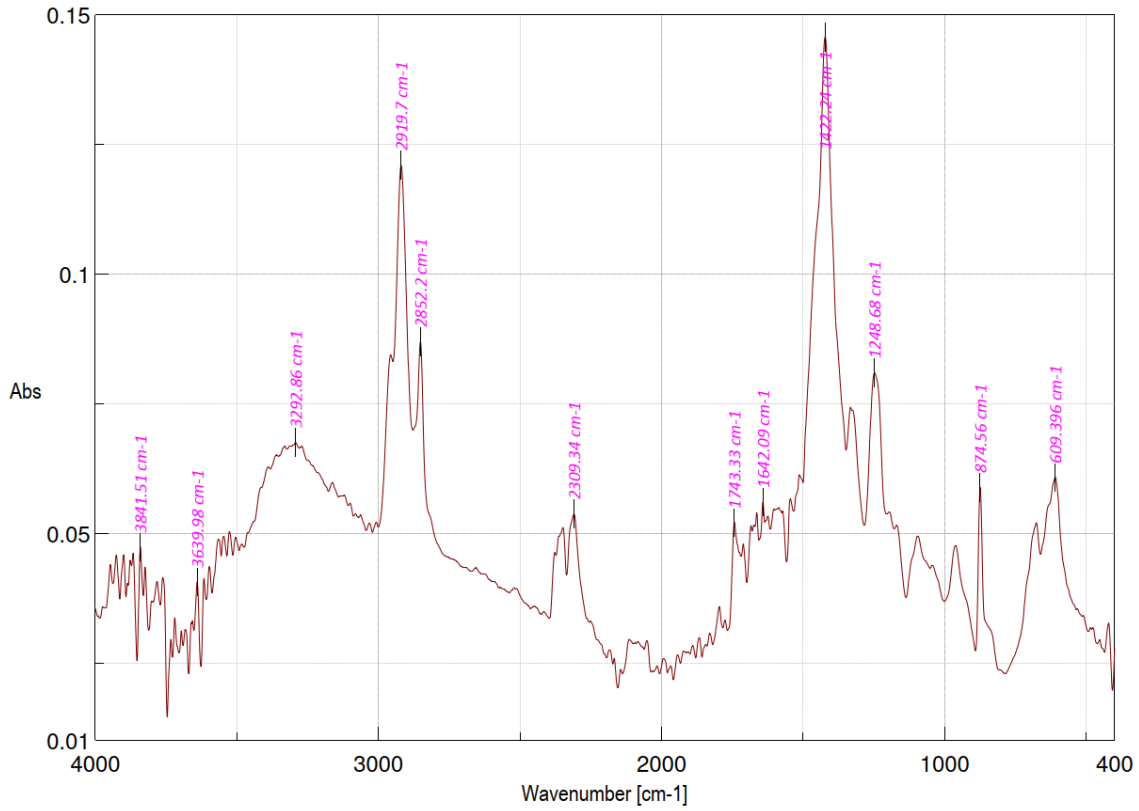

Fig. 4.129. Spectrum of a weld specimen produced at 263 °C for 22 s. Source: Author's own work

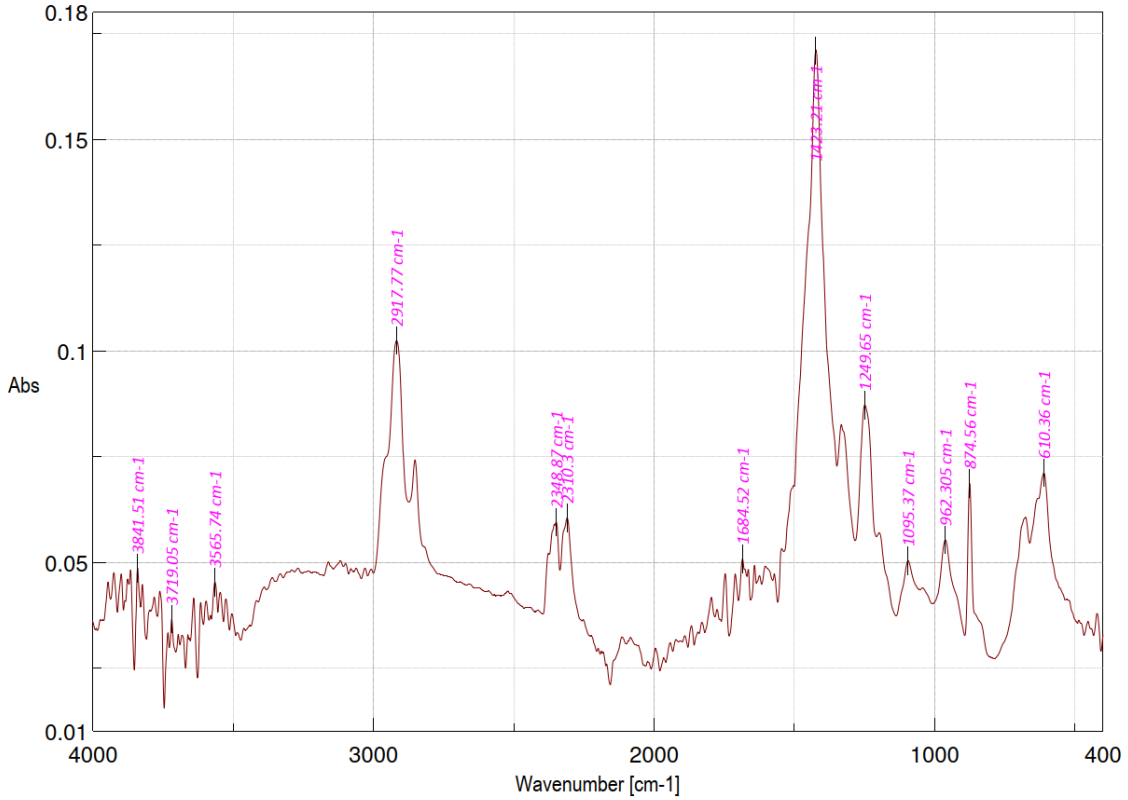

Fig. 4.130. Spectrum of a weld specimen produced at 256 °C for 30 s. Source: Author's own work

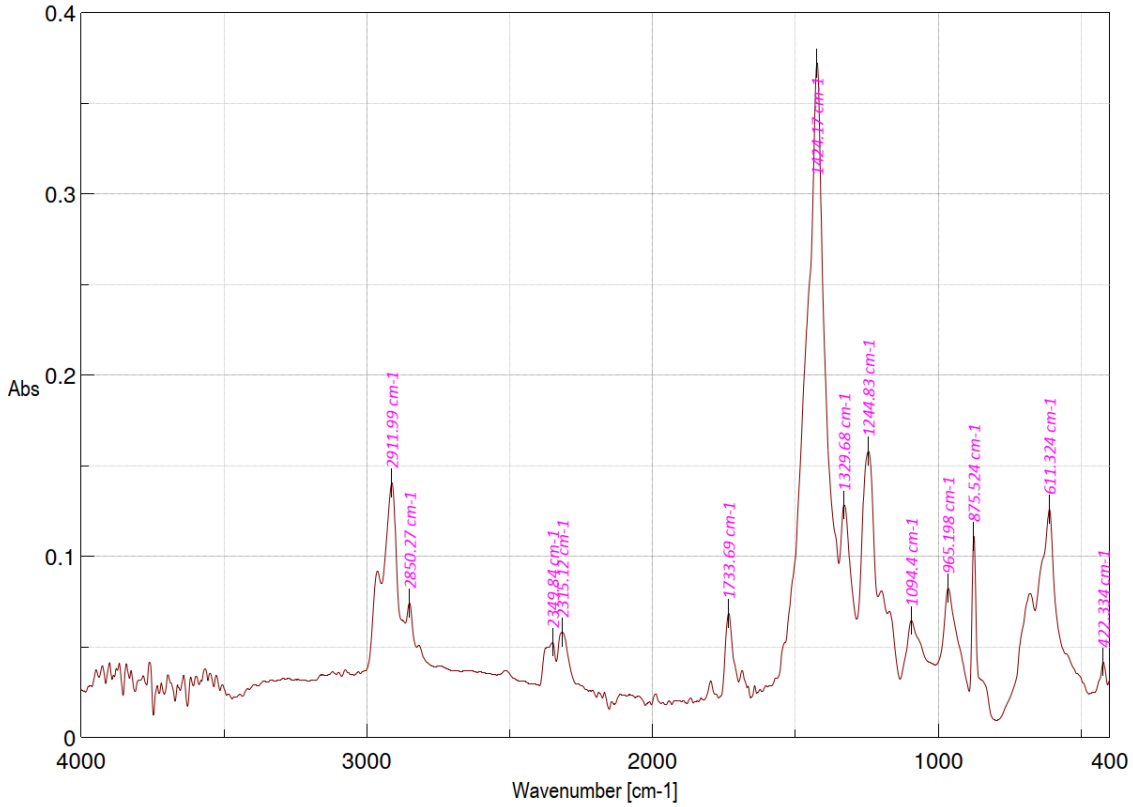

Fig. 4.131. Spectrum of a weld specimen produced at 264 °C for 30 s. Source: Author's own work

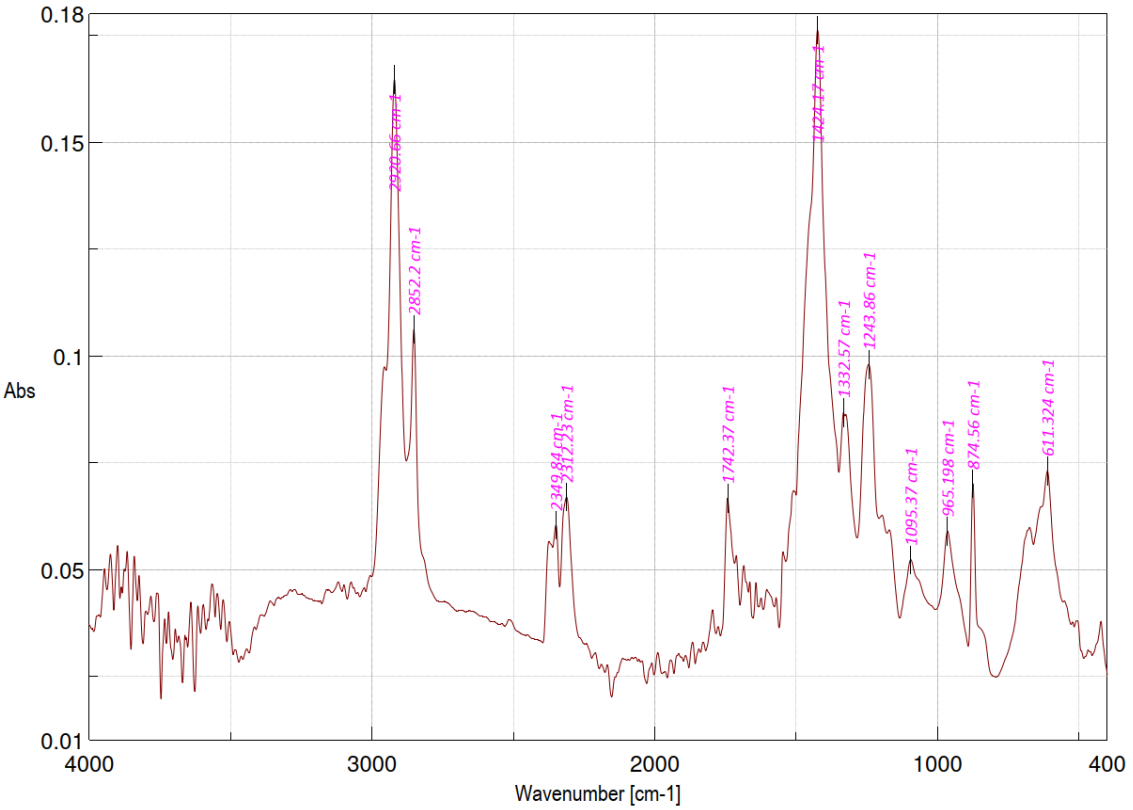

Fig. 4.132. Spectrum of a weld specimen produced at 264 °C for 22 s. Source: Author's own work

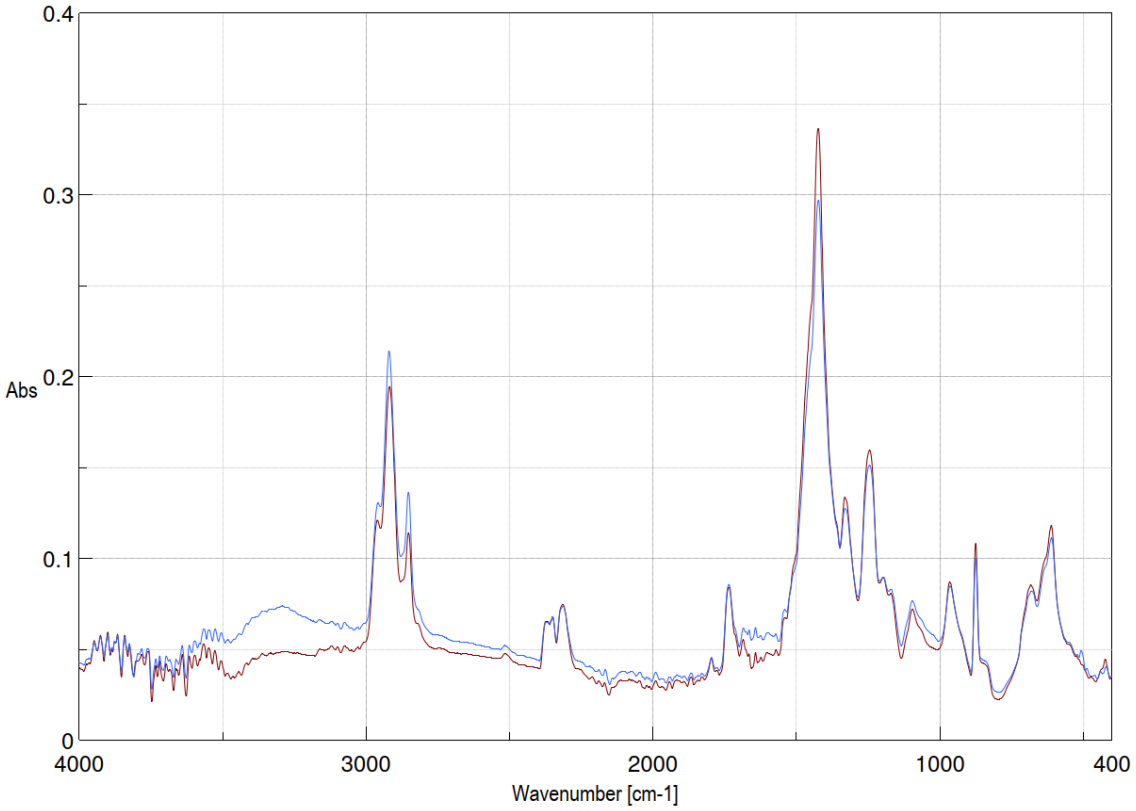

Fig. 4.133. Comparison of FTIR-ATR spectra of weld specimens produced at 264 °C for 22 s and 264 °C for 30 s over the range 4000–400 cm^{-1}. Source: Author's own work

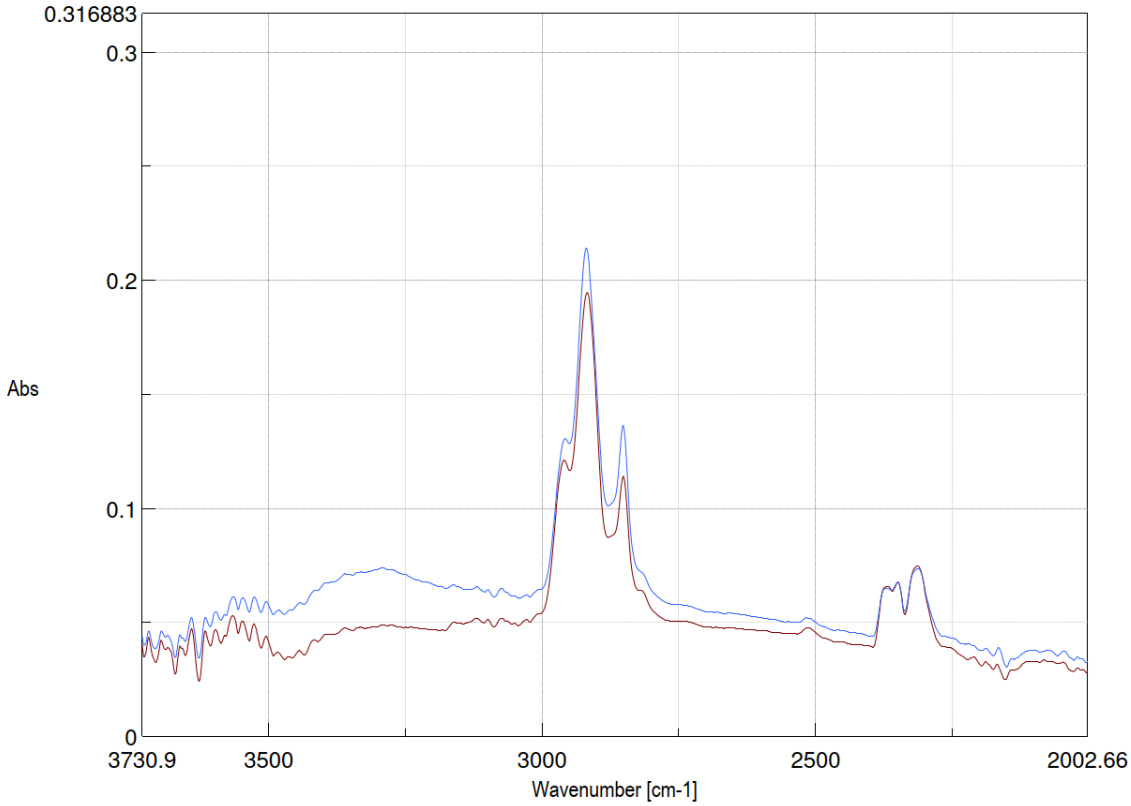

Fig. 4.134. Comparison of FTIR-ATR spectra of weld specimens produced at 264 °C for 22 s and 264 °C for 30 s over the range 3731–2001 cm^{-1}. Source: Author's own work

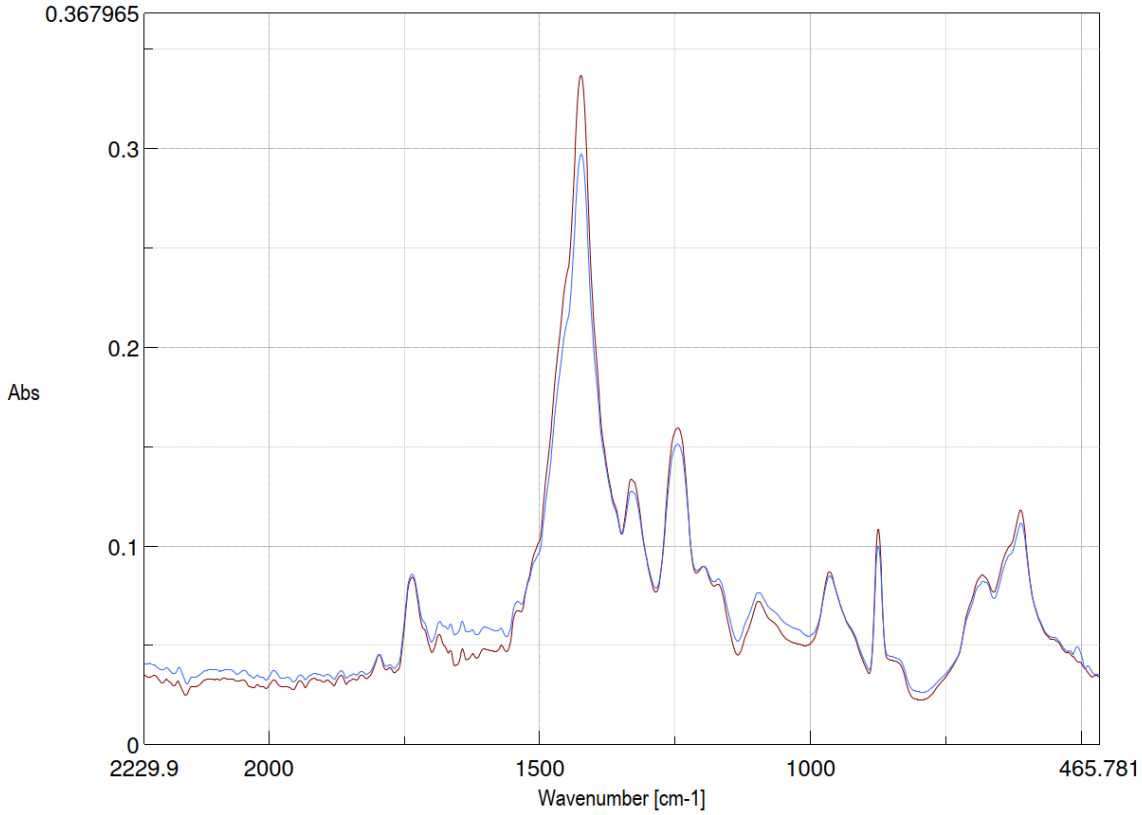

Fig. 4.135. Comparison of FTIR-ATR spectra of weld specimens produced at 264 °C for 22 s and 264 °C for 30 s over the range 2230–464 cm^{-1}. Source: Author's own work

Table 50 presents the main diagnostic FTIR-ATR bands identified for the parent PVC-U profile material and for the analysed weld variants produced under different welding conditions. The comparison focuses on the C–H stretching region, the carbonyl band, and the fingerprint region, which together provide the basis for assessing whether the welding parameters induced detectable changes in the chemical character of the weld material.

Table 50. Main diagnostic FTIR-ATR bands of parent PVC-U and analysed weld variants. Source: Author's own work

Weld condition	C-H stretching bands [cm^{-1}]	C=O band [cm^{-1}]	Main fingerprint [cm^{-1}]
Parent PVC-U profile material	2916.81-2919.70; 2850.27-2851.24	1729.83-1741.41	1420.32-1421.28; 1329-1331; 1245-1249; 1095-1096; 961-964; 874.6; 683-686; 609-611
270 °C / 21 s	2916.81; 2852.20	not labelled in the spectrum	1472.28; 1330.64; 1249.65; 963.27; 874.56; 610.36
263 °C / 22 s	2919.70; 2852.20	1743.33	1422.24; 1248.68; 874.56; 609.40
256 °C / 30 s	2917.77	1684.52	1423.21; 1249.65; 1095.37; 962.31; 874.56; 610.36
264 °C / 30 s	2911.99; 2850.27	1733.69	1424.17; 1329.68; 1244.83; 1094.40;

			965.20; 875.52; 611.32
264 °C / 22 s	2920.66; 2852.20	1742.37	1424.17; 1332.57; 1243.86; 1095.37; 965.20; 874.56; 611.32

The FTIR-ATR comparison confirms that the parent PVC-U profile and all analysed weld variants retain the same principal PVC-related spectral signature. This is evidenced by the repeated occurrence of C–H stretching bands and the characteristic fingerprint-region bands, particularly those near 1420–1424 cm^{-1}, 874–875 cm^{-1}, and 609–611 cm^{-1}. The welds produced at 264 °C / 22 s and 264 °C / 30 s show a highly comparable set of diagnostic bands. The reduction of melting time from 30 s to 22 s at 264 °C therefore did not produce an FTIR-detectable change in the chemical character of the weld material. The remaining weld variants show only local differences in selected peak positions or in the presence of weaker bands. These differences do not indicate a change in the chemical type of the material, but rather remain consistent with minor spectral variability typical of FTIR-ATR measurements.

Figure 4.136 provides a synthetic overview of the investigated process window in the temperature–time domain, showing how the welding conditions were progressively modified towards process-time reduction, process-temperature reduction, and the final target parameter set.

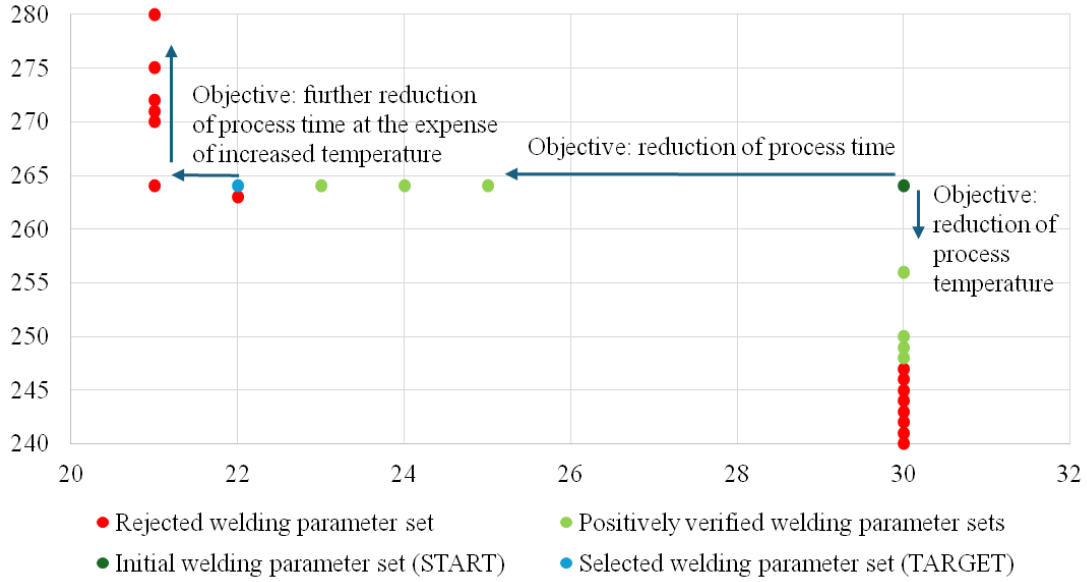

Fig. 4.136. Summary map of verified and rejected welding parameter sets. Source: Author's own work

Figure 4.136. presents a synthetic map of the investigated welding parameter sets in the melting time–welding temperature domain. The initial parameter set was defined by a welding temperature of 264 °C and a melting time of 30 s, after which the experimental programme followed three directions: process-time reduction, process-temperature reduction, and further process-time reduction compensated by an increase in temperature. The positively verified variants were concentrated mainly within the range of 248–264 °C and 22–30 s, with 264 °C and 22 s selected as the target parameter set. Rejected variants occurred both at excessively low temperature and at melting times shorter than 22 s, particularly when the shortened cycle was compensated by higher welding temperature. This indicates that further displacement of

the parameters beyond the defined process window led to a loss of technological stability or deterioration in weld quality.

Against the background of the available literature, the principal significance of the results obtained in this work lies in demonstrating that welding at 264 °C for 22 s does not induce significant chemical or microstructural changes relative to the 264 °C / 30 s variant. Previous studies on welded corners of PVC profiles have focused primarily on the relationship between process parameters and the strength or hardness of joints [17]. In the present work, this perspective was extended by a correlated physicochemical assessment comprising Rockwell hardness testing, microscopy, DSC, and FTIR-ATR. This made it possible to determine not only whether the joint satisfies mechanical requirements, but also whether material stability is preserved within the weld zone.

The material evidence begins with the hardness results, which provide a direct indication of the local mechanical condition of the weld zone. Across the welding-temperature interval from 256 °C to 264 °C, the mean hardness of the welds remained within approximately 65–75 N/mm², with no material differences between the investigated variants. Statistical analysis further confirmed the absence of a significant difference between welds produced at 264 °C with a melting time of 22 s and those produced at 264 °C with a melting time of 30 s. At the same time, weld hardness was lower than that of the parent PVC material, which was approximately 88 N/mm². This reduction is consistent with the formation of a locally plasticised and thermally affected joint zone rather than with degradation. A similar process-oriented interpretation is consistent with studies on welded PVC window-profile corners, where welding parameters, including temperature, were shown to govern joint-zone properties and to require a stable processing window for reproducible performance [17].

Microscopy provided the most direct verification of structural quality. Welds produced within the range of 256–264 °C exhibited a light-coloured weld bead with uneven and locally porous morphology, but no visible features indicative of PVC degradation. In contrast, welding at 270 °C with a melting time of 21 s produced a light-brown discoloration penetrating into the weld bead. This was accompanied by a lower mean hardness of approximately 62 N/mm² and an unequivocally adverse quality outcome. The observed discoloration is consistent with the established degradation pathway of PVC, in which dehydrochlorination is accompanied by HCl evolution and the formation of conjugated polyene sequences responsible for colour change [197], [198]. Consequently, the discoloration observed at 270 °C can be treated as a practical early indicator of degradation processes in the heat-affected region, especially because it coincided with deterioration in the mechanical response.

The DSC results further clarify the material state of the weld zone. Over the investigated temperature interval from 20 °C to 130 °C, the DSC traces were dominated by glass-transition-related effects, without melting or crystallisation peaks. This confirms that the analysed PVC weld material behaves predominantly as an amorphous polymer within this thermal window. Two main thermal response regimes were distinguished. A weak lower-temperature effect occurred at approximately 55–60 °C, mainly in the series welded at 264 °C for 22 s and 30 s, with small ΔCp values of approximately 0.003–0.018 J/g·K. The dominant glass-transition region occurred within approximately 80–95 °C and included the primary PVC response. Within this interval, components near 84–86 °C, 88–90 °C, and 92–95 °C were observed depending on the welding variant. These features should not be interpreted as separate independent Tg values. A more defensible interpretation is that they represent a

broad, heterogeneous glass-transition region containing domains of different segmental mobility. This interpretation is consistent with DSC studies of PVC-based systems, where the thermal response below 130 °C is governed primarily by the ΔCp step associated with Tg rather than by melting phenomena typical of crystalline polymers [122].

The comparison between welding variants shows that temperature and melting time affected the apparent organisation of the amorphous PVC phase in the weld zone. The variants produced at 264 °C for both 22 s and 30 s exhibited the most comparable DSC response. In both cases, a weak lower-temperature effect coexisted with a dominant Tg near 85–86 °C and weaker higher-temperature features between approximately 90 °C and 95 °C. The repeatability of the principal Tg near 85–86 °C and the comparable ΔCp range of approximately 0.19–0.33 J/g·K for the main transition indicate that reducing the melting time from 30 s to 22 s at 264 °C did not cause a qualitatively different reorganisation of the weld material. By contrast, welds produced at 263 °C / 22 s and 256 °C / 30 s exhibited transitions more tightly clustered within approximately 88–95 °C, while the lower-temperature effect was weak or absent. The 270 °C / 21 s variant showed a different response, with the main transition concentrated around 86–90 °C and an additional feature near 94 °C. These differences indicate that welding conditions modify the distribution of segmental mobility, although DSC alone does not permit unambiguous identification of additive type or quantitative determination of gelation degree. Literature on rigid PVC confirms that thermal and thermomechanical history may generate subtle features near Tg associated with relaxation, physical ageing, and processing-related structural reorganisation [195].

The FTIR-ATR results provide the strongest confirmation of chemical stability within the weld zone. Across the parent PVC-U profile specimens, the spectra showed close agreement, including a stable fingerprint set and bands consistent with the C–Cl region. Comparison with a reference PVC spectrum confirmed strong correspondence of the key fingerprint maxima, supporting the identification of PVC as the dominant matrix. For the composite reinforcement, the spectra indicated a polyester-type matrix, including a strong carbonyl C=O band in the region of approximately 1700–1730 cm^{-1} and a characteristic fingerprint pattern associated with C–O and skeletal vibrations. This confirmed that the investigated welded system comprised chemically distinct constituents.

For the welds, all parameter variants retained a common PVC-related spectral core. The most important comparison concerned the 264 °C / 22 s and 264 °C / 30 s variants. In these spectra, the same diagnostic fingerprint bands were retained, with no emergence of new bands and no disappearance of bands decisive for the PVC matrix. The bands associated with C–H stretching, the fingerprint region, and the C–Cl-related range remained consistent with the expected spectral pattern of rigid PVC [199], [200]. Minor peak shifts or intensity differences should be interpreted cautiously, since ATR measurements are sensitive to sample–crystal contact, surface roughness, local topography, and effective penetration depth rather than only to chemical composition [200], [196]. On this basis, the FTIR-ATR evidence supports the conclusion that reducing the melting time from 30 s to 22 s at 264 °C did not produce a detectable chemical transformation of the weld material.

Taken together, the convergence of hardness testing, microscopy, DSC, and FTIR-ATR demonstrates that the 264 °C / 22 s variant provides weld-zone material quality comparable to the 264 °C / 30 s condition, while reducing thermal exposure. The novelty of the present work therefore does not lie merely in showing that welding temperature and melting time affect joint quality. It lies in correlating this effect with the physicochemical state of the weld zone.

The literature contains studies on the strength of welded PVC corners [17] and studies explaining degradation mechanisms and thermal response in rigid PVC [197]–[201], [122], [195], [196]. In the present work, these two interpretative levels were combined. This made it possible to show that, for the PVC-U window-profile and glass-fibre composite-insert system, shortening the melting time from 30 s to 22 s at 264 °C is mechanically and technologically justified without detectable adverse material or microstructural changes in the weld zone. Conversely, increasing the temperature to 270 °C while shortening the melting time to 21 s constitutes a boundary condition that initiates degradation phenomena and should be regarded as technologically unacceptable for the investigated system.

5. Summary and Conclusions

Contemporary construction increasingly requires window joinery to satisfy mechanical, durability, energy-efficiency, and in-service performance criteria at the same time. In this context, the window frame should be regarded as a multi-material and multi-functional system whose performance is governed by the coherence between material behaviour, profile geometry, reinforcement strategy, and joining technology. The welded corner is a critical region of this system because it directly affects load-bearing capacity, dimensional stability, airtightness, and the repeatability of the final product.

The research problem addressed in this dissertation arose from the transition from conventional steel reinforcement towards composite inserts intended to reduce thermal bridging while preserving structural performance. This transition changes the technological character of the welded corner. The joint zone is no longer formed only within a homogeneous PVC-U profile, but becomes an interaction region between PVC-U and a glass-fibre-reinforced composite insert with markedly different thermomechanical behaviour.

The dissertation therefore aimed to identify the cause-and-effect relationships between welding parameters, joint strength, frame dimensional accuracy, weld morphology, and the physicochemical condition of the weld-zone material. The work also aimed to establish a practical process window for welding PVC-U profiles reinforced with glass-fibre composite inserts. This process window had to satisfy strength and dimensional requirements, preserve weld-zone integrity, avoid thermally driven degradation, and reduce process duration and energy demand.

Cognitive conclusions

Thermal testing confirmed that the technological incompatibility between PVC-U and the composite is particularly important under welding conditions. For PVC-U, the Vicat softening temperature was approximately 89–90 °C, while the HDT was approximately 73 °C. By contrast, the composite exhibited a much higher HDT of approximately 202 °C. This shows that PVC-U loses functional stiffness much earlier than the composite under load at elevated temperature. Consequently, welding must be controlled so that PVC-U is sufficiently plasticised, while excessive temperature increase is avoided because it promotes degradation of the PVC matrix.

The pilot trials demonstrated that weld quality is controlled by the coupled influence of insert milling depth, welding-head feed rate, melting time, and welding temperature. Failure load alone did not provide a sufficient basis for process acceptance. Some variants achieved high mean failure loads but failed to satisfy dimensional tolerance, weld symmetry, or weld-bead quality criteria. This confirmed that weld assessment must be multi-criteria rather than strength-based only.

The welding-head feed rate was found to have a direct influence on joint formation. Within the investigated range, 0.25 mm/s provided the most favourable balance between load capacity and process stability. For a milling depth of 1.0 mm, the mean failure load reached 3637 N at 0.25 mm/s, compared with 3157 N at 0.19 mm/s and 3033 N at 0.31 mm/s. This relationship indicates that excessive feed rate limits contact formation and consolidation, whereas excessively low feed rate may impair melt-flow conditions in the weld-bead region.

The melting-time study showed that, under fixed conditions of 264 °C, 0.25 mm/s, and 1.0 mm insert milling, the melting time could be reduced to 22 s without loss of weld quality. Melting times between 22 s and 25 s preserved dimensional tolerance within 1 mm and maintained weld symmetry. A further reduction to 21 s caused systematic dimensional deviations of about 2 mm and loss of symmetry, which indicates insufficient plasticisation and increased resistance to welding-head motion.

The results also showed that the shorter melting time of 22 s is conditional on proper insert preparation. At 22 s, only the 1.0 mm milling depth satisfied the complete set of strength and quality criteria. The 0.5 mm and unmilled variants produced unacceptable dimensional deviations, weld-symmetry defects, or individual failure loads below the expected level. This establishes a clear causal relationship between geometric preparation of the composite insert and the possibility of reducing melting time.

The study showed that at a melting time of 30 s, temperatures from 256 °C to 248 °C produced acceptable geometry and a white weld bead, whereas 247 °C was insufficient for stable and repeatable execution. At the shortened melting time of 22 s, 264 °C was identified as the minimum temperature compatible with stable process execution. At 263 °C, dimensional nonconformity, loss of weld symmetry, actuator overload, and isolated low failure loads were observed.

Increasing welding temperature did not provide a viable route for further shortening the melting time. Conditions in the range of 270–280 °C with a melting time of 21 s could produce high failure loads, but they also caused weld-bead yellowing and, in selected cases, process instability. Microscopic observations and colour changes in the weld zone indicated the onset of PVC degradation. This means that the process cannot be improved by compensating insufficient melting time through excessive temperature increase.

The main verification study confirmed that welding at 264 °C for 22 s, with a welding-head feed rate of 0.25 mm/s and a composite-insert milling depth of 1.0 mm, does not induce adverse material changes relative to welding at 264 °C for 30 s. Hardness measurements in the temperature range from 256 °C to 264 °C remained within approximately 65–75 N/mm², and no statistically meaningful difference was observed between the 264 °C / 22 s and 264 °C / 30 s variants. The lower hardness of the weld compared with parent PVC-U is consistent with local plasticisation and does not, by itself, indicate degradation.

Microscopic examination confirmed that welds produced between 256 °C and 264 °C did not exhibit structural features indicative of degradation. In contrast, welding at 270 °C for 21 s produced discolouration within the weld zone, interpreted as an indication of dehydrochlorination and the onset of PVC degradation. This result defines a technological safety boundary for the investigated system.

DSC analysis supported the conclusion that welding at 264 °C for 22 s did not produce a materially different thermal response from that obtained at 264 °C for 30 s. The observed differences in the glass-transition region and in minor secondary signals were subtle and are consistent with local residual stresses, additive heterogeneity, and thermomechanical history. They do not justify the conclusion that the optimised condition caused a distinct qualitative reorganisation of the PVC weld material.

FTIR-ATR analysis provided the strongest evidence for chemical stability in the weld zone. The spectra of welds produced at 264 °C / 22 s and 264 °C / 30 s showed the same diagnostic fingerprint bands, with no emergence of new bands and no disappearance of characteristic PVC bands. This confirms that reducing melting time from 30 s to 22 s at 264 °C did not produce an FTIR-detectable change in the chemical type of the weld material.

Taken together, the principal cognitive conclusion is that weld quality in PVC-U profiles reinforced with glass-fibre composite inserts is governed by a coupled process–material mechanism, rather than by failure load alone. Within this mechanism, welding temperature and melting time have a quantifiable effect on the mechanical response of the welded corner, as demonstrated by the very strong parameter–response associations obtained for the mean failure load. The correlation coefficient was 0.99 for the failure load–welding temperature dependence and 0.96 for the failure load–melting time dependence. The comparison between weld-zone Rockwell hardness and mean failure load further indicates a positive tendency, whereby higher hardness values are accompanied by a greater likelihood of achieving higher failure loads, although this effect should be interpreted as contributory rather than independently determinative. The decisive condition is therefore the balance between composite-insert preparation, PVC-U plasticisation, welding-head kinematics, thermal input, melt consolidation, weld-zone hardness, dimensional control, and resistance to thermally induced deterioration. Within this integrated mechanism, the 264 °C and 22 s condition represents a stable processing state in which cycle-time reduction is achieved without driving the weld zone towards material instability. This identifies the coherence between technological parameters, strength response, and the material state of the weld zone as the central cognitive outcome of the dissertation.

Methodological conclusions

This methodological framework enabled the integration of mechanical, dimensional, structural, thermal, and spectroscopic evidence within a single experimental approach. It addressed the criteria formulated in Chapter 3 by linking the mechanical response and dimensional accuracy of the welded frames with the thermal, structural, and spectroscopic signatures determined for both the constituent materials and the weld zone.

The staged experimental programme enabled individual process variables to be examined while preserving the system-level interpretation of the welded corner. Insert milling depth, welding-head feed rate, melting time, and welding temperature were varied in a controlled sequence. This supported the identification not only of favourable parameter values, but also of the reasons why specific variants did not meet the combined requirements of strength, dimensional accuracy, weld symmetry, and weld-zone material condition.

The results indicate that reliance on standard mechanical acceptance alone may be insufficient for evaluating welded corners in composite-reinforced PVC-U profiles. A parameter set may provide acceptable or even high failure loads while still producing unacceptable dimensional deviations, weld asymmetry, actuator overload, or visible thermal damage. The methodological implication is that weld quality is more appropriately assessed through an integrated criterion set than through failure load alone.

A comprehensive assessment procedure was developed by linking four evidence levels. The first level comprised corner failure-load testing and mechanical characterisation of the base materials. The second level comprised dimensional inspection and weld-symmetry

evaluation. The third level comprised hardness testing, microscopy, and DSC assessment of the weld zone. The fourth level comprised FTIR-ATR verification of chemical stability. The convergence of these four evidence levels provided a balanced basis for defining the process window while limiting the risk of overinterpretation.

The methodological design also made it possible to consider the practical relevance of the results. Process optimisation was not limited to laboratory-scale strength improvement. It was linked to cycle-time reduction, daily production output, and electricity-cost estimation. This connection between materials characterisation, technological acceptance, and production organisation supports the potential applicability of the findings in industrial implementation.

Taken together, the work produced a cross-correlated evidence base linking mechanical, dimensional, thermal, structural, and spectroscopic results. On this basis, a practical process window was delimited for insert milling depth, welding-head feed rate, welding temperature, and melting time. The study also yielded technologically implementable recommendations for industrial corner welding of PVC-U profiles reinforced with glass-fibre composite inserts.

Application and prognostic conclusions

The principal application result of the dissertation is the definition of an optimal process window for the investigated profile system. The recommended condition comprises a welding temperature of 264 °C, a melting time of 22 s, a welding-head feed rate of 0.25 mm/s, and a composite-insert milling depth of 1.0 mm. This parameter set satisfies corner load-bearing requirements, maintains dimensional accuracy, preserves weld symmetry, avoids FTIR-detectable chemical change, and shows no microscopic evidence of degradation.

The melting time of 22 s should be interpreted as valid only within this complete parameter regime. It should not be treated as an independent optimum transferable to lower or higher temperature conditions, different milling depths, or different feed rates. In particular, the results show that 22 s requires maintaining the welding temperature at 264 °C and milling the composite insert to 1.0 mm.

The optimisation has direct production significance. Reducing the melting time from 30 s to 22 s decreases the controllable melting-plus-joining sequence from 60 s to 52 s. This corresponds to an 8 s reduction and a time saving of more than 13% in the throughput-governing portion of the process.

Under the adopted working-time assumption of 27,900 s per day, the baseline 60 s cycle allows approximately 465 welds per day. The optimised 52 s cycle allows approximately 536 welds per day, which corresponds to an increase of more than 15%. This demonstrates that the identified parameter window is not only scientifically justified, but also operationally meaningful.

The electricity-cost analysis showed that energy expenditure is not the dominant optimisation driver under the adopted assumptions. With a maximum installed machine power of 18.5 kW, a daily working time of 7.75 h, and an electricity price of PLN 1,000 per MWh, daily energy consumption was estimated at approximately 143 kWh, corresponding to about PLN 143. If the electricity price doubled, the estimated daily cost would rise to approximately PLN 286. These values remain relatively low compared with the unit value of finished

frames. In practice, this means that production efficiency is governed mainly by cycle-time reduction, provided that the process remains within a safe technological window.

The results are directly applicable to industrial welding of the investigated six-chamber PVC-U profile reinforced with glass-fibre composite inserts. Their broader applicability is also plausible for similar PVC-U profile systems with composite reinforcement, provided that the material formulation, insert geometry, profile cross-section, and machine kinematics are comparable. However, direct transfer to other profiles, other reinforcement systems, or other welding machines should be preceded by verification using the same multi-criteria assessment logic.

The prognostic implication is that future process development should not focus exclusively on increasing temperature or maximising failure load. Further improvements should instead be based on maintaining an appropriate balance between thermal input, insert preparation, melt flow, weld consolidation, and material stability. Additional work should include long-term ageing, cyclic thermal loading, weathering exposure, fatigue-type response of welded corners, and validation on complete window assemblies.

The main contribution of the dissertation is therefore both scientific and utilitarian. Scientifically, it identifies the causal mechanisms and interdependencies governing weld formation in a PVC-U profile reinforced with a glass-fibre composite insert. Crucially, it demonstrates that the optimised welding regime preserves the material and microstructural integrity of the weld zone, with no evidence of adverse changes detectable by hardness testing, microscopy, DSC, or FTIR-ATR. Technologically, it defines a parameter window that is compatible with industrial implementation and delivers measurable gains in production efficiency without compromising the material stability of the welded joint.

References

[1] Polish Committee for Standardization (PKN), PN-EN 12519:2018-10, *Windows and doors—Terminology*. Warsaw, Poland: PKN, 2018.

[2] Polish Committee for Standardization (PKN), PN-EN 14351-1+A2:2016-10, *Windows and doors—Product standard, performance characteristics—Part 1: Windows and external pedestrian doorsets*. Warsaw, Poland: PKN, 2016.

[3] M. Tutton, E. Hirst, H. Louw, and J. Pearce, *Windows: History, Repair and Conservation*. London, U.K.: Routledge, 2015.

[4] T. Leslie, "Insulation with Vision: The Development of Insulated Glazing, 1930–1980," *APT Bulletin: The Journal of Preservation Technology*, vol. 49, no. 4, pp. 23–32, 2018. [Online]. Available: https://www.jstor.org/stable/26632385. [Accessed: Jan. 4, 2026].

[5] J. Šadauskienė et al., "Investigation of Thermal Bridges of a New High-Performance Window Installation Using 2-D and 3-D Methodology," *Buildings*, vol. 12, no. 5, Art. no. 572, 2022, doi: 10.3390/buildings12050572.

[6] F. Cappelletti, A. Gasparella, P. Romagnoni, and P. Baggio, "Analysis of the influence of installation thermal bridges on windows performance: The case of clay block walls," *Energy and Buildings*, vol. 43, no. 6, pp. 1435–1442, 2011, doi: 10.1016/j.enbuild.2011.02.004.

[7] S. Van Den Bergh, R. Hart, B. P. Jelle, and A. Gustavsen, "Window Spacers and Edge Seals in Insulating Glass Units: A State-of-the-Art Review and Future Perspectives," *Energy and Buildings*, vol. 58, pp. 263–280, 2013, doi: 10.1016/j.enbuild.2012.10.006.

[8] Z. Wang, L. Yao, Y. Shi, D. Zhao, and T. Chen, "Optimizing the Performance of Window Frames: A Comprehensive Review of Materials in China," *Applied Sciences*, vol. 14, no. 14, Art. no. 6091, 2024, doi: 10.3390/app14146091.

[9] A. Gustavsen, D. K. Arasteh, B. P. Jelle, D. C. Curcija, and C. Kohler, "Developing low-conductance window frames: Capabilities and limitations of current window heat transfer design tools," *Journal of Building Physics*, vol. 32, no. 2, pp. 131–153, 2008, doi: 10.1177/1744259108097672.

[10] A. P. Konstantinov and I. S. Aksenov, "Engineering method for calculating temperature deformations of PVC window profiles with a reinforcing steel core," *Buildings*, vol. 13, no. 6, Art. no. 1466, 2023, doi: 10.3390/buildings13061466.

[11] K. Minchenkov, S. Gusev, I. Sergeichev, and A. Safonov, "Improving the thermal performance of PVC windows with pultruded thermoplastic reinforcement," *Sci. Rep.*, vol. 15, Art. no. 1996, 2025, doi: 10.1038/s41598-025-86019-6.

[12] M. Kozielczyk, K. Mencel, J. Kowalczyk, and M. Paczkowska, "Analysis of the Strength and Quality Properties of Welded PVC Profiles with Glass Fiber Composite Reinforcement in the Context of Milling and Weld Head Feed," *Materials*, vol. 18, no. 6, Art. no. 1297, 2025, doi: 10.3390/ma18061297.

[13] M. Kozielczyk, K. Mencel, J. Kowalczyk, and M. Paczkowska, "Selection of Processing Methods and Parameters for Composite Inserts in Window Profiles with Regard to the Strength of Their Welds," *Materials*, vol. 18, no. 1, Art. no. 44, 2025, doi: 10.3390/ma18010044.

[14] M. Kozielczyk, J. Kowalczyk, and M. Paczkowska, "Analysis of the Effects of Weld Melt Duration on Joint Integrity and Surface Quality During Profile Milling," *Applied Sciences*, vol. 15, no. 20, Art. no. 11024, 2025, doi: 10.3390/app152011024.

[15] British Plastics Federation (BPF) Windows Group, "Guidelines for Welding of PVC-U Profiles for Windows and Doors," Publication 332/2, British Plastics Federation,

London, U.K., 2003. [Online]. Available: https://www.bpf.co.uk/windows/windows-standards.aspx. [Accessed: Dec. 30, 2025].
[16] M. Wygoda, M. Paprocki, and W. Adamczyk, "Influence of the Welding Process on the Quality of PVC Frames," *Manufacturing Technology*, vol. 22, pp. 356–366, 2022, doi: 10.21062/mft.2022.037.
[17] P. Postawa, T. Stachowiak, and A. Gnatowski, "Strength analysis of welded corners of PVC window profiles," *IOP Conf. Ser.: Mater. Sci. Eng.*, vol. 225, Art. no. 012003, 2017, doi: 10.1088/1757-899X/225/1/012003.
[18] Polish Committee for Standardization (PKN), PN-EN 514:2018-02, *Plastics—Poly(vinyl chloride) (PVC)-based profiles—Determination of the strength of welded corners and T-joints*. Warsaw, Poland: PKN, 2018.
[19] A. Macfarlane and G. Martin, "A World of Glass," *Science*, vol. 305, no. 5689, pp. 1407–1408, 2004, doi: 10.1126/science.1093597.
[20] N. Van Den Bossche, A. Janssens, and J. Moens, "Pressure equalisation as design strategy for watertight windows," in *Proc. 8th Symp. Building Physics in the Nordic Countries (NSB 2008)*, 2008 (presentation; Zenodo record published Jun. 15, 2008), doi: 10.4122/1.1000000894.
[21] H. J. Gläser, "History of the development and industrial production of low thermal emissivity coatings for high heat insulating glass units," *Applied Optics*, vol. 47, no. 13, pp. C193–C199, 2008, doi: 10.1364/AO.47.00C193.
[22] S. Van Linden and N. Van Den Bossche, "Airtightness of sealed building joints: Comparison of performance before and after artificial ageing," *Building and Environment*, vol. 180, Art. no. 107010, 2020, doi: 10.1016/j.buildenv.2020.107010.
[23] S. C. Park, "The Repair and Thermal Upgrading of Historic Steel Windows," *Preservation Briefs*, no. 13, U.S. Department of the Interior, National Park Service, Heritage Preservation Services, Washington, DC, USA, 1984. [Online]. Available: https://www.nps.gov/orgs/1739/upload/preservation-brief-13-steel-windows.pdf. [Accessed: Dec. 26, 2025].
[24] S. H. Dyvik, B. Manum, J. H. Mork, and M. Luczkowski, "Structural aluminium in architecture – the history and future of aluminium as a structural material," in *Structures and Architecture: Bridging the Gap and Crossing Borders (Proc. ICSA 2019)*, P. J. S. Cruz, Ed. Boca Raton, FL, USA: CRC Press, 2019, pp. 843–844, doi: 10.1201/9781315229126-100.
[25] British Plastics Federation (BPF) Windows Group, "BPF Windows Group Factsheet 1: Environmental Matters," *BPF*. [Online]. Available: https://www.bpf.co.uk/Media/Download.aspx?MediaId=1816. [Accessed: Dec. 26, 2025].
[26] J. Baetens, B. P. Jelle, and A. Gustavsen, "Properties, requirements and possibilities of smart windows for dynamic daylight and solar energy control in buildings: A state-of-the-art review," *Solar Energy Materials & Solar Cells*, vol. 94, no. 2, pp. 87–105, 2010, doi: 10.1016/j.solmat.2009.08.021.
[27] M. L. F. Nascimento, "Brief history of the flat glass patent—Sixty years of the float process," *World Patent Information*, vol. 38, pp. 50–56, 2014, doi: 10.1016/j.wpi.2014.04.006.
[28] A. Barker, "A Window of Opportunity: A third, and domestically focused, Modern Movement in South Africa," *Docomomo Journal*, no. 73, pp. 16–24, 2025, doi: 10.52200/docomomo.73.02.
[29] N. Van Den Bossche, L. Buffel, and A. Janssens, "Thermal Optimization of Window Frames," *Energy Procedia*, vol. 78, pp. 2500–2505, 2015, doi: 10.1016/j.egypro.2015.11.251.

[30] N. Simões, S. A. Moghaddam, and M. G. da Silva, “Review of the Experimental Methods for Evaluation of Windows’ Thermal Transmittance: From Standardized Tests to New Possibilities,” *Buildings*, vol. 13, no. 3, Art. no. 703, 2023, doi: 10.3390/buildings13030703.
[31] S. Gardi, L. Giannone, G. Sarti, and G. Sarti, “Surface Chalking upon Weathering of Dark-Colored PVC Articles and Relevant Stabilizers,” *Polymers*, vol. 16, no. 8, Art. no. 1047, 2024, doi: 10.3390/polym16081047.
[32] O. Ait Khouya, E. H. Sebbar, L. Elfarissi, and N. Laaroussi, “Mechanical performance of recycled PVC window frames: An experimental and numerical investigation,” *Hybrid Advances*, vol. 9, Art. no. 100415, 2025, doi: 10.1016/j.hybadv.2025.100415.
[33] Aluplast, “IDEAL 7000® 85mm Bautiefe,” *Aluplast*. [Online]. Available: https://www.aluplast.net/de/produkte/fenster/ideal/ideal-7000/. [Accessed: Dec. 26, 2025].
[34] VEKA, “SOFTLINE 82 MD Kunststoffprofile für Fenster,” *VEKA*. [Online]. Available: https://www.veka.de/bauherren/produkte/fenster/softline-82-md/. [Accessed: Dec. 26, 2025].
[35] Deceuninck, “Elegant ThermoFibra Infinity,” *Deceuninck*. [Online]. Available: https://www.deceuninck.be/nl-be/pvc-ramen-en-deuren/elegant-thermofibra-infinity.html. [Accessed: Dec. 26, 2025].
[36] REHAU, “ARTEVO – Fiktion wird Realität.,” *REHAU*. [Online]. Available: https://window.rehau.com/de-de/geschaeftskunden/fenster/artevo. [Accessed: Dec. 26, 2025].
[37] REHAU, “SYNEGO Fenster – Wohlfühlen beginnt mit Wärme,” *REHAU*. [Online]. Available: https://window.rehau.com/de-de/fenster-tueren/rehau-fenster/synego-fenster. [Accessed: Dec. 26, 2025].
[38] A. Witek and B. Pietruszka, “Estimating thermal transmittance of the aluminium window profiles in practice,” *E3S Web of Conferences*, vol. 172, Art. no. 24003, 2020, doi: 10.1051/e3sconf/202017224003.
[39] D. Rusin, J. Juraszek, and P. Woźniczka, “Experimental Determination of the Equivalent Moment of Inertia and Stresses of Aluminium Profiles with Thermal Breaks,” *Materials*, vol. 18, no. 1, Art. no. 23, 2025, doi: 10.3390/ma18010023.
[40] F. Yang et al., “Research on the Factors Influencing Broken-Bridge Aluminum Exterior Windows with the Goal of Thermal Performance Improvement,” *Buildings*, vol. 15, no. 12, Art. no. 2101, 2025, doi: 10.3390/buildings15122101.
[41] V. Jirouš-Rajković and J. Miklečić, “Enhancing Weathering Resistance of Wood—A Review,” *Polymers*, vol. 13, no. 12, Art. no. 1980, 2021, doi: 10.3390/polym13121980.
[42] J. H. Oh, H. J. Yoo, and S. S. Kim, “Evaluation of Strategies to Improve the Thermal Performance of Steel Frames in Curtain Wall Systems,” *Energies*, vol. 9, no. 12, Art. no. 1055, 2016, doi: 10.3390/en9121055.
[43] Paris Promeneurs, “Le nouveau siège du groupe Le Monde,” Paris Promeneurs. [Online]. Available: https://paris-promeneurs.com/le-nouveau-siege-du-groupe-le/. [Accessed: Jan. 2, 2026].
[44] R.-A. Pescaru, L. Dumitrescu, I. Baran, and I. Bliuc, “Methods of Assessing the Thermal Performance of Curtain Wall Facades. Specific Energy Audit Problems,” *Bulletin of the Polytechnic Institute of Iași. Construction. Architecture Section*, vol. 68(72), no. 3, pp. 65–80, 2022, doi: 10.2478/bipca-2022-0021.
[45] M. S. Castillo, X. Liu, F. Abd-AlHamid, K. Connelly, and Y. Wu, “Intelligent windows for electricity generation: A technologies review,” *Building Simulation*, vol. 15, no. 10, pp. 1747–1773, 2022, doi: 10.1007/s12273-022-0895-y.

[46] W. Szlezinger and Z. K. Brzozowski, *Tworzywa sztuczne: Chemia, technologia wytwarzania, właściwości, przetwórstwo, zastosowanie*. Krakow, Poland: Wydawnictwo Oświatowe FOSZE, 2012.
[47] Polish Committee for Standardization (PKN), PN-EN ISO 14025:2010, *Environmental labels and declarations—Type III environmental declarations—Principles and procedures*. Warsaw, Poland: PKN, 2010.
[48] A. Gustavsen, S. Grynning, D. K. Arasteh, B. P. Jelle, and H. Goudey, "Key elements of and materials performance targets for highly insulating window frames," *Energy and Buildings*, vol. 43, no. 10, pp. 2583–2594, 2011, doi: 10.1016/j.enbuild.2011.05.010.
[49] Polish Committee for Standardization (PKN), PN-EN 12150-1+A1:2019-06E, *Glass in building—Thermally toughened soda lime silicate safety glass—Part 1: Definition and description*. Warsaw, Poland: PKN, 2019.
[50] Polish Committee for Standardization (PKN), PN-EN 14449:2008, *Glass in building—Laminated glass and laminated safety glass—Evaluation of conformity/product standard*. Warsaw, Poland: PKN, 2008.
[51] M. Ginic-Markovic, N. Roy Choudhury, M. Dimopoulos, and J. G. Matisons, "Weatherability of coated EPDM rubber compound by controlled UV irradiation," *Polymer Degradation and Stability*, vol. 69, no. 2, pp. 157–168, 2000, doi: 10.1016/S0141-3910(00)00053-7.
[52] H. Morawietz, *Polymers: The Origins and Growth of a Science*. New York, NY, USA: Wiley-Interscience, 1985.
[53] R. B. Seymour and T. Cheng, Eds., *History of Polyolefins*. Dordrecht, Netherlands: Reidel Publisher, 1985.
[54] R. W. Tess and G. W. Pochlein, Eds., *Applied Polymer Science*, 2nd ed. Washington, DC, USA: American Chemical Society, 1985.
[55] E. Elliott, *Polymers and People: An Informal History*. Philadelphia, PA, USA: Philadelphia Center for the History of Chemistry, 1986.
[56] P. J. T. Morris, *Polymer Pioneers: A Popular History of the Science and Technology of Large Molecules*. Philadelphia, PA, USA: Philadelphia Center for the History of Chemistry, 1986.
[57] R. B. Seymour and G. S. Kirschenbaum, Eds., *High Performance Polymers: Their Origin and Development*. New York, NY, USA: Elsevier, 1986.
[58] R. B. Seymour and R. D. Deanin, Eds., *History of Composites*. Utrecht, Netherlands: VNU Science, 1987.
[59] *Organic Coatings: Their Origin and Development*. Amsterdam, Netherlands: Elsevier, 1989.
[60] S. T. I. Mossman and P. J. T. Morris, Eds., *The Development of Plastics*. Boca Raton, FL, USA: CRC Press, 1994.
[61] R. E. Hummel, *Understanding Materials Science: History, Properties, Applications*. New York, NY, USA: Springer, 1998.
[62] "Historical development," in *Polymer Science and Technology*, R. O. Ebewele, Ed. Boca Raton, FL, USA: CRC Press, 2000, pt. 1, p. 1.
[63] V. Percec, Ed., *Hierarchical Macromolecular Structures: 60 Years after the Staudinger Nobel Prize I*. Cham, Switzerland: Springer, 2013, doi: 10.1007/978-3-319-01137-0.
[64] A. Duda and R. Szymański, "Konformacja i konfiguracja makrocząsteczek," in *Fizyka materiałów polimerowych: Makrocząsteczki i ich układy*. Warsaw, Poland: WNT, 2008.

[65] J. F. Rabek, *Współczesna wiedza o polimerach. Budowa strukturalna polimerów i metody badawcze*, vol. 1, 1st ed. Warsaw, Poland: PWN, 2017.
[66] R. J. Andrews and E. A. Grulke, "Glass transition temperatures of polymers," in *Polymer Handbook*, 4th ed., J. Brandrup, E. H. Immergut, and E. A. Grulke, Eds. New York, NY, USA: Wiley, 1999, pt. VI, p. 193.
[67] W. Przygodzki and A. Włochowicz, "Stan szklisty," in *Fizyka polimerów*. Warsaw, Poland: PWN, 2001, ch. 6, p. 158.
[68] J. F. Rabek, *Współczesna wiedza o polimerach*. Warsaw, Poland: PWN, 2008.
[69] F. A. Bovey, *Polymer Conformation and Configuration*. New York, NY, USA: Academic Press, 1968.
[70] I. Pasquon, U. Porri, and U. Fiannini, "Stereoregular linear polymers," in *Encyclopedia of Polymer Science and Engineering*, 2nd ed., vol. 15, H. F. Mark, N. M. Bikales, C. G. Overberger, and G. Menges, Eds. New York, NY, USA: Wiley, 1989, p. 632.
[71] L. W. Jelinski, Ed., *Chain Structure and Conformations of Macromolecules*. New York, NY, USA: Academic Press, 1982.
[72] W. Kuran, "Stereoisomerism of α-olefin polymers," in *Procesy polimeryzacji koordynacyjnej*. Warsaw, Poland: Oficyna Wydawnicza Politechniki Warszawskiej, 2000, sec. 3.1, p. 18.
[73] T. Kitayama, "Tacticity," in *Macromolecular Engineering: Precise Synthesis, Materials Properties, Application*, vol. 2, K. Matyjaszewski, Y. Gnanou, and L. Leibler, Eds. Weinheim, Germany: Wiley-VCH, 2007, ch. 1, p. 731.
[74] F. J. Rabek, *Polimery i ich zastosowanie interdyscyplinarne*, vol. 1. Warsaw, Poland: PWN, 2020.
[75] M. Kryszewski and S. Penczek, "Ogólna charakterystyka makrocząsteczek," in *Chemia polimerów*, vol. 1, Z. Florjańczyk and S. Penczek, Eds. Warsaw, Poland: Oficyna Wydawnicza Politechniki Warszawskiej, 2001, ch. 1, p. 11.
[76] J. F. Rabek, *Polimery: Otrzymywanie, metody badawcze, zastosowanie*. Warsaw, Poland: PWN, 2013.
[77] R. N. Haward and R. J. Young, Eds., *The Physics of Glassy Polymers*, 2nd ed. London, U.K.: Chapman & Hall, 1997.
[78] J.-P. Pascault, H. Sautereau, J. Verdu, and R. J. J. Williams, "Glass transition and transformation diagrams," in *Thermosetting Polymers*. New York, NY, USA: Marcel Dekker, 2002, ch. 4, p. 119.
[79] M. Obłój-Muzaj, B. Świerz-Motysia, and B. Szabłowska, *Polichlorek winylu*. Warsaw, Poland: Wydawnictwa Naukowo-Techniczne (WNT), 2016.
[80] *Słownik wyrazów obcych PWN*. Warsaw, Poland: Państwowe Wydawnictwo Naukowe (PWN), 1978.
[81] A. Schellenberg, Ed., *Mała encyklopedia polimerów*, 1st ed. Warsaw, Poland: WNT, 1976.
[82] R. F. T. Stepto, "IUPAC polymer terminology and macromolecular nomenclature," in *Macromolecular Engineering: Precise Synthesis, Material Properties, Application*, vol. 4, K. Matyjaszewski, Y. Gnanou, and L. Leibler, Eds. Weinheim, Germany: Wiley-VCH, 2007, p. 2743.
[83] "PVC," *Wielki Słownik Języka Polskiego (WSJP)*. [Online]. Available: https://wsjp.pl/haslo/podglad/4754/pvc. [Accessed: Jan. 2026].
[84] Z. Florjańczyk and S. Penczek, Eds., *Chemia polimerów*, vols. 1–2. Warsaw, Poland: Oficyna Wydawnicza Politechniki Warszawskiej, vol. 1, 2001 (ISBN 83-7207-265-5); vol. 2, 1977 (ISBN 83-87012-67-X).

[85] Polish Committee for Standardization (PKN), PN-EN 12608-1+A1:2021-02, *Unplasticized poly(vinyl chloride) (PVC-U) profiles for the production of windows and doors—Classification, requirements and test methods—Part 1: Uncoated PVC-U profiles with light-colored surfaces*. Warsaw, Poland: PKN, 2021.
[86] Tworzywa.pl, "Polichlorek winylu miękki (PVC-P)," *Tworzywa.pl*. [Online]. Available: https://www.tworzywa.pl/wiedzopedia/baza-tworzyw/176,polichlorek-winylu-miekki-pvc-p,polimer.html. [Accessed: Jan. 2026].
[87] W. A. Jenkins and R. Osborn, *Plastic Films: Technology and Packaging Applications*. Boca Raton, FL, USA: CRC Press, 1992.
[88] D. Kaplan, *Biodegradable Polymers and Packaging*. Boca Raton, FL, USA: CRC Press, 1993.
[89] S. Selke, J. Culter, and R. Hernandez, *Plastic Packaging: Properties, Processing, Applications and Regulations*. Munich, Germany: Hanser Verlag, 2004.
[90] A. Emblem and H. Emblem, Eds., *Packaging Technology: Fundamentals, Materials and Processes*. Cambridge, U.K.: Woodhead Publishing, 2012.
[91] S. Patrick, *Book Guide to PVC*. Shawbury, U.K.: Smithers Rapra Technology, 2005.
[92] W. V. Titov, *PVC Technology*. Berlin, Germany: Springer, 2012.
[93] M. Shiller, *PVC Additives: Performance, Chemistry, Developments and Sustainability*. Munich, Germany: Hanser, 2015.
[94] L. I. Nass, Ed., *Encyclopedia of PVC: Resin, Manufacture and Properties*, 2nd ed., vols. 1–4. New York, NY, USA: Marcel Dekker, 1988.
[95] A. Stolarzewicz, *Metody syntezy polimerów i ich charakterystyka*. Gliwice, Poland: Wydawnictwo Uniwersytetu Śląskiego, 2003.
[96] H. L. Kricheldorf, O. Nuyken, and G. Swift, *Handbook of Polymer Synthesis*. Boca Raton, FL, USA: CRC Press, 2004.
[97] J. Pielichowski and A. Puszyński, *Chemia polimerów*. Krakow, Poland: TEZA, 2004.
[98] J. Pielichowski and A. Puszyński, *Preparatyka polimerów*. Krakow, Poland: TEZA, 2005.
[99] A. A. Schlüter, C. Hawker, and J. Sakamoto, Eds., *Synthesis of Polymers*. Weinheim, Germany: Wiley-VCH, 2012.
[100] Central Institute for Labour Protection – National Research Institute (CIOP-PIB), "Chloroethene (Chloroeten), CAS 75-01-4," *Hazardous Chemical Substances Database (CHEMPYŁ)*. [Online]. Available: https://www.ciop.pl/CIOPPortalWAR/appmanager/ciop/pl?_nfpb=true&_pageLabel=P27600224401410431343241&id_czynn_chem=105. [Accessed: Apr. 2025].
[101] C. A. Collins, C. A. Daniels, and D. E. Witenhafer, "Physical constants of poly(vinyl chloride)," in *Polymer Handbook*, 4th ed., J. Brandrup, E. H. Immergut, and E. A. Grulke, Eds. New York, NY, USA: Wiley, 1999, p. V/67.
[102] K. J. Saunders, "Poly(vinyl chloride) and related polymers," in *Organic Polymer Chemistry*. Berlin, Germany: Springer, 2018, p. 90.
[103] J. F. Rabek, *Współczesna wiedza o polimerach. Polimery naturalne i syntetyczne, otrzymywanie i zastosowania*, vol. 2, 1st ed. Warsaw, Poland: PWN, 2017.
[104] H. A. Sarvetnick, *Polyvinyl Chloride*. New York, NY, USA: Reinhold Book Corporation, 1969.
[105] R. H. Burgess, Ed., *Manufacture and Processing of PVC*. London, U.K., and New York, NY, USA: Elsevier Applied Science Publishers, 1986.
[106] H. Henson and A. Whelan, Eds., *Developments in PVC Technology*. London, U.K., and New York, NY, USA: Applied Science Publishers Ltd., 1973.
[107] L. I. Nass, *Encyclopedia of PVC*. New York, NY, USA: Marcel Dekker, 1976.

[108] G. Becker, D. Braun, and H. K. Felger, Eds., *Kunststoff-Handbuch: Polyvinylchlorid*. Munich, Germany, and Vienna, Austria: Carl Hanser Verlag, 1986.
[109] M. J. Bunten and N. M. Bikales, *Encyclopedia of Polymer Science and Engineering*, vol. 17. New York, NY, USA: John Wiley & Sons, 1985.
[110] A. Dobraczyński and J. Pochwalski, *Technologia przetwórstwa tłoczyw termoutwardzalnych*. Warsaw, Poland: PWT, 1954.
[111] M. Irzyk, *Nowoczesne metody przetwórstwa tworzyw sztucznych*. Warsaw, Poland: WNT, 1961.
[112] Z. Tadmor and C. G. Gogos, *Principles of Polymer Processing*, 2nd ed. New York, NY, USA: Wiley, 2006.
[113] C. A. Harper, *Handbook of Plastic Technologies: The Complete Guide to Properties and Performance*. New York, NY, USA: McGraw-Hill, 2006.
[114] H. Saechtling, *International Plastics Handbook*, 2nd ed. Munich, Germany; Vienna, Austria; and New York, NY, USA: Hanser, 1987.
[115] E. Turska and M. Obłój-Muzaj, "The influence of selected organic compounds on changes in the polymer thermal stability during suspension polymerization of vinyl chloride," *Acta Polym.*, vol. 32, no. 6, pp. 295–299, 1981, doi: 10.1002/actp.1981.010320602.
[116] R. Tregan and A. Bonnemayre, *Plastiques Modernes et Elastomères*, vol. 23, pp. 220–247, 1971.
[117] R. Tregan, A. Bonnemayre, and R. Tertian, *Proceedings of the Fifth International Congress for Electron Microscopy*, vol. 1, paper BB-10. New York, NY, USA: Academic Press, 1962.
[118] T. Broniewski, A. Iwasiewicz, J. Kapko, and W. Płaczek, *Metody badań i ocena własności tworzyw sztucznych*. Warsaw, Poland: WNT, 1970.
[119] W. J. Freeman, "Characterization of polymers," in *Encyclopedia of Polymer Science and Engineering*, 2nd ed., vol. 3, H. F. Mark, N. M. Bikales, C. G. Overberger, G. Menges, and J. I. Kroschwitz, Eds. New York, NY, USA: Wiley, 1985, p. 290.
[120] D. Braun, "Identification," in *Encyclopedia of Polymer Science and Engineering*, 2nd ed., vol. 8, H. F. Mark, N. M. Bikales, C. G. Overberger, and G. Menges, Eds. New York, NY, USA: Wiley, 1989.
[121] M. Bolger, J. Hubball, J. Groeger, and S. Meronek, *Handbook for the Chemical Analysis of Plastics and Polymer Additives*. Boca Raton, FL, USA: CRC Press, 2007.
[122] W. H. Awad *et al*., "Material properties of nanoclay PVC composites," *Polymer*., vol. 50, no. 8, pp. 1857–1867, 2009, doi: 10.1016/j.polymer.2009.02.007.
[123] W. Ondiek, A. Ridzuan, M. Iwamoto, A. Macadre, and K. Goda, "Comparative Analysis of Mechanical and Morphological Properties of Cordenka and Ramie Fiber-Reinforced Polypropylene Composites," *Materials*, vol. 17, no. 22, Art. no. 5519, 2024, doi: 10.3390/ma17225519.
[124] M. Suzanne, M. M. Delichatsios, and J. Zhang, "Prediction of the Limiting Oxygen Index Using Simple Flame Extinction Theory and Material Properties Obtained from Bench Scale Measurements," in *Fire Safety Science—Proceedings of the Tenth International Symposium*, vol. 10, 2011, pp. 375–387, doi: 10.3801/IAFSS.FSS.10-375.
[125] A. A. Basfar, "Flammability of radiation cross-linked low density polyethylene as an insulating material for wire and cable," *Radiat. Phys. Chem.*, vol. 63, nos. 3–6, pp. 505–508, 2002, doi: 10.1016/S0969-806X(01)00545-X.
[126] E. Sudoł, E. Kozikowska, and E. Choińska, "The Utility of Recycled Rice Husk-Reinforced PVC Composite Profiles for Façade Cladding," *Materials*, vol. 15, no. 10, Art. no. 3418, 2022, doi: 10.3390/ma15103418.

[127] K. Patel, A. Velazquez, H. S. Calderon, and G. R. Brown, “Studies of the solid-state thermal degradation of PVC. I. Autocatalysis by hydrogen chloride,” *J. Appl. Polym. Sci.*, vol. 46, no. 1, pp. 179–187, 1992, doi: 10.1002/app.1992.070460117.
[128] W. H. Starnes, Jr., “Structural and mechanistic aspects of the thermal degradation of poly(vinyl chloride),” *Prog. Polym. Sci.*, vol. 27, no. 10, pp. 2133–2170, 2002, doi: 10.1016/S0079-6700(02)00063-1.
[129] Z. Li *et al*., “An overview of polymer-based thermally conductive functional materials,” *J. Mater. Sci. Technol.*, vol. 218, pp. 191–210, 2025, doi: 10.1016/j.jmst.2024.07.053.
[130] A. Kufel and S. Kuciel, “Hybrid Composites Based on Polypropylene with Basalt/Hazelnut Shell Fillers: The Influence of Temperature, Thermal Aging, and Water Absorption on Mechanical Properties,” *Polymers*, vol. 12, no. 1, Art. no. 18, 2020, doi: 10.3390/polym12010018.
[131] K. Głogowska, P. Pączkowski, and B. Samujło, “Study on the Properties and Structure of Rotationally Moulded Linear Low-Density Polyethylene Filled with Quartz Flour,” *Materials*, vol. 15, no. 6, Art. no. 2154, 2022, doi: 10.3390/ma15062154.
[132] Z. Yu, L. Zhang, W. Wang, X. Xie, H. Sun, Y. Xu, Y. Zhang, Q. Tao, X. Su, and G. Li, “Melt Blending Modification of Commercial Polystyrene with Its Half Critical Molecular Weight, High Ion Content Ionomer, Poly(styrene–ran–cinnamic Acid) Zn Salt, toward Heat Resistance Improvement,” *Polymers*, vol. 12, no. 3, Art. no. 584, 2020, doi: 10.3390/polym12030584.
[133] M. H. Kudzin, E. Piwowarska, N. Festinger, and J. Chruściel, “Risks associated with the presence of polyvinyl chloride in the environment and methods for its disposal and utilization,” *Materials*, vol. 17, no. 1, Art. no. 173, 2024, doi: 10.3390/ma17010173.
[134] M. Saad *et al*., “The impact of heat and humidity on unplasticized poly(vinyl chloride),” *Polym. Degrad. Stab.*, vol. 238, Art. no. 111334, 2025, doi: 10.1016/j.polymdegradstab.2025.111334.
[135] T. Rijavec, M. Strlič, and I. Kralj Cigić, “Plastics in heritage collections: Poly(vinyl chloride) degradation and characterization,” *Acta Chim. Slov.*, vol. 67, no. 4, pp. 993–1013, 2020, doi: 10.17344/acsi.2020.6479.
[136] C. Jubsilp, A. Asawakosinchai, P. Mora, D. Saramas, and S. Rimdusit, “Effects of organic based heat stabilizer on properties of polyvinyl chloride for pipe applications: A comparative study with Pb and CaZn systems,” *Polymers*, vol. 14, no. 1, Art. no. 133, 2022, doi: 10.3390/polym14010133.
[137] Š. Pok, I. Kralj Cigić, M. Strlič, *et al*., “Poly(vinyl chloride) degradation: Identification of acidic degradation products, their emission rates, and implications for heritage collections,” *npj Herit. Sci.*, vol. 13, Art. no. 382, 2025, doi: 10.1038/s40494-025-01955-w.
[138] R. C. Thompson and I. E. Napper, *Microplastic in the Environment*. London, U.K.: Royal Society of Chemistry, 2020.
[139] H. Parapanagioti and I. Kalavrousiotis, Eds., *Microplastic in Water and Wastewater*. London, U.K.: IWA Publishing, 2019.
[140] M. Wagner and S. Lambert, Eds., *Freshwater Microplastics*. Berlin, Germany: Springer, 2019.
[141] Group of Chief Scientific Advisers, *Environmental and Health Risks of Microplastic Pollution*. Brussels, Belgium: European Commission, Directorate-General for Research and Innovation, 2019.
[142] A. P. Leber, “Human exposures to monomers resulting from consumer contact with polymers,” *Chem.-Biol. Interact.*, vols. 135–136, pp. 215–220, 2001, doi: 10.1016/S0009-2797(01)00219-8.

[143] E. Bruchajer, "Toksykometria," in *Podstawy toksykologii*, J. K. Piotrowski, Ed. Warsaw, Poland: WNT, 2008, ch. 2, p. 29.
[144] J. F. Treon, H. Sigmon, H. Wright, and K. V. Kitzmiller, "The toxicity of methyl and ethyl acrylate," *J. Ind. Hyg. Toxicol.*, vol. 31, no. 6, pp. 317–326, Nov. 1949.
[145] G. N. Mir, W. H. Lawrence, and J. Autian, "Toxicological and pharmacological actions of methacrylate monomers II: Effects on isolated guinea pig ileum," *J. Pharm. Sci.*, vol. 62, no. 8, pp. 1258–1261, Aug. 1973, doi: 10.1002/jps.2600620804.
[146] U.S. Environmental Protection Agency, *Toxicological Review of Methyl Methacrylate (CAS No. 80-62-6): In Support of Summary Information on the Integrated Risk Information System (IRIS)*. Washington, DC, USA: U.S. EPA, 1998.
[147] J. Autian, "Structure-toxicity relationships of acrylic monomers," *Environ. Health Perspect.*, vol. 11, pp. 141–152, Jun. 1975, doi: 10.1289/ehp.7511141.
[148] M. A. Pemberton and B. S. Lohmann, "Risk assessment of residual monomer migrating from acrylic polymers and causing allergic contact dermatitis during normal handling and use," *Regul. Toxicol. Pharmacol.*, vol. 69, no. 3, pp. 467–475, 2014, doi: 10.1016/j.yrtph.2014.05.013.
[149] A. Bańkowska, M. Palczewska-Tulińska, and A. Krześlak, "Rejestracja polimerów wg Rozporządzenia REACH," *Polimery*, vol. 61, p. 49, 2016.
[150] M. Kowalewski and M. L. Kowalski, "Alergia na lateks," *Alergia Astma Immunologia*, vol. 2, p. 78, 1998.
[151] M. Chełmińska, "Alergia na lateks," *Pneumonol. Alergol.*, vol. 72, p. 143, 2004.
[152] F. A. Simonsen, M. Stavnsbjerg, L. M. Mollr, and T. Madsen, *Brominated Flame Retardants: Toxicity and Ecotoxicity*. Copenhagen, Denmark: Centre for Integrated Environment and Toxicology, 2000.
[153] National Research Council, *Toxicological Risks of Selected Flame Retardant Chemicals*. Washington, DC, USA: The National Academies Press, 2000.
[154] S. Janssen, *Brominated Flame Retardants: Rising Levels of Concern*. Arlington, VA, USA: Health Care, 2005.
[155] T. G. Osimitz, S. Kacew, and A. W. Hayes, "Assess flame retardants with care," *Science*, vol. 365, p. 992, 2019, doi: 10.1126/science.aay6309.
[156] M. Proshad, T. Kormoker, S. Islam, M. A. Haque, M. M. Rahman, and R. M. Mithu, "Toxic effect of plastic on human health and environment: A consequences of health risk in Bangladesh, a review," *Int. J. Health*, vol. 6, p. 1, 2018.
[157] S. Boryniec and W. Przygodzki, "Procesy spalania polimerów," *Polimery*, vol. 44, p. 87 (pt. I), p. 381 (pt. II), and p. 656 (pt. III), 1999.
[158] G. Janowska, W. Przygodzki, and A. Włochowicz, *Palność polimerów i materiałów polimerowych*. Warsaw, Poland: PWN, 2010.
[159] F. J. Rabek, *Polimery i ich zastosowanie interdyscyplinarne*, vol. 2. Warsaw, Poland: PWN, 2020.
[160] J. Brandrup, M. Bittner, W. Michaeli, and G. Menges, *Recycling and Recovery Plastics*. Munich, Germany: Hanser, 1996.
[161] J. Brandrup, "Gospodarcze i ekologiczne aspekty przerobu odpadów z tworzyw sztucznych," *Polimery*, vol. 42, p. 645, 1997.
[162] A. Kozera-Szałkowska, "Rynek tworzyw sztucznych – produkcja, zapotrzebowanie, zagospodarowywanie odpadów," *Polimery*, vol. 64, p. 751, 2019.
[163] J. Kijeński, "Tworzywa polimerowe w zrównoważonym rozwoju: od potrzeb użycia do potrzeby zużycia, cz. I. Nie ma odwrotu od plastików," *Polimery*, vol. 64, p. 725, 2019.

[164] Z. Zinowicz, J. Gołębiowski, and A. Świć, *Technologiczne problemy zagospodarowywaniem odpadów z tworzyw sztucznych*. Lublin, Poland: Wydawnictwo Politechniki Lubelskiej, 2003.
[165] P. Rejewski and J. Kijeński, "Zużyte polimery – dostęp i perspektywy źródeł surowców dla procesu recyklingu," *Polimery*, vol. 55, p. 721, 2010.
[166] J. Kijeński, A. K. Błędzki, and R. Jeziórska, *Odzyski i recykling materiałów polimerowych*. Warsaw, Poland: PWN, 2011.
[167] A. K. Błędzki and W. Królikowski, "Recykling materiałów polimerowych z dywanowych wykładzin podłogowych," *Polimery*, vol. 45, p. 29, 2000.
[168] K. Butlewski, "Anaerobic digestion and microwave pyrolisis techniques for recycling organic waste," *Polimery*, vol. 64, p. 811, 2019.
[169] S. Ucar, S. Karagoz, T. Karyidrim, and J. Yanik, "Conversion of polymers to fuels in refinery stream," *Polym. Degrad. Stab.*, vol. 75, p. 161, 2002.
[170] J. Scheirs and W. Kaminsky, Eds., *Feedstock Recycling and Pyrolysis of Waste Plastics: Converting Waste Plastics into Diesel and Other Fuels*. Chichester, U.K.: John Wiley & Sons, 2006, doi: 10.1002/0470021543.
[171] D. Kosmalska, H. Kaczmarek, R. Malinowski, and K. Bajer, "Postępy w badaniach degradacji termicznej materiałów polimerowych," *Polimery*, vol. 64, p. 241 (pt. 1) and p. 317 (pt. 2), 2019.
[172] M. Kozłowski, Ed., *Recykling tworzyw sztucznych*. Wroclaw, Poland: Oficyna Wydawnicza Politechniki Wrocławskiej, 2006.
[173] R. Buhl, "Progress in PVC feedstock recycling," *Polimery*, vol. 48, p. 263, 2003.
[174] A. K. Błędzki and W. Nowaczek, "Poli(chlorek winylu) – materiał niezbędny także w przyszłości czy stanowiący potencjalne zagrożenie dla środowiska," *Polimery*, vol. 40, p. 1, 1995.
[175] W. Nowaczek, "Specyficzne problemy recyklingu wyrobów z PVC," in *Recykling materiałów polimerowych*, A. K. Błędzki, Ed. Warsaw, Poland: WNT, 1997, p. 178.
[176] J. Wandrasz and A. Wandrasz, *Paliwa formowane, biopaliwa i paliwa z odpadów w procesach termicznych*. Warsaw, Poland: Seldel-Przywecki, 2006.
[177] Z. Makles, A. Świątkowski, and S. Grzybowska, *Niebezpieczne dioksyny*. Warsaw, Poland: Arkady, 2001.
[178] E. Kowalska, Z. Wielgosz, and T. Bartczak, "Utylizacja odpadów laminatów poliestrowo-szklanych," *Polimery*, vol. 47, p. 110, 2002.
[179] A. Bledzki, K. Goracy, M. Urbaniak, and M. Scheibe, "Problematyka utylizacji wyrobów i odpadów z kompozytów polimerowych, pt. I: Wielkość produkcji, utylizacja kompozytów z włóknami węglowymi, aspekty legislacyjne, recykling przemysłowy," *Polimery*, vol. 64, p. 777, 2019.
[180] M. Scheibe, M. Urbaniak, K. Goracy, and A. K. Błędzki, "Problematyka utylizacji odpadów z kompozytów polimerowych, pt. II: Złomowanie kompozytowych rekreacyjnych jednostek pływających na świecie w perspektywie do roku 2030," *Polimery*, vol. 64, p. 788, 2019.
[181] J. Głowacz, J. W. Kaczmar, and L. Nakonieczny, "Zastosowanie kompozytów polimerowych tworzyw sztucznych w przemyśle samochodowym," *Mechanik*, no. 7, p. 609, 2005.
[182] P. Mayer and J. Pach, "Zastosowanie nowoczesnych kompozytów polimerowych włóknami weglowymi i szklanymi w motoryzacji," *Przegląd Mechaniczny*, no. 9, p. 30, 2010.
[183] InduPlast, "PVC – the most consumed plastic material in Spain," Jul. 23, 2020. *InduPlast*. [Online]. Available: https://induplast.es/en/b/readers-corner/engineering-

plastics/p/pvc-the-most-consumed-plastic-material-in-spain-9-2. [Accessed: Dec. 20, 2025].
[184] Md S. Haque and Mohd. A. Siddiqui, "Plastic Welding: Important Facts and Developments," *American Journal of Mechanical and Industrial Engineering*, vol. 1, no. 2, pp. 15–19, 2016, doi: 10.11648/j.ajmie.20160102.12. [Online]. Available: https://www.sciencepublishinggroup.com/article/10.11648/j.ajmie.20160102.12. [Accessed: Dec. 30, 2025].
[185] A. L. Buxton, "Welding technologies for polymers and composites," TWI Ltd., Cambridge, U.K., paper presented at the I Mech E seminar, "The Joining of Plastics and Polymer Composite Materials," Oct. 24, 2002. [Online]. Available: https://www.twi-global.com/technical-knowledge/published-papers/welding-technologies-for-polymers-and-composites. [Accessed: Dec. 30, 2025].
[186] Directorate-General for Environment (European Commission) and Ramboll, *The Use of PVC (Poly Vinyl Chloride) in the Context of a Non-Toxic Environment*. Luxembourg, Luxembourg: Publications Office of the European Union, 2022, doi: 10.2779/375357.
[187] A. Kumar and R. K. Gupta, *Fundamentals of Polymer Engineering*, 3rd ed. Boca Raton, FL, USA: CRC Press, 2019.
[188] E. Rejman, B. Kiełbasa, P. Bałon, and R. Smusz, "Influence of the shape of reinforcing window profiles on the strength and torsional stiffness of windows," *Mechanik*, vol. 95, no. 8–9, pp. 46–51, 2022, doi: 10.17814/mechanik.2022.8-9.12.
[189] V. Iliev, Z. Y. Geshkova, R. Ivanov, and V. Samichkov, "Constitutive model of unplasticized polyvinyl chloride for numerical stress–strain analysis," *Science, Engineering and Education*, vol. 5, no. 1, pp. 3–8, 2020.
[190] R. Smusz, P. Bałon, B. Kiełbasa, E. Rejman, M. Bembenek, and Ł. Kowalski, "Experimental and numerical characterization of thermal bridges in windows," *Advances in Science and Technology Research Journal*, vol. 17, no. 1, pp. 315–331, 2023, doi: 10.12913/22998624/159070.
[191] F. C. Amorim, J. F. Souza, H. S. da Costa Mattos, and J. Reis, "Temperature effect on the tensile properties of unplasticized polyvinyl chloride," *SPE Polymers*, vol. 3, no. 2, pp. 99–104, 2022, doi: 10.1002/pls2.10067.
[192] M. Etcheverry and S. E. Barbosa, "Glass Fiber Reinforced Polypropylene Mechanical Properties Enhancement by Adhesion Improvement," *Materials*, vol. 5, no. 6, pp. 1084–1113, 2012, doi: 10.3390/ma5061084.
[193] M. Kozielczyk and M. Paczkowska, "Wzornik do oznaczania ciętych pod kątem 45° profili okiennych PVC w celu weryfikacji symetrii zgrzein po procesie zgrzewania," Poland Patent Application P.452695, 28.03.2025.
[194] K. Mathiyazhagan, K. K. Singh, and V. Sivabharathi, "Modeling the interrelationship between the parameters for improving weld strength in plastic hot plate welding: A DEMATEL approach," *J. Elastomers Plast.*, vol. 52, no. 2, pp. 117–141, 2020, doi: 10.1177/0095244318824779.
[195] N. Yarahmadi, I. Jakubowicz, and T. Hjertberg, "The effects of heat treatment and ageing on the mechanical properties of rigid PVC," *Polym. Degrad. Stab.*, vol. 82, no. 1, pp. 59–72, 2003, doi: 10.1016/S0141-3910(03)00163-0.
[196] J. Tomás Ferreira, A. Rizzo, G. Ferreira, F. Carvalho, D. Macário, and S. França de Sá, "Vinyl- and Polyurethane-Coated Fabrics in Fashion Collections: Exploring Material Subtleties Through a Multi-Analytical Approach," *Heritage.*, vol. 8, no. 12, Art. no. 511, 2025, doi: 10.3390/heritage8120511.

[197] J. Yu, L. Sun, C. Ma, Y. Qiao, and H. Yao, “Thermal degradation of PVC: A review,” Waste Management, vol. 48, pp. 300–314, 2016, doi: 10.1016/j.wasman.2015.11.041.
[198] M. Beltrán and A. Marcilla, “Fourier transform infrared spectroscopy applied to the study of PVC decomposition,” European Polymer Journal, vol. 33, no. 7, pp. 1135–1142, 1997, doi: 10.1016/S0014-3057(97)00001-3.
[199] M. Beltrán, J. C. García, and A. Marcilla, “Infrared spectral changes in PVC and plasticized PVC during gelation and fusion,” European Polymer Journal, vol. 33, no. 4, pp. 453–462, 1997, doi: 10.1016/S0014-3057(96)00213-3.
[200] Z. Hadj Amar, S. F. Chabira, M. Sebaa, and B. Ahmed, “Structural Changes Undergone During Thermal Aging and/or Processing of Unstabilized, Dry-blend and Rigid PVC, Investigated by FTIR-ATR and Curve Fitting,” Annales de Chimie - Science des Matériaux, vol. 43, no. 1, pp. 59–68, 2019, doi: 10.18280/acsm.430109.
[201] Z. Hadj Amar, S. F. Chabira, and M. Sebaa, “Thermal aging effects on the microstructure of rigid PVC tubes used for water transportation in sub-Saharan region,” Materials Today: Proceedings, vol. 49, pt. 4, pp. 1035–1040, 2022, doi: 10.1016/j.matpr.2021.09.025.
[202] M. Kozielczyk, J. Kowalczyk, and M. Paczkowska, “The influence of welding temperature on the durability and quality of composite-reinforced window profile joints,” *Inżynieria i Budownictwo*, no. 3, pp. 349–353, 2026, doi: 10.5604/01.3001.0055.7424.